INFORMATION TO USERS

This manuscript has been reproduced from the microfilm master. UMI films the text directly from the original or copy submitted. Thus, some thesis and dissertation copies are in typewriter face, while others may be from any type of computer printer.

The quality of this reproduction is dependent upon the quality of the copy submitted. Broken or indistinct print, colored or poor quality illustrations and photographs, print bleedthrough, substandard margins, and improper alignment can adversely affect reproduction.

In the unlikely event that the author did not send UMI a complete manuscript and there are missing pages, these will be noted. Also, if unauthorized copyright material had to be removed, a note will indicate the deletion.

Oversize materials (e.g., maps, drawings, charts) are reproduced by sectioning the original, beginning at the upper left-hand corner and continuing from left to right in equal sections with small overlaps.

ProQuest Information and Learning
300 North Zeeb Road, Ann Arbor, MI 48106-1346 USA
800-521-0600

UMI®

Université d'Ottawa · University of Ottawa

National Library of Canada
Acquisitions and Bibliographic Services
395 Wellington Street
Ottawa ON K1A 0N4
Canada

Bibliothèque nationale du Canada
Acquisitions et services bibliographiques
395, rue Wellington
Ottawa ON K1A 0N4
Canada

Your file Votre référence

Our file Notre référence

The author has granted a non-exclusive licence allowing the National Library of Canada to reproduce, loan, distribute or sell copies of this thesis in microform, paper or electronic formats.

L'auteur a accordé une licence non exclusive permettant à la Bibliothèque nationale du Canada de reproduire, prêter, distribuer ou vendre des copies de cette thèse sous la forme de microfiche/film, de reproduction sur papier ou sur format électronique.

The author retains ownership of the copyright in this thesis. Neither the thesis nor substantial extracts from it may be printed or otherwise reproduced without the author's permission.

L'auteur conserve la propriété du droit d'auteur qui protège cette thèse. Ni la thèse ni des extraits substantiels de celle-ci ne doivent être imprimés ou autrement reproduits sans son autorisation.

0-612-76426-5

Canada

There is a single light of science,

and to brighten it anywhere

is to brighten it everywhere.

Isaac Asimov

Abstract

This thesis is divided into 5 major sections. The first section covers the reactions of $Ti(NR_2)_4$ (R is methyl or ethyl) with the surface of partially dehydroxylated silica. This leads to the formation of well-defined grafted titanium complexes. The stoichiometry of the grafting reactions depends upon the degree of dehydroxylation of the silica. When the silica is pretreated at 500°C, $\equiv SiOTi(NR_2)_3$ is formed, while on silica which has been dehydroxylated at 200°C, $(\equiv SiO)_2Ti(NR_2)_2$ is the product.

The second section examines the spontaneous transformations experienced by the bis(dialkylamido)titanium fragments upon standing or exposure to vacuum. β-H abstraction results in elimination of one equivalent of amine, leaving an η^2-imine ligand coordinated to titanium. While the N-methylmethanimine complex is stable, the N-ethylethanimine complex undergoes a further loss of ethylene to yield a stable ethylimidotitanium(IV) surface complex. These transformations are catalyzed by the residual surface hydroxyls.

The third section describes the reactivity of the bis(dialkylamido)titanium fragments towards amines. Exposure to ammonia induces β-H abstraction, producing 1 equivalent of dialkylamine and resulting in the formation of η^2-imine complexes instead of the expected transamination products. The N-ethylethanimine complex, under prolonged vacuum, loses ethylene to produce ethylimidotitanium(IV). Other amines, including dialkylamines and aprotic amines such as pyridine and NEt_3, induce the same imine complex formation

The fourth section deals with the reactions of the imine and imido complexes with $Ti(NR_2)_4$. Both reactions result in grafting of an additional 2 wt. % Ti onto the silica, in the absence of surface hydroxyls and the formation of one equivalent of the corresponding amine.

Dinuclear surface complexes containing bridging imine, imido, or siloxo ligands are proposed as products.

The final section involves the characterization of the surface complexes produced upon exposure of partially dehydroxylated silica to $Mo(NR_2)_4$ (R is methyl or ethyl). When R is methyl, grafting on silica pre-treated at 200 or 500°C results in reactions analogous to $Ti(NMe_2)_4$. However, $Mo(NEt_2)_4$ displays a reactivity that is significantly different from its Ti analogue. The maximum Mo loading is double that expected for the number of surface hydroxyl groups available. Furthermore, the amount of diethylamine released is 1.5 times higher than expected (treatment of silica at 500°C) or twice as high (silica pre-treatment at 200°C). Spontaneous β-H abstraction and elimination of diethylamine is proposed to form an N-ethylethanimine complex of molybdenum(IV), which then reacts further with $Mo(NEt_2)_4$ to form a dimolybdenum complex with bridging imine ligands.

Acknowledgements

No scientist ever works in a vacuum, and I am no different. First I would like to thank Susannah. Many times over the (6!!!!) years during which I have had the pleasure of working with her I have been completely lost and discouraged. Always ready with encouraging words and fresh directions, she enabled me to carry on, even when I had no idea where this project was going and was starting to wander down the garden path.

Next, I must thank my mother, who is possibly the strongest person I have ever known. Always there for me with her encouragement, love, friendship, and unwavering belief that (a) I can do it; and (b) I am possibly the smartest person alive; this thesis is as much hers as it is mine. I hope to one day have your strength of character and willpower.

I need to thank my father for instilling me a work ethic that has enabled me to get through this, to never stop working until the job is done, and to never leave something half-finished.

To my girlfriend Geneviève, who has put up with many late nights of me at the computer, there are not enough words to thank you. We have spent almost 18 months together so far, and I look forward to many, many more.

The support and encouragement from people I have worked with over the years, has been very helpful. The people who I started my PhD with in the lab: Gordon, Jamila, Lisa, and Omar. Thank you for your support. The new guard in the lab, Valbona, Eric, and Tagenine, thank you very much for your friendship, I value it greatly. The undergrads who have wandered through over the years, have also been lots of fun...special mention goes to Liz and Huda, who have, more often then they know it, been a great source of stress relief and renewal with their bright-eyed and bushy-tailed view of chemistry and the world around us.

To the lunch gang (if you have to ask, you were never a part of it) Here's to many more lunches filled with laughter, innuendos and a general great time.

There are a number of other people I must thank. Julie and her husband Gianni, thank you for all that you have done for me, for bringing me out to The Liquordome and showing me how to really party. Rob, who I have known for over 13 years now, it has been a hell of a trip, and I look forward to many more years of friendship. Sandra, you are possibly the nicest, kindest person I have ever met. I wish you the strength and willpower to get through your trials. If you ever need a snack, some friendship, or someone to vent to, you know where to reach me. Dave and Cheryl, thank you very much for your friendship. All of my other friends, there is just not enough room for me to mention you here.

I can't say enough about the support staff in the department. Some days, Don, John, Lee, Ian, and Mike are the only things keeping this department from collapsing.

I have been extremely lucky to have had, throughout my life, amazing and passionate teachers. I am a direct result of their love for teaching and learning.

Table of Contents

Abstract iii

Acknowledgements v

Table of Contents vii

List of Figures xii

List of Figures xii

List of Schemes xix

List of Tables xxi

Chapter 1 General introduction 1

1.1 Metal nitrides 1

1.2 Metal nitride thin films 4

1.2.1 Physical vapour deposition (PVD) 4

1.2.2 Chemical vapour deposition (CVD) 5

1.3 Titanium nitride (TiN) 6

1.3.1 Preparation of thin TiN films 6

1.3.2 Origin of carbon contamination 10

1.4 Experimental investigations of CVD chemistry 12

1.4.1 Silica as a substrate 13

1.4.2 Surface organometallic chemistry on silica 18

1.5 References 21

Chapter 2 Experimental techniques 24

2.1 Reactants 24

2.1.1 Silica 24

2.1.2 Metal complexes 24

2.1.3 Liquid reagents 25

2.1.4 Gaseous reagents 25

2.2 Silica preparation 26

2.2.1 Partial dehydroxylation 26

2.2.2 Deuterium labelling 26

2.3 Modification of the silica surface 27

2.3.1 High vacuum techniques 27

2.3.2 Breakseal techniques 27

2.3.3 Grafting of metal complexes 29

2.4 Characterization of modified silicas 32

2.4.1 Infrared spectroscopy 32

2.4.2 Solid state NMR spectroscopy 36

2.4.3 Diffuse-reflectance UV-visible spectroscopy (DRUV-Vis) 36

2.4.4 Elemental analysis 37

2.5 Identification and quantitation of volatile products 39

2.5.1 By gas phase infrared spectroscopy 39

2.5.2 By GC and GC/MS 40

2.6 References 46

Chapter 3 Nature of the initial chemisorption of $Ti(NR_2)_4$ on silica **47**

3.1 Introduction 47

3.2 Stoichiometry of grafting of $Ti(NR_2)_4$ on silica-500 50

3.3 Stoichiometry of grafting of $Ti(NR_2)_4$ on silica-200 52

3.4 Infrared characterization of Ti-modified silicas 54

3.5 NMR characterization of Ti-modified silicas 59

3.6 UV-Vis characterization of Ti-modified silicas 59

3.7 Reactivity of Ti-modified silicas 64

3.7.1 Reaction with t-butanol 64

3.7.2 Reaction with CO_2 68

3.8 Conclusion 70

3.9 References 73

Chapter 4 Spontaneous transformations of silica-supported bis(amido)titanium complexes **75**

4.1 Introduction 75

4.2 Spontaneous transformation of $(\equiv SiO)_2Ti(NMe_2)_2$, **5** 75

4.3 Kinetics of N-methylmethanimine formation 83

4.4 Mechanism of N-methylmethanimine complex formation 91

4.5 Spontaneous transformation of $(\equiv SiO)_2Ti(NEt_2)_2$, **6** 96

4.6 Kinetics of ethylimido complex formation 100

4.7 Mechanism of diethylamine elimination 102

4.8 Conclusion 106

4.9 References 109

Chapter 5 Reactivity of titanium amide-modified silicas towards amines 111

5.1 Introduction 111

5.2 Reactions with dialkylamines 112

5.2.1 Reaction between $(\equiv SiO)_2Ti(NEt_2)_2$, **6**, and $HNMe_2$ 113

5.2.2 Reaction between $(\equiv SiO)_2Ti(NMe_2)_2$, **5**, and $HNEt_2$ 113

5.3 Reaction with a monoalkylamine 115

5.3.1 Reaction of $(\equiv SiO)_2Ti(NMe_2)_2$, **5**, with $CyNH_2$ 117

5.3.2 Reaction of $(\equiv SiO)_2Ti(NEt_2)_2$, **6**, with $CyNH_2$ 121

5.4 Reactions with NH_3 123

5.4.1 Reaction of $(\equiv SiO)_2Ti(NMe_2)_2$ with NH_3 123

5.4.2 Kinetics 128

5.5 Reaction of $(\equiv SiO)_2Ti(NEt_2)_2$ with NH_3 131

5.6 Reactions of $(\equiv SiO)_2Ti(NMe_2)_2$ with aprotic amines 135

5.6.1 Reaction of $(\equiv SiO)_2Ti(NMe_2)_2$ with pyridine 138

5.6.2 Reaction of $(\equiv SiO)_2Ti(NMe_2)_2$ with triethylamine 140

5.6 Conclusion 143

5.7 References 144

Chapter 6 Deposition of $Ti(NR_2)_4$ on Ti-modified silica surfaces 145

6.1 Introduction 145

6.2 Reaction of $Ti(NMe_2)_4$ with $(\equiv SiO)_2Ti(\eta^2\text{-}CH_2NMe)$, **7** 146

6.3 Reaction of $Ti(NEt_2)_4$ with $(\equiv SiO)_2Ti{=}NEt$, **8** 156

6.4 Reaction of $(\equiv SiO)_2Ti{=}NEt$, **6**, with $Ti(NMe_2)_4$ 159

6.5 Conclusion 162

6.6 References 165

Chapter 7 Nature of the chemisorption of $Mo(NR_2)_4$ on silica 166

7.1 Introduction 166

7.2 Stoichiometry of grafting of $Mo(NMe_2)_4$ on silica 167

7.3 Infrared characterization of $Mo(NMe_2)_4$-modified silicas 170

7.4 NMR characterization of $Mo(NMe_2)_4$-modified silicas 170

7.5 Insertion of CO_2 174

7.6 Grafting of $Mo(NEt_2)_4$ on silica 177

7.7 Spectroscopic characterization of $Mo(NEt_2)_4$ modified silicas 180

7.8 Mechanism of grafting of $Mo(NEt_2)_4$ onto silica 180

7.9 Conclusion 183

7.10 References 187

Chapter 8 General conclusions 188

List of Publications 191

Claims to Original Research 192

List of Figures

Chapter 1

Figure 1.1 Crystal structure of TiN. Ti atoms are large, N atoms are small.[4] 2

Figure 1.2 Structures of (a) crystalline (α-quartz) and (b) amorphous silica (presumed).[25] 15

Chapter 2

Figure 2.1 Schematic drawing of a breakseal reactor 28

Figure 2.2 Schematic drawing of an infrared cell 30

Figure 2.3 Schematic drawing of an NMR reactor 31

Figure 2.4 Infrared spectrum of a silica pellet partially dehydroxylated at 200 °C, recorded in an IR cell equipped with KCl windows. 34

Figure 2.5 Infrared spectra of (a) CaF_2; and (b) KCl windows, showing regions of transparency to IR radiation. 35

Figure 2.6 IR calibration curve for $HNEt_2$. 42

Figure 2.7 IR calibration curve for $HNMe_2$. 43

Figure 2.8 IR calibration curve for C_2H_4 44

Figure 2.9 GC calibration curve for C_2H_4 45

Chapter 3

Figure 3.1 *In situ* IR difference spectra of two regions of partial transparency of a self-supporting silica pellet after grafting of $Ti(NEt_2)_4$, **2**, onto silica-200. 55

Figure 3.2 *In situ* IR difference spectra of two regions of partial transparency of a self-supporting silica pellet after grafting of $Ti(NMe_2)_4$, **1**, onto silica-200, including an expansion of the unusual ν(C-H) region. 56

Figure 3.3 ^{13}C CP/MAS spectrum of silica-500 treated with **1** to give $(\equiv SiO)Ti(NMe_2)_3$, **3**, followed by desorption of excess **1** and evacuation of volatiles.....60

Figure 3.4 ^{13}C CP/MAS spectrum of silica-500 treated with **2** to give $(\equiv SiO)Ti(NEt_2)_3$, **4**, followed by desorption of excess **2** and evacuation of volatiles.....61

Figure 3.5 UV-visible spectra of (a) $Ti(NMe_2)_4$ in cyclohexane; (b) silica-200 modified with $Ti(NMe_2)_4$, recorded in diffuse reflectance mode (average of 3 spectra). 62

Figure 3.6 UV-visible spectra of (a) $Ti(NEt_2)_4$ in cyclohexane; (b) silica-200 modified with $Ti(NEt_2)_4$, recorded in diffuse reflectance mode (average of 4 spectra).....63

Figure 3.7 *In situ* IR difference spectra of a self-supporting silica pellet of (a) $(\equiv SiO)Ti(NEt_2)_3$, **4**, and (b) after exposure to $(CD_3)_3COD$. 66

Figure 3.8 *In-situ* IR spectra of (a) $(\equiv SiO)_2Ti(NMe_2)_2$, **5**, (b) after exposure to CO_2.....69

Chapter 4

Figure 4.1 In situ IR difference spectra of a sample of $(\equiv SiO)_2Ti(NMe_2)_2$ (**5**) (2.0 wt. % Ti: 14 mg SiO_2) recorded after dynamic evacuation at room temperature for the following times: (a) 0 h; (b) 3 h; (c) 5 h; (d) 11.5 h.....77

Figure 4.2 Time-resolved evolution of $(\equiv SiO)_2Ti(NMe_2)_2$ (**5**) at room temperature monitored as (a) the % integrated absorbance remaining in the region 3100-2650 cm^{-1}: (b) the intensity of the 2777 cm^{-1} mode.....78

Figure 4. 3 *In situ* IR difference spectra of regions of partial transmission of a self-supporting silica pellet of (a) $(\equiv SiO)_2Ti(\eta^2\text{-}CH_2NCH_3)$, **7**; (b) after exposure to $(CD_3)_3COD$ and evacuation of volatiles.....80

Figure 4.4 Mass spectra of (a) $HN(CH_3)(CH_2D)$ from reaction of **7** with $(CD_3)_3COD$; (b) $DN(CH_3)_2$ from reaction of $Ti(NMe_2)_4$ with $(CD_3)_3COD$; (c) $HNMe_2$; recorded after passing each through a DB-1 column.....81

Figure 4.5 Time-resolved dynamic vacuum evolution of $(\equiv SiO)_2Ti(NMe_2)_2$ on two different silica samples: (a) 0.71 wt. % Ti, 20.0 mg pellet; (b) 1.90 wt. % Ti, 8.0 mg pellet. ...85

Figure 4.6 Time-resolved dynamic vacuum evolution of $(\equiv SiO)_2Ti(NMe_2)_2$; (a) 13.1 mg SiO_2, 0.71 wt. % Ti (open circles), 15.3 mg SiO_2, 0.28 wt. % Ti (filled circles); (b) 17.7 mg SiO_2, 0.67 wt. % Ti (open circles), 13.1 mg SiO_2, 0.71 wt. % Ti (filled circles).....86

Figure 4.7 *In situ* IR spectra of $(\equiv SiO)_2Ti(NMe_2)_2$ (0.71 wt. % Ti), (a) before, and (b) after 900 minutes dynamic evacuation.....88

Figure 4.8 Dependence of k_{obs} for the spontaneous transformation of $(\equiv SiO)_2Ti(NMe_2)_2$ on the number of unreacted hydroxyls present on the silica pellet. 90

Figure 4.9 Time-resolved evolution of $(\equiv SiO)_2Ti(NMe_2)_2$ under static vacuum (14.2 mg SiO_2, 0.84 wt. % Ti, filled circles); dynamic vacuum (13.1 mg SiO_2, 0.71 wt. % Ti, open circles). 92

Figure 4.10 In situ IR difference spectra recorded after dynamic evacuation of $(\equiv SiO)_2Ti(NEt_2)_2$ (6) at room temperature for: (a) 0 h; (b) 3 h; (c) 6 h; (d) 42 h. The silica background spectrum has been subtracted and the spectra vertically offset. 97

Figure 4.11 Time-resolved evolution of $(\equiv SiO)_2Ti(NEt_2)_2$, **6**, at room temperature under dynamic vacuum, monitored as the integrated absorbance from 3100 to 2600 cm^{-1}. 98

Figure 4.12 Time-resolved room temperature dynamic evacuation of $(\equiv SiO)_2Ti(NEt_2)_2$ (1.30 wt. % Ti), monitored as the integrated absorbance from 3100 to 2600 cm^{-1} 101

Figure 4.13 Time-resolved room-temperature transformation of $(\equiv SiO)_2Ti(NEt_2)_2$ (1.30 wt. % Ti, 19.7 mg SiO_2) during periods of static (0-900 min) and dynamic (900-1800 min) vacuum. 103

Chapter 5

Figure 5.1 Spectra of (a) $(\equiv SiO)_2Ti(NEt_2)_2$; (b) after reaction with 30 Torr $HNMe_2$ for 19 hours; (c) after reaction with $HNMe_2$ for 48 hours. 114

Figure 5.2 Spectra of (a) $(\equiv SiO)_2Ti(NMe_2)_2$; (b) after reaction with $HNEt_2$ for 6 hours: (c) after reaction with $HNEt_2$ overnight (18 hours).....116

Figure 5.3 Spectra of (a) $(\equiv SiO)_2Ti(NMe_2)_2$; (b) after reaction with $CyNH_2$ for 60 minutes: (c) after reaction with $CyNH_2$ overnight (8 hours).....118

Figure 5.4 ^{13}C CP/MAS NMR spectrum of **5** after reaction with $CyNH_2$, spin rate 4 kHz.....119

Figure 5.5 Spectrum of (a) **5** after reaction with cyclohexylamine; and (b) after addition of $(CD_3)_3COD$.....120

Figure 5.6 Spectra of (a) $(\equiv SiO)_2Ti(NEt_2)_2$, **6**; (b) after reaction with $CyNH_2$ for 60 minutes: (c) after reaction with $CyNH_2$ overnight (18 hours).....122

Figure 5.7 *In situ* IR difference spectra recorded during the room temperature reaction between $(\equiv SiO)_2Ti(NMe_2)_2$ and 35 Torr NH_3: (a) before addition of NH_3; (b) 4 hrs; (c) 16 hrs; (f) after 41 hrs reaction time and evacuation of NH_3.....124

Figure 5.8 IR spectra of **5** (a) after reaction with NH_3 for 38 hours; (b) after removal of volatiles.....126

Figure 5.9 Comparison of spectra of $(\equiv SiO)_2Ti(NMe_2)_2$ after exposure to either (a) NH_3; (b) prolonged vacuum.....127

Figure 5.10 Time-resolved evolution of the peak height at 2777 cm^{-1} during the reaction between $(\equiv SiO)_2Ti(NMe_2)_2$ and 35 Torr NH_3.....130

Figure 5.11 Time-resolved evolution of peak height at 2777 cm^{-1} during the reaction of **5** with 80 Torr NH_3.....132

Figure 5.12 In situ IR spectra of (a) $(\equiv SiO)_2Ti(NEt_2)_2$; (b) after exposure for 3 hours to 20 Torr NH_3; and (c) after 18 hours exposure to 20 Torr NH_3.....134

Figure 5.13 Spectra of a sample of (a) **6**; (b) after 18 hour exposure to NH_3 to give **9**; (c) prolonged evacuation of the sample in (b).....136

Figure 5.14 Spectra of (a) $(\equiv SiO)_2Ti{=}NEt$, **8** produced by evacuation of $(\equiv SiO)_2Ti(NEt_2)_2$, **6**; (b) produced by evacuation of $(\equiv SiO)_2Ti(N(Et)CHCH_3)$, **9**.....137

Figure 5.15 *In-situ* IR spectra of (a) **5**; and (b) after its exposure to pyridine-d_5.....139

Figure 5.16 Spectra of (a) **5**; (b) after exposure to NEt_3 for 3 hrs; (c) after exposure to NEt_3 for 18 hours.....142

Chapter 6

Figure 6.1 *In-situ* IR spectra of (a) $(\equiv SiO)_2Ti(NMe_2)_2$, **5**; (b) after evacuation to give $(\equiv SiO)_2Ti(\eta^2\text{-}CH_2NCH_3)$, **7**; and (c) after readdition of $Ti(NMe_2)_4$.....147

Figure 6.2 *In-situ* IR spectra of (a) $(\equiv SiO)_2Ti_2(NMe_2)_2(CH_2NMe)_2$; and (b) **10** after alcoholysis with $(CD_3)_2CDCOD$.....148

Figure 6.3 *In-situ* IR spectra of (a) $(\equiv SiO)_2Ti(NMe_2)_2$, **5**; (b) after reaction with NH_3 to give $(\equiv SiO)_2Ti(\eta^2\text{-}CH_2NCH_3)$, **7**; (c) after readdition of $Ti(NMe_2)_4$ to **7**.....150

Figure 6.4 Time-resolved spectra of the reaction between NH_3 and **10** after (a) 0; (b) 0.5; (c) 10; (d) 43; (e) 74; and (f) 100 hours.....151

Figure 6.5 Integrated intensity vs. time for the reaction of NH_3 with **10**.....152

Figure 6.6 IR spectra of (a) $(\equiv SiO)_2Ti(NEt_2)_2$; (b) after evacuation to give $(\equiv SiO)_2Ti{=}NEt$; and (c) after addition of $Ti(NEt_2)_4$ to the sample from (b).....157

Figure 6.7 IR Spectra of (a) $(\equiv SiO)_2Ti(NEt_2)_2$; (b) after exposure to ammonia, followed by 12 hrs evacuation to give $(SiO)_2Ti{=}NEt$; and (c) after addition of $Ti(NEt_2)_4$ to the sample from (b).....158

Figure 6.8 IR spectrum of (a) **12**; (b) after the exposure to 35 Torr NH_3 followed by 2 hours evacuation to give **13**.....160

Figure 6.9 Spectra of (a) $(\equiv SiO)_2Ti(NEt_2)_2$, **6**; (b) after evacuation to give $(\equiv SiO)_2Ti{=}NEt$, **8**; and (c) after the addition of excess $Ti(NMe_2)_4$.....163

Chapter 7

Figure 7.1 *In situ* IR difference spectra of regions of partial transmission of a self-supporting silica pellet after grafting of $Mo(NMe_2)_4$, **15**, onto silica-200.....171

Figure 7.2 ^{13}C CPMAS spectrum of (a) $(\equiv SiO)_2Mo(NMe_2)_2$, **17**, (65,536 scans); and (b) silica-200 after exposure to $Mo(NEt_2)_4$ (123,400 scans).....173

Figure 7.3 In-situ IR spectra of (a) $(\equiv SiO)_2Mo(NMe_2)_2$, **17**, and (b) after exposure to CO_2.....175

Figure 7.4 IR difference spectra of $(\equiv SiO)Mo(NEt_2)_3$.....181

List of Schemes

Chapter 1

Scheme 1.1 Possible decomposition pathways for $TiH_2(NHMe)(NH_2)$ 11

Scheme 1.2 Genealogical tree of colloidal silica[4] 14

Scheme 1.3 Different types of hydroxyl groups present on the surface of silica 17

Chapter 4

Scheme 4.1 Proposed mechanism for the transformation of $(\equiv SiO)_2Ti(NMe_2)_2$, **5**, into $(\equiv SiO)_2Ti(\eta^2\text{-}CH_2NCH_3)$, **7**. 94

Scheme 4.2 Surface hydroxyl group migration, facilitated by a grafted metal complex 95

Scheme 4.3 Proposed mechanism for the transformation of $(\equiv SiO)_2Ti(NEt_2)_2$ (**6**) into $(\equiv SiO)_2TiNEt$ (**8**) 105

Scheme 4.4 Possible reaction pathways for the thermal decomposition of $V(NEt_2)_4$ 107

Chapter 5

Scheme 5.1 Possible mechanism for the reaction of **5** with NH_3 129

Scheme 5.2 Proposed mechanism for the reactions of **5** with aprotic amines. 141

Chapter 6

Scheme 6.1 Possible structures for **10** 154

Scheme 6.2 Possible structures for **11** 155

Scheme 6.3 Possible structures for **12.** 161

Chapter 7

Scheme 7.1 Proposed mechanism for reaction of $Mo(NEt_2)_4$ with silica-500.....184

Scheme 7.2 Proposed mechanism for the reaction of $Mo(NEt_2)_4$ with silica-200.....185

Scheme 7.3 Resonance structures of a bridging N-ethylethanimine ligand 186

List of Tables

Chapter 1

Table 1.1 Comparison of physical properties of TiN, Ti, sapphire (Al_2O_3) and diamond[13].....7

Chapter 3

Table 3.1 Titanium content of silica-500 modified through exposure to $Ti(NR_2)_4$ (R = Me, Et) after complete consumption of surface hydroxyl groups, and quantification of volatile organics released during grafting.....51

Table 3.2 Titanium content of silica-200 modified through exposure to $Ti(NR_2)_4$ (R = Me, Et) after complete consumption of surface hydroxyl groups, and quantification of volatile organics released during grafting.....53

Table 3.3 IR spectra of $Ti(NMe_2)_4$ and silicas modified with $Ti(NMe_2)_4$. 58

Table 3.4 Quantitation of amine liberated by reaction of $Ti(NR_2)_4$-modified silicas with $(CD_3)_3COD$ 67

Table 3.5 Peak positions and assignments for $Ti(O_2CNMe_2)_4$ and $(\equiv SiO)_2Ti(O_2CNMe_2)_2$.....71

Chapter 4

Table 4.1 Zero-order rates of transformation of $(\equiv SiO)_2Ti(NMe_2)_2$ at room temperature under dynamic vacuum 89

Chapter 7

Table 7.1 Analysis of silicas and volatiles resulting from exposure to $Mo(NMe_2)_4$ after complete consumption of surface hydroxyl groups. 168

Table 7.2 IR modes of silicas modified with $Mo(NMe_2)_4$. 172

Table 7.3 Peak positions and assignments for $Ti(O_2CNMe_2)_4$, $(SiO)_2Ti(O_2CNMe_2)_2$, and $(\equiv SiO)_2Mo(O_2CNMe_2)_2$ 176

Table 7.4 Quantitative product analysis for the reaction of $Mo(NEt_2)_4$ with silica 178

Table 7.5 Peak assignments in IR spectra of silica-500 modified with $M(NEt_2)_4$ (M = Ti, Mo) 182

Chapter 1

General introduction

1.1 Metal nitrides

The elements which form nitrides are organized into three classes. Some alkali metals (Li, Na), alkaline earths (Mg, Ca, Sr, Ba), as well as others (Zn), form *ionic nitrides*. These compounds are combinations of the corresponding metal cations with nitride (N^{3-}) anions. Due to their ionic nature, they are described by $(Ca^{2+})_3(N^{3-})_2$, $(Li^{+})_3N^{3-}$, and so on. Their synthesis generally proceeds via either the direct combination of the element with $N_{2(g)}$, or the loss of ammonia during thermolysis of the parent amide (e.g., $Ba(NH_2)_2$).[1] They readily undergo hydrolysis to produce ammonia and the corresponding metal hydroxide.

Cubic (NaCl-type) structures, Figure 1.1, are formed by *interstitial nitrides* of some of the transition metals (e.g., Ti, Zr, Hf), in which the nitrogen atoms occupy vacant sites in the metal lattice.[2] These materials combine the characteristic properties of three different classes of materials. Their extremely high melting points and simple crystal structures are reminiscent of ionic crystals. However, like covalent solids, they exhibit extreme hardness and brittleness. VN, for example, melts at 2570 °C and has a hardness between 9 and 10 on the Moh's scale (diamond is a 10). Finally, their electrical and magnetic properties resemble those of the parent transition metal.[3] Two techniques used for the synthesis of interstitial nitrides are exposure of the metal or metal oxide to ammonia at high temperature (>1000°C), or heating of the metal halides with Li_3N or Na_3N at lower temperatures. Although a large number of metal nitride phases (MN

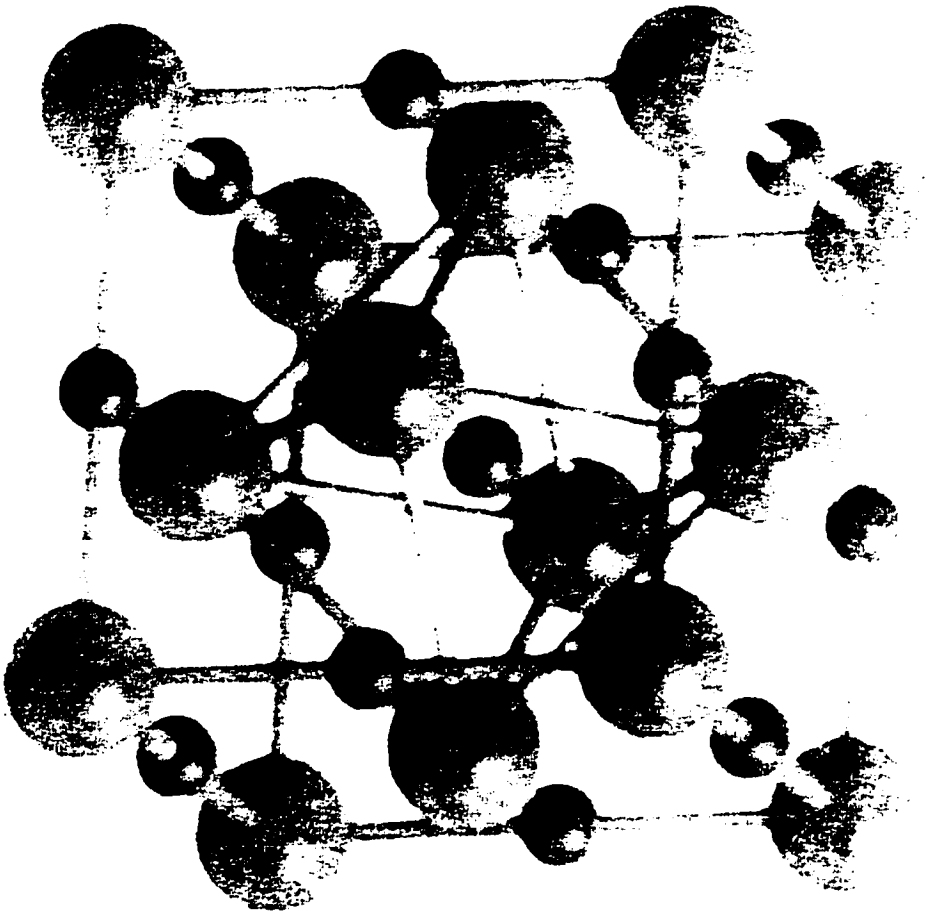

Figure 1.1 Crystal structure of TiN. Ti atoms are large, N atoms are small.[4]

M_2N, M_4N, etc) have been isolated using these techniques, only the stoichiometric nitrides (MN) have been extensively studied. The latter includes VN and TiN as well as nitrides such as Zr_3N_4, Hf_3N_4 and Ta_3N_5, where the metal is in its highest oxidation state.[5]

The final class comprises the *covalent nitrides* such as BN, S_4N_4 and P_3N_5. Their properties vary greatly from compound to compound, depending on the element with which the nitrogen combines.

Due to their attractive physical properties, interstitial metal nitrides have found the widest use in industrial applications. Their chemical inertness, hardness, and thermal stability under inert or reducing atmospheres have made them useful as protective coatings on cutting tools and UHV system components.[6] Crucibles made of titanium or zirconium nitrides have been used as containers in the melting of metals.[6] Their optical properties and colour have made them useful as wavelength-selective transparent films and gold-coloured decorative coatings, respectively.[5] Their electrical properties have led to uses in microelectronics devices.[5]

Transition metal nitrides also find applications as catalysts in a number of reactions traditionally catalysed by noble metals, such as hydrodesulfurization, dehydrogenation, isomerization, methanation, hydrodenitrogenation and ammonia synthesis. In others (hydrogenation and hydrogenolysis), they possess catalytic properties that may be better than those of the noble metal catalysts. Further, their unique catalytic pathways may open the door to desirable product selectivity. Finally, their resistance towards poisoning by S or N is higher than the noble metals.[3]

1.2 Metal nitride thin films

In applications such as coatings and microelectronics circuitry, thin films of metal nitrides are required. Catalyst activity, which is related to surface area, also requires methods of preparation which generate thin films of metal nitrides on a support material. Methods used for the deposition of thin films fall into one of two categories. The first group of techniques is known as physical vapour deposition (PVD). Chemical vapour deposition (CVD) is the second type of technique which finds wide application.

1.2.1 Physical vapour deposition (PVD)

Physical vapour deposition includes all techniques in which at least one of the reactants (usually the metal(s)), not originally in the gas phase, is evaporated in a high-vacuum chamber (10^{-6} – 10^{-9} atm). A number of different techniques may be used to drive the evaporation. Some of the more common ones are heating, sputtering (where an incident beam of atoms or ions is used to knock atoms off a target onto a substrate), and arc-evaporation (heating using a high-voltage electric current).

PVD techniques work best when there is a direct line of sight from the source to the target.[7] While the films produced by PVD routes tend to be very pure, a number of problems arise when trying to coat complex pieces. When they contain features that have high aspect ratios, i.e., a depth / width ratio $\geq$ 1.5, films deposited by PVD techniques show poor step coverage.[7-11] In addition, PVD-produced films are, in general, less conformal (a film is

considered conformal when it uniformly coats all exposed parts of a three-dimensional structure)[11] than the corresponding CVD films, especially in sub-micron devices.[12]

1.2.2 Chemical vapour deposition (CVD)

CVD is distinguished from PVD by the occurrence of surface or gas phase chemical reactions which release ligands or other by-products extraneous to the composition of the film.[13] CVD usually involves one or more gas phase species which contain a core similar to the structure of the desired material (i.e., $M(NR_2)_x$ for the deposition of M_yN_z). As feature sizes in microelectronics descend further into the sub-micron range (for comparison, a human hair is ca. 10 microns in diameter),[7] CVD methods are moving to the forefront due to their advantages over PVD techniques: higher step coverage,[8,9,14] increased density and growth rate,[9] and improved conformality.[12]

A subset of the CVD of thin films which is experiencing rapid growth and study is Atomic Layer Epitaxy (ALE). In ALE, both the gas pressure and the substrate are chosen to ensure that only a single monolayer of gas is chemisorbed onto the substrate; the remainder is removed. Typically, the precursors are delivered in alternating gas pulses. To date, successful ALE has been restricted to the growth of metal oxides (Al_2O_3, Ta_2O_5, and TiO_2) as well as the formation of the binary semiconductors ZnS and GaAs. Although the growth rate in ALE is extremely slow, it provides atomic control over the thickness, as well as conformal growth over surface topography and uniform growth over large surface areas.[11]

1.3 Titanium nitride (TiN)

Titanium nitride (TiN) is the most industrially important of the transition metal nitrides. It is a better conductor than titanium metal, and has optical properties resembling gold. Its hardness is greater than any metal, and comparable to sapphire (Al_2O_3). Finally, it has a melting point of 3220 K, approaching that of diamond, Table 1.1.

TiN has found wide use as a barrier layer in the microelectronics industry. Replacement of aluminum by copper for the interconnects on silicon chips necessitates the use of a barrier layer, placed between the etched silicon wafer and the copper being deposited on the chip.[12] Its function is to prevent the solid state reaction between silicon and copper leading to the formation of copper silicides, $CuSi_n$, which increase the resistance of the copper wire and degrade its performance.[15]

1.3.1 Preparation of thin TiN films

TiN films were originally deposited using PVD methods such as reactive sputtering (sputtering of Ti in a N_2 atmosphere) or by nitriding of a previously sputtered layer of Ti by exposure to NH_3 or N_2 from 300 – 900 K. However, as miniaturization accelerated, the quality (step coverage and conformality) of the films produced via these techniques was no longer acceptable.

CVD methods create higher quality TiN films. However, the transition from PVD to CVD created new problems. The first CVD reaction to be implemented was the thermolysis of $TiCl_4$ in the presence of N_2 and H_2, eq 1.1:

Table 1.1 Comparison of physical properties of TiN, Ti, sapphire (Al_2O_3) and diamond[13]

	Melting Point (K)	Vickers Microhardness (kg / mm^2)	Electrical Resistivity ($\mu\Omega$ cm)
Ti	1933	55	39
TiN	3220	2100	25
C (diamond)	4073[a]	7600	10^{18}
Al_2O_3	2323	2080	10^{18}

[a] Decomposition occurs.

$$TiCl_4 + \frac{1}{2} N_2 + 2 H_2 \rightarrow TiN + 4 HCl \qquad (1.1)$$

The quality of the films produced using this approach is quite high, although the temperature required (>1000°C) for deposition precludes its application with thermally sensitive substrates.[9] In order to reduce the deposition temperature, elemental nitrogen was replaced by a much more reactive form of nitrogen, ammonia. Although the process temperature can then be reduced to 550°C,[9] this is still not low enough for use with systems which involve aluminum.[7,16] Significant Cl contamination in the film occurs at lower temperatures (up to several atomic %). The presence of NH_3 also creates problems. Stable $TiCl_4/NH_3$ adducts and salts form and condense in cool areas of the reactor, hence this approach is "notorious for giving powders that clog the (TiN) deposition apparatus".[17]

Attempts were then made to find single-source precursors to be used in the deposition of TiN. In designing suitable titanium complexes, several requirements were noted.[18] First, the precursor must already contain the chemical bonds (Ti-N) required. Second, the core of the molecule should resemble that of the material being deposited (as in the deposition of AlN, where $[(CH_3)_2AlN]_3$ is the precursor). Finally, the Ti-N bonds must be stronger than other bonds in the compound. If this is not the case, the decomposition of the precursor is complex and non-selective. Furthermore, there are several requirements to ensure the economic viability of a CVD process.[19] The precursor must have good volatility, as well as good thermal stability during evaporation and transport. It must be readily available both at high purity and low cost. In addition to low (or no) toxicity, it should be a non-pyrophoric liquid with a long shelf-life. A

number of single-source precursors were studied, including azido[20] and imido[20-22] complexes of titanium, however, the films produced were of poor quality.

The titanium(IV) dialkylamides also fit the above requirements. While a large number of dialkylamido complexes are readily available, either commercially or through a relatively trivial synthesis, only the dimethyl- and diethylamido complexes are viable CVD precursors. With alkyl groups larger than ethyl (i.e., isopropyl, tert-butyl), in order to create an appreciable vapour pressure the temperature must be raised precariously close to the decomposition temperature of the complex.[12] Up to 350°C, only a fine powder was formed during deposition of TiN using $Ti(NR_2)_4$ (R = Me, Et). Above this temperature, films were formed, however, they were highly contaminated with carbon.[12] Curiously, films formed from $Ti(NMe_2)_4$ (initial C / Ti = 8) contained almost twice as much carbon contamination than the corresponding films formed from $Ti(NEt_2)_4$ (initial C / Ti = 16).[12]

The presence of NH_3 in the CVD reactor lowers the level of carbon contamination in $Ti(NR_2)_4$-derived TiN films, presumably by assisting in the removal of dialkylamido ligands. Adding NH_3 also drastically lowers the temperature required for TiN deposition compared to deposition from $TiCl_4$ and NH_3, rendering TiN CVD compatible with a wide variety of possible substrates. Deposition of TiN films on stainless steel and polyester was thus achieved at temperatures lower than 250°C. Unfortunately, ammonia is not completely effective at removing dialkylamido ligands. TiN films grown from $Ti(NMe_2)_4$ and NH_3 under a variety of different conditions (gas flow, deposition temperature, inlet diameter, etc) always showed significant C incorporation, ranging from 2-20 at%, in the film.[9] As the temperature increased, C contamination also increased.

1.3.2 Origin of carbon contamination

In their discussion of TiN films deposited using either of the single-source precursors $Ti(NMe_2)_3(^tBu)$ or $[Ti(\mu\text{-}N^tBu)(NMe_2)_2]_2$, Gordon and co-workers[22] identified two different types of carbon contamination: organic carbon, defined as carbon bound only to other carbon, oxygen or nitrogen, and carbidic carbon, in which the carbon is found in the primary coordination sphere of titanium, i.e., $Ti\text{-}CH_2\text{-}$, Ti=CH-, or TiC (carbide).

The mass spectral pattern of a molecular compound can be used to predict its decomposition pathways in a CVD chamber. $[TiCl_2(N^tBu)(NH_2{}^tBu)_2]_3$, $[TiCl_2(N^tBu)(NH_2{}^tBu)_3]$, $[TiCl_2(N^tBu)(NH_2{}^tBu)_{0.4}]$, $[TiCl_2(N^tBu)(NH_2{}^tBu)_2]_x$, and $[TiCl_2(N^tBu)(TMEDA)]$ were synthesized and their fragmentation patterns examined.[16] One of the major peaks, at *m/e* 323, was assigned to the loss of an ^{t}butyl fragment from the common intermediate $[TiCl_2(N^tBu)]_2$. This is an important observation since cleavage of nitrogen-carbon bonds is crucial to the CVD of carbon-free titanium nitride films.

Calculations were performed to elucidate both the source of carbon contamination as well as the mechanism by which the ligands are eliminated during deposition. Possible pathways by which the model compound $TiH_2(NHMe)(NH_2)$ may decompose are shown in Scheme 1.1.[23] The 1,2-elimination of ammonia, methane, molecular hydrogen or methylamine leads to the formation of an imidotitanium complex, $L_nTi{=}NR$ (R = Me, H). β-H elimination yields either H_3TiNH_2, via extrusion of methylamine, or a 3-membered azametallacycle containing coordinated methylimine.

Scheme 1.1 Possible decomposition pathways for $TiH_2(NHMe)(NH_2)$

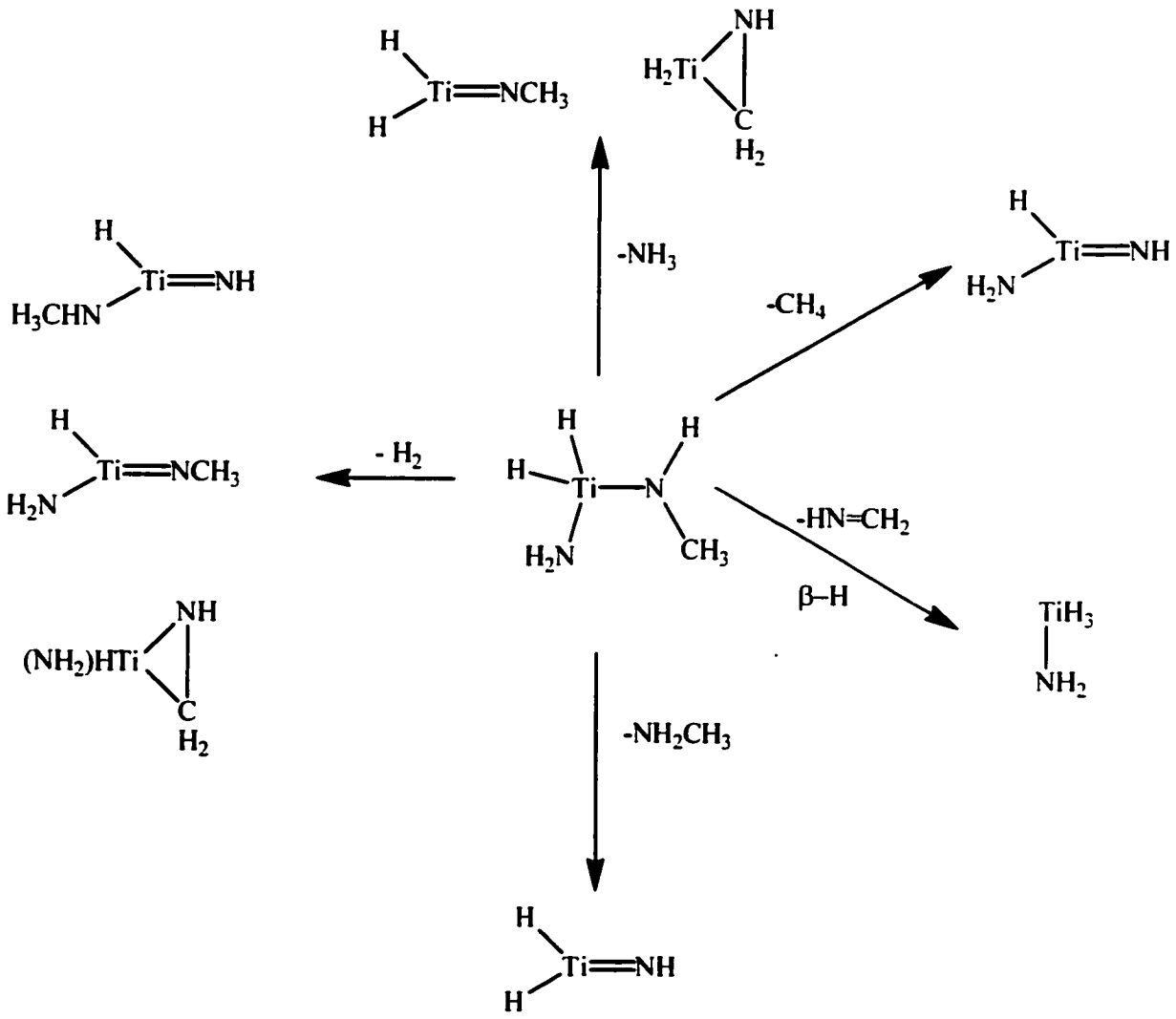

Extrusion of methylimine was found not to be competitive, either thermodynamically or kinetically. Of the remaining pathways, those that lead to cyclization are only slightly less favourable than 1,2-elimination reactions, and may be competitive under CVD conditions.

The experimental mass spectrum of $Ti(NMe_2)_4$ shows evidence of cyclization products ($HNMe_2$ and $(Me_2N)_2Ti(CH_2NMe)$). In contrast to theoretical predictions, β-hydride elimination products ($H_2C{=}NMe$ and $(Me_2N)_3TiH$) were also observed. However, products resulting from one 1,2-elimination pathway (NMe_3 and $(Me_2N)_2Ti{=}NMe$) were not observed. Galakhov found evidence of β-H elimination in the thermolysis of $[\{Cp^*Ti(NMe_2)\}_3(\mu\text{-}O)_3]$.[24] When heated in toluene, dimethylamine was lost and a complex with a bridging imine ligand was formed, $[Cp^*_3Ti_3(NMe_2)(\mu\text{-}\eta^2\text{-}CH_2NMe)(\mu\text{-}O)_3]$.

1.4 Experimental investigations of CVD chemistry

The reactions which control the purity of CVD films can occur either in the gas phase or on the surface of the substrate. When the reactions occur in the gas phase (as is the case for *A*tmospheric *P*ressure *C*hemical *V*apour *D*eposition), the higher the temperature, the cleaner (less carbon contamination) the resulting film. When the majority of the reactions involved occur on the surface of the substrate (as is the case for *L*ow *P*ressure *C*hemical *V*apour *D*eposition), it is at low temperatures that the cleanest films are produced. Modern substrates prohibit the high temperatures required in APCVD, thus, it is the surface reactions that control the LPCVD of TiN which must be optimized.

Accurate modelling of LPCVD requires knowledge of the way in which the CVD precursor interacts with the substrate surface. In the microelectronics industry, the substrate to be modelled is the surface of the silicon wafers upon which the microcircuits are printed. Unless this surface has been rigorously cleaned and kept in an inert atmosphere, oxygen from the atmosphere will rapidly oxidize the silicon surface to SiO_2. Thus, in the deposition of TiN onto silicon substrates, it is not the interaction of TiN with silicon that is important, but its interaction with SiO_2 on the surface. Thus a reasonable choice for use as a model substrate is silica itself.

1.4.1 Silica as a substrate

Silica is the most abundant oxide present on the surface of the earth. It occurs naturally, primarily as α-quartz. Other common forms of silica are β-quartz, β-cristobalite, and HP tridymite. α-Quartz is one of the hardest materials on earth, with a Moh's hardness of 10. This property, as well as its low solubility in water, aids it in resisting weathering. All phases of silica are built up from SiO_4 tetrahedra,[25] although certain phases, especially those formed under high pressure conditions (e.g., stishovite) or extremely high temperatures (e.g., silica glass), also contain SiO_6 octahedra.[25]

A great number of different types of silica are available commercially. Degussa alone offers almost 60 different types of silica, among them fumed silicas, precipitated silicas and chemically prepared silicas. Names given to them depend on the technique used to prepare the silica, Figure 1.2. The method of preparation also determines how the SiO_4 tetrahedra are linked, as in either crystalline or amorphous polymorphs, Figure 1.3.

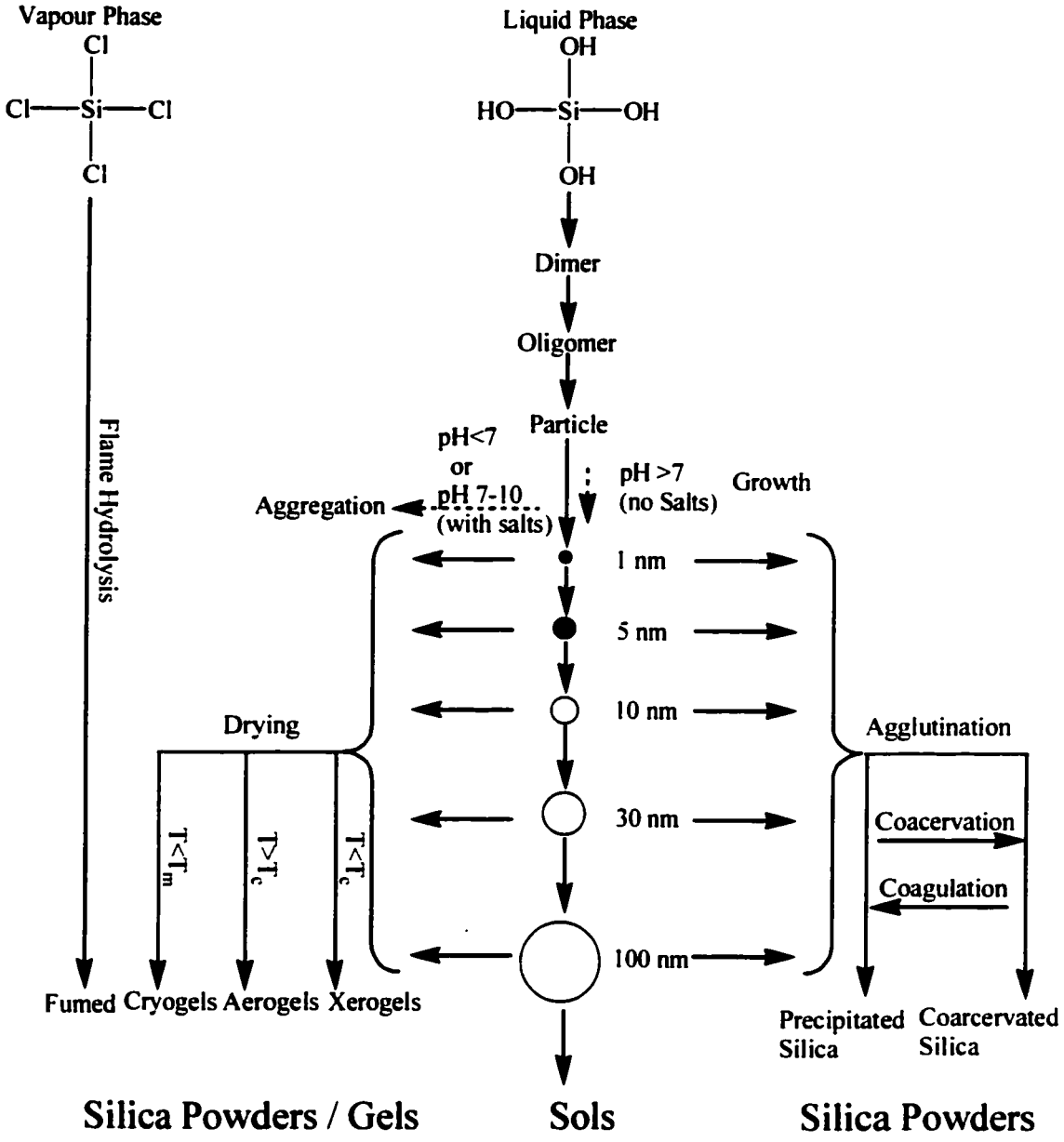

Scheme 1.2 Genealogical tree of colloidal silica[4]

a

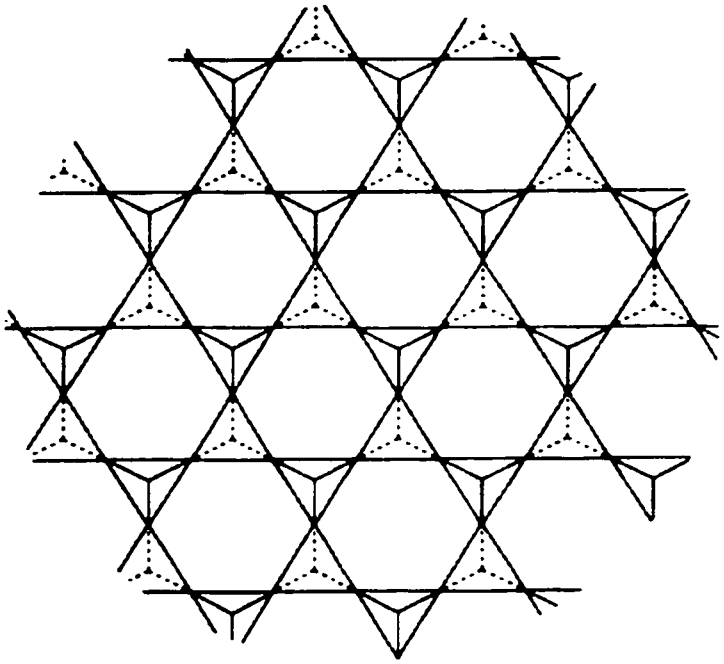

b

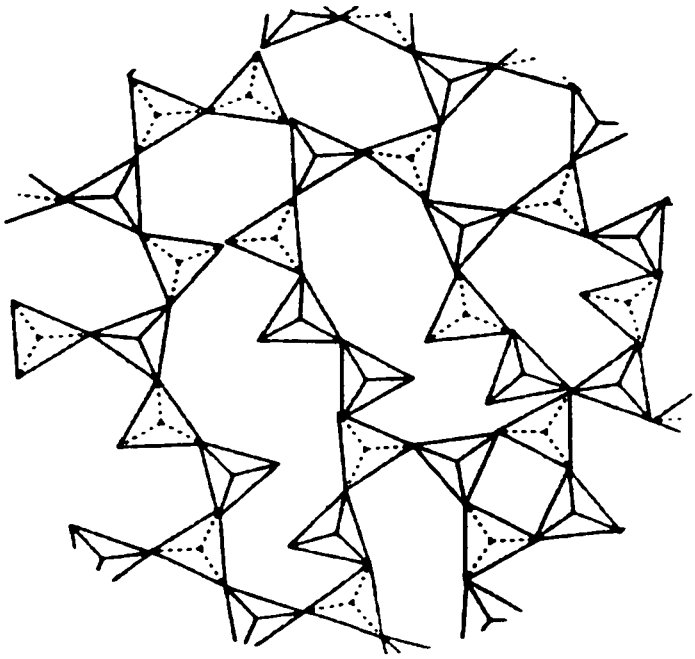

Figure 1.2 Structures of (a) crystalline (α-quartz) and (b) amorphous silica (presumed).[25]

The surface of silica is terminated by hydroxyl groups. Under most conditions, it is these hydroxyl groups which are responsible for the reactivity of silica. In an infrared spectrum, isolated hydroxyl groups (those that are not coordinated to either water or other hydroxyl groups in the vicinity) vibrate at 3747 cm^{-1} (ν(SiO-H)). Hydroxyl groups which are hydrogen-bonded to other surface hydroxyl groups absorb in the infrared at lower frequencies, down to 3200 cm^{-1}. In the air at room temperature, the surface of silica adsorbs several layers of hydrogen-bonded water molecules. Heating under vacuum results first in dehydration of the silica then progressive dehydroxylation.[4] Dehydroxylation results in the formation of siloxane bridges, eq 1.3:

$$2 \equiv SiOH \rightarrow \equiv Si\text{-}O\text{-}Si\equiv + H_2O \qquad (1.3)$$

Depending on the history of the silica, different types of hydroxyl groups may be present on its surface, Scheme 1.3. As soon as dehydration is complete (i.e., all of the physisorbed water has been driven off), the surface population consists mainly of hydrogen-bonded OH groups. Elimination of hydrogen-bonding via condensation leaves a mixture of three other types of hydroxyl groups: geminal, vicinal, and isolated. Geminal OH groups are a minor component, but are thought to persist on the surface at temperatures up to 800°C,[4] since they do not undergo internal condensation. After dehydroxylation at 200°C, the surface hydroxyl groups exist primarily as vicinal pairs. Dehydroxylation at higher temperatures (450 – 500°C) results in further condensation so that only isolated hydroxyl groups are left on the surface.

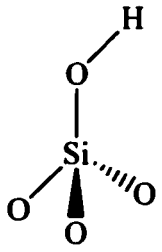

Isolated

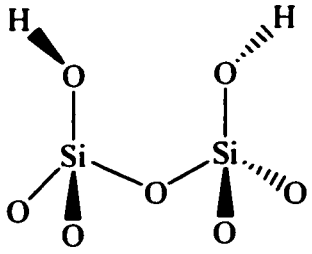

Vicinal

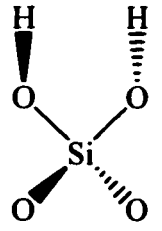

Geminal

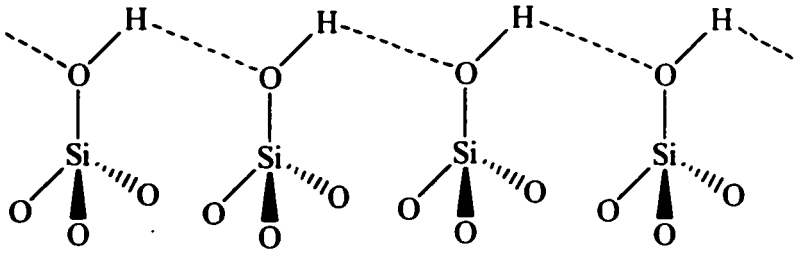

Hydrogen-bonded

Scheme 1.3 Different types of hydroxyl groups present on the surface of silica

1.4.2 Surface organometallic chemistry on silica

Due to the importance of silica as a catalyst support, the main impetus for the study of the reactivity of species chemisorbed on silica has come from the field of catalysis. Bridging the gap between molecular (homogeneous) organometallic chemistry and heterogeneous catalysis, *s*urface *o*rgano*m*etallic *c*hemistry (SOMC) comprises three closely related areas of study.[26] First is the reactivity of organometallic compounds with surfaces. Second is the characterization of the resulting surface organometallic fragments. Last but not least is an examination of the reactivity of supported complexes. Applying principles from organometallic chemistry to probe the surface, a map of surface reactivity may be obtained,[26,27] as well as the knowledge to eventually design and predict surface chemistry.[28]

During LPCVD, the metal complex is transported intact from source to substrate. Once adsorbed (either physically or chemically) onto the surface, it must then undergo controlled thermolysis. SOMC can model both the adsorption and subsequent thermal decomposition of CVD precursors as surface organometallic fragments.

For example, tetraneopentyl complexes of Ti, V and Cr have been used as single-source precursors in the CVD of metal carbide films. The thermolysis mechanisms have been suggested to involve neopentylidene (M = Ti) or metallacyclobutane (M = Cr) intermediates. Due to their very short lifetimes, neither of these intermediates was directly observed during the CVD process. However, the reactions of MNp_4 (M = Ti, V, Cr) with silica have been extensively studied. On Aerosil silica pretreated at 200°C, grafting results in the formation of bis(neopentyl)

surface organometallic fragments and is accompanied by the evolution of two equivalents of neopentane, eq 1.4.[29]

$$2\ \equiv SiOH + MNp_4 \rightarrow (\equiv SiO)_2MNp_2 + 2\ NpH \qquad (1.4)$$

Mild thermolysis (<150°C) of $(\equiv SiO)_2MNp_2$ resulted in the liberation of one additional equivalent of neopentane. Deuterium labeling experiments and reactivity studies confirmed that the thermolysis process corresponds to α-H elimination and results in the formation of silica-stabilized neopentylidene complexes, eq 1.5.[29]

$$(\equiv SiO)_2MNp_2 \xrightarrow{\Delta} (\equiv SiO)_2M{=}CHCMe_3 + NpH \qquad (1.5)$$

Thus a key proposed intermediate in metal carbide CVD was positively identified via surface organometallic chemistry.

SOMC has also shed light on the CVD of metal oxide films. A number of such films, including ZrO_2, Al_2O_3, TiO_2, and Ta_2O_5,[30] have been deposited via the thermolysis of the corresponding metal alkoxides. Metal oxoalkoxides such as $[Ti_3O_4(OR)_4]_n$ and $ZrO(O^tBu)_2$ (in the deposition of TiO_2 and ZrO_2 from $Ti(OR)_4$ and $Zr(O^tBu)_4$, respectively) have been proposed as intermediates.[31] The reaction of $Ti(O^iPr)_4$ with silica was recently shown to produce dinuclear supported titanium oxoisopropoxides via spontaneous disproportionation of the alkoxide ligands, eq 1.6-1.7.[32]

$$2\ \equiv SiOH + Ti(O^iPr)_4 \rightarrow (\equiv SiO)_2Ti(O^iPr)_2 + 2\ {}^iPrOH \qquad (1.6)$$

$$(\equiv SiO)_2Ti(O^iPr)_2 + Ti(O^iPr)_4 \rightarrow (\equiv SiO)_2Ti_2O(O^iPr)_4 + {}^iPrOH + C_3H_6 \qquad (1.7)$$

To date, no investigation of the grafting of $Ti(NR_2)_4$ on silica surfaces has been reported, although such reactions could be considered to model the first step in the LPCVD of TiN. This chemistry, as well as subsequent transformations of the supported titanium dialkylamide fragments relevant to CVD, will be described with the goal of better understanding the reactions which lead to TiN formation and impurities in TiN films.

1.5 References

(1) Cotton, F. A.; Wilkinson, G.; Murillo, C. A.; Bochmann, M. *Advanced Inorganic Chemistry*; 6th ed.; Wiley Interscience: Toronto, 1999.

(2) Hector, A. L.; Parkin, I. P. *Polyhedron* **1995**, *14*, 913-917.

(3) Chen, J. G. *Chem. Rev.* **1996**, *96*, 1477-1498.

(4) Bergna, H. E., Ed. *The Colloid Chemistry of Silica*; American Chemical Society: Washington, DC, 1994.

(5) Hoffman, D. M. *Polyhedron* **1994**, *13*, 1169-1179.

(6) Gillan, E. G.; Kaner, R. B. *Inorg. Chem* **1994**, *33*, 5693-5700.

(7) Ekerdt, J. G.; Sun, Y.-M.; Szabo, A.; Szulczewski, G. J.; White, J. M. *Chem. Rev.* **1996**, *96*, 1499-1517.

(8) Cale, T. S.; Chaara, M. B.; Raupp, G. B.; Raaijmakers, I. J. *Thin Solid Films* **1993**, *236*, 294-300.

(9) Fix, R.; Gordon, R. G.; Hoffman, D. M. *Chem. Mater.* **1991**, 1138-1148.

(10) Buiting, M. J.; Otterloo, A. F.; Montree, A. H. *J. Electrochem. Soc.* **1991**, *138*, 500-505.

(11) Gates, S. M. *Chem. Rev.* **1996**, *96*, 1519-1532.

(12) Raaijmakers, I. J. *Thin Solid Films* **1994**, 85-93.

(13) Oyama, S. T. *The Chemistry of Transition Metal Carbides and Nitrides*; Blackie Academic & Professional: New York, 1996.

(14) Sun, S. C.; Tsai, M. H. *Thin Solid Films* **1994**, *253*, 440-444.

(15) Liu, X.; Wu, Z.; Cai, H.; Yang, Y.; Chen, T.; Vallet, C. E.; Zuhr, R. A.; Beach, D. B.; Peng, Z.-H.; Wu, Y.-D.; Concolino, T. E.; Rheingold, A. L.; Xue, Z. *J. Am. Chem. Soc.* **2001**, *123*, 8011-8021.

(16) Lewkebandara, T. S.; Sheridan, P. H.; Heeg, M. J.; Rheingold, A. L.; Winter, C. H. *Inorg. Chem* **1994**, *33*, 5879-5889.

(17) Jayaratne, K. C.; Yap, G. P. A.; Haggerty, B. S.; Rheingold, A. L.; Winter, C. H. *Inorg. Chem.* **1996**, *35*, 4910-4920.

(18) Maury, F. *J. Phys. IV* **1995**, *5*, 449-463.

(19) Maury, F.; Gueroudij, L.; Vahlas, C. *Surf. Coat. Technol.* **1996**, *86-87*, 316-324.

(20) Carmalt, C. J.; Whaley, S. R.; Lall, P. S.; Cowley, A. H.; Jones, R. A.; McBurnett, B. G.; Ekerdt, J. G. *J. Chem. Soc., Dalton Trans.* **1998**, 553-557.

(21) Winter, C. H.; Sheridan, P. H.; Lewkebandara, T. S.; Heeg, M. J.; Proscia, J. W. *J. Am. Chem. Soc.* **1992**, *114*, 1095-1097.

(22) Fix, R. M.; Gordon, R. G.; Hoffman, D. M. *Chem. Mater.* **1990**, 235-241.

(23) Cundari, T. R.; James M. Morse, J. *Chem. Mater.* **1996**, *8*, 189-196.

(24) Galakhov, M.; Gómez-Sal, P.; Martín, A.; Mena, M.; Yélamos, C. *Eur. J. Inorg. Chem.* **1998**, 1319-1325.

(25) Heaney, P. J.; Prewith, C. T.; Gibbs, G. V., Eds. *Silica: Physical Behaviour, Geochemistry and Materials Applications*; Mineralogical Society of America: Washington, DC, 1994.

(26) Cornils, B.; Herrmann, W. A.; Schlögl, R.; Wong, C.-H., Eds. *Catalysis from A to Z: A Concise Encyclopedia*; Wiley-VCH: Toronto, 2000.

(27) Basset, J.-M.; Lefebvre, F.; Santini, C. *Coord. Chem. Rev.* **1998**, *178-180*, 1703-1723.

(28) Amor Nait Ajjou, J.; Rice, G. L.; Scott, S. L. *J. Am. Chem. Soc.* **1998**, *120*, 13436-13443.

(29) Beaudoin, M. C.; Womiloju, O.; Fu, A.; Nait Ajjou, J. A.; Rice, G. L.; Scott, S. L. *J. Mol. Cat. A: Chem.* **2002**, in Press.

(30) Caulton, K. G.; Hubert-Pfalzgraf, L. G. *Chem. Rev.* **1990**, *90*, 969-995.

(31) Bradley, D. C. *Chem. Rev.* **1989**, *89*, 1317-1322.

(32) Bouh, A. O.; Rice, G. L.; Scott, S. L. *J. Am. Chem. Soc.* **1999**, *121*, 7201-7210.

Chapter 2

Experimental techniques

2.1 Reactants

2.1.1 Silica

Aerosil-200, an amorphous silica produced by Degussa Corporation, is the support used in this study. It is a non-porous, high purity silica (> 99.8% SiO_2), fabricated via the flame pyrolysis of $SiCl_4$, eq 2.1 and 2.2:[1]

$$SiCl_4 + O_2 \rightarrow SiO_2 + 2\ Cl_2 \qquad (2.1)$$

$$2\ H_2O + 2\ Cl_2 \rightarrow 4\ HCl + O_2 \qquad (2.2)$$

It has a BET surface area of (183.1 ± 0.94) m^2/g, with an average primary particle size of 12 nm.

2.1.2 Metal complexes

Titanium-modified silicas were prepared from two different titanium precursors. $Ti(NMe_2)_4$ (99.9%, Alfa-Æsar) was purified of its dimethylamine impurity by evacuation at room temperature. A similar method was used to remove the diethylamine impurity present in $Ti(NEt_2)_4$ (99.99%, Alfa-Æsar). The $Ti(NR_2)_4$ complexes (R = Me, Et) are yellow (Me) or dark yellow (Et), air- and light-sensitive liquids.

Molybdenum-modified silicas were prepared using two different molybdenum precursors, $Mo(NR_2)_4$ (R = Me, Et). Both were synthesized using standard Schlenk techniques according to literature procedures,[2] and purified via sublimation at room temperature and 70°C for R = Me and Et, respectively. Once purified, $Mo(NMe_2)_4$, has the form of dark purple crystals, while $Mo(NEt_2)_4$ is a dark purple oil. Both molybdenum complexes are extremely sensitive to O_2 and moisture, decomposing immediately upon exposure to air.

All metal complexes were stored in Schlenk tubes under vacuum (ca. 10^{-2} Torr).

2.1.3 Liquid reagents

tert-Butylamine (98%, Aldrich) was stored over activated molecular sieves (3 Å). The deuterated alcohols $(CD_3)_2CDOD$ (98%, Aldrich) and $(CD_3)_3COD$ (99%, Aldrich) were dried by shaking in Schlenk tubes over activated molecular sieves, followed by trap-to-trap distillation into Schlenk tubes containing fresh molecular sieves. Before use, each reactant was subjected to three freeze-pump-thaw cycles to remove dissolved gases. Reactant transfers were performed via the vapour phase through a high vacuum manifold using a liquid nitrogen trap.

2.1.4 Gaseous reagents

NH_3 (anhydrous, 99.99% min, Matheson) and ND_3 (99% atom D, Matheson) were used as received and were stored in glass bulbs with high vacuum stopcocks. In order to prevent loss of deuteration, Krytox®, a fluorinated grease produced by Dupont, was used for the stopcock of the storage bulb for ND_3. Oxygen was used as received from Air Products (Ultrapure Carrier Grade)

or Praxair (99.5%, Industrial Grade). DCl (99% atom D, Cambridge Isotopes) was either used as received or stored in a glass bulb. CO_2 (99.98 %, Air Products) was stored in a glass bulb containing fresh molecular sieves. Precise gas pressures were measured with a capacitance manometer.

2.2 Silica preparation

2.2.1 Partial dehydroxylation

In order to ensure reproducible surface chemistry, a standard pre-treatment protocol was used. The temperature to which the silica is heated under vacuum determines the density of hydroxyl groups on the surface. Aerosil silicas partially dehydroxylated at 200 and 500°C contain 2.6 and 1.2 OH/nm^2, respectively.[1] These materials will be denoted as silica-200 and silica-500, respectively, where the appended number indicates the temperature at which the silica was treated prior to exposure to a metal complex. Thus silica-500 was prepared by dehydroxylation for a minimum of 4 hours under dynamic vacuum ($< 10^{-4}$ Torr) at a temperature of 500°C: identical conditions were used for silica-200, except that the temperature used was 200°C.

2.2.2 Deuterium labelling

Exchange of the protons in the surface hydroxyl groups for deuterium was performed following dehydroxylation of the silica at the desired temperature. The cell was flooded with 35 Torr of DCl for 10 minutes, then evacuated. The degree of deuterium enrichment was estimated by

measuring the decrease in intensity of the ν(SiO-H) band at 3747 cm^{-1}. Exchange was considered essentially complete when the peak at 3747 cm^{-1} had decreased in intensity by at least 90%.

2.3 Modification of the silica surface

2.3.1 High vacuum techniques

All experiments were performed using a glass high vacuum system consisting of a high vacuum manifold and a gas manifold. The system is evacuated by a mercury diffusion pump backed by a rotary pump (Edwards). Pressure in the line was monitored by two capacitance manometers with a combined range of 10^{-3} to 1000 Torr. Reactors were connected to the vacuum system via high vacuum stopcocks and spherical joints.

2.3.2 Breakseal techniques

The glass breakseal reactor shown in Figure 2.1 was constructed and its ability to hold static vacuum verified on the high vacuum line. Reactants were introduced into the reactor using a variety of methods. When the reactant is a liquid with low viscosity, as is the case for $Ti(NR_2)_4$ (R = Me, Et), it was transferred into the reactor by syringe under flowing nitrogen. When the reactant is either a liquid of high viscosity (e.g., $Mo(NEt_2)_4$), or a volatile solid which does not pour readily (e.g., $Mo(NMe_2)_4$), the reactor was connected to the Schlenk storage tube containing the reactant via a "U"-shaped tube and sublimed until the desired amount was present in the breakseal reactor. Once filled, the reactor was attached to the vacuum line and any volatile

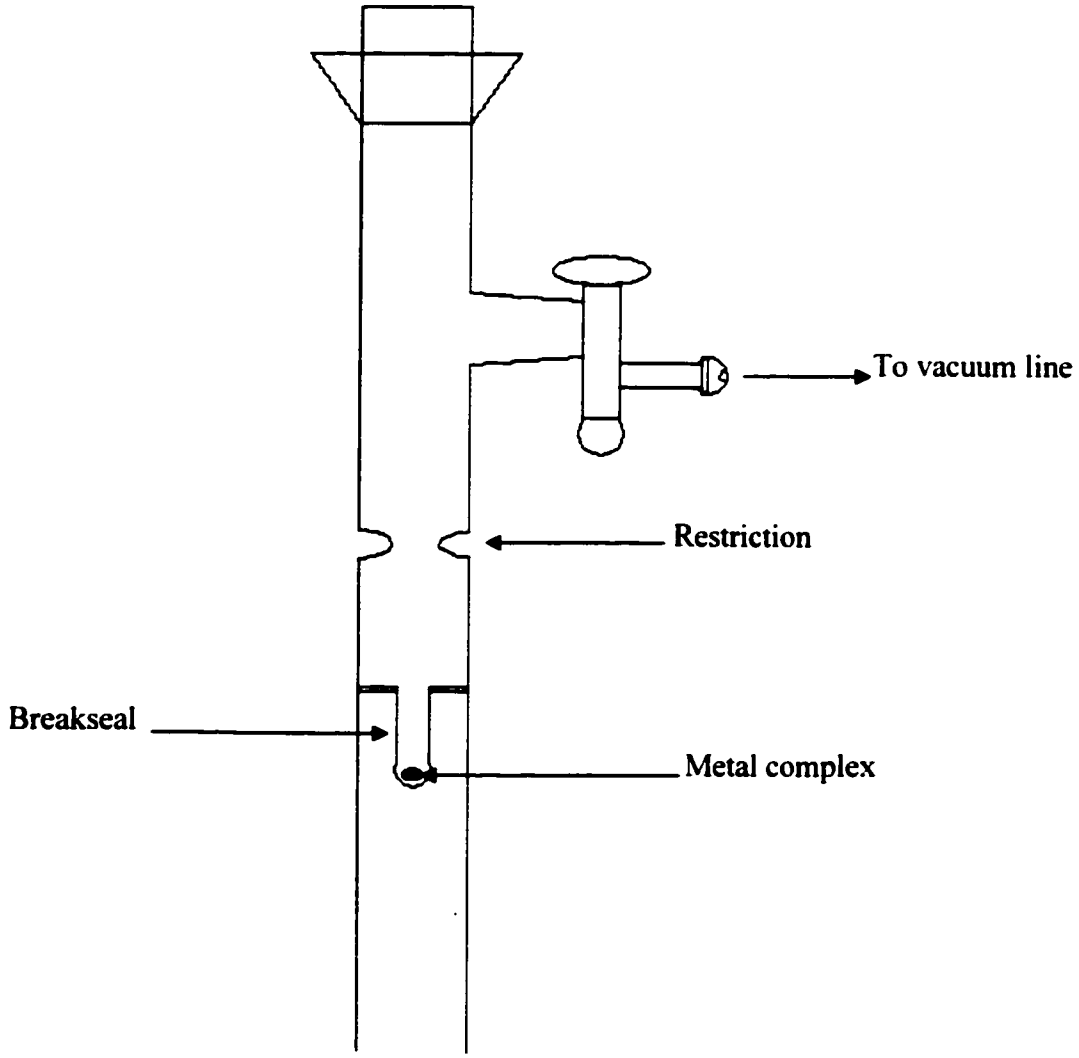

Figure 2.1 Schematic drawing of a breakseal reactor

impurities or decomposition products were removed by evacuation. While under vacuum, with the breakseal immersed in liquid nitrogen, the reactor was sealed off at the level of the restriction. The metal complexes were thus sealed into breakseals under static vacuum (ca. 10^{-4} Torr).

A hammer, typically a short piece of iron sealed inside a glass tube, was inserted into the open end of the breakseal and held in place with a magnet fixed to the outside of the breakseal. A second restriction was then made in the glass between the hammer and the open end of the breakseal to permit later sealing of the breakseal under vacuum. Finally, the open end of the breakseal tube was welded onto to the desired reactor, as depicted in Figures 2.2 (IR) and 2.3 (NMR).

2.3.3 Grafting of metal complexes

After the silica had been thermally treated and allowed to cool to room temperature, the breakseal containing the metal complex was broken using the hammer. To facilitate the reaction between silica pellets and $M(NMe_2)_4$ (M = Ti, Mo), the pellet holder was positioned above the breakseal and the reactant allowed to sublime onto the silica. To accelerate the reaction of silica with less volatile $M(NEt_2)_4$ (M = Ti, Mo), the silica was positioned in the thermal treatment zone of the IR cell where it was plunged in liquid nitrogen. The reactant was allowed to sublime for a period of time determined by its volatility (ca. 2 hrs for $Ti(NEt_2)_4$, ca. 16 hrs for $Mo(NEt_2)_4$). Once sublimation was complete, the liquid nitrogen bath was removed, the silica was allowed to warm up to room temperature and the complex left to react for varying periods of time depending on its reactivity and the metal loading desired.

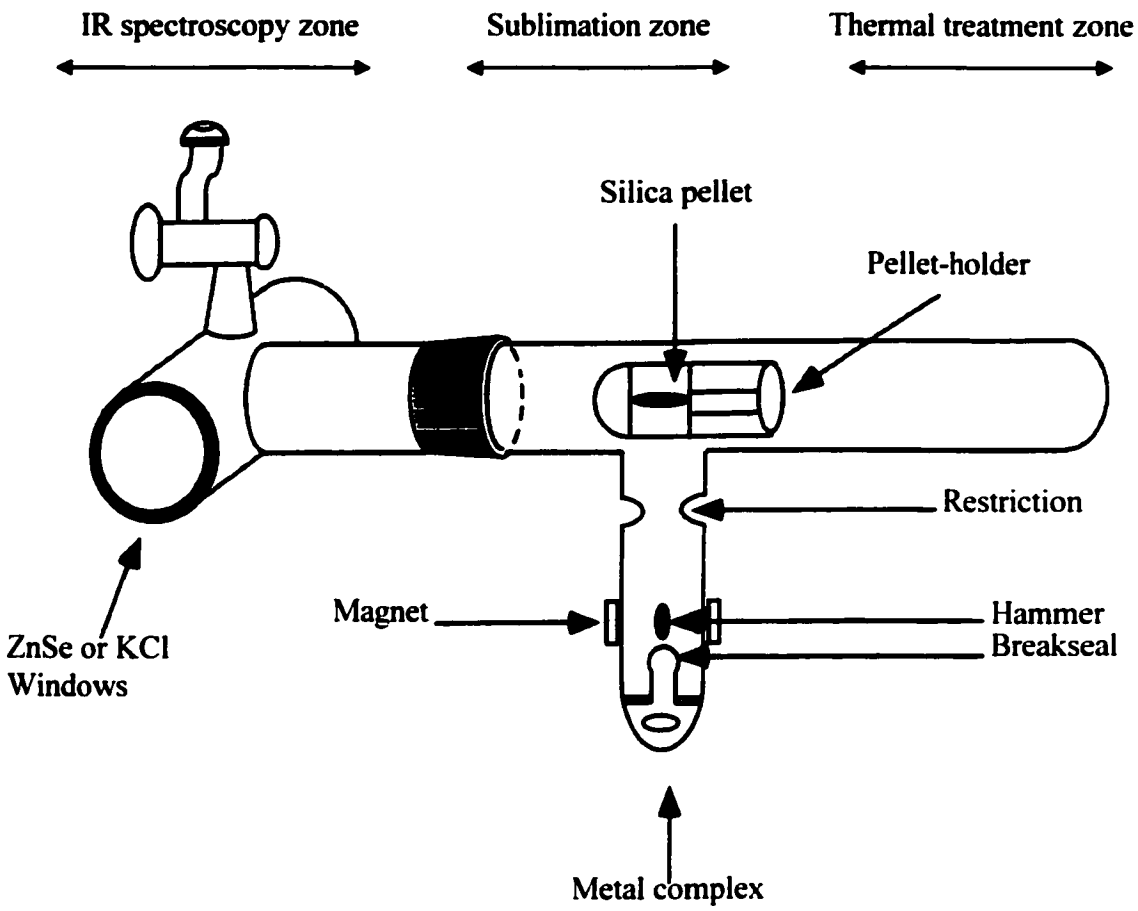

Figure 2.2 Schematic drawing of an infrared cell

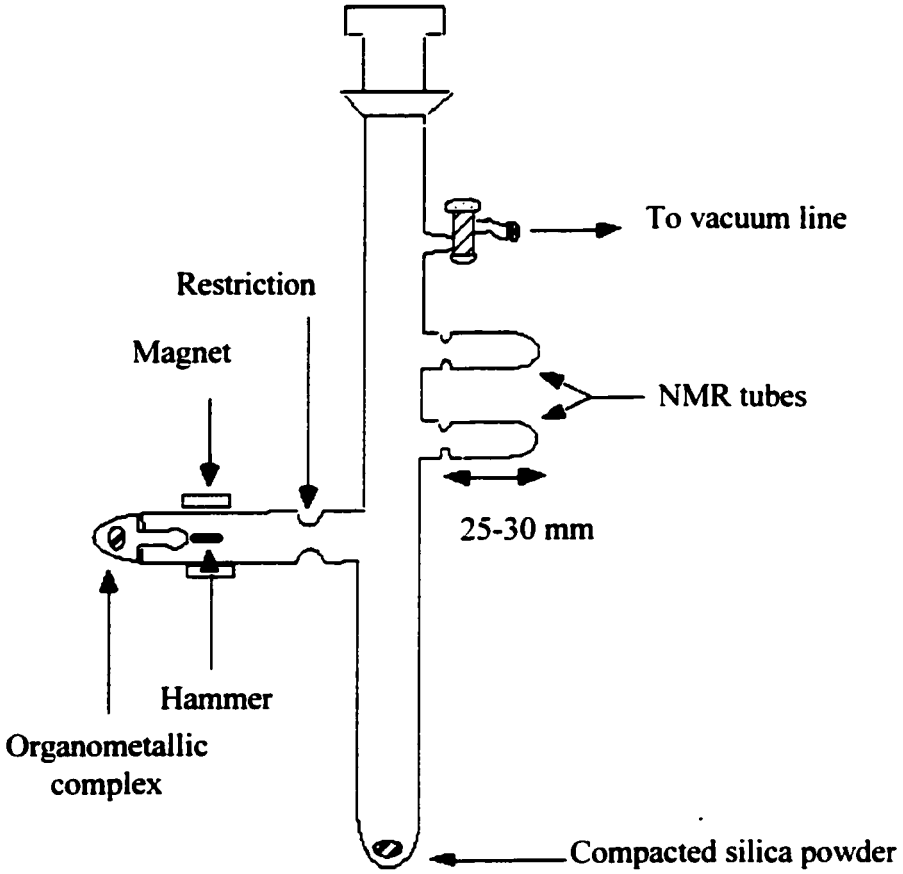

Figure 2.3 Schematic drawing of an NMR reactor

Unreacted metal complex was subsequently desorbed into the breakseal sidearm using a liquid nitrogen trap. In general, desorption was conducted for at least the same period of time as the sublimation. Finally, the breakseal was sealed off under vacuum at the restriction, isolating the modified silica and allowing further manipulations to take place in the absence of ungrafted metal complex.

2.4 Characterization of modified silicas

2.4.1 Infrared spectroscopy

Infrared spectroscopy experiments were performed *in situ* in specially designed IR cells. Figure 2.2, with a volume of ca. 300 mL. They are equipped with windows, either KCl or CaF_2, which are transparent to infrared radiation and are attached to the IR cell using TorrSeal (Varian). These cells are capable of holding a static vacuum ($<10^{-4}$ Torr) for several days.

Transmission IR spectra were recorded on a Mattson Research Series FTIR equipped with a DTGS detector. The sample compartment was purged with dry air, from which both carbon dioxide and water vapour has been removed. 32 scans at 2 cm^{-1} resolution were averaged for both background and sample spectra.

2.4.1.1 Infrared spectra of silica pellets

Between 5 and 25 mg of silica were pressed at a pressure of ca. 125 kg/m^2 into a pellet 1.6 cm in diameter. The pellets were then placed in a sample holder which was inserted into an infrared

cell, Figure 2.2. The sample holder was first positioned in the thermal treatment zone, where calcination and dehydroxylation treatments were performed. After cooling, IR spectra were recorded of both the silica pellet, Figure 2.4, and the windows, Figure 2.5. Next the pellet was exposed to the metal complex, as described above. The progress of the reaction was followed by recording spectra at various stages of the experiment. These spectra were obtained by sliding the sample holder into the head of the IR cell, and aligning it such that the silica pellet was parallel to the windows, i.e., perpendicular to the infrared beam. Spectra of gas phase products were obtained by sliding the sample holder back while ensuring that the IR beam continued to pass through the cell windows.

2.4.1.2 Kinetic studies

In experiments which required spectra to be recorded continuously while the sample was held under dynamic vacuum, a slightly modified cell was used. The stopcock was located below the taper joint, just above the breakseal, remaining outside the sample compartment of the IR spectrometer. The IR cell could then be connected to the high vacuum manifold via flexible Polyflo tubing. Through the use of the macro-writing software provided with the WinFIRST™ program, it was possible to automate the acquisition of spectra and derive time-resolved spectral information (e.g., peak area or intensity).

To observe kinetics of reactions with ammonia, approximately 30 Torr of dry anhydrous ammonia was added to the IR cell and immediately condensed into a sidearm using a liquid nitrogen bath. Keeping the ammonia frozen, the IR cell was moved to the IR spectrometer and aligned so that the beam sampled the supported metal complex. A spectrum was taken, then the

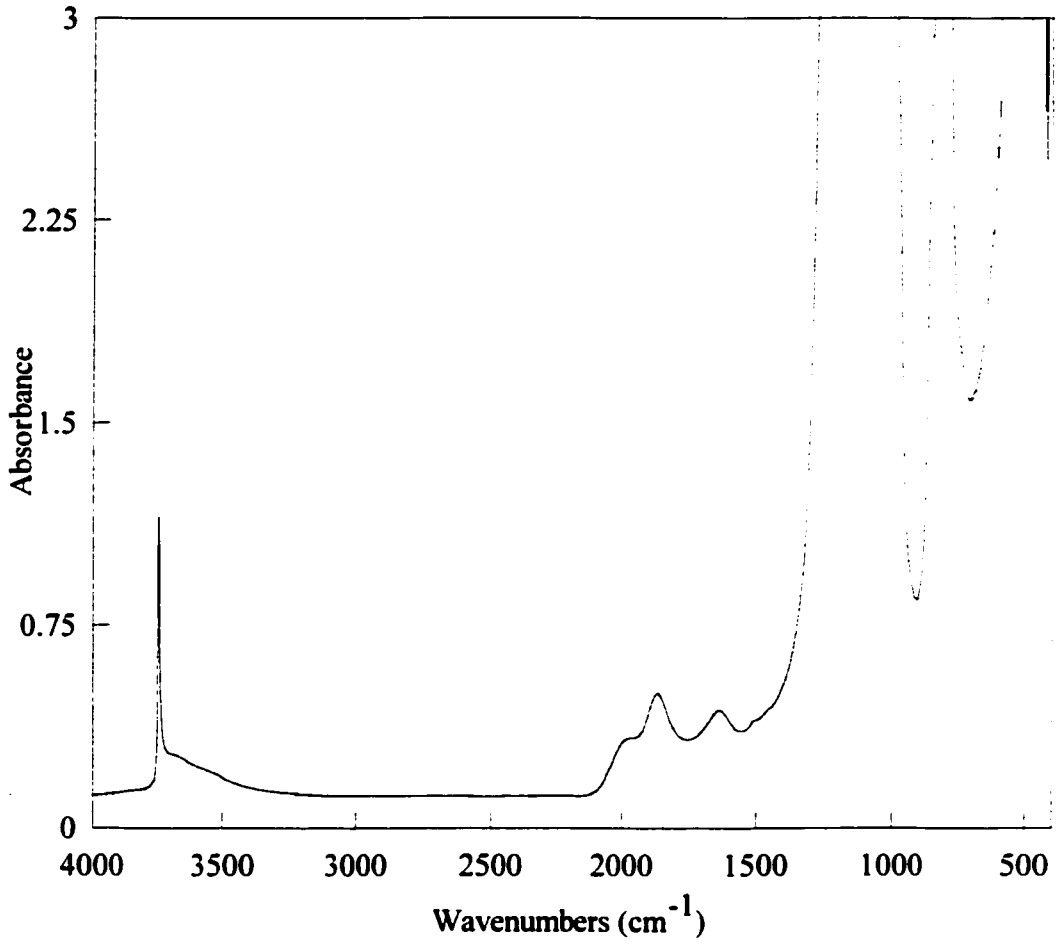

Figure 2.4 Infrared spectrum of a silica pellet partially dehydroxylated at 200 °C, recorded in an IR cell equipped with KCl windows.

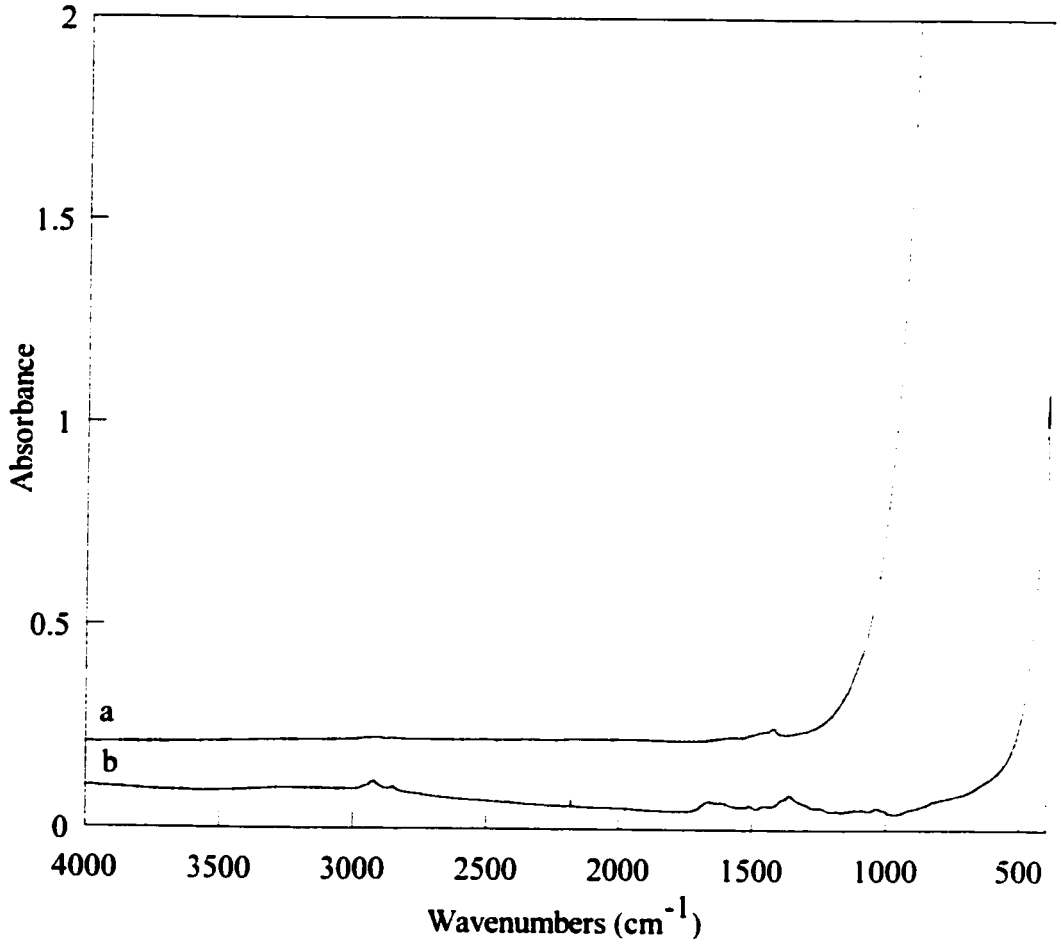

Figure 2.5 Infrared spectra of (a) CaF_2; and (b) KCl windows, showing regions of transparency to IR radiation.

cold bath was removed, the sidearm immersed in room temperature water and the transformation on the silica surface monitored.

2.4.2 Solid state NMR spectroscopy

For NMR experiments, the silica was first compacted in the form of thick pellets (50-60 mg) which were ground to a fine powder in a mortar. The resulting compacted silica was placed in a modified Schlenk reactor equipped with a high vacuum stopcock, as well as one or more pyrex NMR tubes (5 mm x 30 mm) glassblown onto the body of the reactor at 90° angles.

After dehydroxylation of the compacted silica and subsequent cooling to room temperature, the silica was modified with a metal complex according to procedures previously described for silica pellets. Without breaking vacuum, 50-75 mg of the modified silica was then poured into one of the NMR tubes, which was flame-sealed to give a sealed sample tube of length less than 30 mm. ^{13}C spectra were recorded using CP/MAS (Cross- Polarization/Magic-Angle-Spinning) techniques on a Bruker ASX-200 spectrometer. Spectra were accumulated using 4.4 μsec 90° proton pulses with a 2 msec contact time and 2 sec relaxation delay.

2.4.3 Diffuse-reflectance UV-visible spectroscopy (DRUV-Vis)

The techniques used for the preparation of DRUV-Vis samples were similar to those used in the preparation of NMR samples. However, instead of transferring the sample into an NMR tube, the sample was poured into a rectangular 2 x 5 mm quartz tube, sealed onto the pyrex reactor via a quartz-pyrex graded seal. Once filled, they were sealed off at a restriction situated between the

graded seal and the main body of the reactor. Spectra were recorded on a Cary 100 spectrophotometer (Varian) fitted with a diffuse-reflectance accessory referenced to a PTFE disk.[3]

2.4.4 Elemental analysis

2.4.4.1 Titanium

The amount of chemisorbed titanium was determined at the end of each experiment. Quantitative extraction of the titanium was achieved by adding a sample of modified silica to a mixture of 3 mL 3.6 M H_2SO_4 and 0.3 mL H_2O_2 (30 % w/w aqueous solution) to form the yellow peroxo titanium complex.[4,5] After stirring for ca. 45 minutes, the sample was made up to 10 mL with 3.6 M H_2SO_4 and filtered to remove suspended silica particles. UV-visible spectra were recorded in 10 mm square quartz cuvettes on a Cary 100 spectrophotometer (Varian). The blank was a solution containing all components except Ti.

The absorbance at λ_{max} 408 nm was converted into Ti concentration using a calibration curve, Figure 2.6, prepared with a titanium standard solution, 1.000 g Ti/L (Aldrich).

2.4.4.2 Molybdenum

The amount of chemisorbed molybdenum was determined at the end of each experiment. Quantitative extraction was achieved by stirring each sample of modified silica in 4 mL 1:3 HCl:HNO_3 solution at room temperature for 45 minutes, then boiling for 45 minutes. After

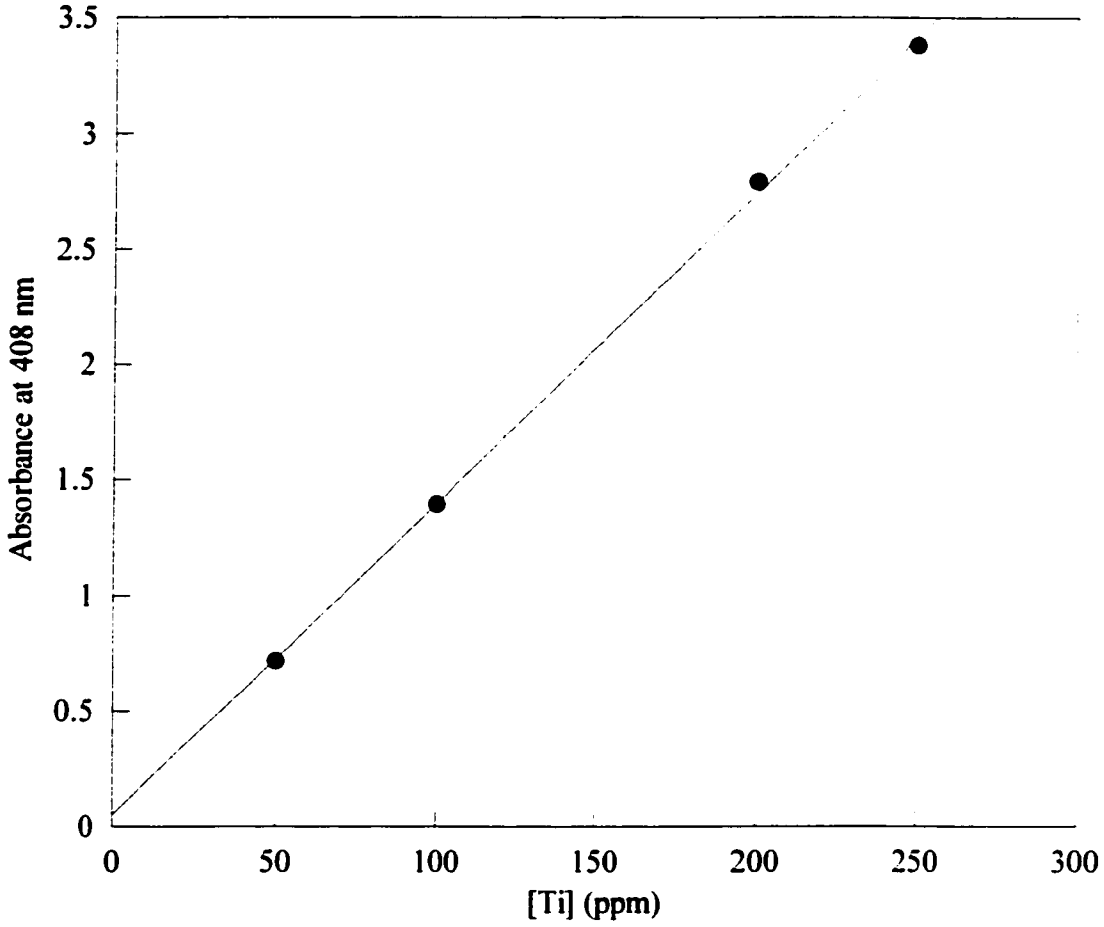

	Abs= m*[Ti] + b
m	0.0134 ± 0.0003
b	0.054 ± 0.046
Chisq	0.0036173
R	0.9996

Figure 2.6 UV-Vis calibration curve for titanium (pathlength 1 cm).

cooling, the solution was diluted to 25 mL with water, followed by filtration to remove suspended silica. ICP analysis of Mo was performed on a Thermo Jarrell Ash Atom Scan 25. The amount of molybdenum was determined by comparing the absorbance at 202.030 nm against a one-point calibration curve prepared using a standard containing 100 ppm Mo in 5% HNO_3.

2.5 Identification and quantitation of volatile products

2.5.1 By gas phase infrared spectroscopy

By comparing the infrared spectrum of a volatile product produced during grafting on the silica surface with the spectrum of a pure compound, it may be possible to identify it. However, IR analysis was always confirmed by GC (see below). When a single product was present, it was also possible to quantify it by IR spectroscopy. In order to do so, a calibration curve was prepared using the pure gas, with either integration of a spectral region or measurement of the peak absorbance as a function of pressure.

To prepare each calibration curve, a known pressure of gas was introduced into the IR cell of pathlength 7 cm. An infrared spectrum was recorded with a resolution of 2 cm^{-1}. This procedure was repeated at various pressures covering the range expected for products of the surface reactions. IR calibration curves were generated in this way for $HNEt_2$, $HNMe_2$ and C_2H_4. Figures 2.6-2.8. For CO_2, a previously prepared calibration curve was used, where I is the integrated absorbance from 2500 – 2000 cm^{-1} and P is the pressure in Torr. The equation of the curve is shown in eq 2.3:

$$I = 0.908P - 14.749 \quad (2.3)$$

2.5.2 By GC and GC/MS

By comparing the retention time and mass spectrum of volatile products of surface reactions with those of the pure compounds, it is possible to conclusively identify them. Gases present in the reactors were first condensed into Schlenk tubes equipped with a rubber septum. 1 mL of the gas phase was sampled using a gas-tight syringe. GC analysis was performed on an HP 5730A Gas Chromatograph with a Carbopack column designed for amine separation and an FID detector. Samples were run isothermal at 50°C using N_2 as a carrier gas. GC/MS analysis was performed on a combination HP 5973 Mass Selective Detector/6890 Series Gas Chromatograph using a PLOT column at 50°C with He as a carrier gas.

In experiments where the IR extinction coefficient of a product was low or the presence of another gaseous product precluded IR quantitation, analysis was performed by GC. A GC calibration curve was produced for C_2H_4, Figure 2.9, where A is the area under the peak, and P is the pressure in Torr. For $HNMe_2$, a previously prepared calibration curve was used, where A is the area under the peak and n is the quantity injected in μmoles. The equation is shown in eq 2.4.

$$A = (9.7618 \times 10^6)n + 600 \quad (2.4)$$

A known pressure of the gas was introduced into a Schlenk tube of known volume equipped with a rubber septum. 0.2 mL of the gas was sampled with a gas-tight syringe and injected into

the GC. This procedure was repeated at various pressures covering the range expected for products of the surface reactions.

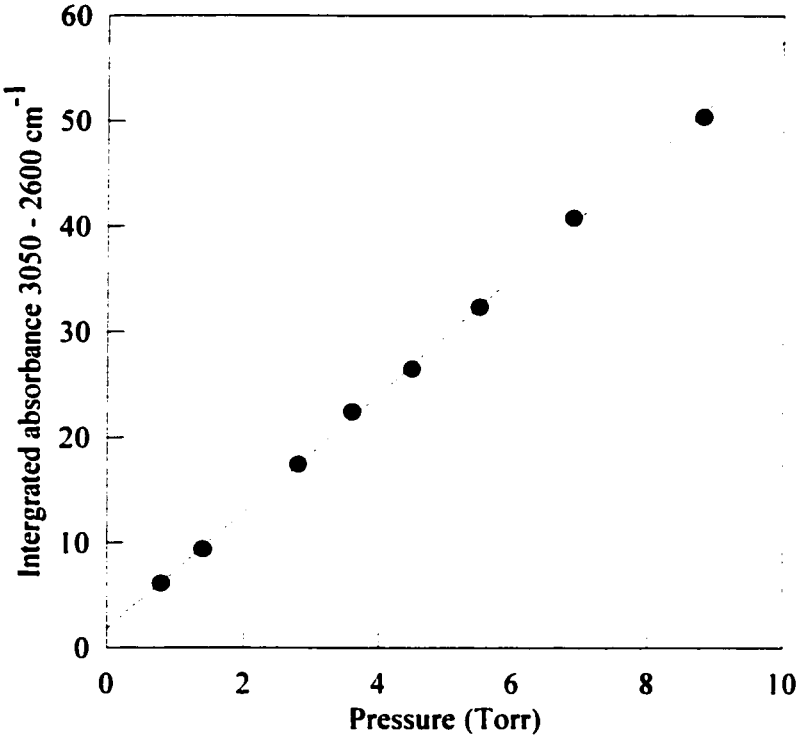

	Abs= m*P + b
m	5.57 ± 0.06
b	1.9 ± 0.3
Chisq	1.0702
R	0.99967

Figure 2.7 IR calibration curve for $HNEt_2$..

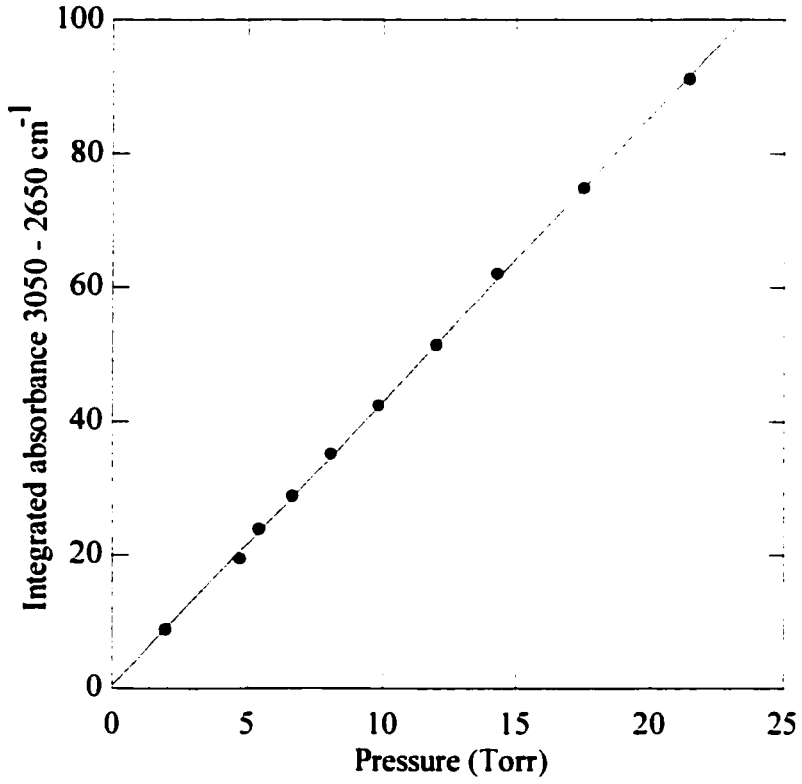

	Abs= m*P + b
m	4.25 ± 0.03
b	0.6 ± 0.4
Chisq	2.697
R	0.99978

Figure 2.8 IR calibration curve for $HNMe_2$.

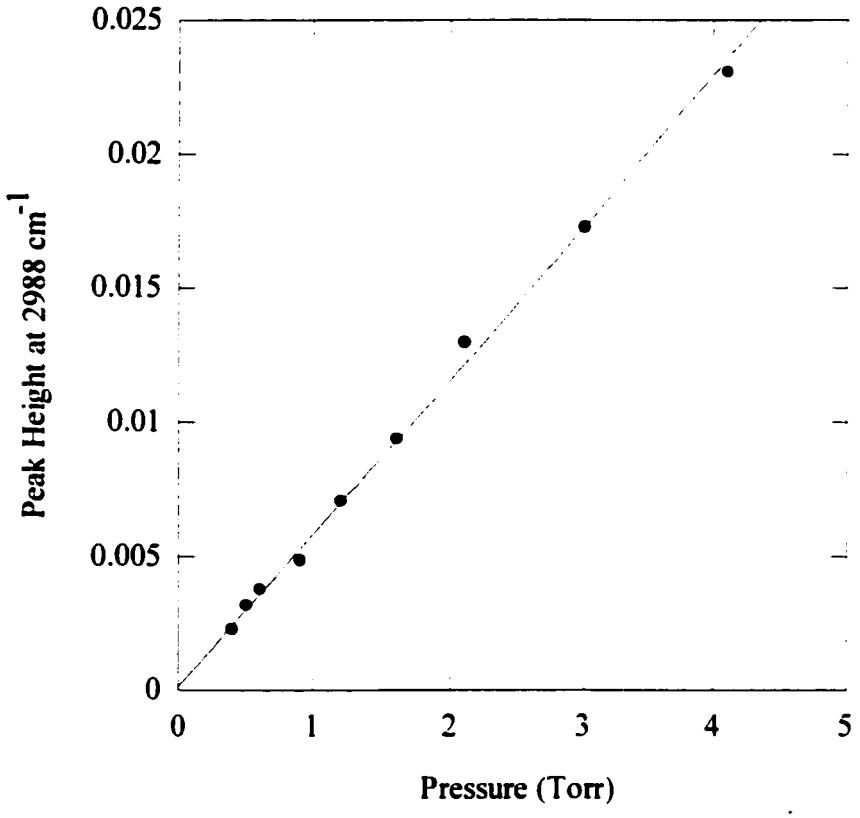

	Height= m*P + b
m	0.0057 ± 0.0001
b	0.0002 ± 0.0002
Chisq	1.4328×10^{-6}
R	0.99854

Figure 2.9 IR calibration curve for C_2H_4

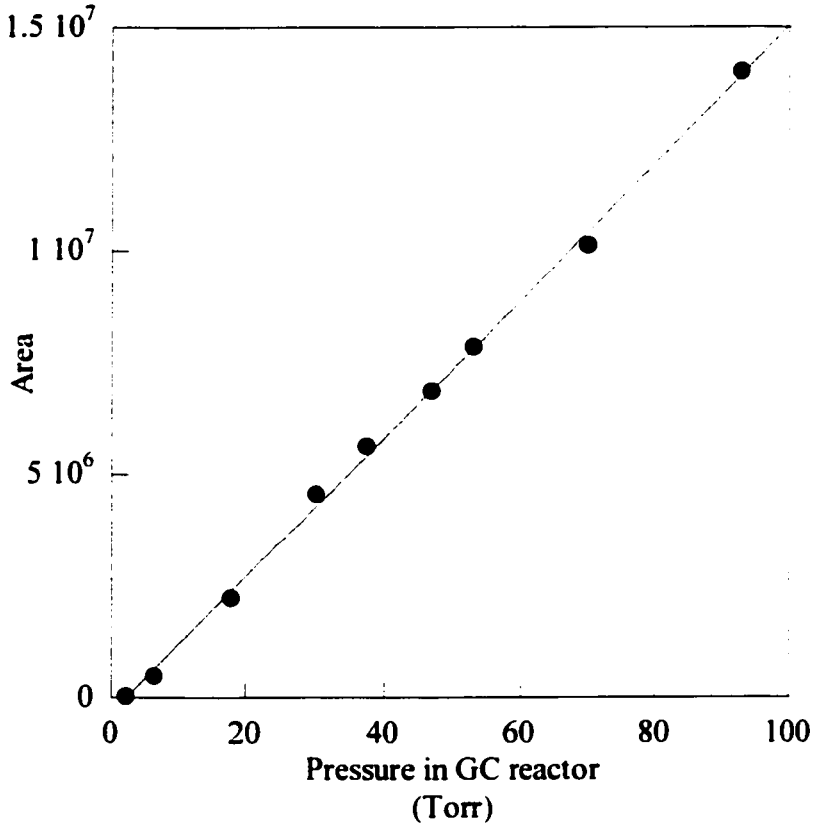

A = m*P + b	
m	(152 ± 2) x 10^3
b	(-2.4 ± 1.0) x 10^5
Chisq	3.5884 x 10^{11}
R	0.99909

Figure 2.10 GC calibration curve for C_2H_4

2.6 References

(1) Heaney, P. J.; Prewith, C. T.; Gibbs, G. V., Eds. *Silica: Physical Behaviour, Geochemistry and Materials Applications*; Mineralogical Society of America: Washington, DC, 1994.

(2) Bradley, D. C.; Chisholm, M. H. *J. Chem. Soc (A)* **1971**, 2741-2744.

(3) Amor Nait Ajjou, J.; Scott, S. L. *Organometallics* **1997**, *16*, 86-92.

(4) Haukka, S.; Saastamoinen, A. *Analyst* **1992**, *117*, 1381-1384.

(5) Vogel, A. J. *A Textbook of Quantitative Inorganic Analysis*; Longman: London, 1961.

Chapter 3

Nature of the initial chemisorption of $Ti(NR_2)_4$ on silica

3.1 Introduction

Transition metal complexes with many different kinds of ligands (e.g., $Ti(O^iPr)_4$,[1] $Cr(CH_2CMe_3)_4$,[2] $V(CH_2SiMe_3)_4$,[3] $VOCl_3$,[4] $Sn(^nC_4H_9)_4$,[5] $Re(\equiv C^tBu)(=CH^tBu)(CH_2^tBu)_2$)[6] have been shown to react with silica at the surface hydroxyl groups which terminate its surface. These reactions generally occur via electrophilic attack of the protons associated with the hydroxyl groups on the donor atoms of one or more ligands. eq 3.1.

$$n \equiv SiOH + ML_x \rightarrow (\equiv SiO)_nML_{x-n} + n\,HL \qquad (3.1)$$

Ideally, the product HL has little or no affinity for the silica surface under mild reaction conditions, such that the grafted metal complex is obtained in high yield without interference from side-reactions of HL.

The analogous grafting reactions of homoleptic metal amide complexes on silica have not been extensively investigated. Similar reactivity towards silica "silanols" is expected, based on precedents in molecular chemistry in the reactions between metal amides and alcohols or molecular silanols,[7] eq 3.2.

$$M(NR_2)_4 + 4\,R'OH \rightarrow M(OR')_4 + 4\,HNR_2 \qquad (3.2)$$

M = Ti, R = Me, Et, ^{n}Pr, ^{i}Bu; M = Zr, R = Me, Et; R' = ^{n}Bu, $SiEt_3$

Bouh *et al* examined the reactivity of $Ti(NEt_2)_4$ with partially dehydroxylated Aerosil-200, and found irreversible grafting occurred, giving tris- and bis(diethylamido)titanium(IV) surface fragments on silicas dehydroxylated at 500 and 200°C, respectively, eq 3.3.[1]

$$n \equiv SiOH + Ti(NEt_2)_4 \rightarrow (\equiv SiO)_nTi(NEt_2)_{4-n} + n\ HNEt_2 \qquad (n = 1, 2) \qquad (3.3)$$

Anwander *et al.* reported the reactions of silylamido complexes of the lanthanides (Sm, Y, Nd) towards MCM-41, eq 3.4.[8]

$$6 \equiv SiOH + Nd(N(SiMe_3)_2)_3 \rightarrow 4 \equiv SiOSiMe_3 + (\equiv SiO)_2NdN(SiMe_3)_2 + NH_3 \qquad (3.4)$$

The metal-amide bond undergoes electrophilic attack by the silanol group, resulting in the loss of amine, and the formation of a metal-oxygen bond.[8-11]

Alcoholysis reactions of metal amides are controlled by both steric and electronic effects. For a homologous series $M(NR_2)_4$, the most reactive complex is the one containing the least electronegative metal. Steric effects are particularly important in compounds where the central metal atom is small and/or in a high coordination state. For example, the rate of alcoholysis of $W(NMe_2)_6$ follows the order MeOH > EtOH > PrOH >> ^{t}BuOH, while Me_3CCH_2OH and Et_3SiOH do not react at all at room temperature.[12] In some instances, the metal changes oxidation state, such as when Nb(IV) amides are oxidized to Nb(V) alkoxides upon reaction with excess alcohols or Et_3SiOH.[12] In addition, some amine may remain coordinated to the metal, eq 3.5.

$$[Ti(NMe_2)_3]_2 + 4\ PhOH \rightarrow [Ti(OPh)_4(HNMe_2)] + \text{"}Ti^{II}\text{"} \qquad (3.5)$$

In order to establish the nature of the reaction between metal amide complexes and silica, an important question to address is the stoichiometry of the grafting reaction, since a given transition metal complex may interact with just one or more than one surface hydroxyl group. For example, depending on the degree of dehydroxylation of the silica, the homoleptic alkyl complexes CrR_4 may react with either one or two hydroxyl groups,[2] according to eq 3.6.

$$CrR_4 + n\ \equiv SiOH \rightarrow (\equiv SiO)_nCrR_{4-n} + n\ RH \qquad (3.6)$$

$$n = 1, 2$$

In contrast, $VOCl_3$ and $VO(O^iPr)_3$ always react with only one hydroxyl group on the silica surface, regardless of the degree of surface dehydroxylation,[4] eq 3.7.

$$VOX_3 + \equiv SiOH \rightarrow \equiv SiOVOX_2 + HX \qquad (3.7)$$

$$X = Cl, O^iPr$$

Finally, the reaction between $Ti(O^iPr)_4$ and silica hydroxyls occurs with either 2:1 or 2:2 stoichiometry, eq 3.8-3.9, resulting in the exclusive formation of dinuclear surface complexes.[1]

$$2\ Ti(O^iPr)_4 + 2\ \equiv SiOH \rightarrow [(\equiv SiO)Ti(O^iPr)_2]_2(O) + 3\ ^iPrOH + C_3H_6 \qquad (3.8)$$

silica-200

$$2\ Ti(O^iPr)_4 + \equiv SiOH \rightarrow (\equiv SiO)Ti_2(O^iPr)_5(O) + 2\ ^iPrOH + C_3H_6 \qquad (3.9)$$

silica-500

In each of the examples cited above, the grafting reaction is unique. That is, regardless of the stoichiometry with respect to the surface hydroxyls (2:1, 1:1, 1:2 or 2:2), a single supported metal complex is formed on a given silica surface. In this chapter, the stoichiometry of grafting of $Ti(NR_2)_4$ on silica surfaces will be established, and the nature of the resulting supported metal complexes investigated.

3.2 Stoichiometry of grafting of $Ti(NR_2)_4$ on silica-500

Exposure of silica pretreated at 500°C (silica-500) to an excess of $Ti(NR_2)_4$ vapour (R = Me (**1**), Et (**2**)) in an sealed reactor (base pressure < 10^{-4} Torr) results in an irreversible chemisorption of the metal complex onto the surface. The silica, initially colourless, acquires a yellow colour over the course of the reaction (ca. 20 min and 2 hours for $Ti(NMe_2)_4$ and $Ti(NEt_2)_4$, respectively), while volatiles are released into the gas phase. After unreacted $Ti(NR_2)_4$ was removed via desorption into a liquid nitrogen cold trap, the amount of chemisorbed Ti was measured to be (2.00 ± 0.04) and (1.95 ± 0.07) wt. % for grafting of **1** and **2**, respectively. These values are highly reproducible, Table 3.1. In each case, the amount of chemisorbed Ti corresponds to 1.0 Ti/≡SiOH and a surface coverage of 1.25 Ti/nm^2.

Table 3.1 Titanium content of silica-500 modified through exposure to $Ti(NR_2)_4$ (R = Me, Et) after complete consumption of surface hydroxyl groups, and quantification of volatile organics released during grafting.

Complex	Wt. % Ti	Ti[a] mmol / g	HNR_2[a] mmol / g	Ti / ≡SiOH [b]	HNR_2 / Ti
$Ti(NMe_2)_4$	1.95	0.41	0.40	1.02	0.98
1	2.03	0.42	0.43	1.06	1.01
	2.02	0.42	0.42	1.05	1.00
Avg.	2.00 ± 0.04	0.42 ± 0.01	0.42 ±0.02	1.04 ± 0.02	1.00 ± 0.02
$Ti(NEt_2)_4$	1.90	0.40	0.41	0.99	1.03
2	1.85	0.39	0.40	0.97	1.04
	2.05	0.43	0.44	1.07	1.03
	2.01	0.42	0.41	1.05	0.98
	1.99	0.42	0.40	1.04	0.96
	1.89	0.39	0.35	0.99	0.89
	2.03	0.42	0.40	1.06	0.97
	1.95	0.41	0.43	1.02	1.06
	1.91	0.40	0.39	1.00	0.98
Avg.	1.95 ± 0.07	0.41 ± 0.01	0.40 ± 0.03	1.02 ± 0.04	0.99 ± 0.05

[a] Values normalized per g of silica.

[b] Based on a hydroxyl content of (0.40 ± 0.02) mmol / g.[4]

During grafting of **1** and **2**, the sole gas phase product is the corresponding amine HNR_2, identified by GC and GC/MS. The amount of amine released during the reaction between $Ti(NR_2)_4$ and silica was quantified by *in situ* gas phase IR spectroscopy and is reproducible, Table 3.1, regardless of the quantity of silica used provided the titanium complex is in excess. It corresponds to 1.0 HNR_2 / Ti. Thus, the stoichiometry of the grafting reactions on silica-500 can be written as in eq 3.10:

$$\equiv SiOH + Ti(NR_2)_4 \rightarrow (\equiv SiO)Ti(NR_2)_3 + HNR_2 \qquad (3.10)$$

1, 2 **3, 4**

R = Me (**1**, **3**), Et (**2**, **4**)

This 1:1 stoichiometry implies that the OH groups terminating the surface of silica-500 are isolated and capable of reacting with only one titanium complex each.

3.3 Stoichiometry of grafting of $Ti(NR_2)_4$ on silica-200

Exposure of silica pretreated at 200°C (silica-200) to the vapour of **1** or **2** also results in irreversible chemisorption of the titanium amide complex. The colour change is identical to that on silica-500, from colourless or white to yellow, and volatile organics are again released into the gas phase. Once the reaction was complete and the excess $Ti(NR_2)_4$ removed to a liquid nitrogen cold trap, the titanium content was determined to be (1.93 ± 0.04) wt % Ti for **1** and (1.93 ± 0.07) wt % Ti for **2**, Table 3.2. These values are highly

Table 3.2 Titanium content of silica-200 modified through exposure to $Ti(NR_2)_4$ (R = Me, Et) after complete consumption of surface hydroxyl groups, and quantification of volatile organics released during grafting.

Complex	Wt. % Ti	Ti [a] mmol / g	HNR_2 [a] mmol / g	Ti / ≡SiOH [b]	HNR_2 / Ti
$Ti(NMe_2)_4$	1.95	0.41	0.80	0.47	1.96
1	2.02	0.42	0.85	0.49	2.01
	1.89	0.39	0.76	0.46	1.96
	2.05	0.43	0.88	0.50	1.99
	2.10	0.44	0.88	0.51	2.01
	1.90	0.40	0.81	0.46	2.04
	1.95	0.41	0.81	0.47	1.96
	2.03	0.42	0.81	0.49	1.91
	2.04	0.43	0.85	0.50	2.00
	2.00	0.42	0.79	0.49	1.89
	1.99	0.42	0.78	0.48	1.88
	1.86	0.39	0.80	0.45	2.06
	1.87	0.39	0.79	0.45	2.02
Avg.	1.97 ± 0.08	0.41 ± 0.02	0.81 ± 0.03	0.48 ± 0.02	1.97 ± 0.06
$Ti(NEt_2)_4$	1.98	0.41	0.82	0.48	1.98
2	2.01	0.42	0.85	0.49	2.02
	1.89	0.39	0.80	0.46	2.03
	1.85	0.39	0.76	0.45	1.97
	1.90	0.40	0.78	0.46	1.97
Avg.	1.93 ± 0.07	0.40 ± 0.01	0.80 ± 0.03	0.47 ± 0.02	1.99 ± 0.03

[a] Values normalized per g of silica.

[b] Based on a hydroxyl content of (0.86 ± 0.02) mmol / g.[4]

reproducible and correspond to 0.5 Ti/≡SiOH. As in the reaction with silica-500, the sole gas phase products are the corresponding amines, $HNMe_2$ and $HNEt_2$, identified by GC and GC/MS. The quantity of amine released is also reproducible, Table 3.2, and amounts to 2.0 HNR_2/Ti. Thus, the stoichiometry of grafting of $Ti(NR_2)_4$ onto silica-200 can be written as in eq. 3.11:

$$2\ \equiv SiOH + Ti(NR_2)_4 \rightarrow (\equiv SiO)_2Ti(NR_2)_2 + 2\ HNR_2 \qquad (3.11)$$

1, 2 **5, 6**

R = Me (**1**, **5**), Et (**2**, **6**)

Calcination of the resulting solid material at 800°C in O_2 yielded 4.1 CO_2 / Ti for **5** and 7.9 CO_2 / Ti for **6**. This 2:1 grafting stoichiometry implies that the OH groups terminating the surface of silica-200 exist in close proximity and react preferentially in pair-wise fashion with the amide complexes.

3.4 Infrared characterization of Ti-modified silicas

Upon reaction of **1** and **2** with either silica-500 or -200, the intense ν(SiO-H) mode of silica, located at 3747 cm^{-1}, disappears, Figures 3.1 and 3.2. At the same time, new bands appear. The high frequency modes consist of bands in the C-H stretching and deformation regions. Qualitatively, the spectra of **3** and **4** ($Ti(NR_2)_4$ grafted on silica-500) are very similar to the spectra of **5** and **6** ($Ti(NR_2)_4$ grafted on silica-200).

All but one of the peaks present in IR spectra of $(\equiv SiO)_nTi(NEt_2)_{4-n}$ are readily assigned to vibrations of the diethylamido ligands. The four peaks in the ν(C-H) region consist of

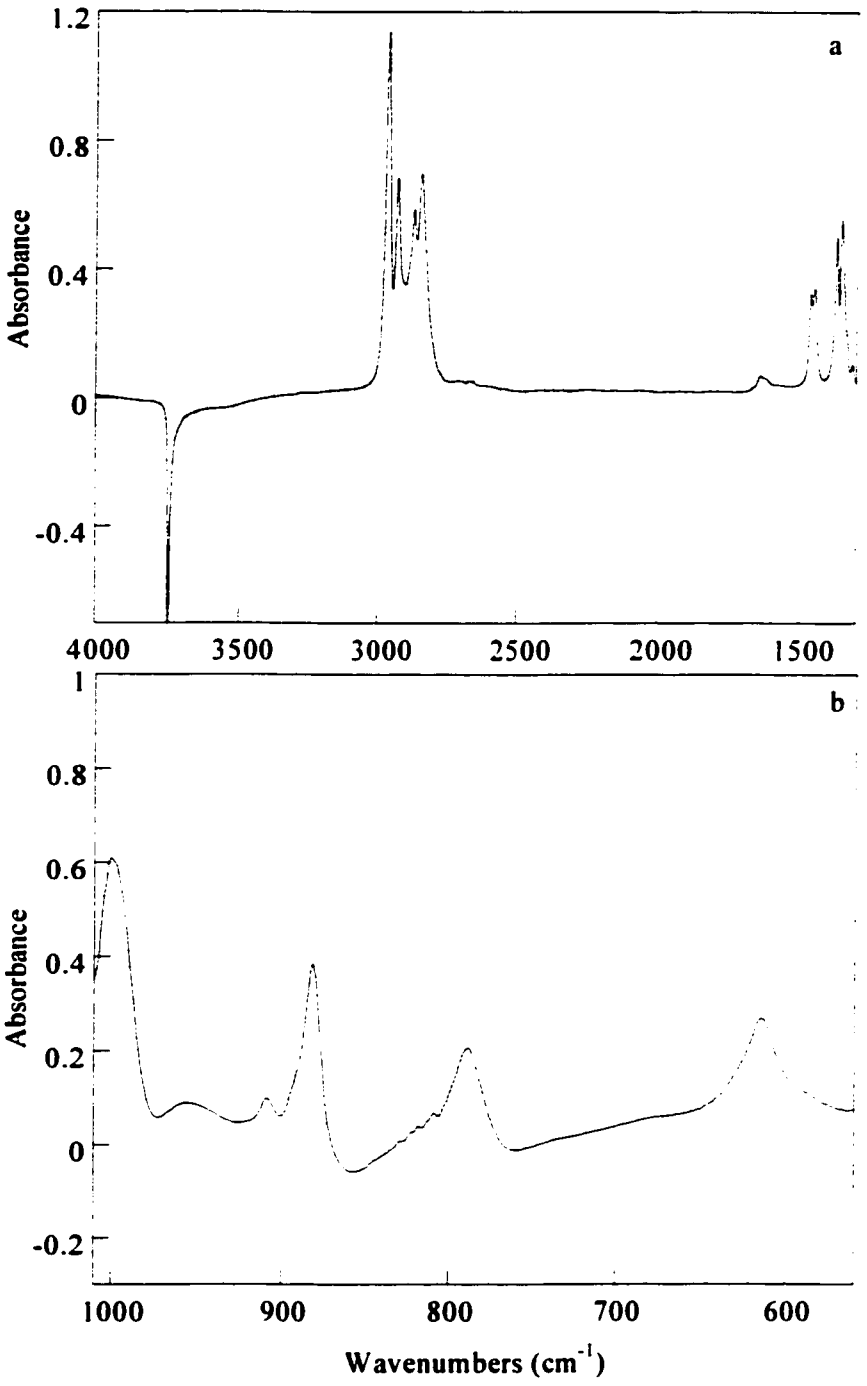

Figure 3.1 *In situ* IR difference spectra of two regions of partial transparency of a self-supporting silica pellet after grafting of $Ti(NEt_2)_4$, **2**, onto silica-200. Excess **2** has been desorbed and the volatiles removed. A reference spectrum of silica-200 has been subtracted, thus negative peaks signify modes that disappear upon reaction.

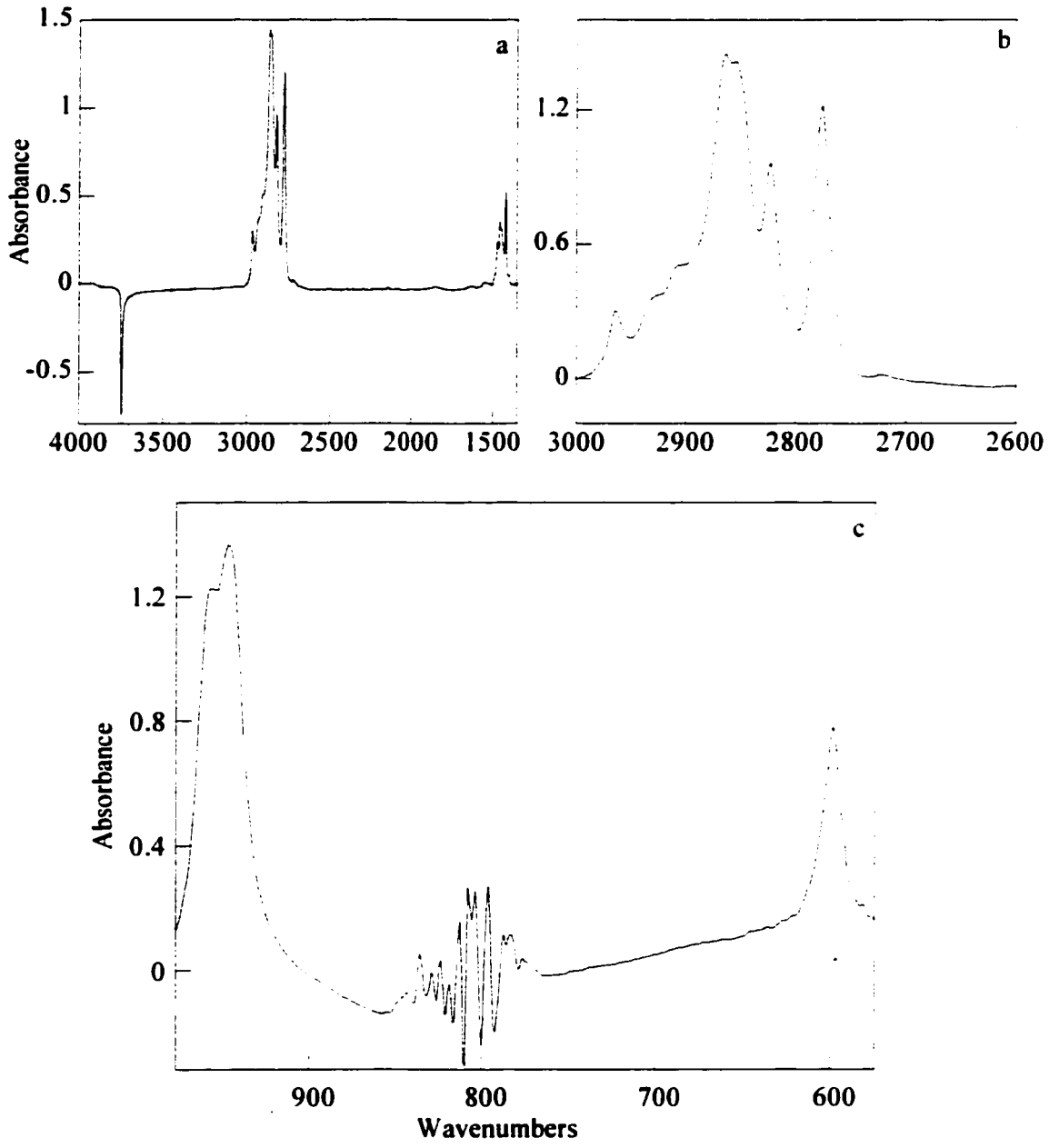

Figure 3.2 *In situ* IR difference spectra of two regions of partial transparency of a self-supporting silica pellet after grafting of $Ti(NMe_2)_4$, **1**, onto silica-200, including an expansion of the unusual ν(C-H) region. Excess **1** has been desorbed and the volatiles removed. A reference spectrum of silica-200 has been subtracted, thus negative peaks signify modes that disappeared upon reaction.

asymmetric (2973, 2937 cm^{-1}) and symmetric (2880, 2848 cm^{-1}) C-H stretching vibrations of CH_3 and CH_2 groups. The symmetric and asymmetric deformations of the CH_3 groups appear at 1373 and 1448 cm^{-1},[13] while the CH_2 deformation is observed at 1464 cm^{-1}.[13,14] The low frequency peaks at 992, 882, 790, and 616 cm^{-1} all have analogues in the cyclohexane IR spectrum of $Ti(NEt_2)_4$. The peaks at 992 and 616 cm^{-1} are assigned to $\nu_s(NC_2)$ and ν(Ti-N), respectively, while the peaks at 882 and 790 cm^{-1} are unassigned.[15]

Only the peak at 957 cm^{-1} has no corresponding peak in the spectrum of $Ti(NEt_2)_4$. In previous work using $H_2{}^{18}O$, it was possible to label the surface hydroxyl groups of partially dehydroxylated silica so that most (>80%) are $Si^{18}OH$ rather than $Si^{16}OH$. Upon reaction with $Ti(NEt_2)_4$, the peak usually observed at 957 cm^{-1} shifts to 936 cm^{-1}.[1] By comparison to spectra of other silica-supported ^{18}O-labelled complexes, it was established that the appropriate peak assignment is ν(Si-OTi).

The IR spectra of $(\equiv SiO)_nTi(NMe_2)_{4-n}$ are somewhat more complicated, but consistent with reported spectra for $Ti(NMe_2)_4$.[16,17] In the C-H stretching region, seven peaks appear due to extensive coupling of the vibrational modes, Figure 3.2b and Table 3.3. In the portion of the low frequency region of the spectrum not obscured by the absorbance of the silica matrix, peaks at 955 and 945 cm^{-1} (for $(\equiv SiO)_2Ti(NMe_2)_2$) are assigned to in-phase and out-of-phase components of $\nu(NC_2)$, respectively (they are not resolved for $(\equiv SiO)Ti(NMe_2)_3$).[16] The peak at ca. 600 cm^{-1} is assigned to ν(TiN). It was not possible to observe the peak due to ν(Si-OTi) due to superposition of the intense $\nu(NC_2)$ modes, located in the same region.

Table 3.3 IR spectra of $Ti(NMe_2)_4$ and silicas modified with $Ti(NMe_2)_4$.

$Ti(NMe_2)_{4(g)}$ [16]	$Ti(NMe_2)_{4(l)}$ [17]	$(\equiv SiO)_nTi(NMe_2)_{4-n}$		Assignment[16,17]
		n = 1	n = 2	
2964	2959	2966	2965	$\nu(CH_3)$
2943	2934	2933	2930	"
2918	2907	2907	2908	"
2865		2866	2865	"
2852	2855	2855	2856	"
2827	2838	2824	2824	"
	2814			"
2779	2768	2777	2777	$\nu_s(CH_3)$
		1470	1470	$\delta(CH_3)$
1458	1450, 1440	1455	1455	"
1424	1413	1423	1422	"
1254	1249	[a]	[a]	Not assigned
1156	1152, 1145	[a]	[a]	$\rho(CH_3)$
1121		[a]	[a]	Not assigned
1059	1057	[a]	[a]	$\nu_{as}(NC_2)$
949	945	947	955, 945	$\nu_s(NC_2)$
594	590	599	600	$\nu(TiN)$

[a] Not observed due to intense absorbance of the silica lattice from 1000-1300 cm^{-1}.

3.5 NMR characterization of Ti-modified silicas

The ^{13}C CP/MAS NMR spectra of **3** and **5** both consist of one peak located at 43 ppm. Figure 3.3. It is assigned to the carbon present in the dimethylamido ligands, by comparison to the $^{13}C\{^1H\}$ NMR spectrum of $Ti(NMe_2)_4$ in C_6D_6 (44.4 ppm). The spectra of **4** and **6** both contain two peaks, located at 14 and 46 ppm. Figure 3.4. They are assigned to the methyl and methylene carbons, respectively, of the diethylamido ligands by comparison to the $^{13}C\{^1H\}$ NMR spectrum of $Ti(NEt_2)_4$ in $CDCl_3$ (13.3 and 45.0 ppm).

3.6 UV-Vis characterization of Ti-modified silicas

The UV-visible spectrum of $Ti(NMe_2)_4$ and the diffuse reflectance spectrum of silica-200 modified with $Ti(NMe_2)_4$ are very similar. In cyclohexane, $Ti(NMe_2)_4$ gives a broad, intense peak in the UV, composed of three components located at approximately 309, 255 and 238 nm. Figure 3.5a. The diffuse reflectance spectrum of $(\equiv SiO)_2Ti(NMe_2)_2$ also consists of three peaks, at ca. 322, 258 and 228 nm, Figure 3.5b, albeit with different relative intensities. Tailing of the lowest energy UV band into the visible confers the yellow colour on both the molecular complex and the modified silica. The corresponding spectra of $Ti(NEt_2)_4$ and $Ti(NEt_2)_4$-modified silica are likewise virtually identical. In cyclohexane, $Ti(NEt_2)_4$ has three overlapping UV peaks at ca. 309, 260 and 235 nm, Figure 3.6a. The diffuse reflectance spectrum of $(\equiv SiO)_2Ti(NEt_2)_2$ consists of three peaks located at 309, 260 and 235 nm, Figure 3.6b.

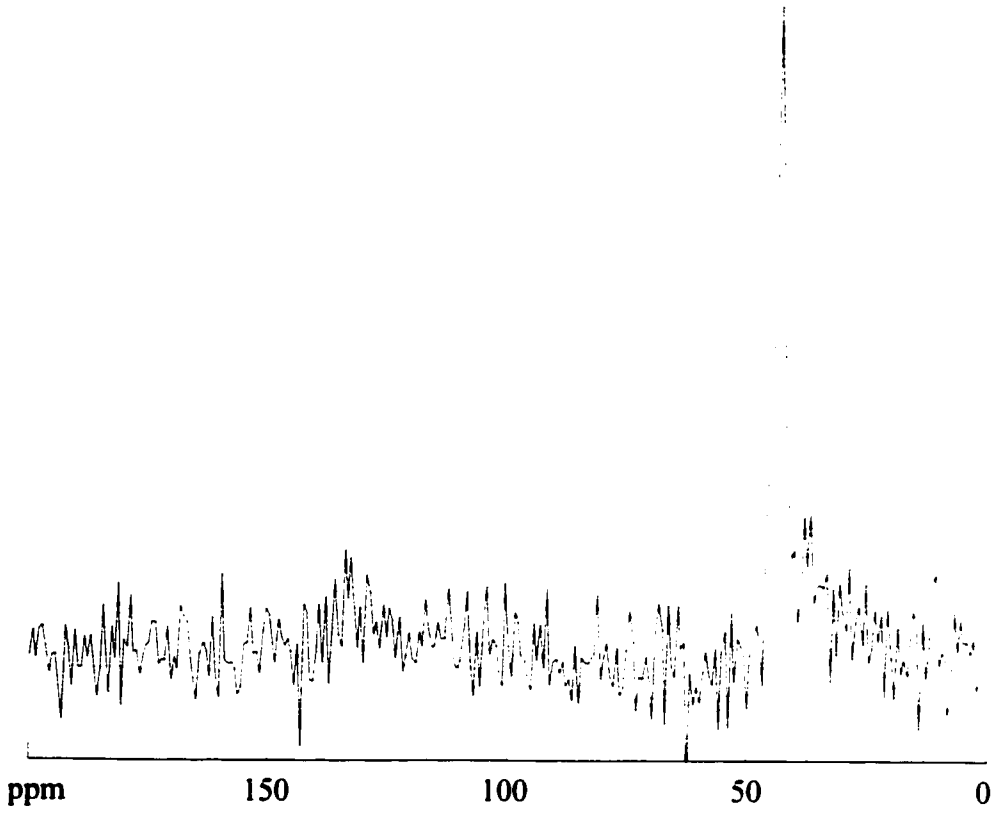

Figure 3.3 ^{13}C CP/MAS spectrum of silica-500 treated with **1** to give $(\equiv SiO)Ti(NMe_2)_3$. **3.** followed by desorption of excess **1** and evacuation of volatiles. Spin rate. 4 kHz.

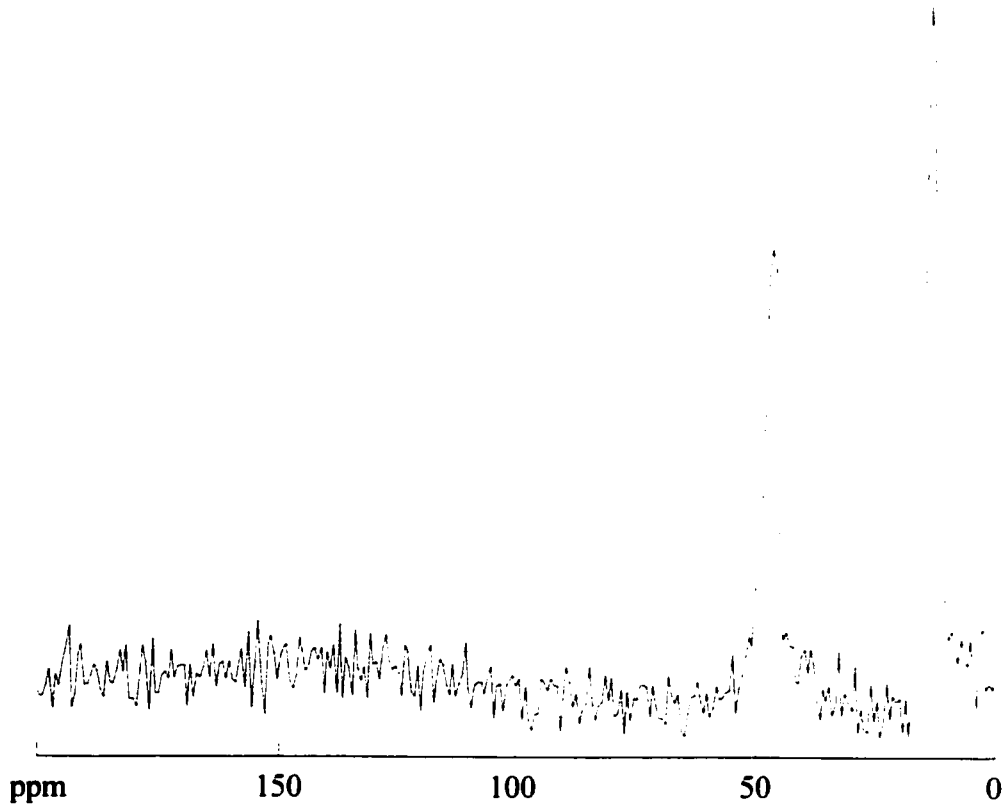

Figure 3.4 ^{13}C CP/MAS spectrum of silica-500 treated with **2** to give $(\equiv SiO)Ti(NEt_2)_3$. **4.** followed by desorption of excess **2** and evacuation of volatiles. Spin rate, 4 kHz.

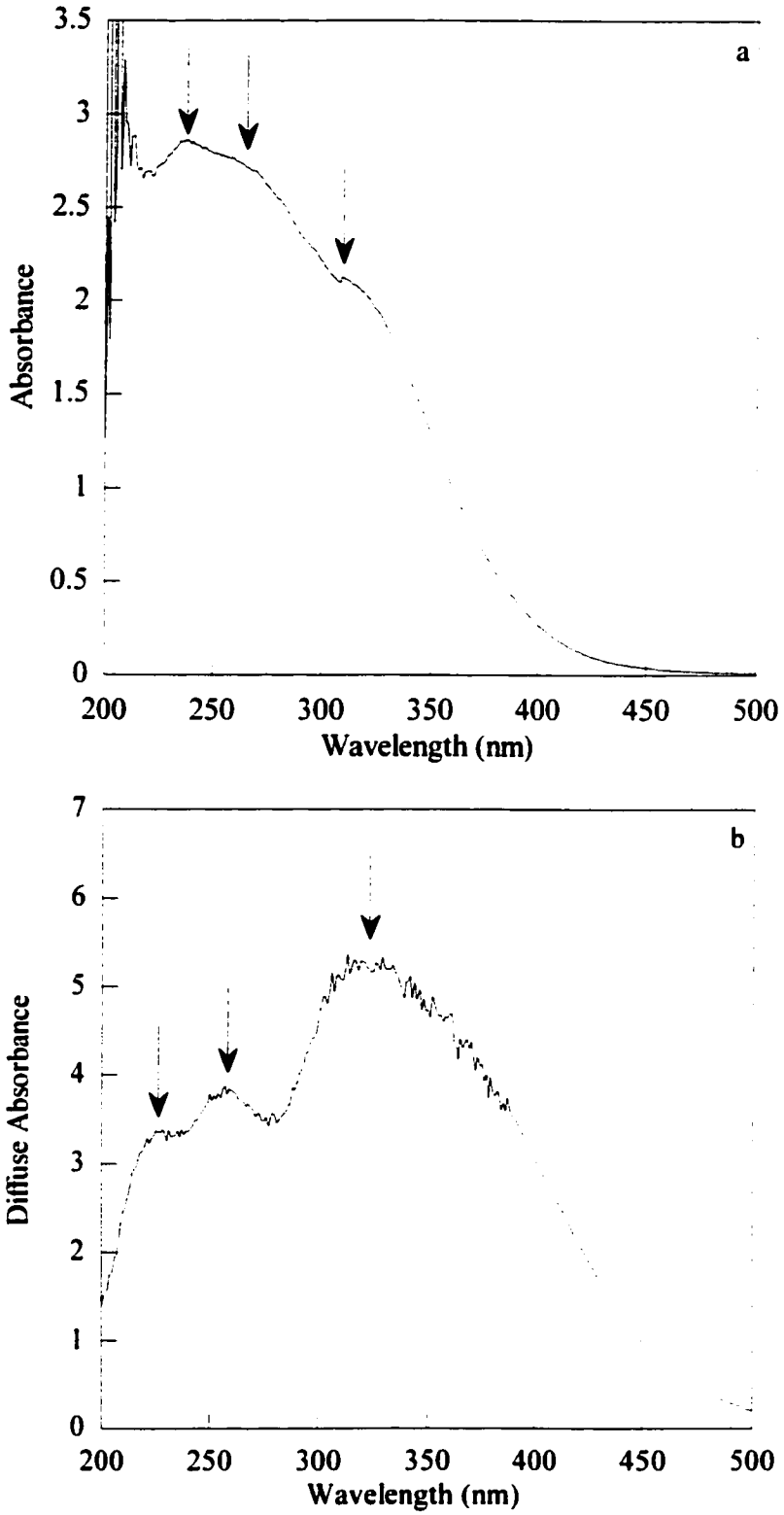

Figure 3.5 UV-visible spectra of (a) $Ti(NMe_2)_4$ in cyclohexane; (b) silica-200 modified with $Ti(NMe_2)_4$, recorded in diffuse reflectance mode (average of 3 spectra).

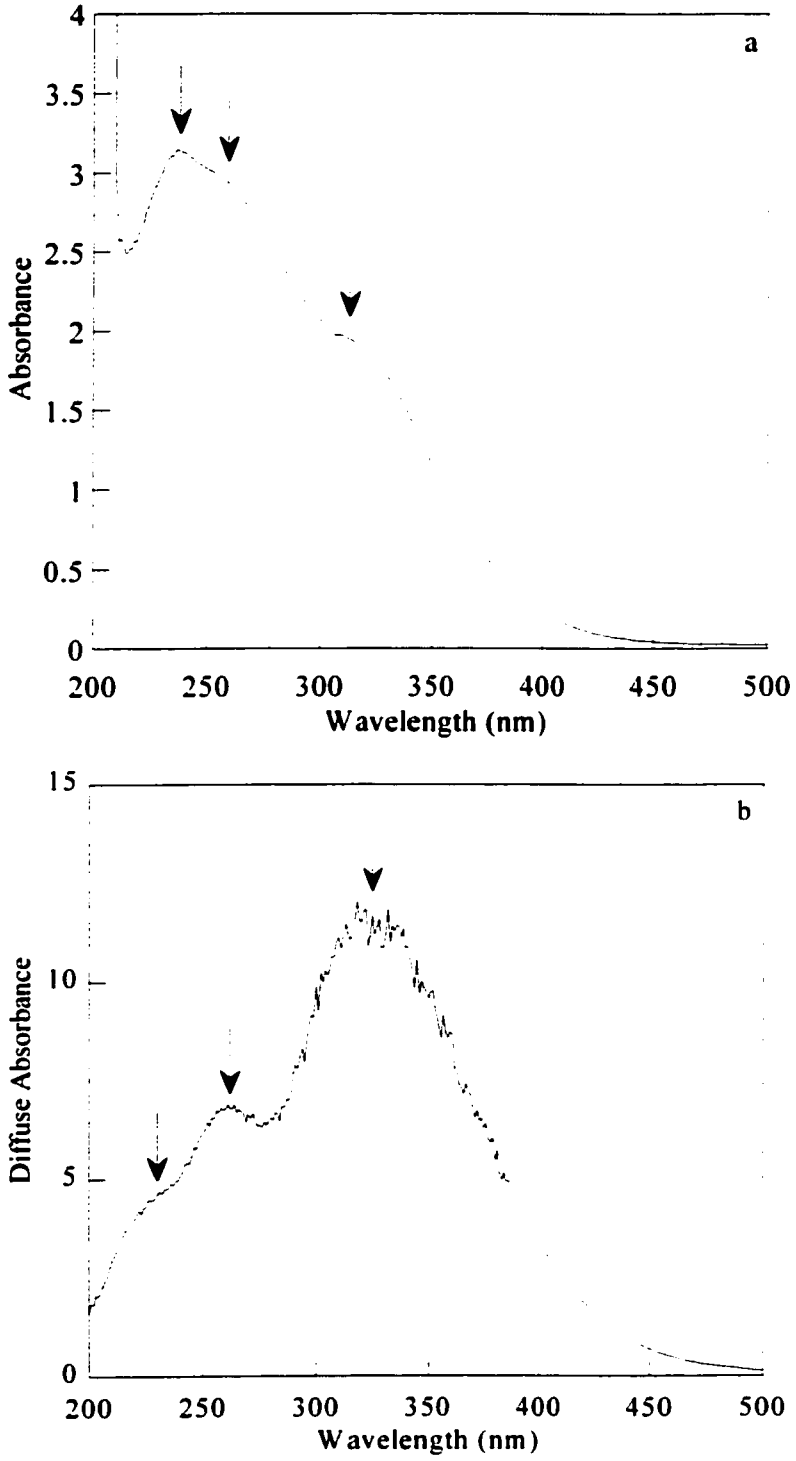

Figure 3.6 UV-visible spectra of (a) $Ti(NEt_2)_4$ in cyclohexane; (b) silica-200 modified with $Ti(NEt_2)_4$, recorded in diffuse reflectance mode (average of 4 spectra).

The similarity in peak positions between solution and solid spectra suggests that the electronic transitions are due to amide ligand-based or amide→Ti charge transfers which are not appreciably perturbed by the partial substitution of amide ligands upon grafting on the silica. The relative intensities of the bands in the diffuse reflectance spectra should not be compared with those found in the solution spectra. As particle size decreases, DRUV extinction coefficients also decrease due to more efficient scattering, resulting in the incident radiation not penetrating the sample as deeply.[18] This effect is wavelength-dependent.

3.7 Reactivity of Ti-modified silicas

3.7.1 Reaction with t-butanol

The displacement of amide ligands of molecular metal complexes by alcohols is well-known, eq 3.2.[7] The reactivity of supported-metal amide complexes towards alcohols, although much less extensively studied,[1] has been found to mimic the reactivity seen in solutions. $Nd(N(SiMe_3)_2)_3$ grafted on MCM-41, will react with a wide range of alcohols to produce the corresponding alkoxo complex, eq 3.12.[8]

$$(\equiv SiO)_2NdN(SiMe_3)_2 + ROH \rightarrow (\equiv SiO)_2NdOR + HN(SiMe_3)_2 \qquad (3.12)$$

$$R = Me, Et, {}^{i}Pr, C^{t}Bu$$

The reactions of **3-6** with excess *tert*-butyl alcohol vapour results in an immediate colour change from yellow to white, and nearly complete (ca. 95%) displacement of the amido ligands as HNR_2, eq 3.13-3.14.

$$(\equiv SiO)Ti(NR_2)_3 + 3\ {}^tBuOH \rightarrow (\equiv SiO)Ti(O^tBu)_3 + 3\ HNR_2 \qquad (3.13)$$

3, 4

$$(\equiv SiO)_2Ti(NR_2)_2 + 2\ {}^tBuOH \rightarrow (\equiv SiO)_2Ti(O^tBu)_2 + 2\ HNR_2 \qquad (3.14)$$

5, 6

In the IR spectrum of **4** treated with $(CD_3)_3COD$, the ν(C-H) vibrations of the diethylamido ligands decreased in intensity by 96%, Figure 3.7, while new bands were observed at 2235, 2135, 2076 and 2054 cm^{-1}, assigned to the ν(C-D) vibrations of perdeuterio-*tert*-butyl groups which are strongly chemisorbed.

The amount of amine liberated was quantified by gas phase IR spectroscopy, Table 3.4, avoiding spectral overlap through the use of $(CD_3)_3COD$. When the silica was pre-treated at 500°C, exposure of the surface complexes **3** or **4** to $(CD_3)_3COD$ resulted in 2.85 and 2.81 equivalents of HNR_2 (R = Me, **3**, and Et, **4**), being released into the gas phase. When silica-200 was used, 1.98 and 1.95 equivalents of HNR_2 (R = Me, **5**, and Et, **6**) were released upon exposure of **5** or **6** respectively, to an excess of $(CD_3)_3COD$.

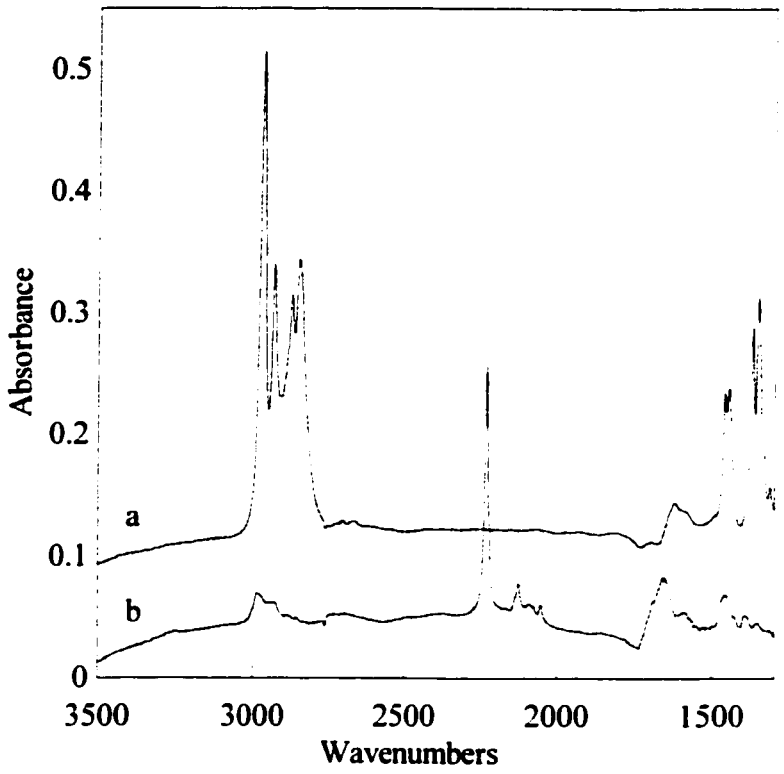

Figure 3.7 *In situ* IR difference spectra of a self-supporting silica pellet of (a) $(\equiv SiO)Ti(NEt_2)_3$. **4**, and (b) after exposure to $(CD_3)_3COD$. Volatiles have been evacuated and a reference spectrum of silica-200 has been subtracted.

Table 3.4 Quantitation of amine liberated by reaction of $Ti(NR_2)_4$-modified silicas with $(CD_3)_3COD$

Complex	Products of grafting				Product of Alcoholysis	
	Wt. % Ti	Ti[a] mmol / g	HNR_2 [a] mmol / g	HNR_2 / Ti	DNR_2 [a] mmol / g	HNR_2 / Ti
$(\equiv SiO)Ti(NMe_2)_3$, **3**	1.95	0.41	0.40	0.98	1.17	2.85
$(\equiv SiO)Ti(NEt_2)_3$, **4**	2.05	0.43	0.44	1.07	1.21	2.81
$(\equiv SiO)_2Ti(NMe_2)_2$, **5**	1.90	0.40	0.81	2.04	0.79	1.98
$(\equiv SiO)_2Ti(NEt_2)_2$, **6**	1.85	0.39	0.76	1.97	0.76	1.95

[a] Values normalized per g of silica.

3.7.2 Reaction with CO_2

Insertion of CE_2 (E = O, S) into the metal-nitrogen bonds of metal amides (M = Ti, Zr, V, Nb, Ta) is facile and quantitative.[12,19] The resulting dimethylcarbamato (E = O) or dimethyldithiocarbamato (E = S) ligands can be either mono- or bidentate. Reaction of $Ti(NR_2)_4$ (R = Me, Et) with CO_2 gives a tetrakis(dimethylcarbamate) complex in which all four ligands are bidentate, eq 3.14.[19]

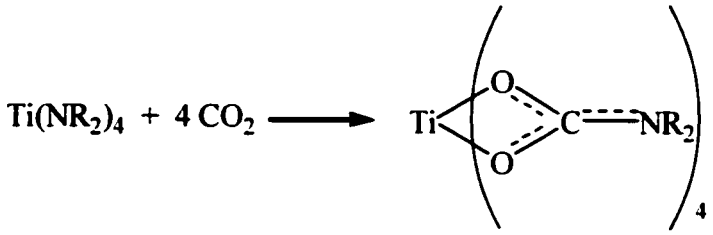

(3.14)

Monodentate dimethylcarbamato ligands, verified by X-ray crystallography, are formed when CO_2 inserts into three of the W-N bonds of $W(NMe_2)_6$, eq 3.15.[19]

$$W(NMe_2)_6 + xs\ CO_2 \rightarrow W(NMe_2)_3(O_2CNMe_2)_3 \qquad (3.15)$$

Upon reaction with CO_2, $M(NMe_2)_5$ (M = Nb, Ta), were found to generate both mono- and bidentate dimethylcarbamato ligands. For example, the X-ray structure of $Nb(O_2CNMe_2)_5$ shows three bidentate carbamato ligands, while the remaining two are monodentate.

Exposure of **5** to an excess of dry $CO_{2(g)}$ resulted in an immediate, dramatic change in its IR spectrum, Figure 3.8, as well as a colour change from bright yellow to orange. The

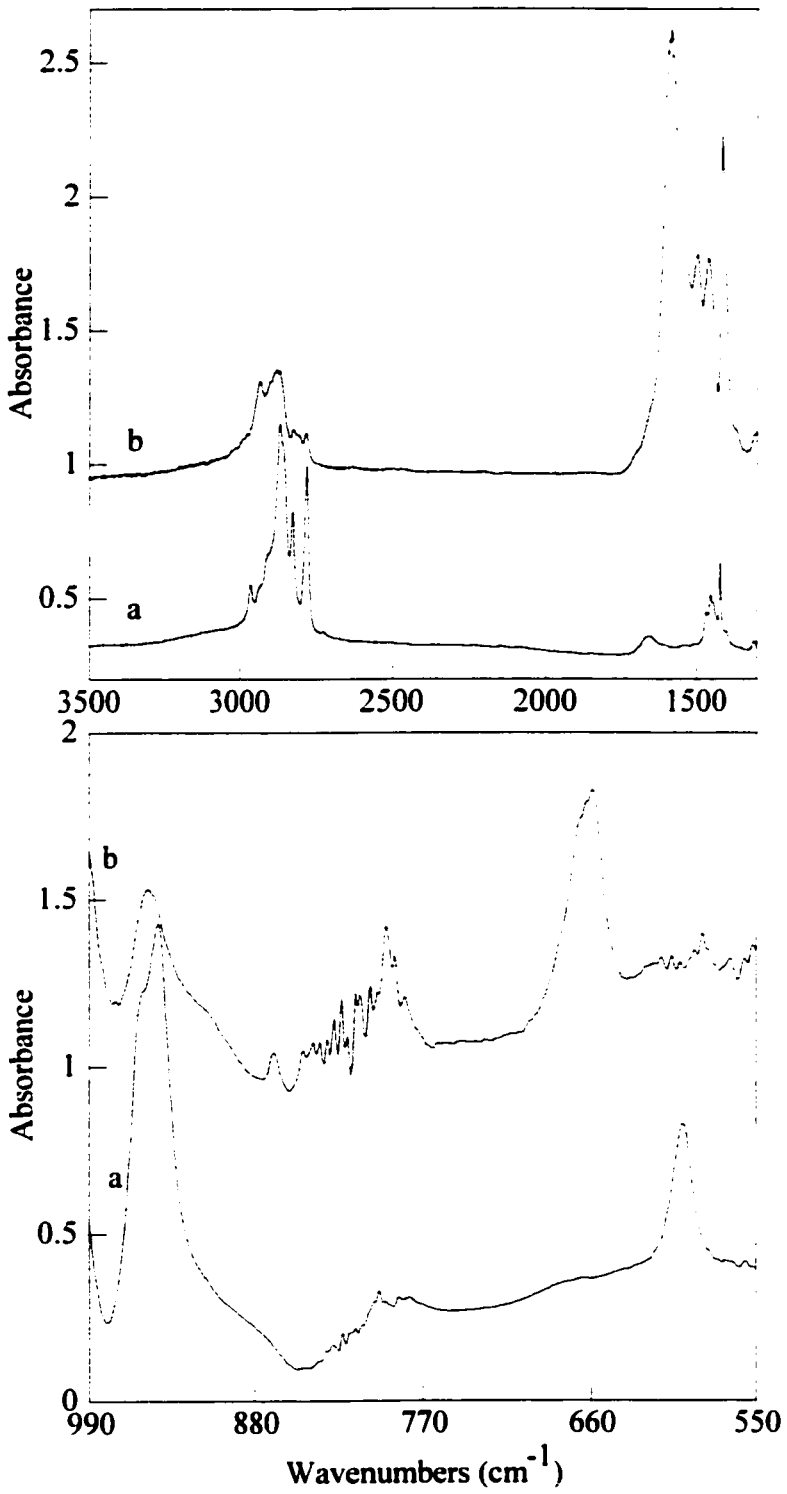

Figure 3.8 *In-situ* IR spectra of (a) $(\equiv SiO)_2Ti(NMe_2)_2$, **5**, (b) after exposure to CO_2. In each case, a reference spectrum of silica-200 has been subtracted and all volatiles evacuated.

characteristic ν(C-H) pattern due to the dimethylamido ligands was replaced by a much less intense and less well-resolved pattern. Intense new bands appeared. Table 3.5. The peaks at 1581, 1499, 1461 and 1416 cm^{-1} are assigned to $\nu_{as}(O_2C)$ and $\nu_s(O_2C)$. By comparison. the IR spectrum of $Ti(O_2CNMe_2)_4$ is reported to contain a band at 1589 cm^{-1}.[19] In the low frequency region, new peaks are seen at 867 and 660 cm^{-1}. The latter is assigned to $\delta(O_2CN)$ by analogy to the vibration at 650 cm^{-1} in $Ti(O_2CNMe_2)_4$. The $\nu(NC_2)$ modes at 945 and 955 cm^{-1} decrease in intensity and are no longer resolved. resulting in a much less intense peak at 951 cm^{-1}. also present in the spectrum of $Ti(O_2CNMe_2)_4$. Finally, the ν(Ti-N) peak located at ca. 600 cm^{-1} completely disappeared, confirming that insertion occurred in both Ti-N bonds.

Based on these observations, the reaction occurring on the silica surface is inferred to proceed as shown in eq 3.16.

$$(\equiv SiO)_2Ti(NMe_2)_2 + 2\ CO_2 \rightarrow (\equiv SiO)_2Ti(O_2CNMe_2)_2 \qquad (3.16)$$

3.8 Conclusion

In this chapter, four supported titanium dialkylamide complexes resulting from the reaction of $Ti(NR_2)_4$ (R = Me, Et) with silica have been synthesized and characterized. The formation of well-defined surface complexes with the formula $(\equiv SiO)_nTi(NR_2)_{4-n}$ (R = Me, Et; n = 1, 2) has been demonstrated. The nature of the surface complex obtained depends on the thermal pretreatment of the silica. On silica-500, each titanium dialkylamide reacts with a single hydroxyl (i.e., n = 1), whereas on silica-200, reaction occurs with a pair of hydroxyl groups (i.e.,

Table 3.5 Peak positions and assignments for $Ti(O_2CNMe_2)_4$ and $(\equiv SiO)_2Ti(O_2CNMe_2)_2$

$Ti(O_2CNMe_2)_4$[19]	$(\equiv SiO)_2Ti(O_2CNMe_2)_2$	Assignment[19]
1738	Not observed	
1690	1700	
1589	1587	$\nu_{str}(O_2CN)$ (bidentate)
1512	Not observed	
1503	1500	
	1461	
1408	1416	
1266	1276	
1170	[a]	
1153	[a]	
1058	[a]	
1042	[a]	
950	953	
865	867	
784	[a]	
650	660	$\delta(O_2CN)$
446	[a]	ν_{str}(M-O)
352	[a]	
250	[a]	

[a] Not observed due to intense absorbance of the silica lattice from 1000-1300, 775-850, and 400-600 cm^{-1}.

n = 2).

Spectroscopic characterization of the supported complexes is consistent with the retention of intact dialkylamido ligands, as well as the formation of Ti-O-Si linkages to the silica surface. The driving force for the replacement of one or more Ti-amide bonds by Ti-silica bonds is the respective bond strengths, since Ti-O is stronger than Ti-N by ca. 34 kcal/mol.[20] Relative acidities also favour the formation of ≡SiO-Ti bonds since the hydroxyl groups terminating the Aerosil surface are much more acidic (pK_a ca. 3.6 – 4.3)[21] than the dialkylamines (pK_a ca. 40).[22] Finally, grafting is driven by entropy, through the evolution of a gaseous product (HNR_2).

The supported bis(dialkylamido)titanium complexes show reactivity characteristic of metal-amide bonds, specifically alcoholysis and CO_2 insertion. However, this reactivity is only observed if the Ti-modified silicas are exposed to these reagents soon after their preparation. Upon standing for several hours/days, characteristic amide reactivity is lost and the supported metal complexes spontaneously evolve to new surface species. The nature of this transformation, which initially complicated our efforts to understand the chemistry of $(\equiv SiO)_nTi(NR_2)_{4-n}$, will be reported in Chapter 4.

3.9 References

(1) Bouh, A. O.; Rice, G. L.; Scott, S. L. *J. Am. Chem. Soc.* **1999**, *121*, 7201-7210.

(2) Amor Nait Ajjou, J.; Scott, S. L. *Organometallics* **1997**, *16*, 86-92.

(3) Amor Nait Ajjou, J.; Rice, G. L.; Scott, S. L. *J. Am. Chem. Soc.* **1998**, *120*, 13436-13443.

(4) Rice, G. L.; Scott, S. L. *Langmuir* **1997**, *13*, 1545-1551.

(5) Humblot, F.; Didillon, D.; Lepeltier, F.; Candy, J. P.; Corker, J.; Clause, O.; Bayard, F.; Basset, J. M. *J. Am. Chem. Soc.* **1998**, *120*, 137-146.

(6) Chabanas, M.; Baudouin, A.; Coperet, C.; Basset, J.-M. *J. Am. Chem. Soc.* **2001**, *123*, 2062-2063.

(7) Chandra, G.; Lappert, M. F. *J. Chem. Soc (A)* **1968**, 1940-1945.

(8) Anwander, R.; Palm, C. *Stud. Surf. Sci. Cat.* **1998**, *117*, 413-420.

(9) Nagl, I.; Widenmeyer, M.; Grasser, S.; Köhler, K.; Anwander, R. *J. Am. Chem. Soc.* **2000**, *122*, 1544-1545.

(10) Anwander, R.; Görlitzer, H. W.; Gerstberger, G.; Palm, C.; Runte, O.; Spiegler, M. *J. Chem. Soc., Dalton Trans.* **1999**, 3611-3615.

(11) Anwander, R.; Roesky, R. *J. Chem. Soc., Dalton Trans.* **1997**, 137-138.

(12) Lappert, M. F.; Patil, D. S.; Sanger, A. R.; Srivastava, R. C. *Metal and Metalloid Amides: Syntheses, Structures, and Physical and Chemical Properties*; Wiley: Toronto, 1980.

(13) Conley, R. T. *Infrared Spectroscopy*; Allyn and Bacon: Boston, 1970.

(14) Bellamy, L. J. *Advances in Infrared Group Frequencies*; Chaucer: Bungay, 1968.

(15) Bradley, D. C.; Gitlitz, M. H. *J. Chem. Soc. (A)* **1969**, 980-984.

(16) Dubois, L. H.; Zegarski, B. R.; Girolami, G. S. *J. Electrochem. Soc.* **1992**, *139*, 3603-3609.

(17) Bürger, H.; Stammreich, H.; Sans, T. T. *Monatsh. Chem.* **1966**, *97*, 1276-1279.

(18) Frei, R. W.; Frodyma, M. M.; Lieu, V. T. *Instrumentation for Spectroscopy, Analytical Atomic Absorption and Fluorescence Spectroscopy, Diffuse Reflectance Spectroscopy*; Elsevier Scientific: New York, 1975.

(19) Chisholm, M. H.; Extine, M. W. *J. Am. Chem. Soc.* **1977**, *99*, 782-792.

(20) Lappert, M. F.; Patil, D. S.; Pedley, J. B. *J. Chem. Soc., Chem. Comm.* **1975**, 830-831.

(21) *Technical Bulletin No. 16: Analytical Methods for Synthetic Silicas and Silicates*; 3rd ed.; Degussa: Frankfurt, 1992.

(22) McMurry, J. *Organic Chemistry*; Brooks/Cole: Pacific Grove, 1988.

Chapter 4

Spontaneous transformations of silica-supported bis(amido)titanium complexes

4.1 Introduction

Surface organometallic fragments are usually stable in the absence of an external agent, be it chemical or thermal. Studies of many silica-supported complexes including $(\equiv SiO)_nM(CH_2E(CH_3)_3)_{4-n}$ (M = Cr, V, E = C, Si; M = Ti, E = C; n = 1-2),[1-3] $(\equiv SiO)VOCl_2$,[4] and $(\equiv SiO)_nTi_2O(O^iPr)_{6-n}$ (n = 1-2),[5] revealed no evidence of spontaneous transformations.

As described in the previous chapter, the silica-supported amide complexes $(\equiv SiO)_2Ti(NR_2)_2$ (R = Me (**5**), Et (**6**)), are stable at room temperature under static vacuum (ca. 10^{-4} Torr) for short periods of time, ca. 2 hours. However, upon standing (> 2 hrs), both complexes undergo spontaneous irreversible transformations. As we shall see, such reactions provide a unique opportunity to identify and study some of the intermediates in the deposition of $Ti(NR_2)_4$ leading to the CVD of TiN.

4.2 Spontaneous transformation of $(\equiv SiO)_2Ti(NMe_2)_2$, 5

As shown in Chapter 3, when the surface hydroxyl groups of a partially dehydroxylated silica have been completely consumed through reaction with **1**, a monolayer of **5** is present on the surface in an amount corresponding to ca. 2 wt % Ti. Upon standing under either static or dynamic vacuum, the IR spectrum of **5** undergoes a dramatic change both in appearance, Figure 4.1, and intensity, Figure 4.2, consistent with the loss of hydrocarbon (i.e., ligands) from the

surface. By the time the reaction reaches completion, the colour of the pellet has changed from bright yellow to pale yellow. Standing for longer periods of time resulted in no further change in the IR spectrum. An increase in the temperature from room temperature to 60 °C resulted in a more rapid loss of hydrocarbon from the surface.

Inspection of the final IR spectrum reveals a small amount of hydrocarbon remaining on the surface. In fact, the integrated absorbance in the ν(C-H) region stabilized reproducibly at (24 ± 1)% of its initial value (average of seven expts), Figure 4.2a. The progress of the reaction can also be monitored via the intensity of the characteristic $\nu_s(CH_3)$ mode of the dimethylamide ligands at 2777 cm^{-1}, which disappears almost completely, Figure 4.2b.

Volatiles produced during this transformation were trapped in liquid N_2. GC and GC-MS analysis showed the presence of a single gaseous product, $HNMe_2$. By *in situ* IR, the yield was evaluated as 0.9 $HNMe_2$ per grafted Ti. Calcination of the resulting solid in O_2 at 800°C resulted in the complete removal of all remaining hydrocarbon fragments from the surface. This procedure generated 2.1 CO_2 per Ti present on the surface.

On the basis of these results, we infer that **5** loses one-half of its carbon atoms as $HNMe_2$ during its transformation. We therefore propose that **5** evolves to the N-methylmethanimine complex **7**, eq 4.4:

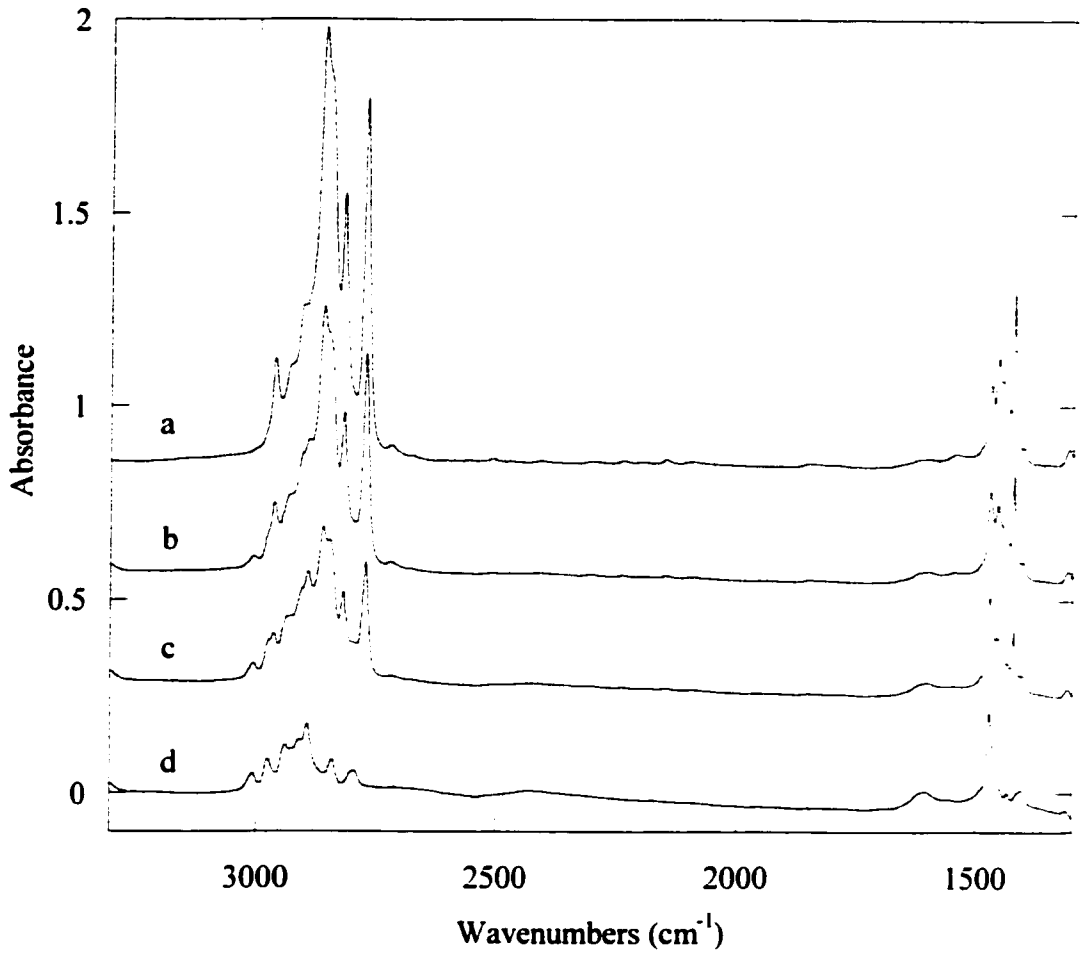

Figure 4.1 In situ IR difference spectra of a sample of $(\equiv SiO)_2Ti(NMe_2)_2$ (**5**) (2.0 wt. % Ti: 14 mg SiO_2) recorded after dynamic evacuation at room temperature for the following times: (a) 0 h; (b) 3 h; (c) 5 h; (d) 11.5 h. The silica background spectrum has been subtracted and the spectra vertically offset.

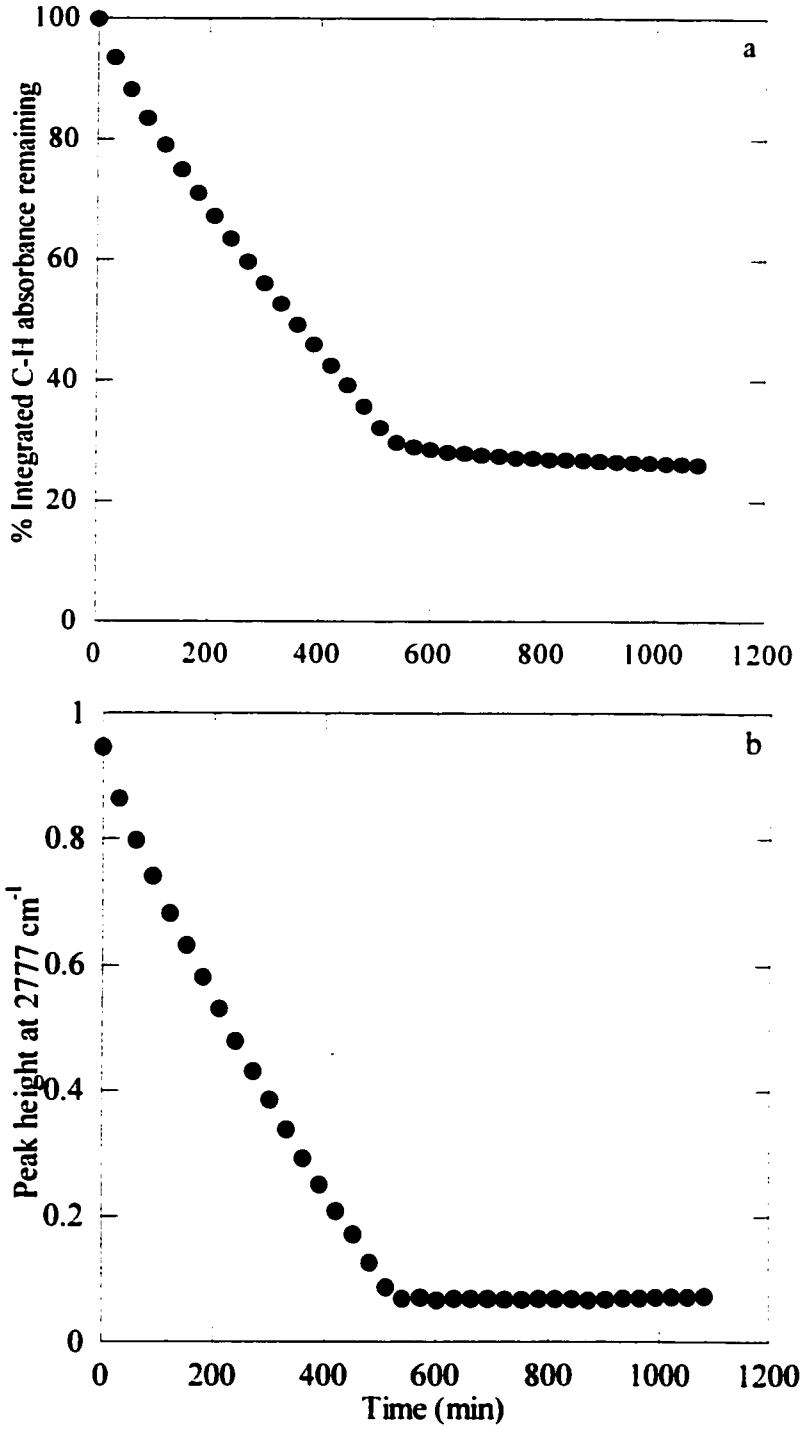

Figure 4.2 Time-resolved evolution of $(\equiv SiO)_2Ti(NMe_2)_2$ (**5**) at room temperature monitored as (a) the % integrated absorbance remaining in the region 3100-2650 cm^{-1}; (b) the intensity of the 2777 cm^{-1} mode.

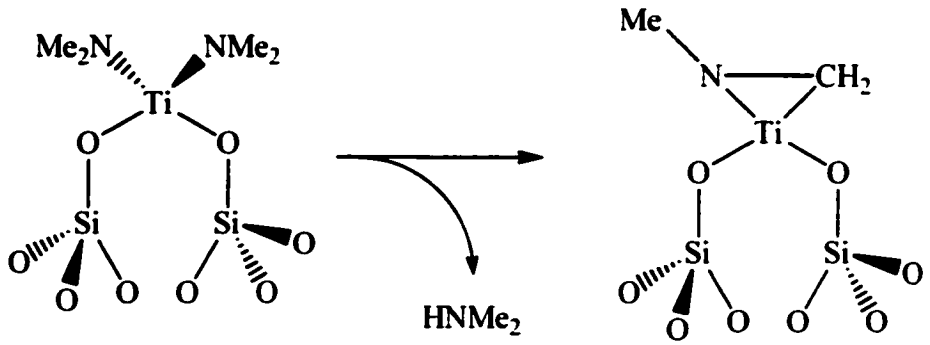

(4.4)

5 7

The transformation of **5** to **7** is irreversible: addition of a four-fold excess of $HNMe_2$ to a freshly prepared sample of **7** does not regenerate the IR spectrum of **5**, as judged by the failure of the peak at 2777 cm^{-1} to reappear.

The ^{13}C CP/MAS spectrum of **7** is very similar to that of **5** (Figure 3.3), with a signal at 43 ppm corresponding to the methyl carbon. Unfortunately, the spectrum does not show any new peak assignable to the methylene carbon. However, its signal is expected to be difficult to detect in the solid state, both due to its low abundance and its lack of mobility.

Additional evidence for the proposed formulation of **7** was sought through its reactivity. Exposure of **7** to an excess of $(CD_3)_3COD$ resulted in the loss of most of the remaining C-H vibrations from the surface, Figure 4.3, and the liberation of 0.9 equivalents of dimethylamine / Ti into the gas phase. GC/MS analysis identified the isotopomer as dimethylamine-d_1, with a molecular ion at m/z = 46 (p+1/p = 0.428), Figure 4.4a, where p is the intensity of the fragment at m/z = 45 (corresponding to M^+ for unlabelled $HNMe_2$). GC/MS of an authentic sample of $DN(CH_3)_2$, prepared by reaction of $Ti(NMe_2)_4$ with $(CD_3)_3COD$, resulted in the detection of only $HN(CH_3)_2$ (m/z = 45, p+1/p = 0.040), resulting from complete N-D/N-H exchange on the GC

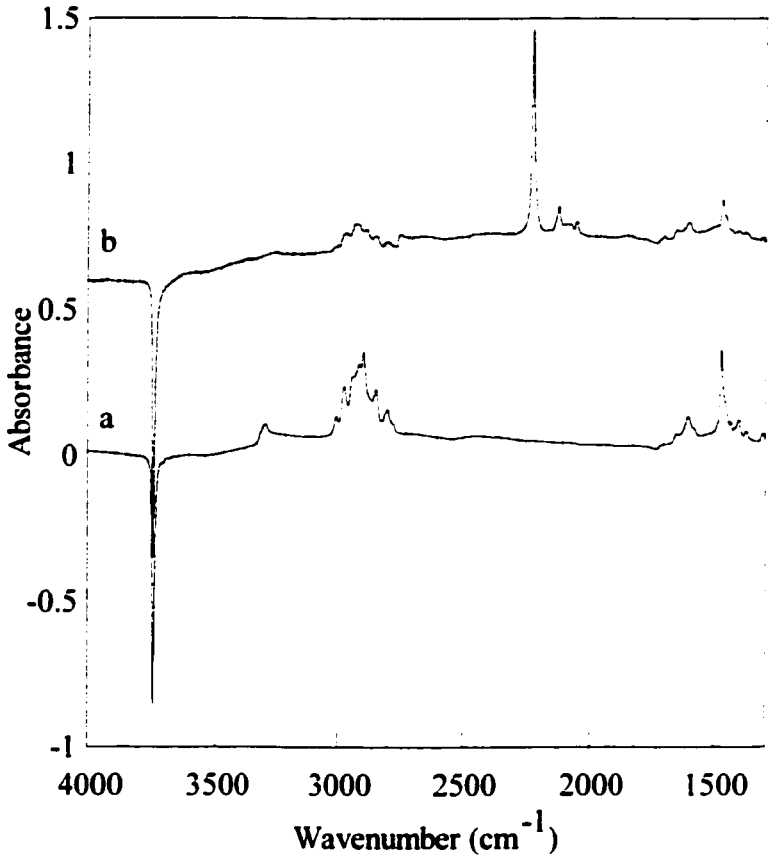

Figure 4. 3 *In situ* IR difference spectra of regions of partial transmission of a self-supporting silica pellet of (a) $(\equiv SiO)_2Ti(\eta^2\text{-}CH_2NCH_3)$, **7**; (b) after exposure to $(CD_3)_3COD$ and evacuation of volatiles.

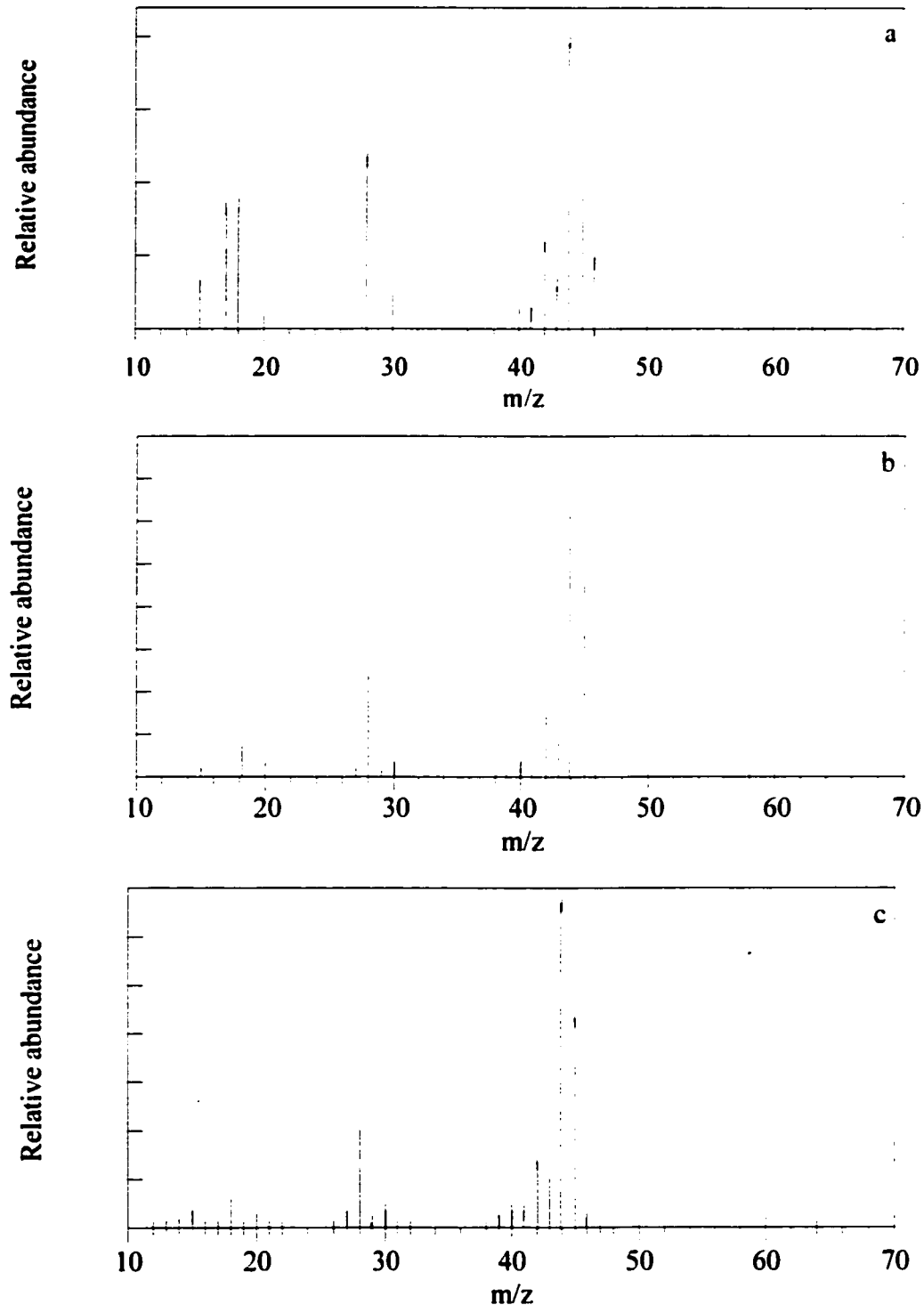

Figure 4.4 Mass spectra of (a) $HN(CH_3)(CH_2D)$ from reaction of **7** with $(CD_3)_3COD$; (b) $DN(CH_3)_2$ from reaction of $Ti(NMe_2)_4$ with $(CD_3)_3COD$; (c) $HNMe_2$; recorded after passing each through a DB-1 column.

column, Figure 4.4b. The mass spectrum is virtually identical to that of undeuterated dimethylamine, Figure 4.4c, p+1/p = 0.023. Thus, alcoholysis of **7** clearly results in incorporation of a non-exchangeable deuterium atom bound to carbon, eq 4.5-4.6:

$$(\equiv SiO)_2\overbrace{Ti(CH_2NMe)} + xs\ (CD_3)_3COD \longrightarrow (\equiv SiO)_2Ti(O^tBu)_2 + DN(CH_3)(CH_2D) \qquad (4.5)$$

7

$$DN(CH_3)(CH_2D) \xrightarrow{GC\ column} HN(CH_3)(CH_2D) \qquad (4.6)$$

$m/z = 47$ $\qquad\qquad$ $m/z = 46$

An analogous displacement of an η^2-imine ligand by deuterated alcohol was reported for the deuterolysis of N-ethylethaniminetris(diethylamido)tantalum. $HNEt(CHDCH_3)$ was detected as its molecular ion at m/z = 74, p+1/p = 0.32.[6]

The formation of imine complexes of early transition metals from their dialkylamides is not unusual. Although $Ti(NMe_2)_4$ is stable, an examination of fragments in its mass spectrum revealed products resulting from metallacycle formation ($HNMe_2$ and $(Me_2N)_2Ti(CH_2NMe)$) as well as β-hydride elimination ($H_2C{=}NMe$ and $(Me_2N)_3TiH$).[7] The formation of stable molecular imine complexes is also well-precedented. Pentakis(diethylamido)tantalum, when distilled, decomposes to N-ethylethaniminetris(diethylamido)tantalum(V), eq 4.5.[6]

$$Ta(NEt_2)_5 \dashrightarrow (Et_2N)_3Ta(CH_3CH{=}NEt) + HNEt_2 \qquad (4.5)$$

Another tantalum complex, $Cp^*Ta(NMe_2)Me_3$, decomposes at 25°C to give an imine complex, $Cp^*Ta(CH_2NMe)Me_2$ with evolution of methane.[8] A number of dimeric tungsten species also

produce imines upon thermolysis at or above room temperature. $W_2Cl_3(NMe_2)_3L_2(\mu\text{-}C_2H_2)$ (L = PMe_2Ph or PMe_3), in either benzene or toluene, evolves to give a complex having a $W_2(\mu\text{-}C_2H_3)(\mu\text{-}CH_2NMe)$ core.[9]

4.3 Kinetics of N-methylmethanimine formation

As Figure 4.2 shows, the transformation of **5** to **7** on silica follows zero-order kinetics. The rate law can therefore be represented as

$$-\frac{d[5]}{dt} = k_{obs} \qquad (4.6)$$

At room temperature and with a fully loaded sample of **5** (19.3 mg SiO_2, 1.85 wt. % Ti), the observed rate constant is $(0.00113 \pm 0.00001)\ min^{-1}$ under dynamic vacuum.

Unfortunately, the overall zero-order rate law (eq 4.6) is uninformative about the nature of the chemical transformation taking place. However, zero-order behaviour is a common phenomenon in temperature-programmed desorption from surfaces, where it characterizes the existence of an equilibrium state involving an adsorbed gas.[10] For example, Xe adsorbed on Pt(111) desorbs in a zero-order fashion, ascribed to the presence of a two-phase (2D gas-condensate) adsorbate in internal equilibrium.[11] At the desorption temperature (ca. 100 K), surface diffusion and desorption of Xe atoms from the borders of condensed Xe islands are fast enough to allow the adsorbate to maintain its equilibrium structure. Similar phenomena have been observed for more complex, molecular adsorbates such as trimethylsilane on graphite at

multilayer as well as monolayer coverages.[12] Surface reactions may exhibit zero-order kinetics if they consist of at least two consecutive steps: 1) transformation of reactant to product, followed by 2) desorption of product into the gas phase, and are carried out at low enough temperatures such that desorption is rate limiting.[12]

Two factors were found to alter appreciably the rate of formation of **7**. The first and more dramatic of these is the effect of Ti loading. Figure 4.5 shows kinetic curves for two silica pellets of different sizes, loaded with the same amount of Ti. On the heavier pellet (20.0 mg, 0.71 wt. % Ti, 3.0 μmol Ti), k_{obs} is 0.0098 μmol Ti/min, while on the lighter pellet (8.0 mg, 1.90 wt. % Ti, 3.2 μmol Ti), k_{obs} is 0.0020 μmol Ti/min. Less than full loading of the silica surface with **5** was achieved by decreasing the contact time between $Ti(NMe_2)_4$ and silica during grafting.

The same effect was seen, although to a lesser extent, on silica pellets of similar size (13.1 and 15.3 mg), when the Ti loading was decreased from 0.71 wt. % to 0.28 wt. %. The result was a doubling of the k_{obs} from 0.006 μmol Ti/min to 0.014 μmol Ti/min at room temperature under dynamic vacuum, Figure 4.6a.

The Ti loading of silica is inversely proportional to its residual hydroxyl content. Since unmodified silica-200 contains 0.86 mmol OH/g, deposition of 0.71 wt. % Ti (0.15 mmol Ti / g) causes the hydroxyl content to decrease to 0.56 mmol/g, while at full coverage (1.90 wt. % Ti, 0.40 mmol Ti / g), there are < 0.06 mmol OH/g remaining. An obvious explanation for the accelerated rate of transformation of **5**→**7** as the Ti loading decreases is that the reaction involves these surface hydroxyls. Inspection of the IR spectrum of partially loaded **5** before and after reaction does not reveal consumption of unreacted OH groups, Figure 4.7. Furthermore, since the reaction proceeds quantitatively even when the number of residual OH groups is very

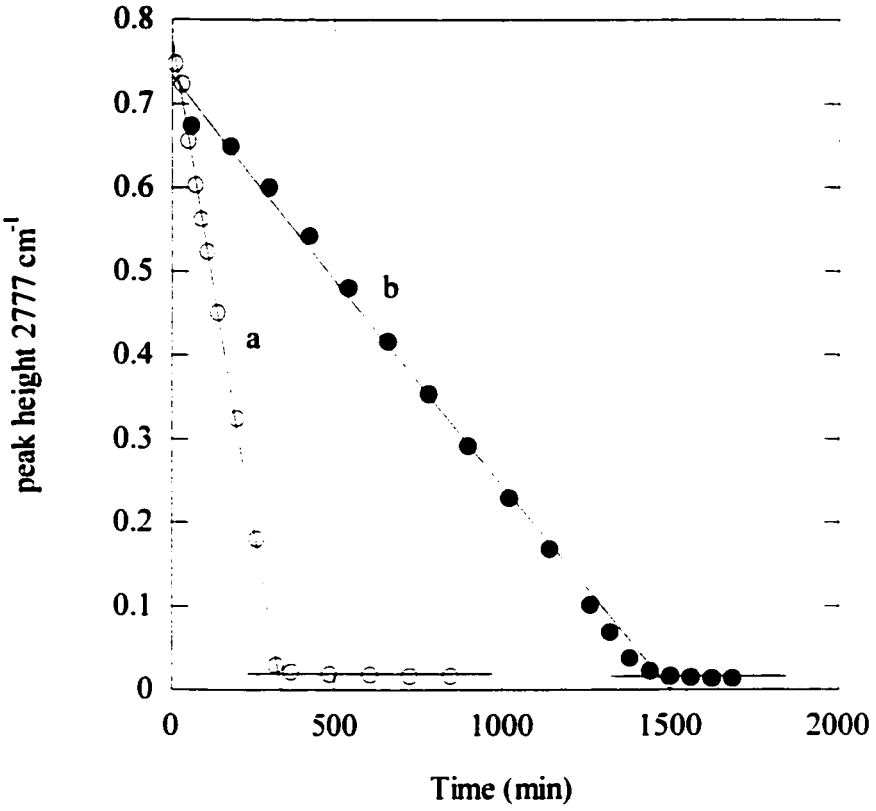

Figure 4.5 Time-resolved dynamic vacuum evolution of $(\equiv SiO)_2Ti(NMe_2)_2$ on two different silica samples: (a) 0.71 wt. % Ti, 20.0 mg pellet; (b) 1.90 wt. % Ti, 8.0 mg pellet.

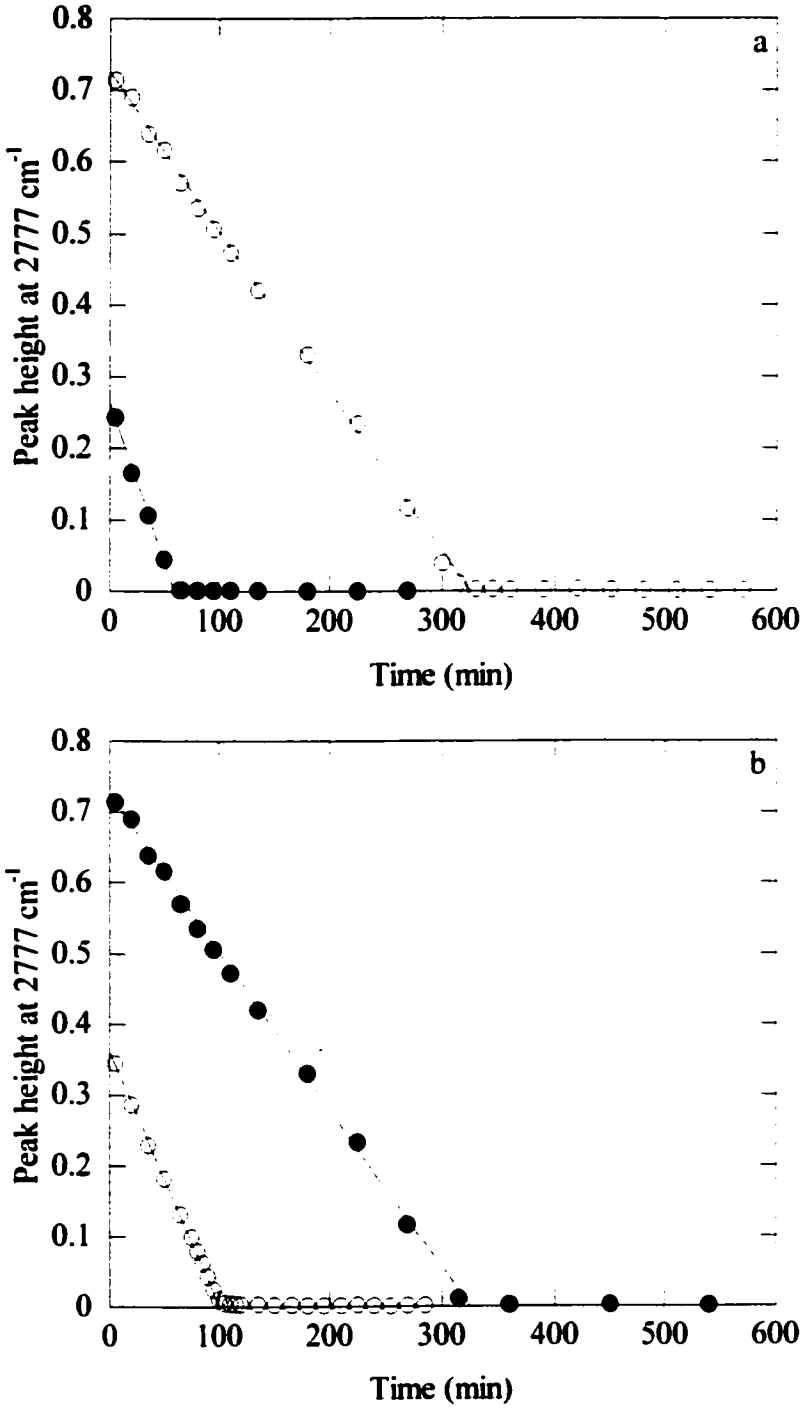

Figure 4.6 Time-resolved dynamic vacuum evolution of $(\equiv SiO)_2Ti(NMe_2)_2$; (a) 13.1 mg SiO_2, 0.71 wt. % Ti (open circles), 15.3 mg SiO_2, 0.28 wt. % Ti (filled circles); (b) 17.7 mg SiO_2, 0.67 wt. % Ti (open circles), 13.1 mg SiO_2, 0.71 wt. % Ti (filled circles)

low, the surface hydroxyls must play a catalytic rather than a stoichiometric role in the transformation. Kinetically, the catalytic role of the surface hydroxyls is consistent with the observed zero-order behaviour, eq 4.7.

$$k_{obs} = k\, n_{SiOH} = \text{constant} \qquad (4.7)$$

Furthermore, the dependence of k_{obs} on n_{SiOH} implies that the zero-order kinetics are not a consequence of rate-limiting desorption of $HNMe_2$ from the surface.

Interestingly, it is not the density of residual surface OH (n_{SiOH} / nm^2) groups which controls the rate but the absolute number, n_{SiOH}. As the mass of the silica pellet increases, n_{SiOH} likewise increases although the density remains constant. The effect on dimethylamine elimination from **5** is dramatic. Figure 4.6b shows kinetic curves for two silica pellets of different sizes, loaded with similar amounts of Ti. On the heavier pellet (17.7 mg, 0.67 wt. % Ti, 2.5 μmol Ti), k_{obs} is 0.025 μmol Ti/min, while on the lighter pellet (13.1 mg, 0.71 wt. % Ti, 1.9 μmol Ti), k_{obs} is 0.006 μmol Ti/min. The hydroxyl contents in these experiments are 7.4 μmol for the 13.1 mg pellet and 10.3 μmol for the 17.7 mg pellet. Table 4.1 shows a list of kinetic runs, organized by decreasing wt.% Ti. A plot of k_{obs} vs μmol OH remaining shows no discernable trend, Figure 4.8. Clearly, the total amount of OH remaining on the surface is not the only factor that affects the rate of transformation.

The second variable which affects the rate of conversion of **5**→**7** is the total pressure. When **5** is maintained under dynamic vacuum (base pressure ca. 10^{-5} Torr), the volatile product $HNMe_2$ is constantly removed from the reactor. However, if **5** is allowed to stand under static vacuum, i.e., the reactor is isolated from the pumping system, then the pressure in the reactor

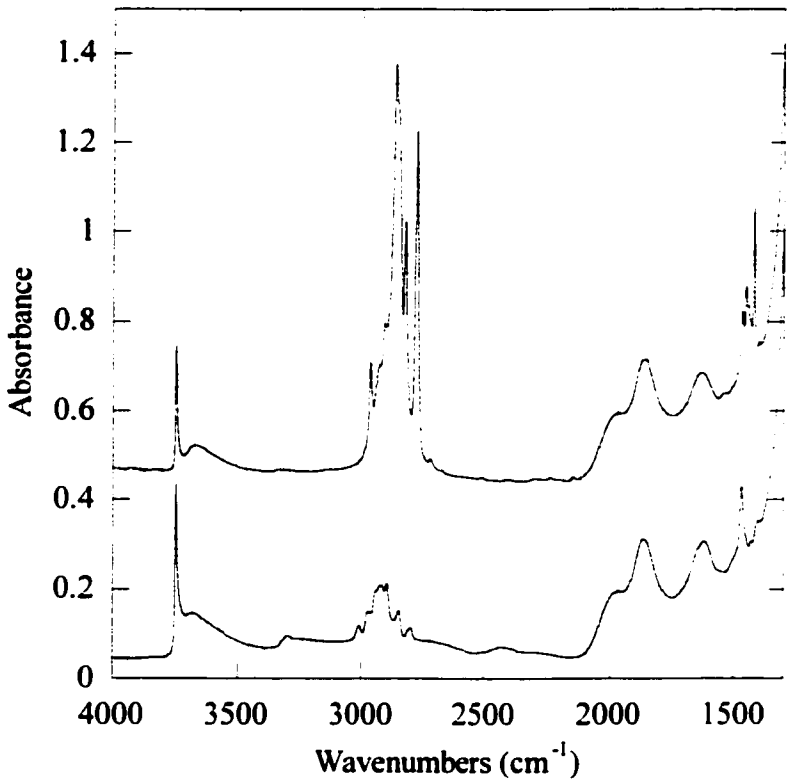

Figure 4.7 *In situ* IR spectra of $(\equiv SiO)_2Ti(NMe_2)_2$ (0.71 wt. % Ti). (a) before, and (b) after 900 minutes dynamic evacuation.

Table 4.1 Zero-order rates of transformation of $(\equiv SiO)_2Ti(NMe_2)_2$ at room temperature under dynamic vacuum

Mass SiO_2 (mg)	wt. % Ti	μmol Ti	mmol Ti/g	μmol OH remaining	μmol OH/g remaining	k_{obs} μmol Ti/min
52.6	1.80	19.79	0.376	5.69	0.108	0.013
35.8	1.76	13.16	0.368	4.47	0.125	0.004
30.6	1.63	10.42	0.340	5.48	0.179	0.016
21.2	1.3	5.76	0.272	6.72	0.317	0.022
15.4	1.27	4.08	0.265	5.07	0.329	0.017
17.7	0.67	2.48	0.140	10.3	0.580	0.022
17.8	0.35	1.30	0.073	12.7	0.714	0.005
15.3	0.28	0.90	0.058	11.4	0.743	0.014

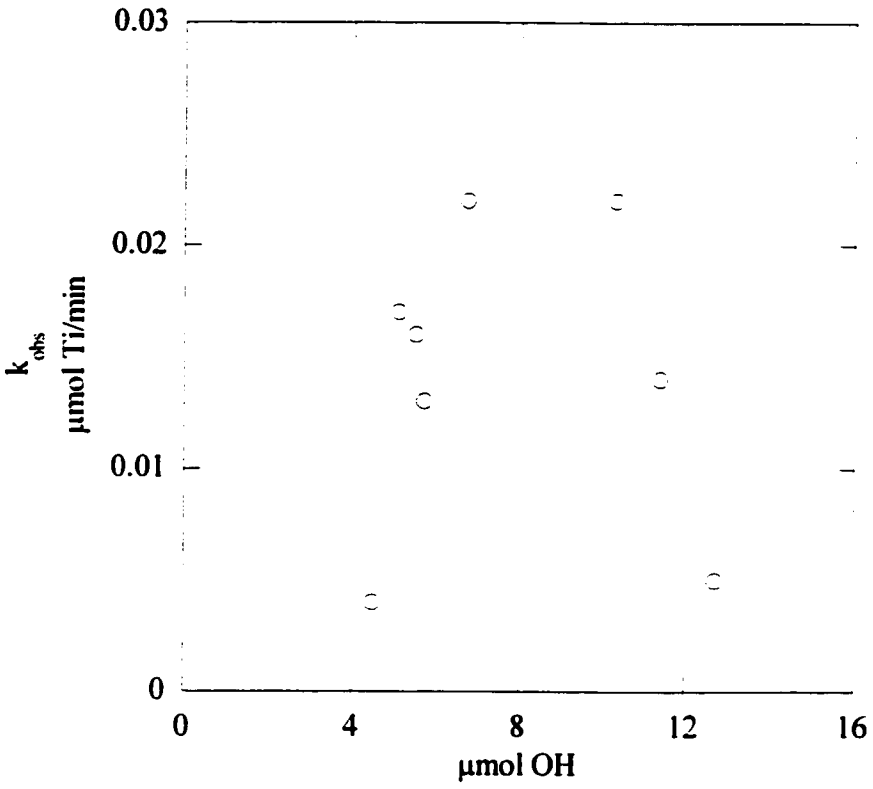

Figure 4.8 Dependence of k_{obs} for the spontaneous transformation of $(\equiv SiO)_2Ti(NMe_2)_2$ on the number of unreacted hydroxyls present on the silica pellet.

increases over the course of the reaction, to a final value of ca. 0.5 Torr. Reaction profiles for the transformation of similar samples of **5** under dynamic vacuum (13.1 mg SiO_2, 0.71 wt. % Ti) and static vacuum (14.2 mg SiO_2, 0.84 wt. % Ti) are shown in Figure 4.9. Both are zero-order. The value of k_{obs} decreases slightly, from (0.00223 ± 0.00002) min^{-1} to (0.00180 ± 0.00009) min^{-1}, when the reactor is isolated, despite the pressure change of four orders of magnitude.

4.4 Mechanism of N-methylmethanimine complex formation

The observation of overall zero-order kinetics for the transformation of **5** to **7**, combined with the catalytic role of the surface hydroxyls, is consistent with a Michaelis-Menten-type mechanism consisting of two consecutive reactions:

$$A + B \underset{k_{-1}}{\overset{k_1}{\rightleftharpoons}} A \cdot B \xrightarrow{k_2} A + C \qquad (4.8)$$

where A is the catalyst (hydroxyl) which converts reagent B to product C. The rate law for this mechanism is

$$-\frac{d[B]}{dt} = \frac{k_1 k_2 [B][cat]}{k_{-1} + k_1[B]} \qquad (4.9)$$

where [cat] = [A] + [A·B]. One limiting form of this rate law, under conditions such that $k_1[B] \gg k_{-1}$, is

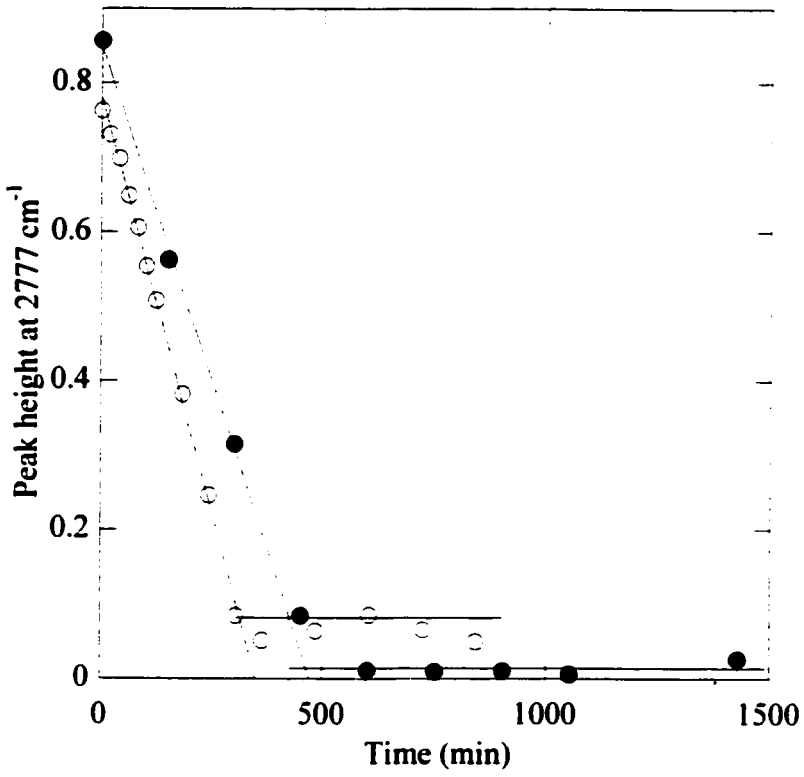

Figure 4.9 Time-resolved evolution of $(\equiv SiO)_2Ti(NMe_2)_2$ under static vacuum (14.2 mg SiO_2, 0.84 wt. % Ti, filled circles); dynamic vacuum (13.1 mg SiO_2, 0.71 wt. % Ti, open circles).

$$-\frac{d[\mathrm{B}]}{dt} = k_2[\mathrm{cat}] = k_{obs} \qquad (4.10)$$

i.e., the rate of the reaction is independent of the concentration of B, or pseudo-zero-order.

A mechanism consistent with this rate law is shown in Scheme 4.1. Reversible addition of a surface hydroxyl across one of the Ti-N bonds of **5** generates coordinated dimethylamine, and a five-coordinate Ti site which then undergoes β-H abstraction to regenerate the surface hydroxyl. Provided $k_1[\mathbf{5}] \gg k_{-1}$, the expected rate law is

$$-\frac{d[\mathbf{5}]}{dt} = k_2 n_{OH} = k_{obs} \qquad (4.11)$$

in agreement with the observed behaviour. Catalysis of this surface reaction by hydroxyls requires their ready migration across the silica surface from one grafted Ti site to another. Although proton mobility on silica surfaces is well-established, mobility of hydroxyl groups is more difficult to document. It may be facilitated by the presence of the grafted metal complexes, Scheme 4.2.[13]

It is interesting that intramolecular β-H abstraction is spontaneous for **5** but not for **1**. Scheme 4.1 shows an increase in coordination number precedes imine formation. It may be that the required transition state, which requires considerable distortion of the dimethylamide ligand, cannot be achieved in the more sterically congested complex **1**. It is also possible that coordination of a third siloxo ligand renders the Ti more electrophilic and the C-H bond more acidic, thereby facilitating proton abstraction.

Scheme 4.1 Proposed mechanism for the transformation of $(\equiv SiO)_2Ti(NMe_2)_2$, **5**, into $(\equiv SiO)_2Ti(\eta^2\text{-}CH_2NCH_3)$, **7**.

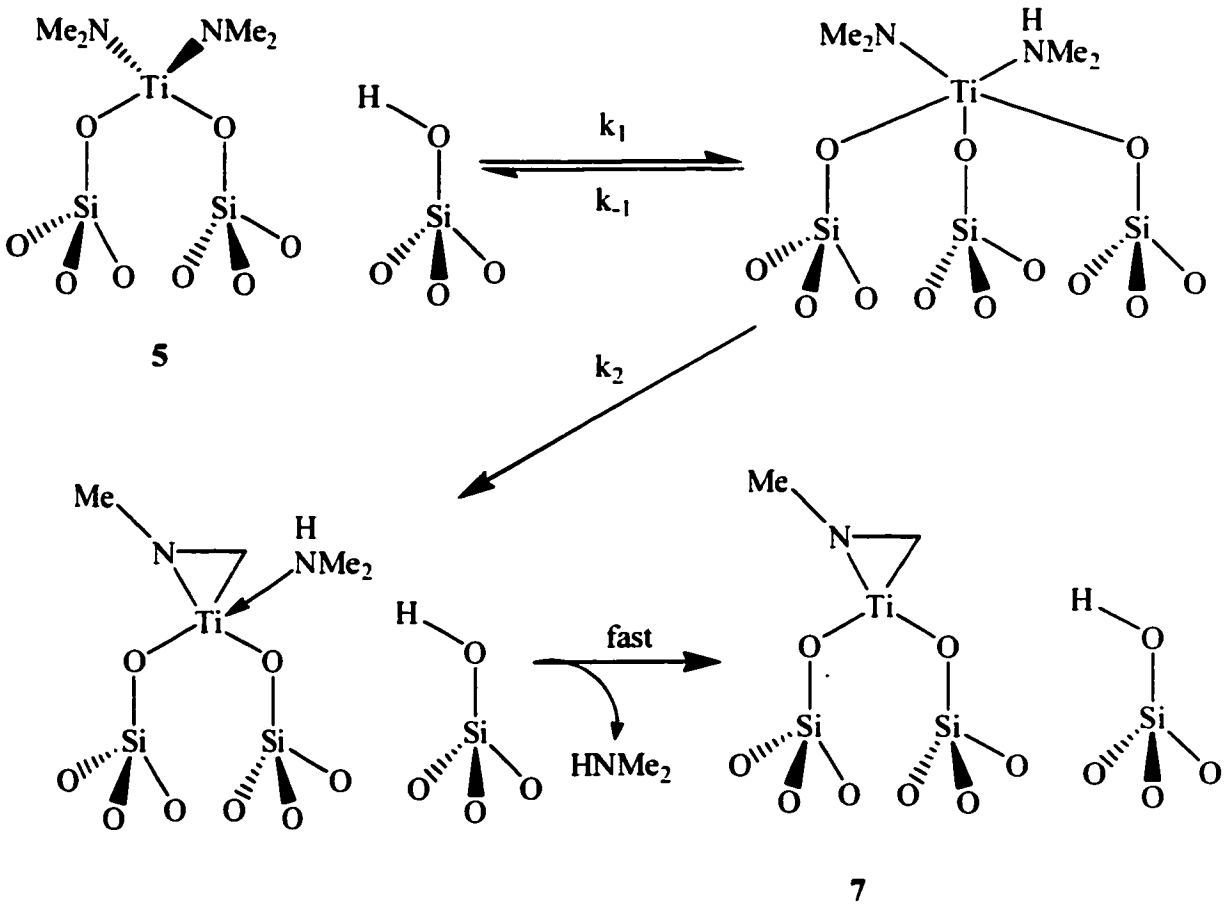

Scheme 4.2 Surface hydroxyl group migration. facilitated by a grafted metal complex.

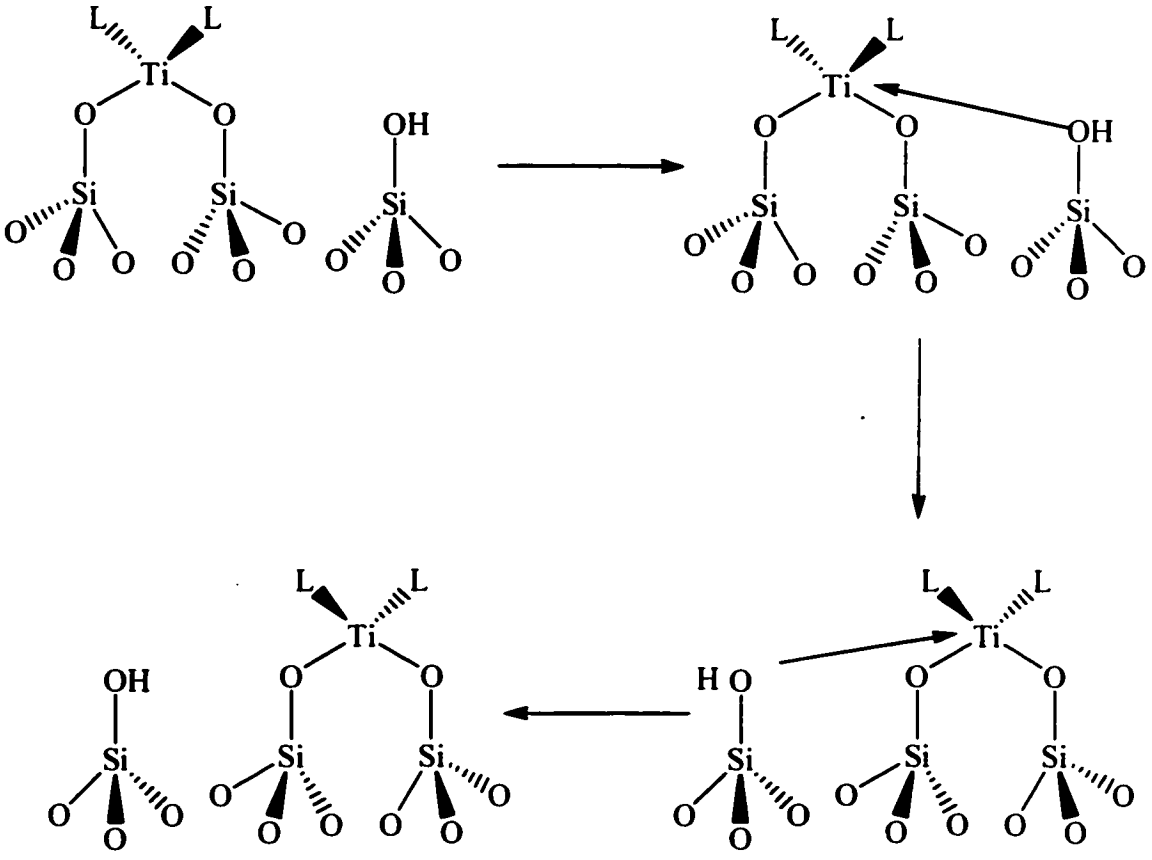

4.5 Spontaneous transformation of $(\equiv SiO)_2Ti(NEt_2)_2$, 6

Upon consumption of the surface hydroxyl groups of partially dehydroxylated silica via reaction with **2**, a monolayer of **6** is present upon the surface, with a titanium content corresponding to ca. 2 wt. %. Complex **6** is significantly more stable than **5** under static vacuum: it can be left standing for longer periods of time (ca. 16 hours) with no noticeable change in either the ν(C-H) or $\delta(CH_3)$ regions of its IR spectrum. However, upon heating or exposure to dynamic vacuum (ca. 10^{-5} Torr), there are substantial changes both in the appearance, Figure 4.10, and the intensity, Figure 4.11, of the stretching and deformation regions.

The final IR spectrum contains reproducibly (27 ± 4) % of the ν(C-H) intensity initially present on the surface (average of 5 experiments). Volatiles produced during this transformation were trapped in liquid N_2. GC and GC/MS analysis showed the presence of two volatile products, $HNEt_2$ and C_2H_4. *In situ* IR quantitation revealed the presence of 0.8 $HNEt_2$ and 0.5 C_2H_4 per grafted Ti.

Calcination of the resulting solid in O_2 resulted in the complete removal of all remaining hydrocarbon fragments from the surface, and generated 1.8 CO_2 per Ti present on the surface. On the basis of these results, we propose that **6** is transformed to the ethylimido complex **8**, eq 4.12:

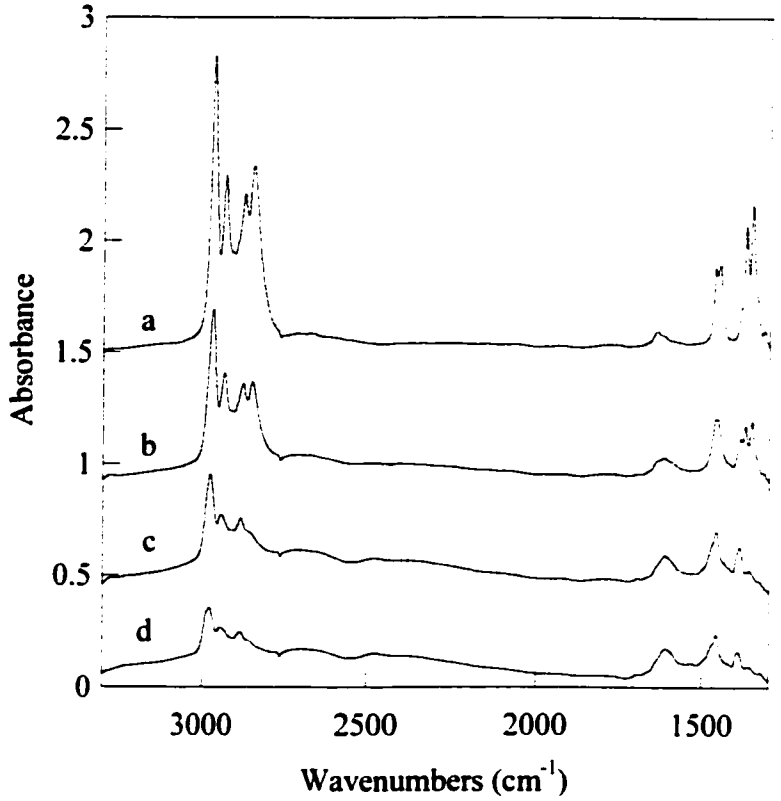

Figure 4.10 In situ IR difference spectra recorded after dynamic evacuation of $(\equiv SiO)_2Ti(NEt_2)_2$ **(6)** at room temperature for: (a) 0 h; (b) 3 h; (c) 6 h; (d) 42 h..The silica background spectrum has been subtracted and the spectra vertically offset.

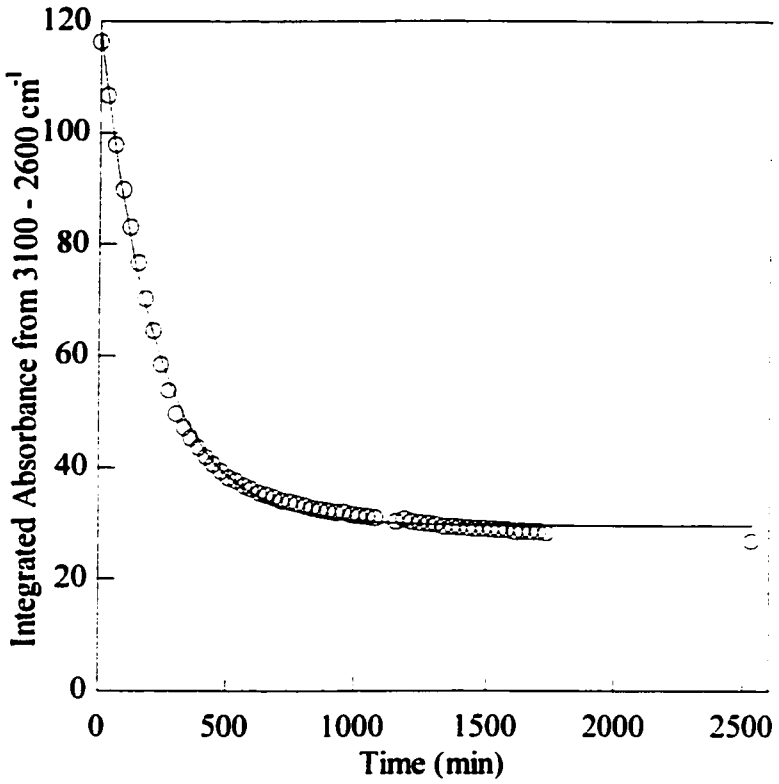

$A_t = A_\infty + (A_0 - A_\infty)e^{-kt}$	
A_∞	29.5 ± 0.2
A_0	118.1 ± 0.8
k (min^{-1})	0.0451 ± 0.0001

Figure 4.11 Time-resolved evolution of $(\equiv SiO)_2Ti(NEt_2)_2$, **6**, at room temperature under dynamic vacuum, monitored as the integrated absorbance from 3100 to 2600 cm^{-1}.

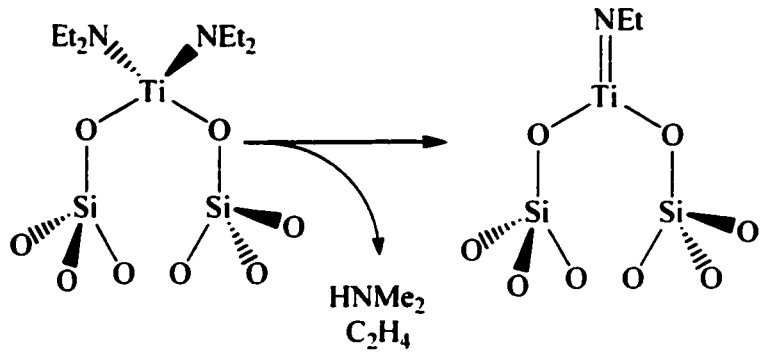

(4.12)

6 **8**

Complete recovery of the C_2H_4 expected from the transformation of **6** to **8** proved difficult. Its low boiling point (-169°C) is close to that of the liquid nitrogen cold trap (-196°C) which was used to trap the volatiles.

The ^{13}C CP/MAS NMR spectrum of **8** is qualitatively indistinguishable from that of **6**. Therefore, evidence for the proposed formulation of **8** was sought through its reactivity. Exposure of **8** to $(CD_3)_3COD$ resulted in no change in the IR spectrum. Exposure of **8** to $^tBuNH_2$ resulted in the liberation of a single gas phase product, H_2NEt, verified by GC and GC-MS. The formation of this product is consistent with metathetical displacement of the ethylimido ligand, eq 4.13:

$$(\equiv SiO)_2Ti{=}NEt + H_2N^tBu \rightarrow (\equiv SiO)_2Ti{=}N^tBu + H_2NEt \qquad (4.13)$$

8

Imido-ligand metathesis to produce new imidotitanium complexes is well known. For example, reaction of $TiCl_2(py)_3(N^tBu)$ with aniline results in the formation of $^tBuNH_2$ and

$TiCl_2(py)_3(NPh)$.[14] Imido-group exchange was also used in the synthesis of a series of imidotitanium complexes by Mountford, eq 4.14.[15]

$$[Ti(N^tBu)Cl_2py_3] + H_2NAr \rightarrow [Ti(NAr)Cl_2py_3] + H_2N^tBu \qquad (4.14)$$

where Ar = phenyl, methylphenyl, nitrophenyl, 2,6-diisopropylphenyl, or 2,6-dimethylphenyl.

4.6 Kinetics of ethylimido complex formation

As the plot of integrated ν(C-H) absorbance shows, Figure 4.11, the transformation of **6** to **8** follows first-order kinetics. Therefore, the rate law for the transformation can be written as follows:

$$-\frac{d[\mathbf{6}]}{dt} = k[\mathbf{6}] \qquad (4.15)$$

At room temperature with a fully loaded sample of **6** (1.85 wt. % Ti, 22.7 mg SiO_2), the rate constant is 0.0045 ± 0.0001 min^{-1}.

The titanium loading on the silica pellet plays a role in the rate of transformation of 6, as in the transformation of **5**. A decrease in the Ti loading from 1.77 wt. % Ti to 1.30 wt. % Ti results in an increase in the rate constant from 0.0045 min^{-1} to 0.0055 min^{-1}, Figure 4.12. In the

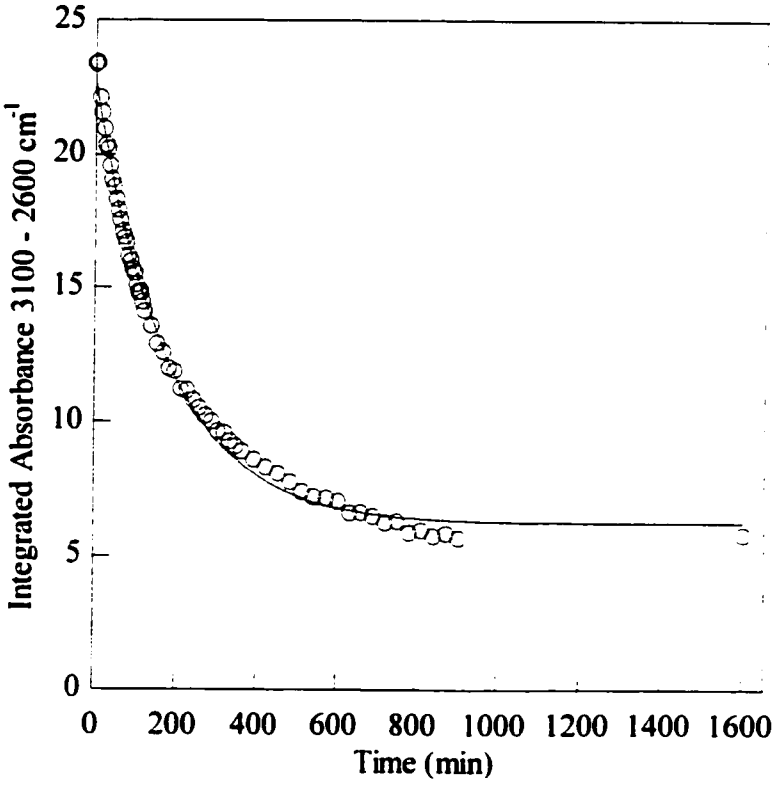

$A_t = A_\infty + (A_0 - A_\infty)e^{-kt}$	
A_∞	6.1 ± 0.1
A_0	22.6 ± 0.2
k (min^{-1})	0.0055 ± 0.0002

Figure 4.12 Time-resolved room temperature dynamic evacuation of $(\equiv SiO)_2Ti(NEt_2)_2$ (1.30 wt. % Ti), monitored as the integrated absorbance from 3100 to 2600 cm^{-1}.

latter experiment, 0.32 mmol OH / g are present, while in the former only 0.12 mmol OH / g remain.

Pressure has a much greater effect on the transformation of **6** than it did in the case of **5**. When **6** is maintained under static vacuum, the rate of transformation is much slower than under dynamic vacuum. This phenomenon is illustrated in Figure 4.13, which shows the reaction profile of a sample of $(\equiv SiO)_2Ti(NEt_2)_2$ (1.30 wt. % Ti) which was first held under static vacuum for 15 hours, followed by dynamic evacuation for 15 hours. Examination of the plot reveals two very distinct regions. Over the first 15 hours, the rate of transformation is slow but not zero. The second 15 hours show a much greater rate of transformation.

4.7 Mechanism of diethylamine elimination

Although the transformation of **6** to **8** is kinetically different from the corresponding formation of **7** from **5**, it can still be accommodated by a Michaelis-Menten treatment, eq 4.9, by postulating another limiting form of the rate law, viz., $k_{-1} \gg k_1[B]$. Under these conditions, the rate law becomes

$$-\frac{d[B]}{dt} = \frac{k_1 k_2 [B][cat]}{k_{-1}} = k_{obs}[B] \qquad (4.16)$$

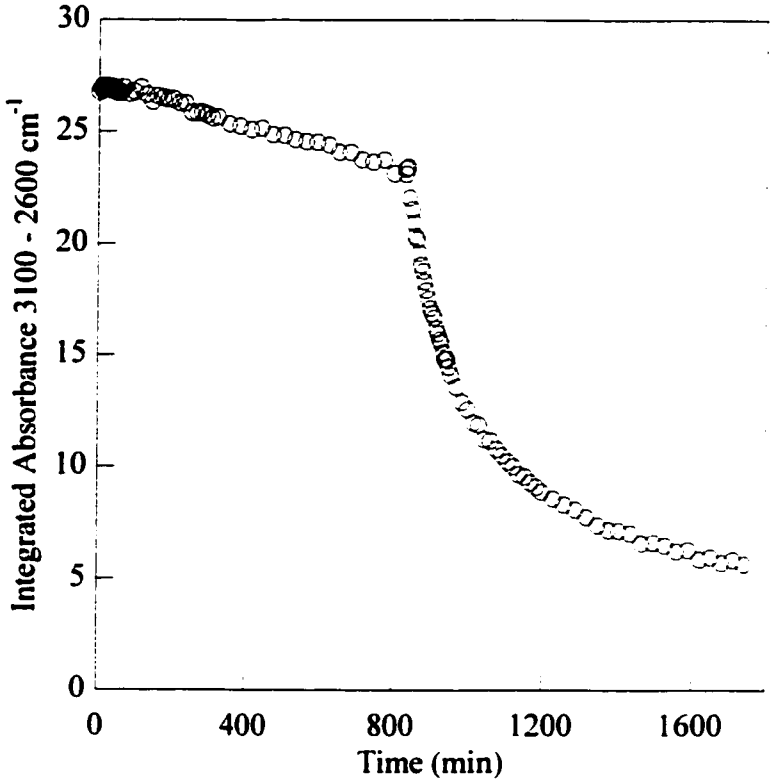

Figure 4.13 Time-resolved room-temperature transformation of $(\equiv SiO)_2Ti(NEt_2)_2$ (1.30 wt. % Ti, 19.7 mg SiO_2) during periods of static (0-900 min) and dynamic (900-1800 min) vacuum.

and is pseudo-first-order. The change in limiting forms of the Michaelis-Menten rate law for thermolysis of 5 vs. 6 amounts to a shift in the position of the preequilibrium, eq 4.17:

$$(\equiv SiO)_2Ti(NR_2)_2 + \equiv SiOH \rightleftharpoons (\equiv SiO)_3Ti(NR_2)(NHR_2) \qquad (4.17)$$

which must lie to the right for **5** and to the left for **6**. This change may be a consequence of steric factors: the smaller dimethylamido ligands can more readily accommodate the coordination of an additional siloxo ligand than can the more bulky diethylamido ligands. The rate law for R = Et thus becomes

$$-\frac{d[\mathbf{6}]}{dt} = k_{obs}[\mathbf{6}], \quad \text{where} \quad k_{obs} = \frac{k_1 k_2 n_{OH}}{k_{-1}}. \qquad (4.18)$$

The proposed mechanism is shown in Scheme 4.3 and is analogous to the suggested mechanism of formation of **7**. However, when R = Et, the η^2-imine complex **9** is not the final product. It rapidly extrudes ethylene to yield the observed ethylimido complex **8**.

The formation of ethylene was reported previously in the distillation of $Ta(NEt_2)_5$.[6] In this case, N-ethylethaniminotris(diethylamido)tantalum(V) was initially isolated, eq 4.5. It is presumably an intermediate in the pathway leading to the thermodynamic product ethylimidotris(diethylamido)tantalum(V), eq 4.19.

$$(Et_2N)_3Ta(CH_3CH{=}NEt) \rightarrow (Et_2N)_3Ta{=}NEt + C_2H_4 \qquad (4.19)$$

Scheme 4.3 Proposed mechanism for the transformation of $(\equiv SiO)_2Ti(NEt_2)_2$ (**6**) into $(\equiv SiO)_2TiNEt$ (**8**)

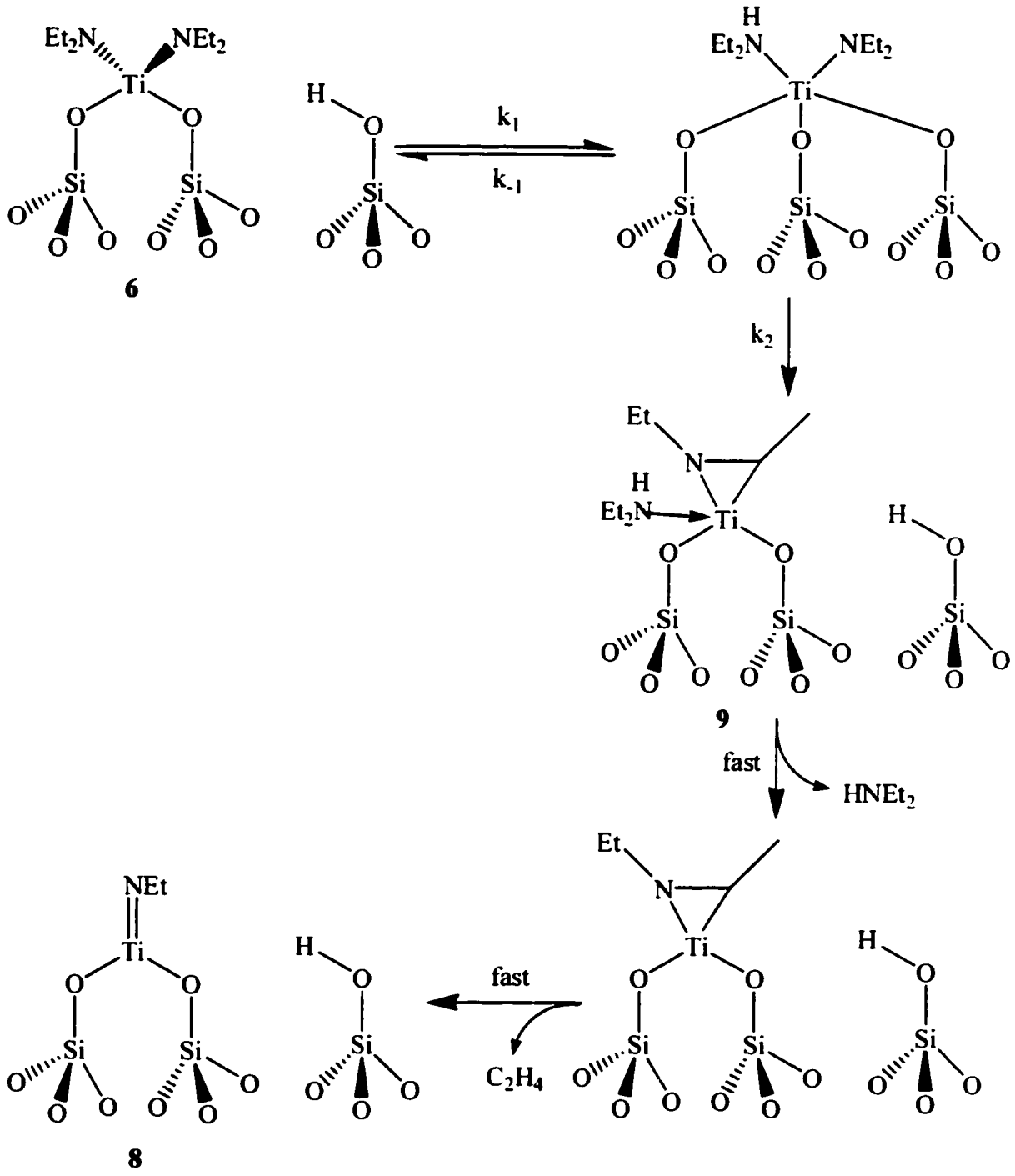

Similarly, in a study of the thermolysis of $V(NEt_2)_4$, Maury reported that the predominant mechanism by which the NEt_2 ligands are removed is intramolecular β-H elimination.[16] The resulting azametallacycle intermediate can then release EtN=CHMe, C_2H_4, or HN=CHMe, Scheme 4.4.

4.8 Conclusion

In this chapter, the spontaneous transformations of two supported bis(dialkylamido)titanium(IV) complexes have been identified and probed. N-methylmethanimine and ethylimido complexes were shown to evolve from $(\equiv SiO)_2Ti(NMe_2)_2$ and $(\equiv SiO)_2Ti(NEt_2)_2$, respectively. Their formation is greatly accelerated by the presence of surface hydroxyls, which play a catalytic role suggested to be addition across a Ti-N bond. The N-methylmethanimine ligand was identified by deuterolysis giving $DN(CH_3)(CH_2D)$, while the ethylimido ligand undergoes exchange with $^tBuNH_2$ to give H_2NEt.

The relevance of these reactions to TiN CVD is two-fold. First, both processes result in the extrusion of HNR_2, which reduces the carbon, nitrogen and hydrogen content of the film. Second, the remaining ligands (N-methylmethanimine and ethylimido) will exhibit different reactivity towards transamination by ammonia than the parent dialkylamido ligands. In the eventuality that they are less readily eliminated, the transformations may result in a greater fraction of the carbon content remaining in the films derived from $Ti(NMe_2)_4$ than from $Ti(NEt_2)_4$ (50% vs. 25%, respectively).

Scheme 4.4 Possible reaction pathways for the thermal decomposition of $V(NEt_2)_4$

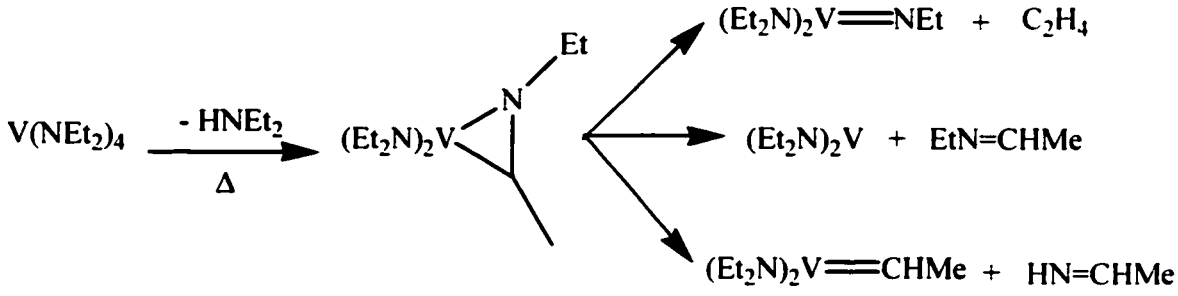

The nature of the transamination of $Ti(NR_2)_4$ by NH_3 is thought to be relatively straightforward. however parent amido (NH_2^-) complexes are rarely isolated. Our attempts to characterize products of the reactions of bis(dialkylamido) complexes **5** and **6** with ammonia. as well as transaminations by other amines, will be reported in Chapter 5 and compared with the transamination behaviour of the N-methylmethanimine and ethylimido complexes.

4.9 References

(1) Beaudoin, M. C.; Womiloju, O.; Fu, A.; Nait Ajjou, J. A.; Rice, G. L.; Scott, S. L. *J. Mol. Cat. A: Chem.* **2002**, in Press.

(2) Amor Nait Ajjou, J.; Rice, G. L.; Scott, S. L. *J. Am. Chem. Soc.* **1998**, *120*, 13436-13443.

(3) Amor Nait Ajjou, J.; Scott, S. L. *Organometallics* **1997**, *16*, 86-92.

(4) Rice, G. L.; Scott, S. L. *Langmuir* **1997**, *13*, 1545-1551.

(5) Bouh, A. O.; Rice, G. L.; Scott, S. L. *J. Am. Chem. Soc.* **1999**, *121*, 7201-7210.

(6) Takahashi, Y.; Onoyama, N.; Ishikawa, Y.; Motojima, S.; Sugiyama, K. *Chem. Lett.* **1978**, 525-528.

(7) Norton, E. T.; Amato-Wierda, C. *Chem. Mater.* **2001**, *13*, 4655-4660.

(8) Mayer, J. M.; Curtis, C. J.; Bercaw, J. E. *J. Am. Chem. Soc.* **1983**, *105*, 2651-2660.

(9) Ahmed, K. J.; Chisholm, M. H.; Folting, K.; Huffman, J. C. *J. Am. Chem. Soc.* **1986**, *108*, 989-999.

(10) Norton, P. R.; Bindner, P. E. *Surf. Sci.* **1986**, *169*, L259-L265.

(11) Widdra, W.; Trischberger, P.; Frieb, W.; Menzel, D.; Payne, S. H.; Kreuzer, H. J. *Phys. Rev. B* **1998**, *57*, 4111-4126.

(12) Wehner, S.; Zecho, T.; Küppers, J. *J. Phys. Chem. B* **2001**, *105*, 1799-1804.

(13) Santini, C. C.; Scott, S. L.; Basset, J.-M. *J. Mol. Cat.* **1996**, *107*, 263-271.

(14) Blake, A. J.; Collier, P. E.; Dunn, S. C.; Li, W.-S.; Mountfoford, P.; Shishkin, O. V. *J. Chem. Soc., Dalton Trans.* **1997**, 1549-1558.

(15) Mountford, P. *Chem. Comm.* **1997**, 2127-2134.

(16) Bonnefond, P.; Feurer, R.; Reynes, A.; Maury, F.; Chansou, B.; Choukroun, R.; Cassoux, P. *J. Mater. Chem* **1996**, *6*, 1501-1506.

Chapter 5

Reactivity of titanium amide-modified silicas towards amines

5.1 Introduction

Despite the accepted role of transamination reactions in the deposition of TiN from $Ti(NR)_4$ in the presence of ammonia, studies of reactions between metal dialkylamides and NH_3 are few.[1,2] Solution reactions of titanium dialkylamides with primary and secondary amines are however, well-known. For example, exposure of $Ti(NMe_2)_4$ to excess diethylamine results in partial transamination, eq 5.1:[3]

$$Ti(NMe_2)_4 + 3\ HNEt_2 \rightarrow Ti(NMe_2)(NEt_2)_3 + 3\ HNMe_2 \qquad (5.1)$$

Displacement of the fourth dimethylamido ligand is presumably prohibited for steric reasons. In contrast, reactions of $Ti(NMe_2)_4$ with monoalkylamines H_2NR (R = ^{n}Pr, ^{i}Pr, ^{t}Bu, ^{s}Bu, cyclohexyl) result in the formation of insoluble extended polymers with the formula $Ti(NR)_2$.[3]

Nitrido (N^{3-}), imido (NH^{2-}) and amido (NH_2^-) ligands bridging metal centres have been observed in the ammonolysis of various organometallic derivatives of Ti, Zr, and Hf.[4] The reaction between $Zr(NEt_2)_4$ and NH_3 was suggested to proceed as in eq 5.2:

$$Zr(NEt_2)_4 + xs\ NH_3 \rightarrow [Zr(NH_2)_4]_x \rightarrow [Zr(NH)(NH_2)_2]_x \qquad (5.2)$$

After 24 hours at 330 K, a species with the empirical formula $[Zr(NH_2)_2]_x$ was obtained.[1] Ammonolysis of $Ti(NMe_2)_4$ results in absorptions which have been assigned to NH_x fragments of oligomeric intermediates with a $[Ti_2(\mu\text{-}NH)_2]$ core.[4]

5.2 Reactions with dialkylamines

In order to gain a clearer idea of how close the reactivity of silica-supported bis(dialkylamido)titanium(IV) parallels the reactivity of the molecular dialkylamides, simple transamination by dialkylamines was attempted. The reaction of **6** with $HNMe_2$ and the reaction of **5** with $HNEt_2$ were investigated. The expected products are **5** and **6**, respectively, as shown in eq 5.3 and 5.4.

$$(\equiv SiO)_2Ti(NEt_2)_2 + \text{xs } HNMe_2 \rightarrow (\equiv SiO)_2Ti(NMe_2)_2 + 2\ HNEt_2 \qquad (5.3)$$

6 **5**

$$(\equiv SiO)_2Ti(NMe_2)_2 + \text{xs } HNEt_2 \rightarrow (\equiv SiO)_2Ti(NEt_2)_2 + 2\ HNMe_2 \qquad (5.4)$$

5 **6**

Barring steric effects, the extent of transamination should be driven mainly by Lechatelier's principle, since the basicities of the two amines are similar (pK_b of 3.00 for $HNEt_2$ and 3.27 for $HNMe_2$) and we assume that the amide basicities are likewise close. As shown in Chapter 3, the IR spectra of **5** and **6** are different in the ν(C-H) region, making it simple to monitor the progress of the reaction. The replacement of a diethylamido ligand by dimethylamido should be characterized by the appearance of the intense ν(CH) band at 2777

cm^{-1}. By the same token, the progress of dimethylamido replacement by diethylamido ligands can be followed by the disappearance of this peak, as well as by the appearance of the ν(CH) band at 2966 cm^{-1}.

5.2.1 Reaction between $(\equiv SiO)_2Ti(NEt_2)_2$, 6, and $HNMe_2$

A silica sample fully-loaded with **6** was exposed to a large excess (30 Torr) of $HNMe_2$. After ca. 19 hours, only a small amount of $-NEt_2$ had been exchanged for $-NMe_2$, as judged by the appearance of a small peak at 2777 cm^{-1}, Figure 5.1. A small ν(NH) peak at 3300 cm^{-1} due to adsorbed amine is also visible. Unexpectedly, longer reaction times resulted in less, rather than more, intensity at 2777 cm^{-1}. After 48 hours, the integrated intensity of the ν(CH) region had decreased by 48% relative to the initial spectrum of **6**, and the spectrum no longer resembles that of either $(\equiv SiO)_2Ti(NEt_2)_2$ or $(\equiv SiO)_2Ti(NMe_2)_2$. Rather, it appears that added amine induces β-H elimination, eq 5.5:

$$(\equiv SiO)_2Ti(NEt_2)_2 + HNMe_2 \rightarrow (\equiv SiO)_2Ti(CH(CH_3)NEt)/(\equiv SiO)_2Ti(CH_2NMe)$$
$$\mathbf{6} \qquad\qquad + HNMe_2/HNEt_2 \qquad (5.5)$$

5.2.2 Reaction between $(\equiv SiO)_2Ti(NMe_2)_2$, 5, and $HNEt_2$

Six hours after addition of a large excess of $HNEt_2$ to a silica sample fully loaded with **5**, a small increase in the ν(CH) band at 2966 cm^{-1} was observed, while the band at 2777 cm^{-1} had

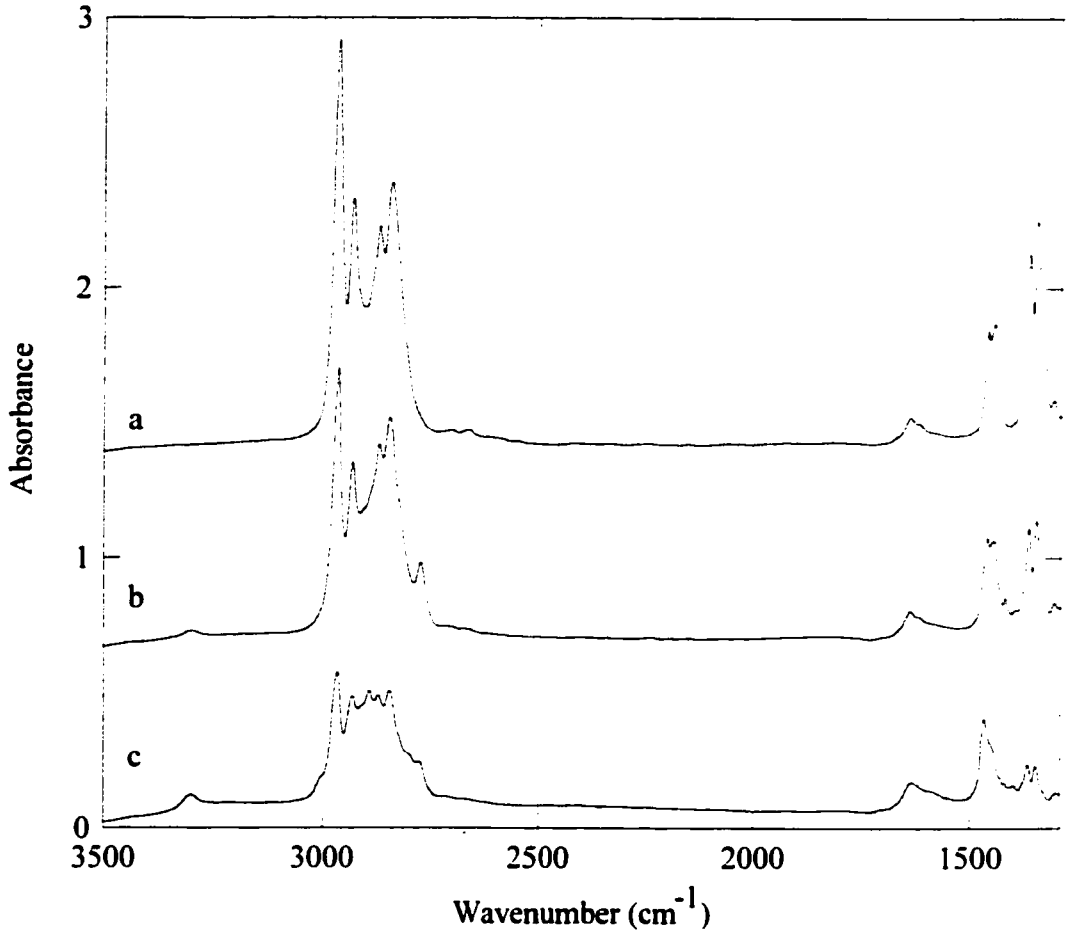

Figure 5.1 Spectra of (a) $(\equiv SiO)_2Ti(NEt_2)_2$; (b) after reaction with 30 Torr $HNMe_2$ for 19 hours; (c) after reaction with $HNMe_2$ for 48 hours. In each spectrum, volatiles have been condensed in liquid nitrogen and a background spectrum of silica-200 has been subtracted and the individual spectra offset.

decreased in intensity, Figure 5.2. Allowing the reaction to proceed overnight resulted in a more dramatic change in the IR spectrum. The peak at 2777 cm^{-1}, indicative of the presence of dimethylamido ligands, disappeared completely, however, the peak at 2966 cm^{-1} of diethylamido ligands did not become more intense. Once again, it appears that the final product is a mixture of imine complexes, eq 5.6:

$$(\equiv SiO)_2Ti(NMe_2)_2 + HNEt_2 \rightarrow (\equiv SiO)_2Ti(CH_2NMe)/(\equiv SiO)_2Ti(CH(CH_3NEt)$$

$$\mathbf{6} \qquad + HNMe_2/HNEt_2 \qquad (5.6)$$

5.3 Reaction with a monoalkylamine

In solution, reaction of tetrakis(dimethylamido)titanium(IV) with monoalkylamines results in the formation of oligomers held together by bridging imido ligands. On the silica surface, reaction of $(\equiv SiO)_2Ti(NR_2)_2$ with RNH_2 is not expected to result in oligomerization because of the immobilization of the titanium centres.

The monoalkylamine chosen to investigate transamination is cyclohexylamine. Its IR spectrum is distinctive in the ν(CH) region, consisting only of CH_2 vibrations (ν_{as} and ν_s at 2930 and 2865 cm^{-1}, respectively). Also, cyclohexylamine is only slightly less basic (pK_b of 3.33) than the dialkylamines being displaced.

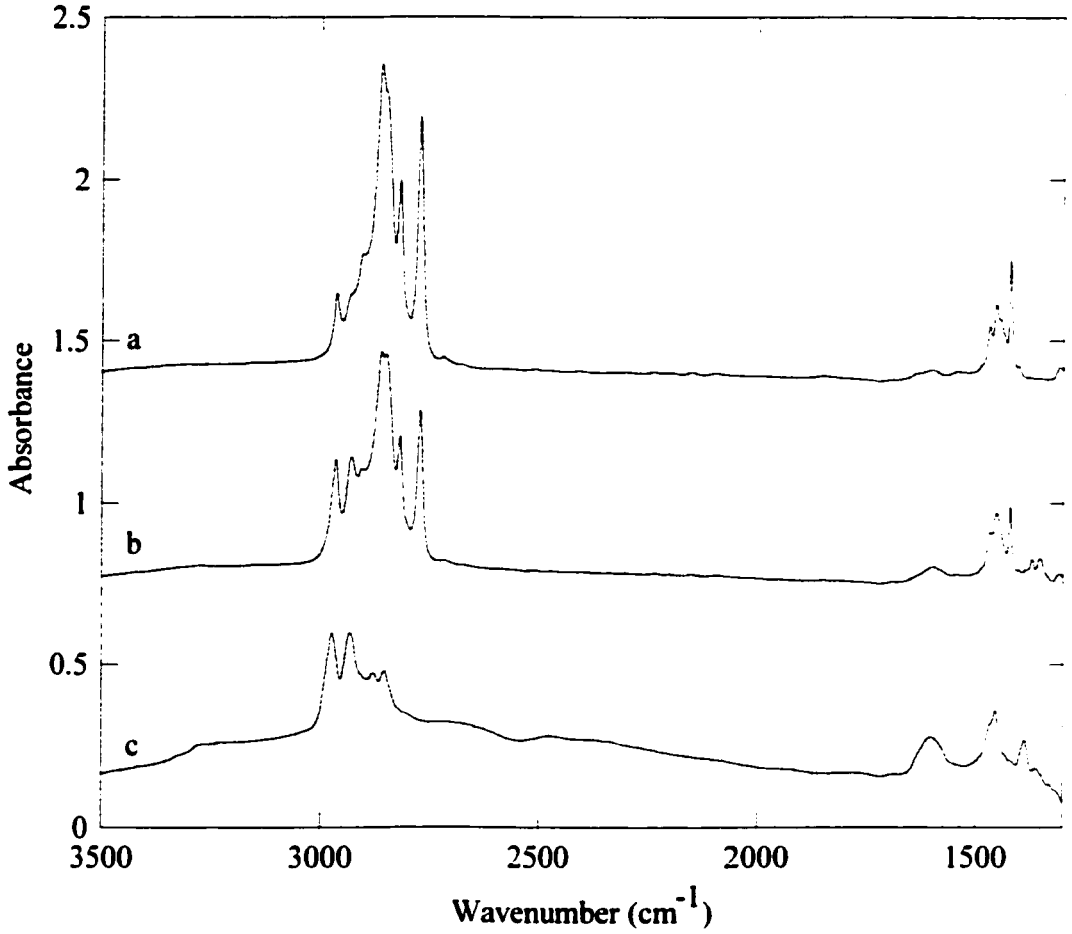

Figure 5.2 Spectra of (a) $(\equiv SiO)_2Ti(NMe_2)_2$; (b) after reaction with $HNEt_2$ for 6 hours; (c) after reaction with $HNEt_2$ overnight (18 hours). In each spectrum, volatiles have been condensed in liquid nitrogen and a background spectrum of silica-200 has been subtracted from each of the spectra and the individual spectra offset.

5.3.1 Reaction of $(\equiv SiO)_2Ti(NMe_2)_2$, 5, with $CyNH_2$

A silica sample fully-loaded with **5** was exposed to an excess of cyclohexylamine vapor. After 60 minutes, a decrease in the intensity of the peak at 2777 cm^{-1} was observed, with a corresponding increase at 2930 and 2856 cm^{-1}, Figure 5.3. A longer exposure time (8 hours) resulted in a further decrease of the characteristic peaks of **5**. The final IR spectrum is dominated by cyclohexyl vibrations.

Evidence for coordinated intact $CyNH_2$ can also be discerned. Two ν(NH) vibrations are present at 3322 and 3280 cm^{-1}, assigned to ν_{as} and ν_s, respectively. Also, two $\delta(NH_2)$ modes are seen at 1593 and 1580 cm^{-1}. ^{13}C CP/MAS NMR, Figure 5.4, shows three signals. The peaks at 45 and 38 ppm can be assigned to the ipso and ortho carbons, respectively, of the cyclohexyl ring, by comparison to the solution spectrum of cyclohexylamine (50.0 and 36.5 ppm for the ipso and ortho carbons, respectively). The peak at 26 ppm is assigned to both meta and para carbons of the cyclohexyl ring. In solution, these carbons resonate at 25.3 (meta) and 24.8 (para) ppm.

In order to probe the nature of the ligands present, the sample was exposed to $(CD_3)_3COD$ vapour. The alcohol is expected to displace amine ($CyNH_2$) and amido (CyNH) ligands, but not imido (CyN) ligands. (Recall from Chapter 3 that $(\equiv SiO)_2Ti{=}NEt$ is stable in the presence of $(CD_3)_3COD$.) A sample of **5** which had been exposed to cyclohexylamine was subjected to a large excess of ^tBuOD. After removal of volatiles, the IR spectrum shown in Figure 5.5 was recorded. The appearance of ν(CD) vibrations of the coordinated alcohol is accompanied by a decrease in intensity of the ν(CH) vibrations of cyclohexyl groups, as well as the complete disappearance of ν(NH) and $\delta(NH_2)$ vibrations. From this, we infer the

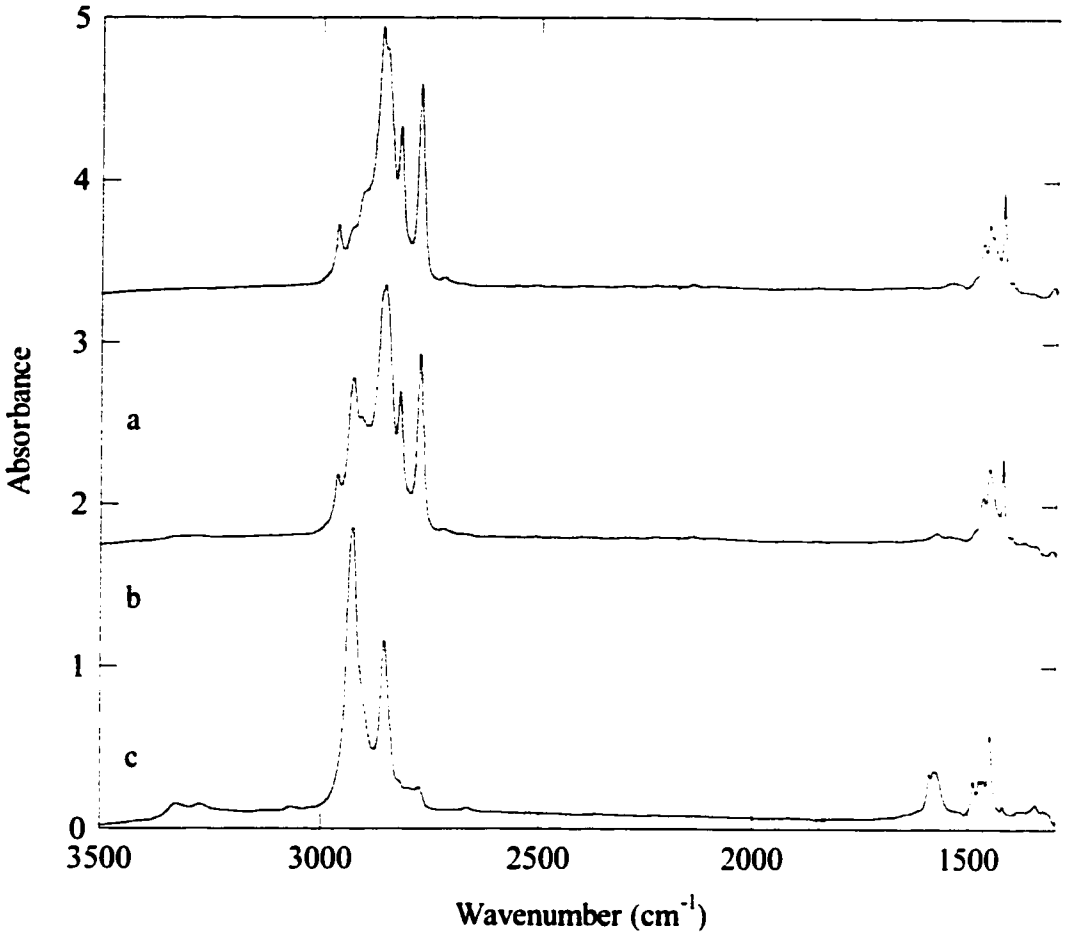

Figure 5.3 Spectra of (a) $(\equiv SiO)_2Ti(NMe_2)_2$; (b) after reaction with $CyNH_2$ for 60 minutes; (c) after reaction with $CyNH_2$ overnight (8 hours). In each spectrum, volatiles have been condensed in liquid nitrogen and a background spectrum of silica-200 has been subtracted from each of the spectra and the individual spectra offset.

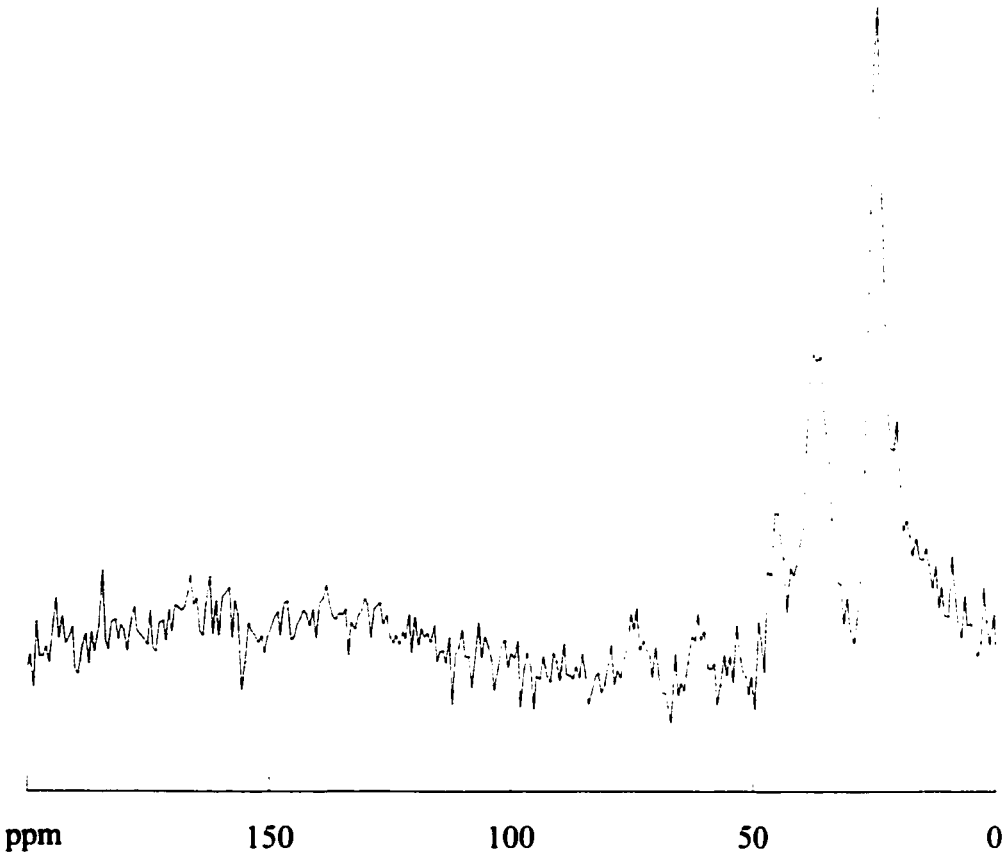

Figure 5.4 ^{13}C CP/MAS NMR spectrum of **5** after reaction with $CyNH_2$, spin rate 4 kHz.

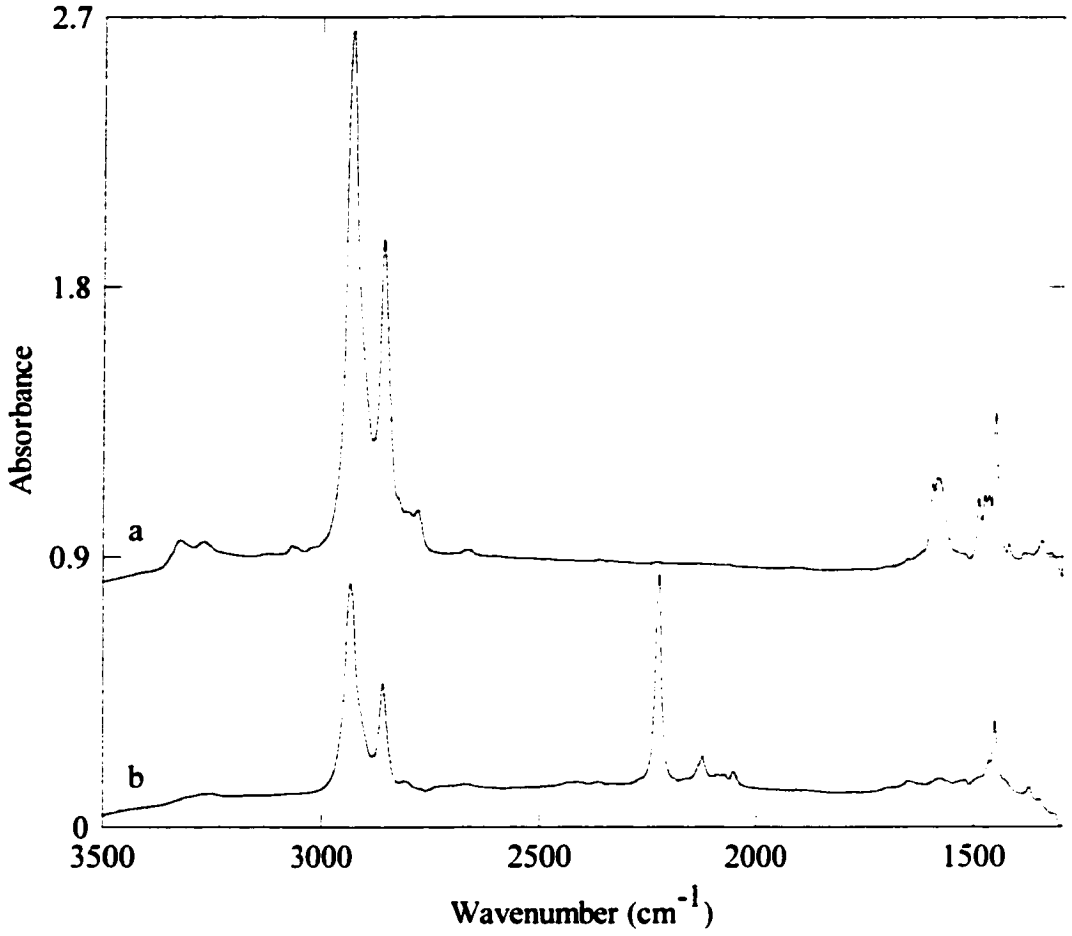

Figure 5.5 Spectrum of (a) **5** after reaction with cyclohexylamine; and (b) after addition of $(CD_3)_3COD$. All volatiles have been removed, a background spectrum of silica-200 has been subtracted from each spectrum and the individual spectra offset.

displacement of coordinated cyclohexylamine. The retention of some cyclohexyl groups on the surface is also evident in the spectrum, presumably as non-displaceable cyclohexylimido ligands. Repeated addition of alcohol, even with heating (70°C), failed to alter the intensity of the remaining ν(CH) bands.

The observed decrease in integrated ν(CH) intensity upon reaction with $(CD_3)_3COD$ is 66%. Therefore the transamination of **5** by $CyNH_2$ is inferred to generate a titanium complex with one (non-displaceable) cyclohexylimido ligand and two (displaceable) coordinated cyclohexylamines, eq 5.7-5.8.

$$(\equiv SiO)_2Ti(NMe_2)_2 + 3\ CyNH_2 \rightarrow (\equiv SiO)_2Ti(=NCy)(NH_2Cy)_2 + 2\ HNMe_2 \qquad (5.7)$$

5

$$(\equiv SiO)_2Ti(=NCy)(NH_2Cy)_2 + 2\ {}^tBuOD \rightarrow (\equiv SiO)_2Ti(=NCy)({}^tBuOD)_2 + 2\ H_2NCy \qquad (5.8)$$

Therefore transamination proceeds as expected for $CyNH_2$, by analogy to the molecular reactivity of titanium dialkylamides.

5.3.2 Reaction of $(\equiv SiO)_2Ti(NEt_2)_2$, 6, with $CyNH_2$

Similar observations were made upon the reaction of **6** with cyclohexylamine. A short term (60 min) exposure of a fully-loaded sample of $(\equiv SiO)_2Ti(NEt_2)_2$ to excess cyclohexylamine resulted in a rapid change in the IR spectrum, Figure 5.6, corresponding to loss of ca. 20% of the diethylamido ligands (as judged by the decrease in peak height at 2965 cm^{-1}). Longer exposure

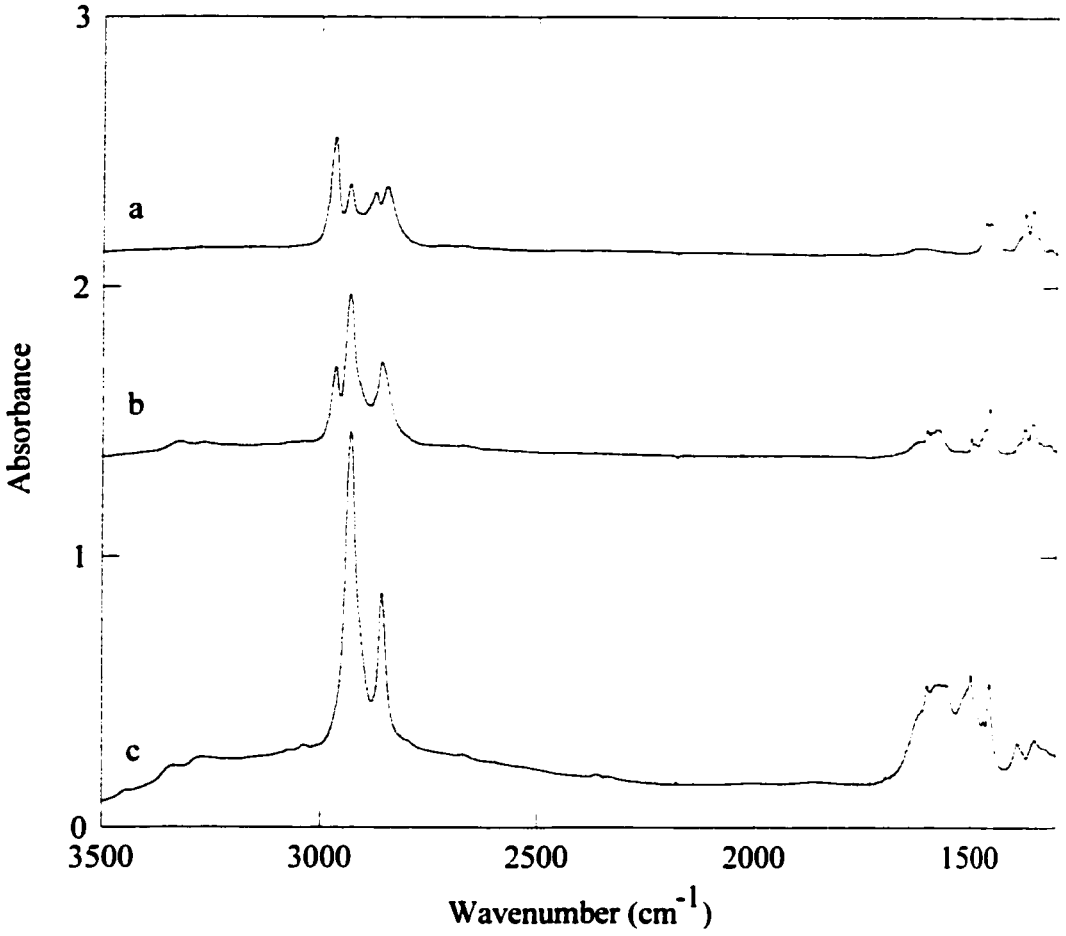

Figure 5.6 Spectra of (a) $(\equiv SiO)_2Ti(NEt_2)_2$, **6**; (b) after reaction with $CyNH_2$ for 60 minutes; (c) after reaction with $CyNH_2$ overnight (18 hours). Prior to recording each spectrum, volatiles were condensed in liquid nitrogen, a background spectrum of silica-200 was subtracted and the individual spectra offset.

(18 hrs) resulted in complete loss of the 2965 cm^{-1} band. The ν(CH) peaks which appear at 2931 and 2958 cm^{-1} correspond to cyclohexyl vibrations. Once again, ν(NH) and δ(NH_2) vibrations suggest the presence of coordinated $CyNH_2$. The reaction is therefore formulated as shown in eq 5.9.

$$(\equiv SiO)_2Ti(NEt_2)_2 + 3\ CyNH_2 \rightarrow (\equiv SiO)_2Ti(=NCy)(NH_2Cy)_2 + 2\ HNEt_2 \qquad (5.9)$$

6

5.4 Reactions with NH_3

Based on the encouraging results of transamination with $CyNH_2$, in which cyclohexylimidotitanium complexes were formed but (presumably) prevented from oligomerizing by the strong Si-O-Ti bonds anchoring the complexs to the silica surface, we undertook to observe transamination by NH_3, expecting to obtain imido (Ti=NH) or even nitrido (Ti≡N) products.

5.4.1 Reaction of $(\equiv SiO)_2Ti(NMe_2)_2$ with NH_3

Exposure of $(\equiv SiO)_2Ti(NMe_2)_2$, **5**, to 35 Torr NH_3 results in a dramatic change in the appearance of the ν(C-H) region of the IR spectrum, Figure 5.7. The modified silica, initially bright yellow, gradually changes to a less intense yellow colour over the course of the reaction.

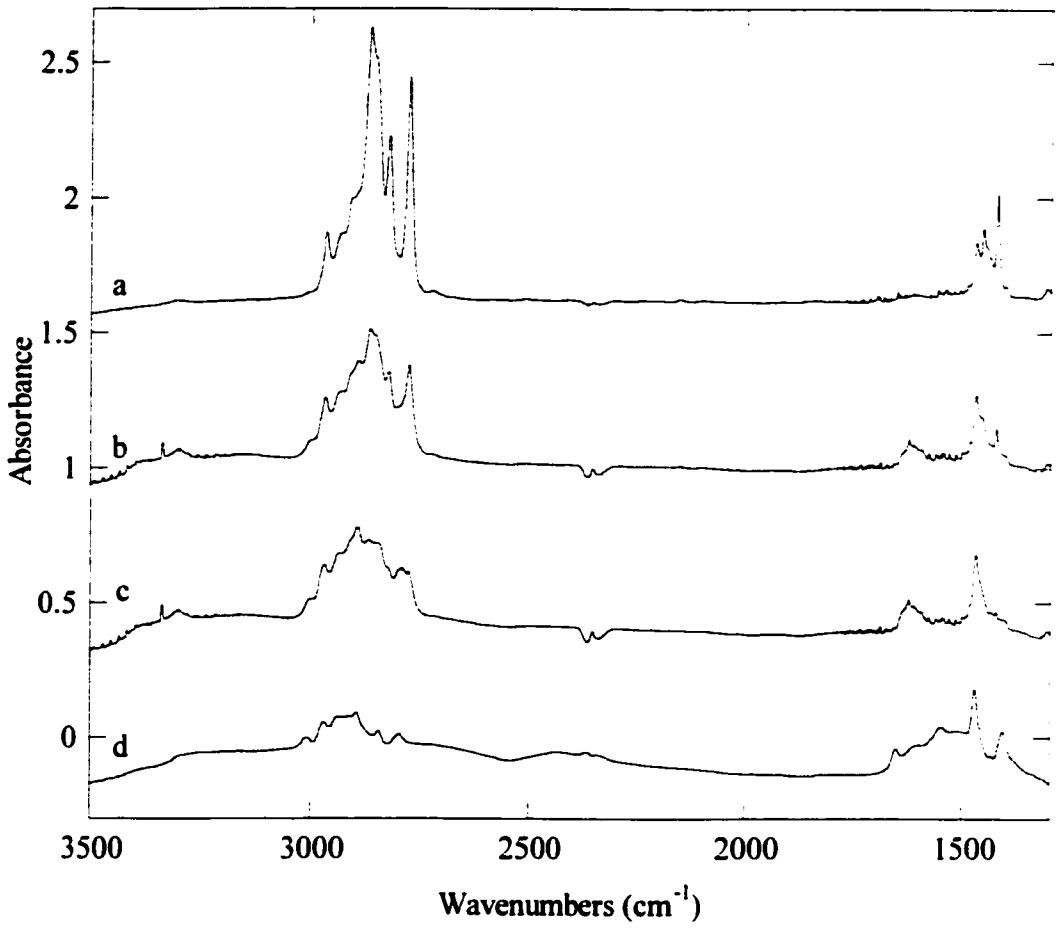

Figure 5.7 *In situ* IR difference spectra recorded during the room temperature reaction between $(\equiv SiO)_2Ti(NMe_2)_2$ and 35 Torr NH_3: (a) before addition of NH_3; (b) 4 hrs; (c) 16 hrs; (f) after 41 hrs reaction time and evacuation of NH_3. A reference spectrum of silica-200 was subtracted from each spectrum and the individual spectra offset.

Once the reaction had reached completion (after ca. 1600 min, as judged by the complete disappearance of the $\nu_s(CH_3)$ peak at 2777 cm^{-1}), volatiles were collected in a liquid nitrogen cold trap. By GC and GC-MS, the sole product of the reaction was determined to be $HNMe_2$. Attempts were made to determine the amount of $HNMe_2$ released during the reaction with NH_3 via *in situ* IR spectroscopy. Surprisingly, we observed that the simultaneous presence of NH_3 in the gas phase alters the intensity of the $HNMe_2$ spectrum. This effect was confirmed by recording the spectrum of 1.2 Torr $HNMe_2$ alone and in the presence of ca. 30 Torr of NH_3. The integrated absorbance in the ν(C-H) region increased by 36% in the presence of NH_3. Since quantitation by IR spectroscopy was not feasible, the $HNMe_2$ liberated through reaction of **5** with NH_3 was analyzed by GC. The recovery of $HNMe_2$ was 0.9 equivalents / Ti.

The presence of NH_3 also has an effect on the intensity and appearance of the ν(CH) region of the IR spectrum of the silica surface, Figure 5.8. After evacuation of the NH_3, the integrated ν(CH) intensity has decreased to 25% of its original value prior to reaction with NH_3. Examination of the final spectrum reveals a striking similarity to the spectrum of **7**, Figure 5.9. Exposure of the resulting surface complex to $(CD_3)_3COD$ resulted in the loss of the remaining ν(C-H) vibrations and the appearance of new ν(C-D) vibrations. *In-situ* IR quantitation showed the formation of 0.9 $HNMe_2$ / Ti. The sole gas phase products of the alcoholysis reaction were ammonia and $HNMe(CH_2D)$, detected by GC/MS ($p+1/p = 0.15$). The degree of deuteration is lower than that seen in the alcoholysis of **7** produced by evacuation. This is presumably due to loss of deuteration in the alcohol through exchange with NH_3 which remains coordinated.

Based on its IR spectrum and its reaction with $(CD_3)_3COD$, the product of reaction of **5** with NH_3 is identified as the N-methylmethanimine complex **7**, eq 5.10:

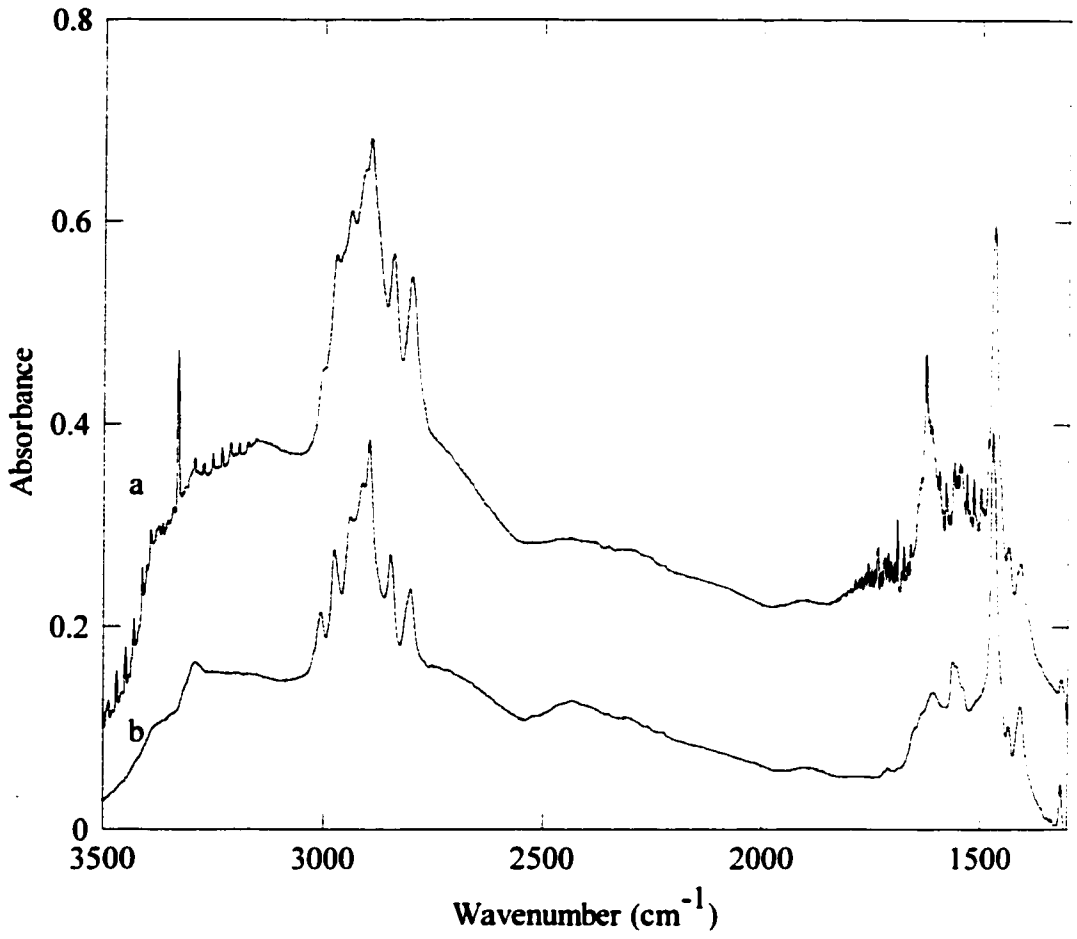

Figure 5.8 IR spectra of **5** (a) after reaction with NH_3 for 38 hours; (b) after removal of volatiles. A background spectrum of silica-200 was subtracted from each of the spectra and the individual spectra offset.

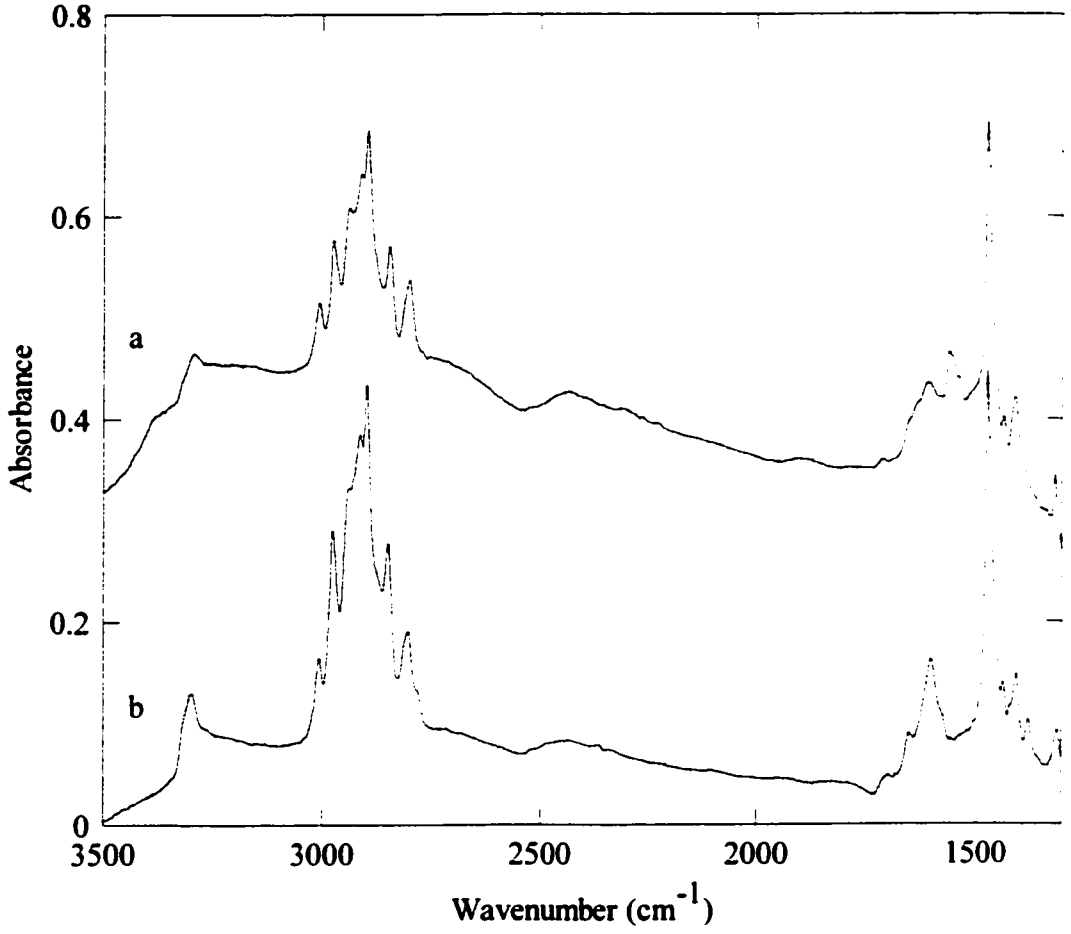

Figure 5.9 Comparison of spectra of $(\equiv SiO)_2Ti(NMe_2)_2$ after exposure to either (a) NH_3: (b) prolonged vacuum. A background spectrum of silica-200 was subtracted from each of the spectra and the individual spectra offset.

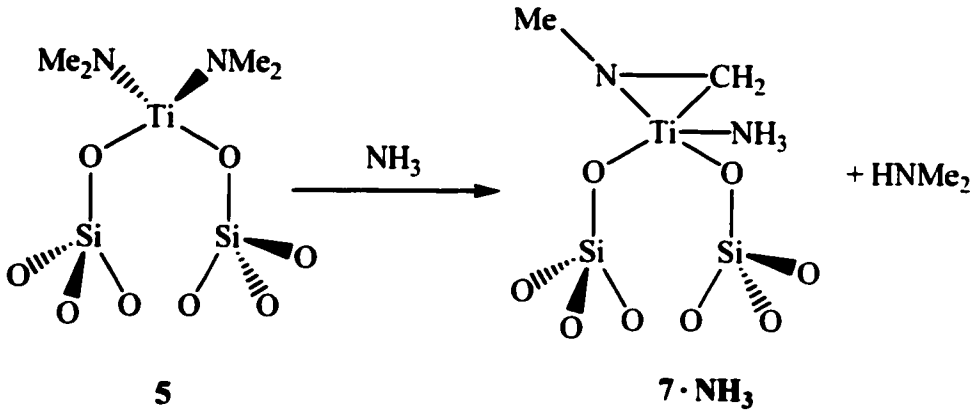

Thus exposure of **3** to an excess of NH_3 does not result in complete removal of carbon from the coordination sphere of Ti by transamination; only 50% is removed. Evacuation of the volatiles followed by repeated exposure to NH_3 does not alter the IR spectrum of the product. A possible mechanism for the NH_3-induced transformation of **5** is shown in Scheme 5.1. In this mechanism, transamination results in the formation of the mixed amide complex $(\equiv SiO)_2Ti(NMe_2)(NH_2)$ with the liberation of 1 eq. of $HNMe_2$ Instead of further transamination or deprotonation of the NH_2 ligand, β-H abstraction from the dimethylamido ligand generates the observed product. (Since NH_3 is regenerated in this step, its role in the transformation of **5** to **7** is catalytic.)

5.4.2 Kinetics

The kinetics of the reaction between $(\equiv SiO)_2Ti(NMe_2)_2$ and NH_3 were monitored by following the decrease in absorbance at 2777 cm^{-1}, Figure 5.10. The addition of 35 Torr of NH_3 at room temperature to a 16.0 mg SiO_2 pellet fully loaded with **5** (2.0 wt. % Ti) resulted in the gradual loss of absorbance shown. The reaction is not pseudo-first order. The data were fit with a biexponential equation yielding two rate constants: (0.0315 ± 0.0008) min^{-1} and (0.00219 ±

Scheme 5.1 Possible mechanism for the reaction of **5** with NH_3

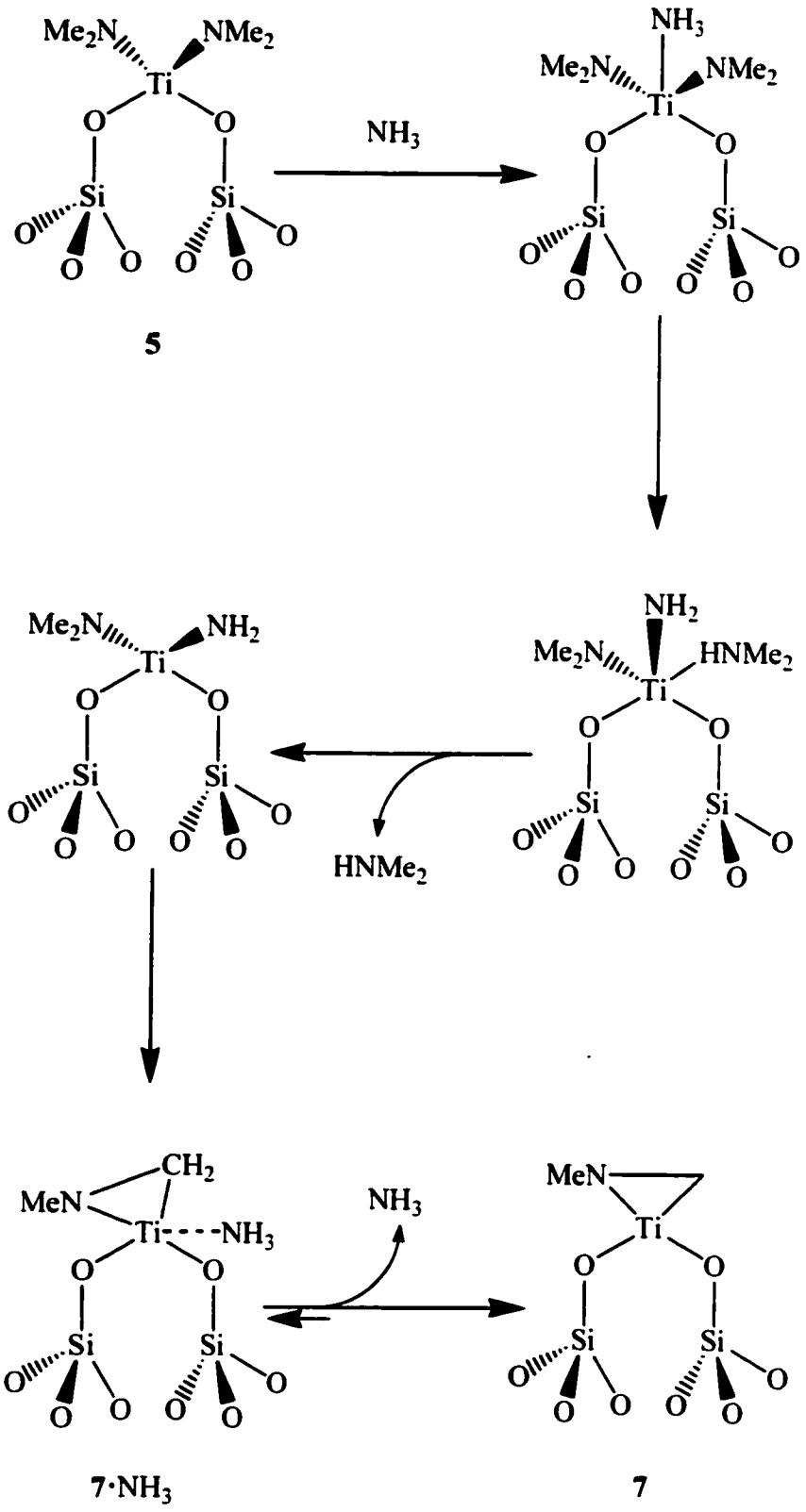

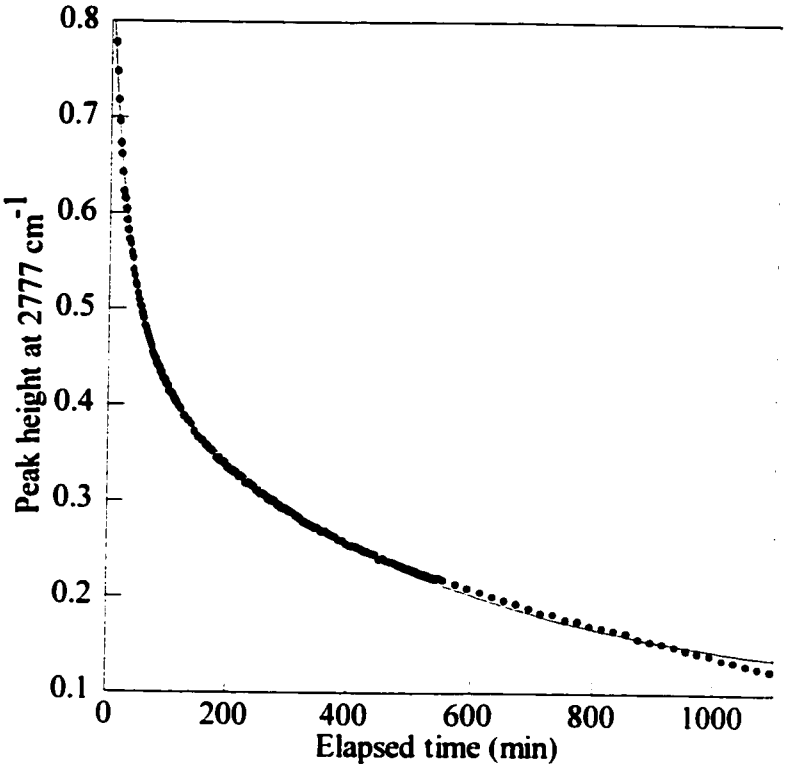

$Abs_t = A_\infty + \alpha e^{-k_1 t} + \beta e^{-k_2 t}$	
Abs_∞	0.103 ± 0.004
α	0.367 ± 0.004
k_1	0.0315 ± 0.0008
β	0.369 ± 0.003
k_2	0.00219 ± 0.00001
Chisq	0.0045017
R	0.99932

Figure 5.10 Time-resolved evolution of the peak height at 2777 cm^{-1} during the reaction between $(\equiv SiO)_2Ti(NMe_2)_2$ and 35 Torr NH_3.

0.00001) min^{-1}. This behaviour is typical of a reaction with consecutive elementary steps. eq 5.12.

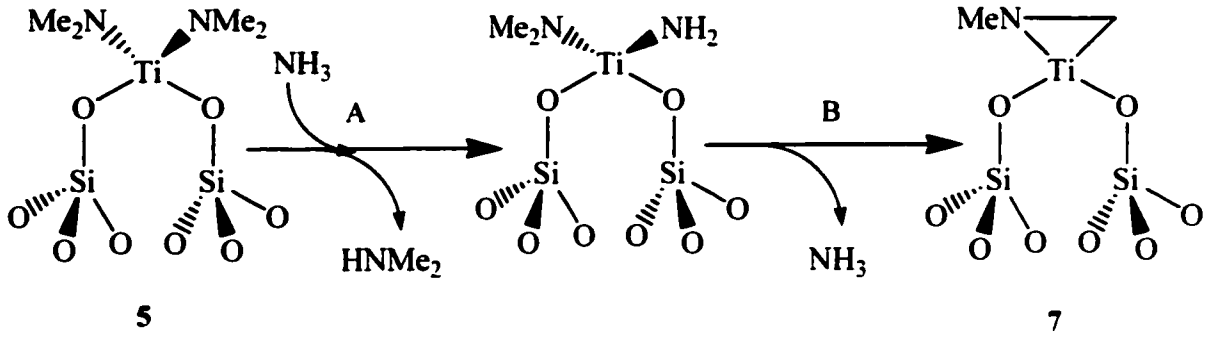

(5.12)

In order to investigate the rate law further, the induced transformation of **5** → **7** was repeated with a different pressure of ammonia. The kinetic profile for the transformation of 22.0 mg SiO_2 loaded with 1.87 wt. % Ti in the presence of 80 Torr NH_3 is shown in Figure 5.11. The reaction is completed in a much shorter time and is closer to pseudo-first order. Interestingly, the rate constants extracted from biphasic fit have increased by much more than the expected factor of two based on the increase in $P(NH_3)$. Although an in-depth study of the kinetics was not pursued, the evidence points to a non-linear effect of $P(NH_3)$ which may effect the C-content of TiN films.

5.5 Reaction of $(\equiv SiO)_2Ti(NEt_2)_2$ with NH_3

Exposure of a fully-loaded sample (2.0 wt. % Ti, 18.5 mg SiO_2) of **6** to 20 Torr NH_3 resulted in a dramatic change in the ν(CH) region of the IR spectrum, which decreased in intensity by 42%

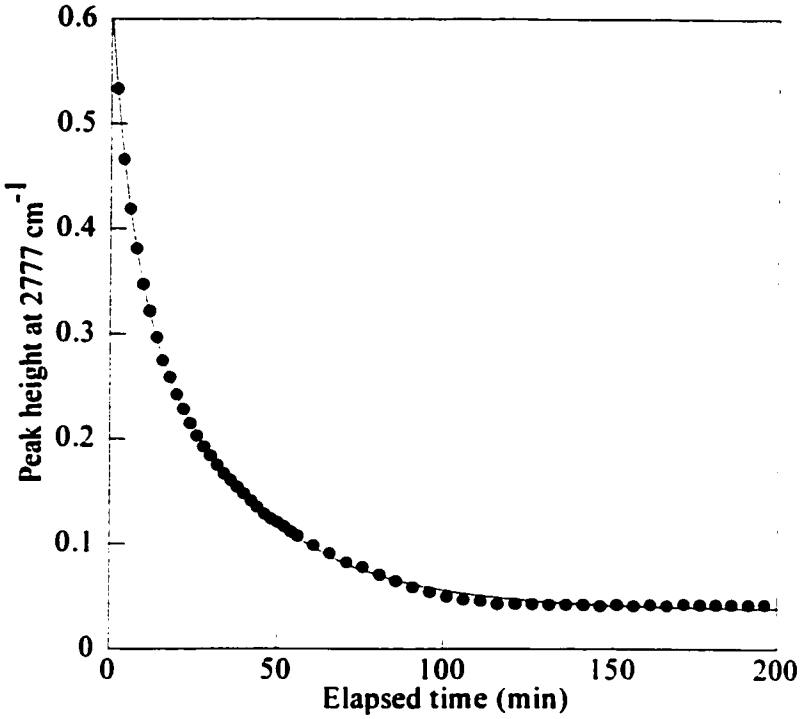

$Abs_t = A_\infty + \alpha e^{-k_1 t} + \beta e^{-k_2 t}$	
Abs_∞	0.0370 ± 0.0008
α	0.223 ± 0.007
k_1	0.1542 ± 0.009
β	0.351 ± 0.008
k_2	0.0292 ± 0.0007
Chisq	0.00036501
R	0.99977

Figure 5.11 Time-resolved evolution of peak height at 2777 cm^{-1} during the reaction of **5** with 80 Torr NH_3. The line is the non-linear least squares curve fit to the biexponential rate equation.

after 3 hours, Figure 5.12. Extending the reaction time to 18 hours resulted in a further, slight decrease in intensity (for a total loss of 51% of the original ν(CH) absorbance). GC analysis of the volatiles showed only the presence of $HNEt_2$ and NH_3. The recovery of $HNEt_2$ was 0.9 equivalents / Ti. Evacuation of the NH_3 produced no change in the IR spectrum. Thus, exposure of **6** to NH_3 does not result in complete removal of the hydrocarbon ligands. Judging by the changes observed in the ν(CH) region, it appears that one of the two diethylamido ligands has been displaced. The loss of 50% of the ν(CH) intensity in the reaction of **6** with NH_3 contrasts with the loss of 75% observed upon prolonged evacuation of **6** (Chapter 4). Further, the absence of C_2H_4 among the volatiles indicates that ammonolysis generates a different product from thermolysis. The IR spectra and quantitative results are consistent with the formation of the N-ethylethanimine complex, eq 5.12.

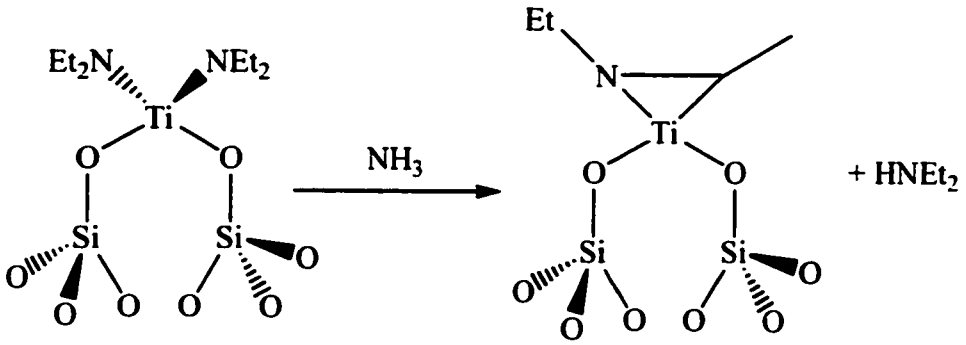

(5.12)

6 **9**

The mechanism for this transformation is proposed to be analogous to that shown in Scheme 5.1, involving initial transamination followed by β-H elimination and extrusion of NH_3.

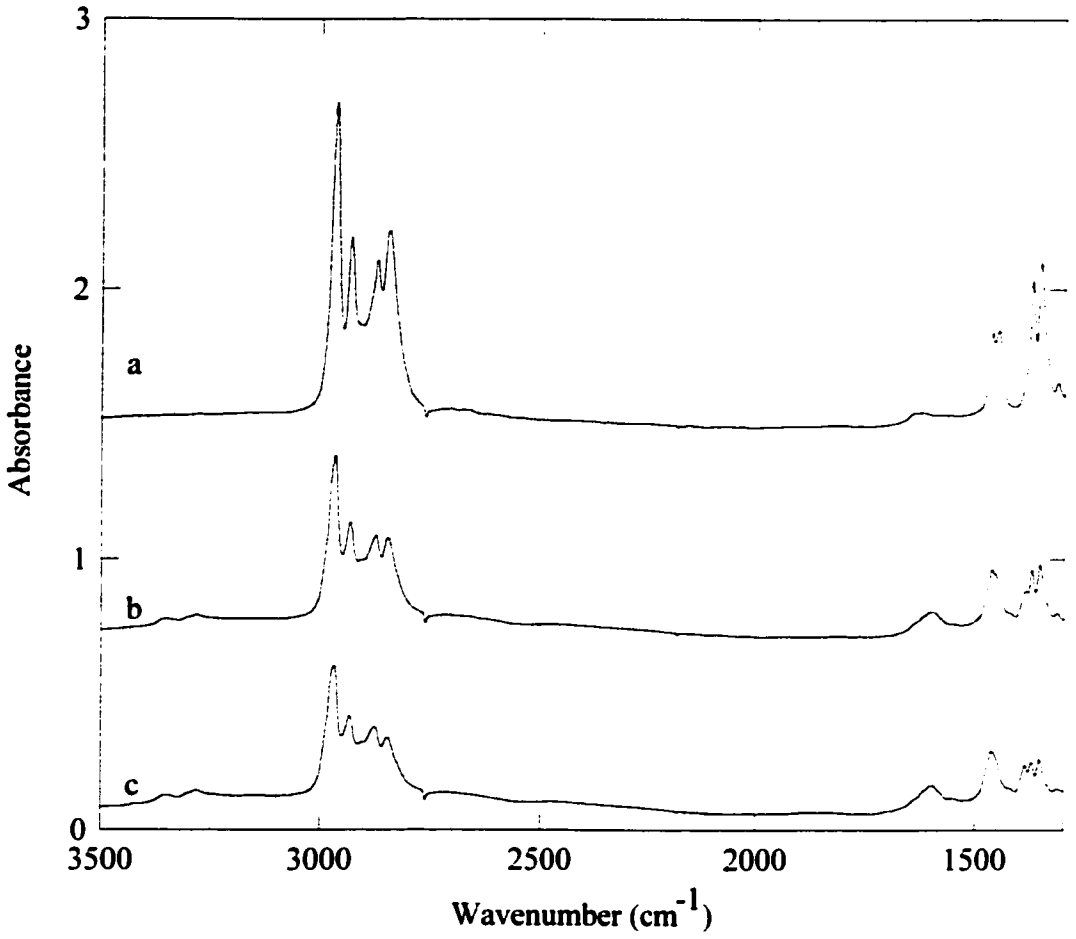

Figure 5.12 In situ IR spectra of (a) $(\equiv SiO)_2Ti(NEt_2)_2$; (b) after exposure for 3 hours to 20 Torr NH_3; and (c) after 18 hours exposure to 20 Torr NH_3. In each spectrum, volatiles have been condensed in liquid nitrogen and a background spectrum of silica-200 has been subtracted from each spectrum and the individual spectra offset.

The nature of **9** was probed by prolonged room temperature evacuation. After 18 hours, the intensity in the ν(CH) region had decreased by half, Figure 5.13. As expected, the integrated absorbance stabilized at 25% of its original value in the initial spectrum of **6**. Thus we infer that the N-ethylethanimine **9** complex extrudes C_2H_4 to generate the ethylimido complex **8**, eq. 5.13.

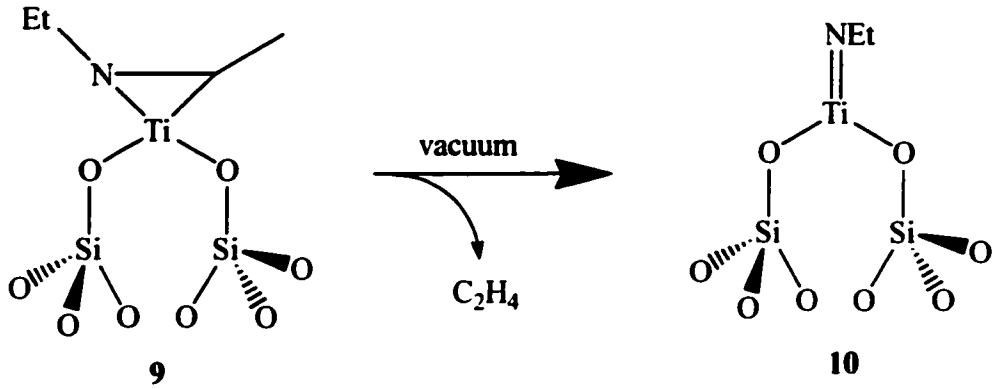

9 **10** (5.13)

The final spectrum is very similar to the spectrum of **8** obtained by thermolysis, Figure 5.14.

5.6 Reactions of $(\equiv SiO)_2Ti(NMe_2)_2$ with aprotic amines

The first step in the reactions of dialkylamines, monoalkylamines and ammonia with $(\equiv SiO)_2Ti(NR_2)_2$ (R = Me, Et) has been proposed to be transamination. However, in the case of the dialkylamines and ammonia, the surface products do not appear to contain amido ligands, therefore the amine acts as a catalyst for the β-H elimination reaction. We therefore decided to investigate whether transamination necessarily precedes β-H elimination, via the reactions of the dialkylamides with aprotic amines.

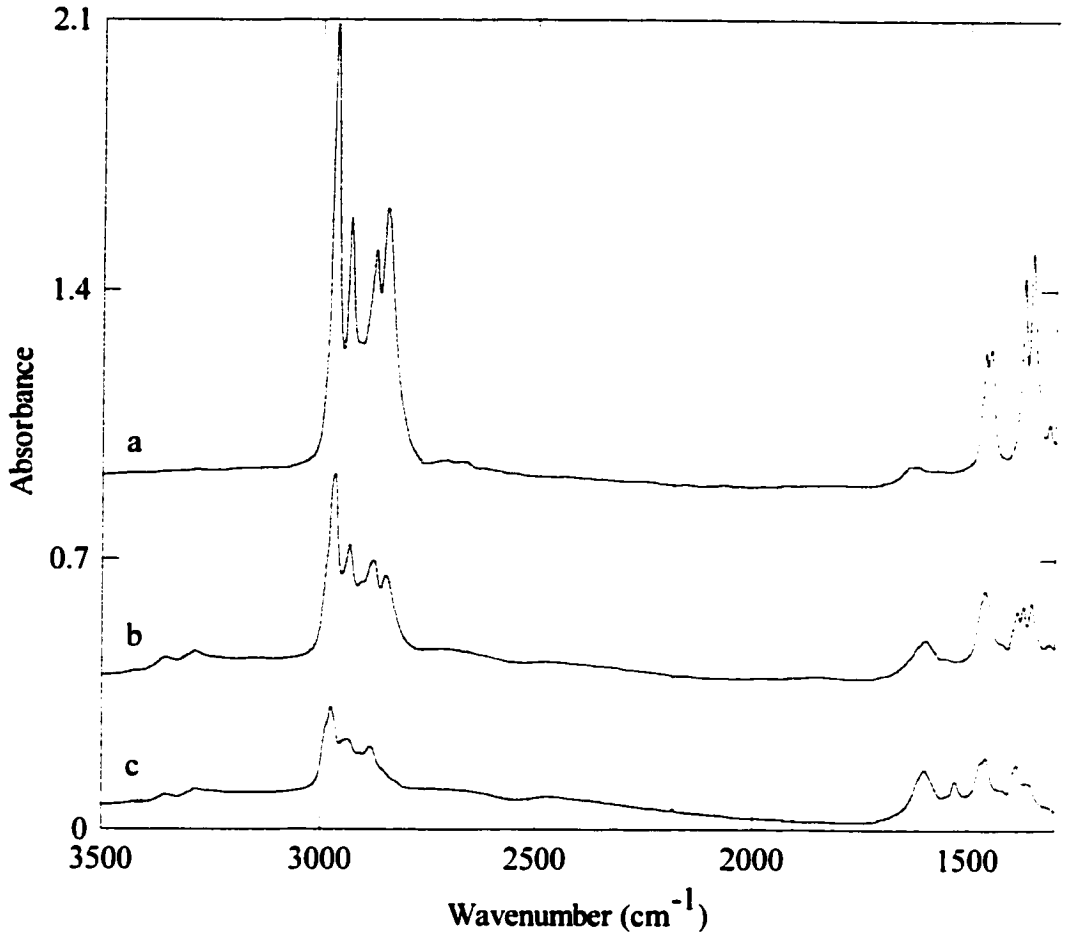

Figure 5.13 Spectra of a sample of (a) **6**; (b) after 18 hour exposure to NH_3 to give **9**: (c) prolonged evacuation of the sample in (b). All volatiles have been removed and a reference spectrum of silica-200 has been subtracted and the individual spectra offset.

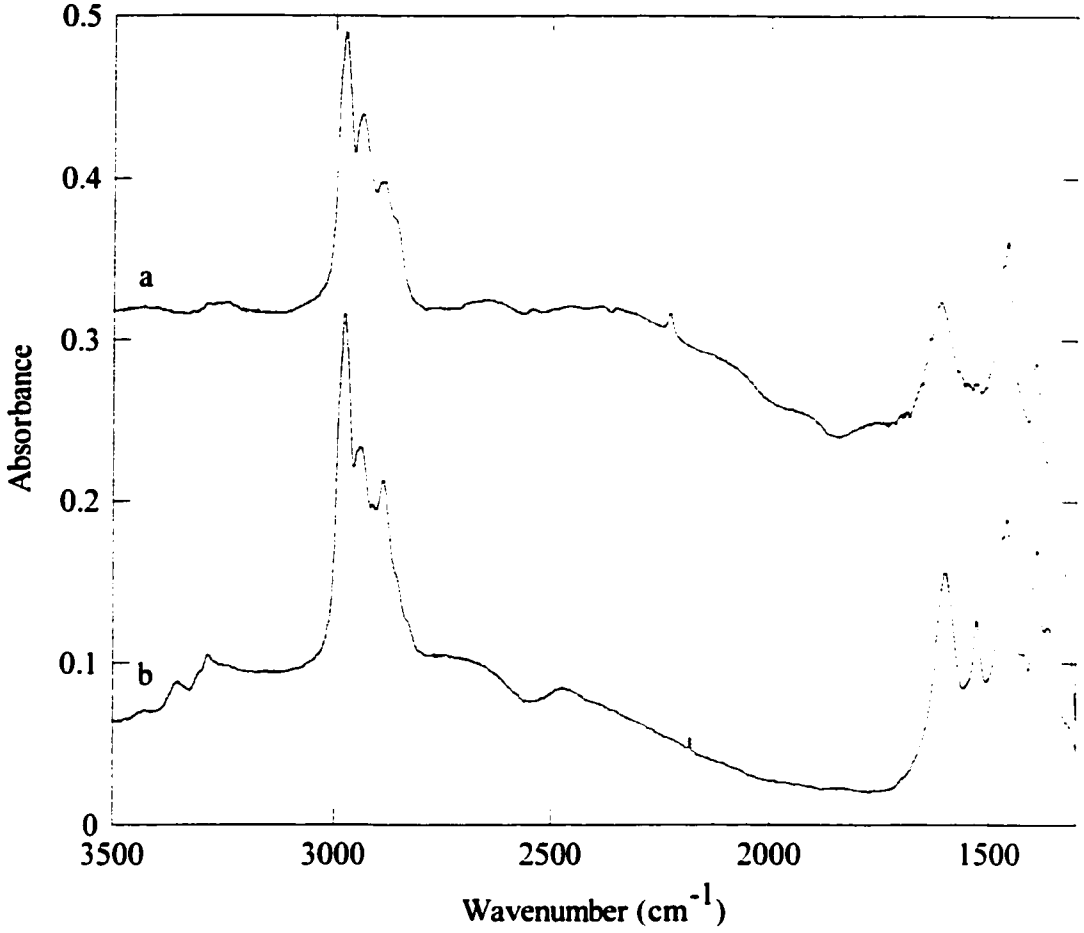

Figure 5.14 Spectra of (a) $(\equiv SiO)_2Ti{=}NEt$, **8** produced by evacuation of $(\equiv SiO)_2Ti(NEt_2)_2$, **6**: (b) produced by evacuation of $(\equiv SiO)_2Ti(N(Et)CHCH_3)$, **9**. A reference spectrum of silica-200 has been subtracted from each spectrum and the individual spectra offset.

5.6.1 Reaction of $(\equiv SiO)_2Ti(NMe_2)_2$ with pyridine

Pyridine-d_5 was chosen because its ν(C-D) vibrations do not overlap those due to the dimethylamido ligands. When an excess of pyridine was added to a sample of **5**, an immediate change in the intensity and appearance of the IR spectrum was observed, Figure 5.15. The integrated ν(CH) intensity decreased by 80%. GC analysis of the volatile products showed only $HNMe_2$, in an amount corresponding to 0.9 $HNMe_2$ / Ti. Alcoholysis of the resulting material with ^tBuOH removed 95% of the ν(CH) intensity remaining on the surface. GC analysis of the volatiles again revealed $HNMe_2$, in an amount corresponding to 0.9 / Ti.

These results are consistent with the pyridine-induced transformation of **5** to **7**, eq 5.14.

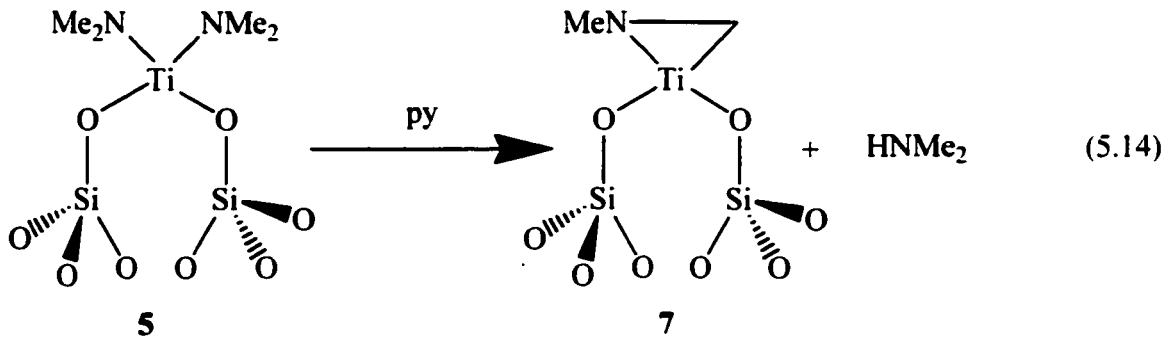

(5.14)

The IR spectrum of **5** after its reaction with pyridine-d_5 contains peaks at 1562 and 1538 cm^{-1} due to ring vibrations of coordinated pyridine.[5] Weak ν(CD) vibrations are also evident at ca. 2280 cm^{-1}.

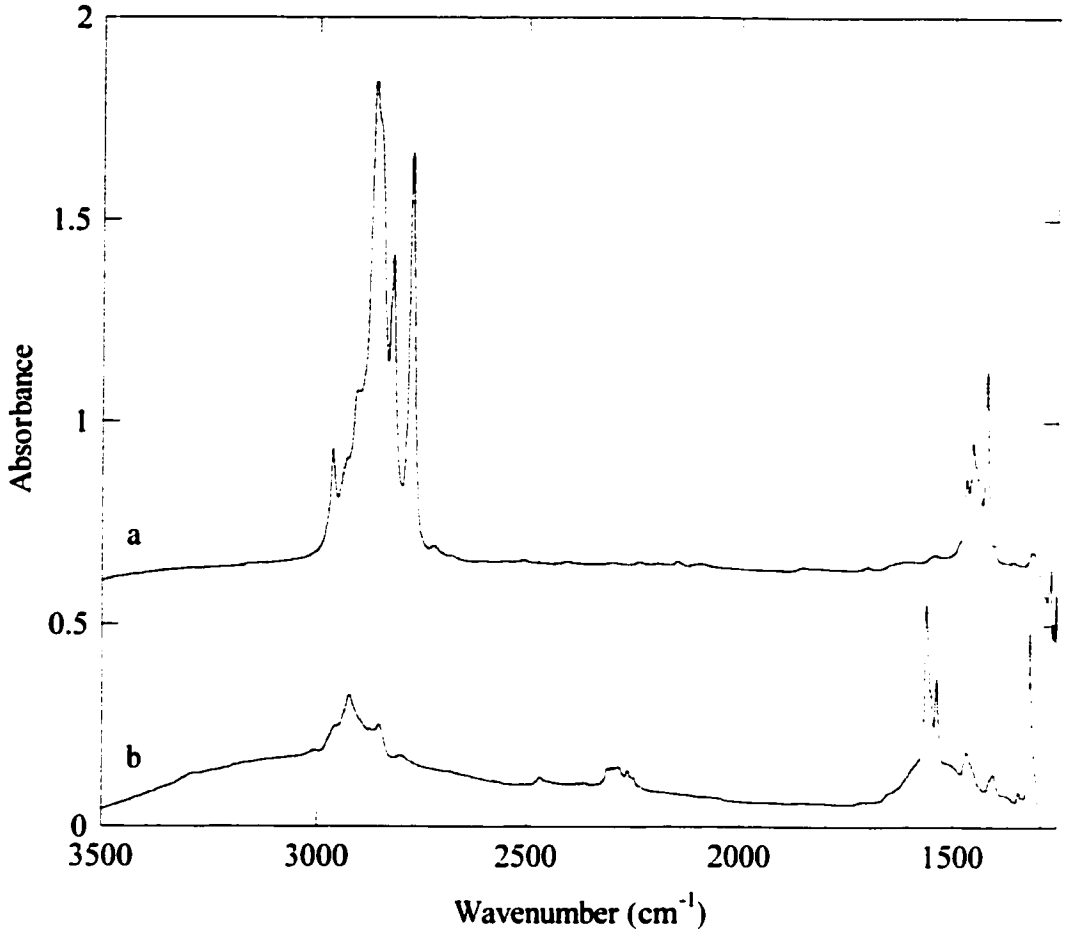

Figure 5.15 *In-situ* IR spectra of (a) **5**; and (b) after its exposure to pyridine-d_5. All volatiles have been removed, a background spectrum of silica-200 has been subtracted and the individual spectra offset.

Evidently pyridine, despite its inability to perform transamination, is nonetheless able to induce the transformation of **5** to **7**. A possible mechanism is shown in Scheme 5.2. We propose that coordination of pyridine increases steric crowding in the coordination sphere of Ti, which accelerates β-H abstraction from a dimethylamido ligand.

5.6.2 Reaction of $(\equiv SiO)_2Ti(NMe_2)_2$ with triethylamine

When an excess of NEt_3 was added to a fully loaded sample of **5** (23 mg SiO_2, 1.92 wt. % Ti), little change in the IR spectrum was observed after 3 hours, Figure 5.16. However, after a longer reaction time (18 hours), a small ν(NH) peak was visible at 3300 cm^{-1}, and the ν(CH) and $\delta(CH_3)$ regions show dramatic changes. Analysis of the gas phase products revealed only $HNMe_2$.

Despite prolonged evacuation (2 hours), it was not possible to remove all of the NEt_3 from the surface. Because of the presence of physisorbed amine, it was not possible to determine, via integration of the IR spectrum, the extent of loss of dimethylamido groups from the surface. We propose a triethylamine-induced transformation of **5** to **7**, eq 5.15.

$$(\equiv SiO)_2Ti(NMe_2)_2 + \text{xs } NEt_3 \rightarrow (\equiv SiO)_2Ti(\eta^2\text{-}CH_2NMe)(NEt_3) + HNMe_2 \qquad (5.15)$$

5 **7·NEt₃**

The suggested mechanism is the same as for the reaction of **5** with pyridine, Scheme 5.2.

Scheme 5.2 Proposed mechanism for the reactions of **5** with aprotic amines.

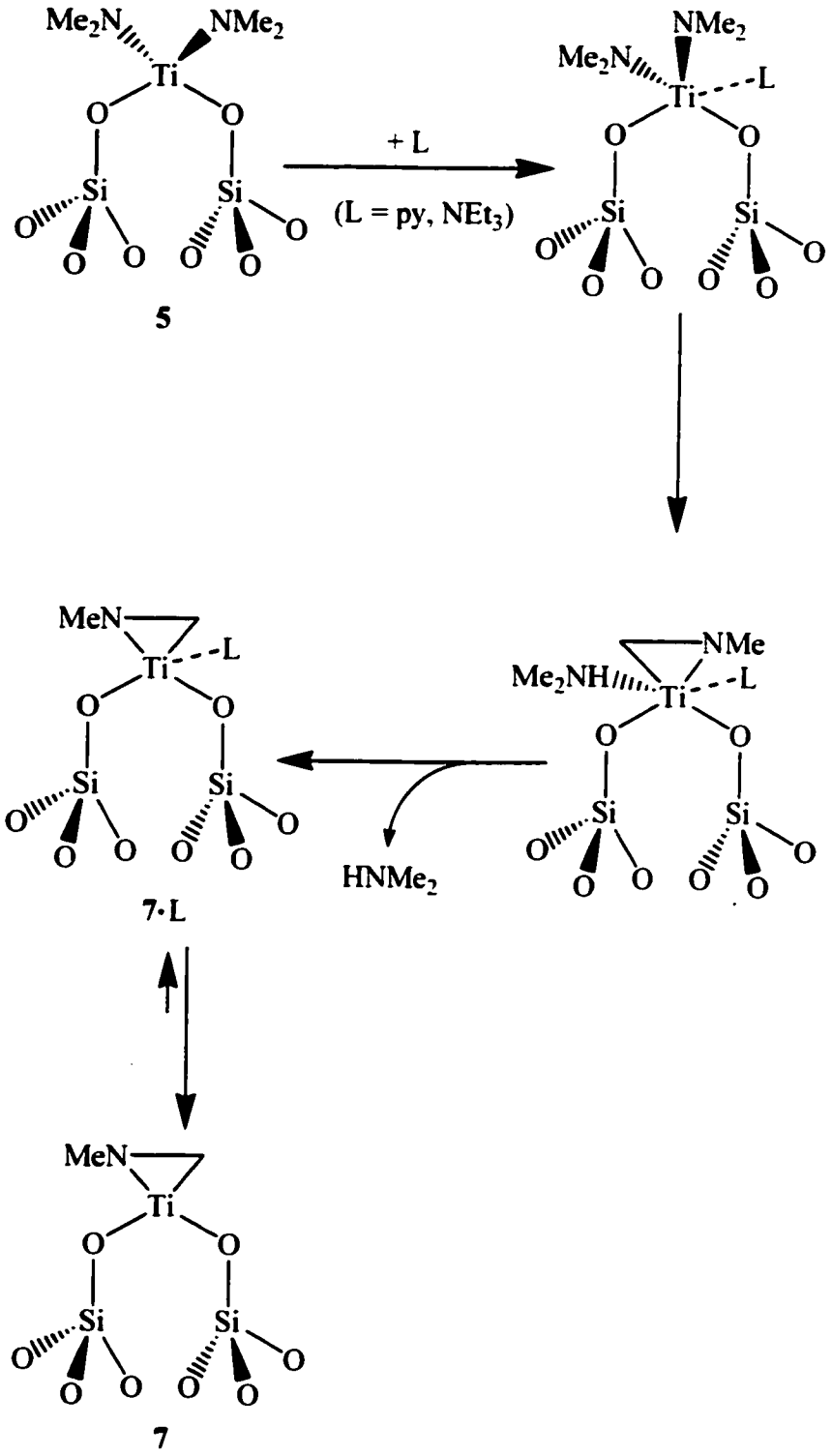

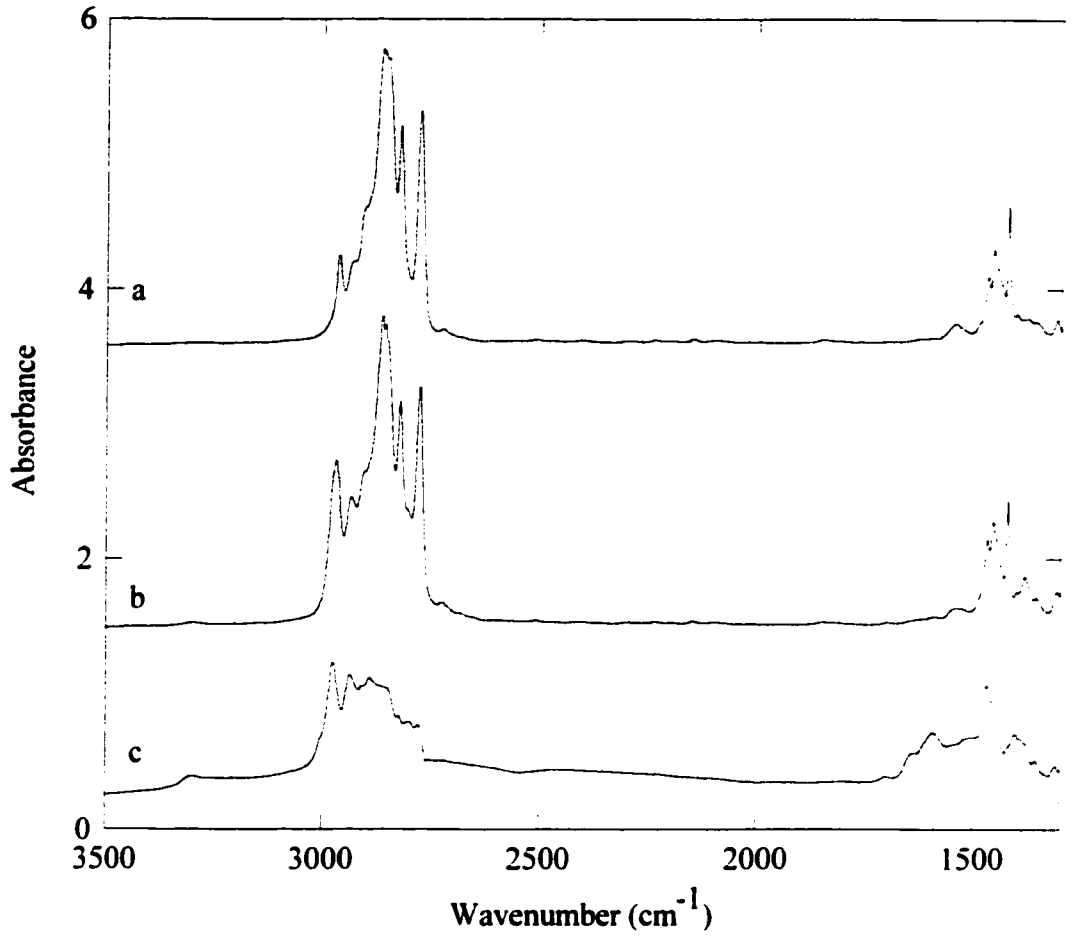

Figure 5.16 Spectra of (a) **5**; (b) after exposure to NEt_3 for 3 hrs; (c) after exposure to NEt_3 for 18 hours. All volatiles have been removed and a reference spectrum of silica-200 has been subtracted and the individual spectra offset.

5.6 Conclusion

In solution, both mono- and dialkylamines react rapidly with metal dialkylamides, resulting in transamination, and, in the case of the monoalkylamines, oligomerization. On the silica surface, bis(dialkylamido)titanium fragments undergo vastly different reactions with mono- and dialkylamines. As a consequence of the immobility conferred upon the titanium centres as a result of grafting, cyclohexylamine forms isolated cyclohexylimido complexes. Dialkylamines, on the other hand, induce not transamination, but β-H elimination to form imine complexes. Acceleration of β-H elimination was also observed when aprotic amines were coordinated to the supported titanium complexes.

Solution reactions of dialkylamido complexes with ammonia rapidly result in the formation of insoluble oligomers containing bridging NH_2^-, NH^{2-} and N^{3-} ligands. However, exposure of silica-supported bis(dialkylamido)titanium complexes to ammonia results in the removal of only one dialkylamido ligand. The remaining imino ligand resists ammonolysis. Increasing the pressure of ammonia increases the rate of imine formation, in a non-linear fashion. This may have important implications for CVD deposition of TiN, since it relates to how carbon is incorporated into the film. The removal of carbon from the coordination sphere of titanium is crucial and necessary for the deposition of clean films. Since the imine ligand is ammonia-stable, its reactivity towards $Ti(NR_2)_4$ present in the CVD chamber may be an important pathway through which carbon is irreversibly incorporated into titanium nitride films. This topic will be explored in the next chapter.

5.7 References

(1) Dubois, L. H.; Zegarski, B. R.; Girolami, G. S. *J. Electrochem. Soc.* **1992**, *139*, 3603-3609.

(2) Baxter, D. M.; Chisholm, M. H.; Gama, G. J.; DiStasi, V. F. *Chem. Mater.* **1996**, *8*, 1222-1228.

(3) Bradley, D. C.; Torrible, E. G. *Can. J. Chem.* **1963**, *41*, 134-138.

(4) Abarca, A.; Gómez-Sal, P.; Martin, A.; Mena, M.; Poblet, J. M.; Yélamos, C. *Inorg. Chem.* **2000**, *39*, 642-651.

(5) Lambert, J. B.; Shurvell, H. F.; Lightner, D.; Cooks, R. G. *Introduction to Organic Spectroscopy*; Macmillan: New York, 1987.

Chapter 6

Deposition of $Ti(NR_2)_4$ on Ti-modified silica surfaces

6.1 Introduction

While there has been a great deal of study on the CVD of TiN, there is very little information on the carbon which is incorporated in TiN films. Films deposited from $Ti(NEt_2)_4$ have less carbon than do analogous films deposited with $Ti(NMe_2)_4$, despite containing more carbon initially. The type of carbon also depends on the precursor chosen. Films derived from $Ti(NEt_2)_4$ contain primarily organic carbon, while films derived from $Ti(NMe_2)_4$, contain both organic and titanium-bound carbon.[1]

Deposition of films using isotopically labeled $^{15}NH_3$ showed that as the amount of carbon present in the film increased, the amount of ^{15}N in the film decreased. At 20 atomic % carbon, almost no ^{15}N is present. When the film is contaminated with 12 or 5 atomic % carbon, the amount of ^{15}N present in the film increases to 80% and 94%, respectively.[2]

AlN films deposited from $AlCl_3$ and NH_3 have been proposed to go through nanometer-sized clusters as intermediates. Similar clusters have been proposed to occur in the gas phase reaction of ammonia with $Ti(NMe_2)_4$. The mass spectrum of the reaction mixture shows all of the peaks between m/e 60 and 300 decreasing, with no new features appearing. The lack of new peaks is attributed to the formation of high molecular weight (> 300 amu) reactive intermediates.[2] MS analysis of some pyridine-soluble oligomers of the solution ammonolysis of $Ti(NEtMe)_4$ showed a spectrum containing significant ions, none of which had recognizable fragmentation patterns, at m/e 923, 940, and 1245 m/e.[3]

6.2 Reaction of $Ti(NMe_2)_4$ with $(\equiv SiO)_2Ti(\eta^2\text{-}CH_2NMe)$, 7

A sample of **5**, prepared by prolonged evacuation of $(\equiv SiO)_2Ti(NMe_2)_2$ (2.0 wt. % Ti), and containing virtually no remaining hydroxyl groups, was treated with an excess of $Ti(NMe_2)_4$. An immediate colour change occurred, from pale yellow to orange. After desorption of unreacted material, new peaks appeared in the ν(CH) and δ(CH) regions of the IR spectrum. Their positions and intensities identify them as belonging to dimethylamido ligands bound to titanium, Figure 6.1.

At the end of the reaction, after removal of unreacted $Ti(NMe_2)_4$, the samples contain up to (3.9 ± 0.3) wt. % Ti (average of 3 experiments), i.e., their Ti content has doubled relative to samples of **7**. As well, the sole gas phase product was $HNMe_2$. The amount generated was quantified by *in situ* IR, (0.47 ± 0.02) $HNMe_2$ / Ti (average of 2 experiments). These results suggest the occurrence of the reaction shown in eq 6.2.

$$(\equiv SiO)_2Ti(NCH_2CH_3) + Ti(NMe_2)_4 \rightarrow (\equiv SiO)_2Ti_2(NMe_2)_2(CH_2NMe)_2 + HNMe_2 \quad (6.2)$$

7 **10**

Alcoholysis of **10** with $(CD_3)_2CDOD$ resulted in removal of ca. 95% of the hydrocarbon ligands as judged by the decrease in integrated intensity in the ν(CH) stretching region, Figure 6.2. The ligands were removed in the form of $DNMe_2$. The amount formed corresponds to 1.8 $DNMe_2$ / Ti compared to the expected amount, based on the proposed formula for **10**, of 2.0 $DNMe_2$ / Ti, eq 6.3.

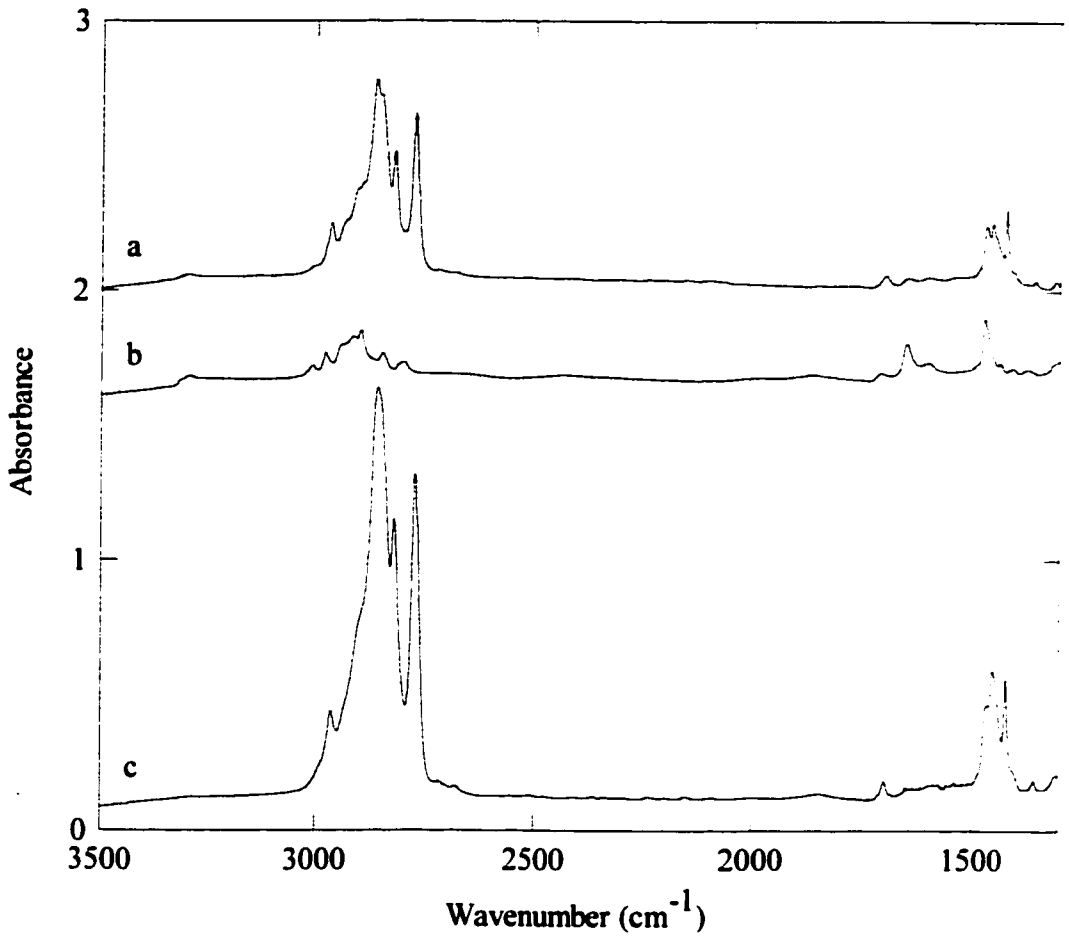

Figure 6.1 *In-situ* IR spectra of (a) $(\equiv SiO)_2Ti(NMe_2)_2$, **5**; (b) after evacuation to give $(\equiv SiO)_2Ti(\eta^2\text{-}CH_2NCH_3)$, **7**; and (c) after readdition of $Ti(NMe_2)_4$. Volatiles have been removed and a reference spectrum of silica-200 has been subtracted from each spectrum.

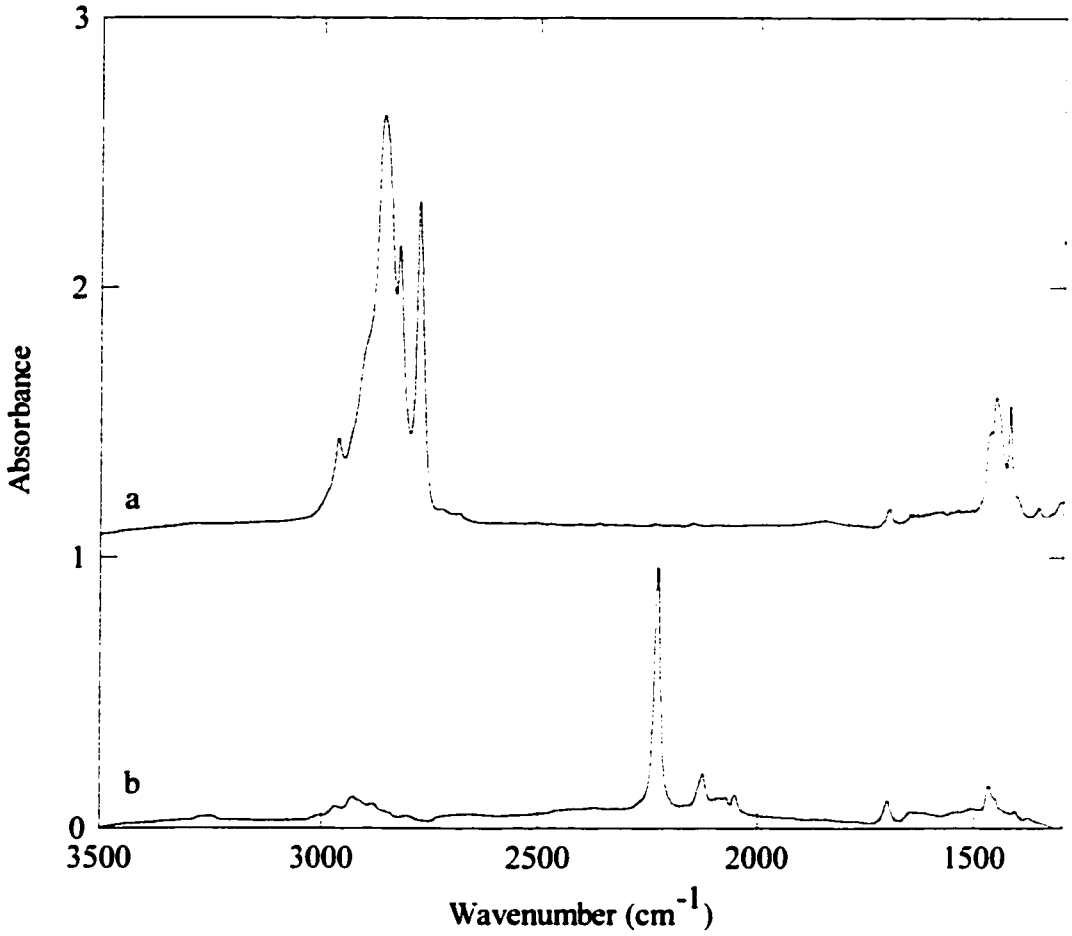

Figure 6.2 *In-situ* IR spectra of (a) $(\equiv SiO)_2Ti_2(NMe_2)_2(CH_2NMe)_2$; and (b) **10** after alcoholysis with $(CD_3)_2CDCOD$. Volatiles have been removed and a reference spectrum of silica-200 has been subtracted from each spectrum.

$$(\equiv SiO)_2Ti_2(NMe_2)_2(CH_2NMe)_2 + xs\ (CD_3)_2CDOD \rightarrow (\equiv SiO)_2Ti_2O(O^iPr)_4 + 4\ DNMe_2 \quad (6.3)$$

Identical spectral and quantitative results were obtained for **5** treated first with NH_3 followed by $Ti(NMe_2)_4$, Figure 6.3. At the end of the reaction, after removal of unreacted $Ti(NMe_2)_4$, the samples contain up to (4.0 ± 0.2) wt. % Ti (average of 2 experiments). As well, the sole gas phase product was (0.52 ± 0.03) $HNMe_2$ / Ti (average of 2 experiments).Thus NH_3 appears to facilitate the grafting of a second layer of titanium amide.

Exposure of **10** to NH_3 resulted in changes both in the appearance, Figure 6.4, and the intensity, Figure 6.5, of the IR spectrum which resemble those of the reaction of **5** with NH_3. The intensity of the ν(CH) bands decreased by ca. 50 %. $HNMe_2$ was evolved in an amount corresponding to 0.44 $HNMe_2$ / Ti. Further exposure to NH_3 had no effect. These results suggest that the reaction of NH_3 with **10** occurs in the same manner as the reaction of NH_3 with $(\equiv SiO)_2Ti(NMe_2)_2$. The proposed reaction is shown in eq 6.4.

$$\underset{\textbf{10}}{(\equiv SiO)_2Ti_2(NMe_2)_2(CH_2NMe)_2} \xrightarrow{NH_3} \underset{\textbf{11}}{(\equiv SiO)_2Ti_2(CH_2NMe)_3} + HNMe_2 \quad (6.4)$$

Consistent with this formulation, alcoholysis of **11** with $(CD_3)_3COD$ resulted in the loss of 95 % of the ligands in the form of $DNMe_2$ in an amount corresponding to 1.4 $DNMe(CH_2D)$ / Ti ($p+1/p = 0.18$).

The nature of binding of the imine ligands is, at present, unknown. However, a likely possibility is that some or all of them bridge the two titanium centers. Molecular complexes with this coordination mode are known. For example, a dinuclear tungsten complex,

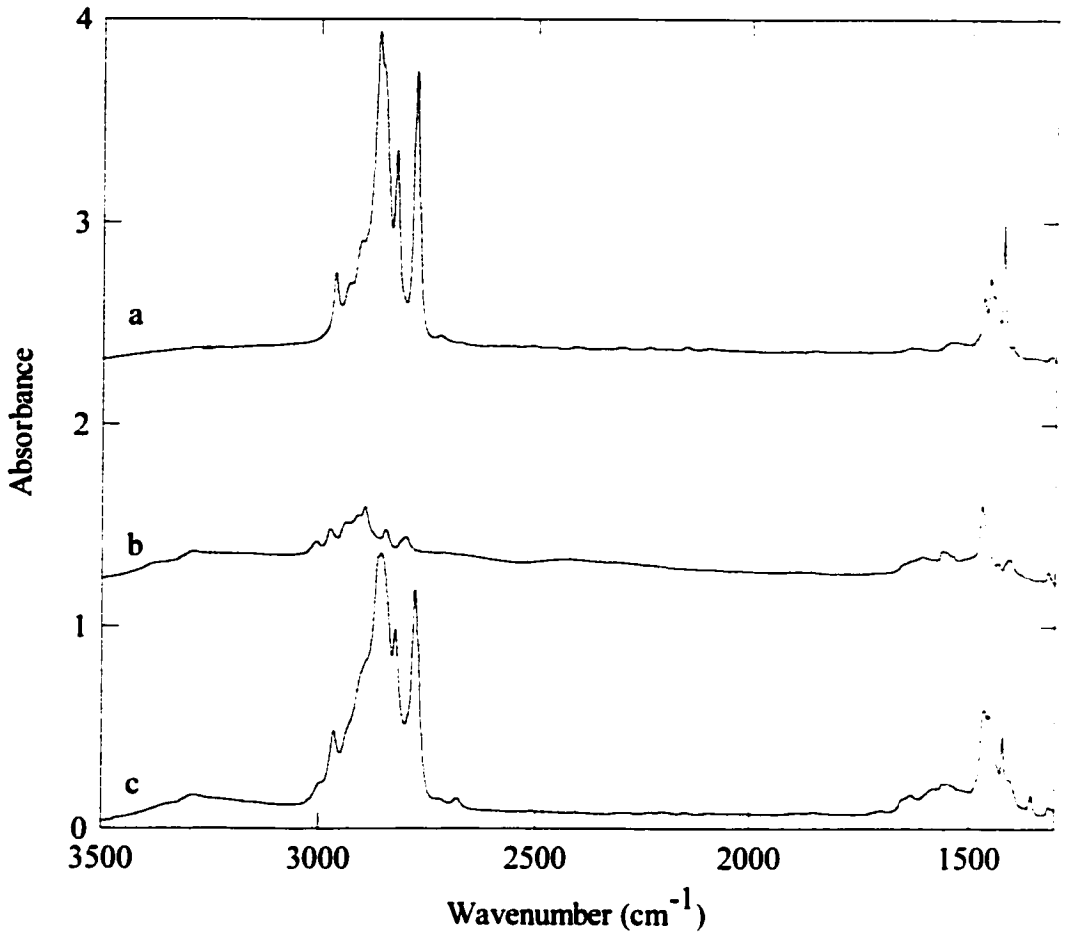

Figure 6.3 *In-situ* IR spectra of (a) $(\equiv SiO)_2Ti(NMe_2)_2$, **5**; (b) after reaction with NH_3 to give $(\equiv SiO)_2Ti(\eta^2\text{-}CH_2NCH_3)$, **7**; (c) after readdition of $Ti(NMe_2)_4$ to **7**. Volatiles have been removed and a reference spectrum of silica-200 has been subtracted from each spectrum.

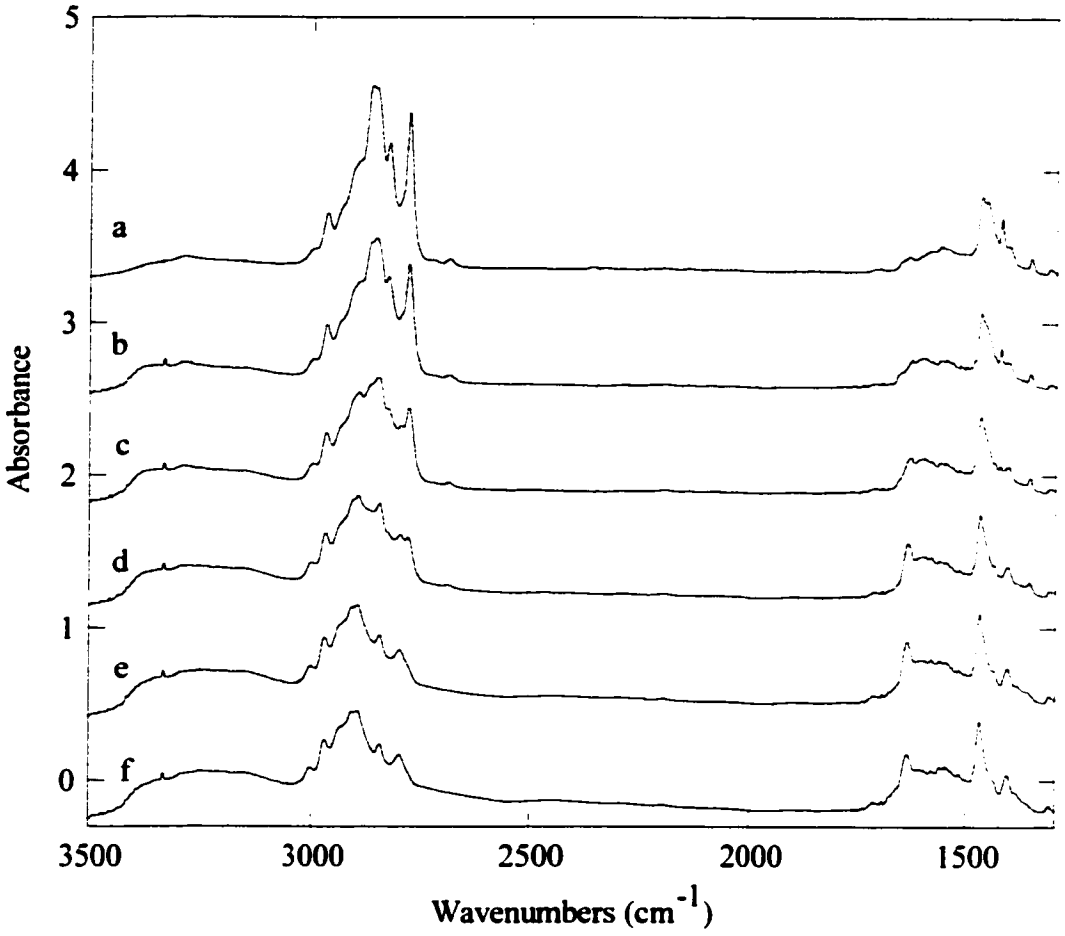

Figure 6.4 Time-resolved spectra of the reaction between NH_3 and **10** after (a) 0; (b) 0.5; (c) 10; (d) 43; (e) 74; and (f) 100 hours. A reference spectrum of silica-200 has been subtracted from each spectrum.

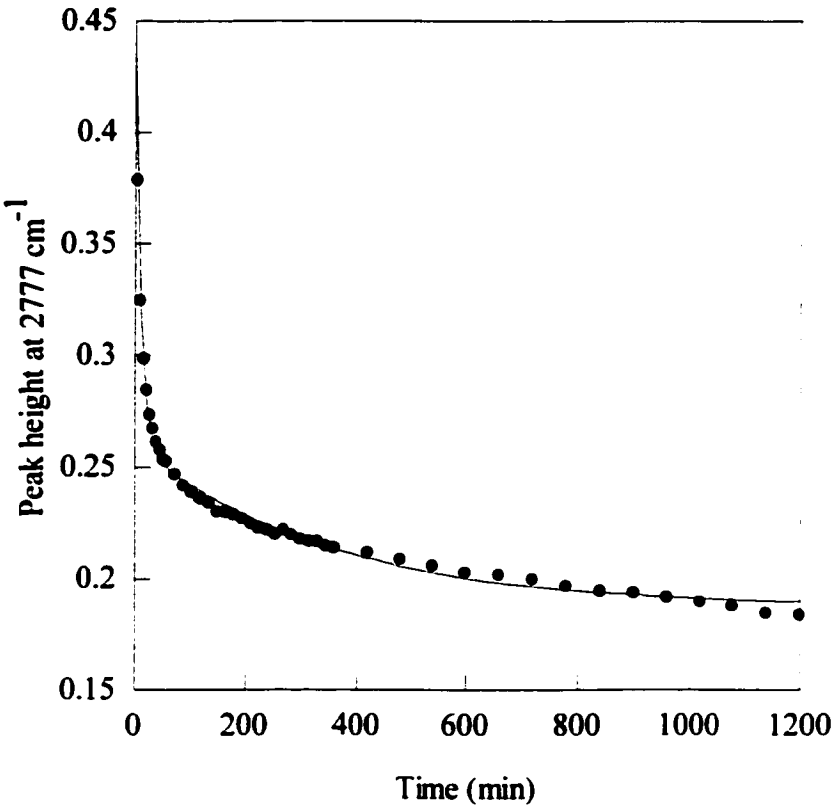

$Abs_t = A_\infty + \alpha e^{-k_1 t} + \beta e^{-k_2 t}$	
Abs_∞	0.187 ± 0.001
α	0.072 ± 0.001
k_1	0.0029 ± 0.0001
β	0.173 ± 0.003
k_2	0.086 ± 0.003
Chisq	0.0013416
R	0.99659

Figure 6.5 Integrated intensity vs. time for the reaction of NH_3 with **10**. The line is a non-linear least squares fit to a biphasic rate equation.

$W_2Cl_3(NMe_2)_2L_2(\mu\text{-}C_2H_2)(\mu\text{-}NMe_2)$, undergoes β-H activation of one of its amido ligands upon heating to 65°C in toluene. The product contains a bridging N-methylmethanimine ligand, eq. 6.5:[4]

$$W_2Cl_3(NMe_2)_2L_2(\mu\text{-}C_2H_2)(\mu\text{-}NMe_2) \xrightarrow{\Delta} W_2Cl_3(NMe_2)_2L_2(\mu\text{-}C_2H_3)(\mu,\eta^2\text{-}CH_2NMe) \qquad (6.5)$$

Similarly, the cyclic, trinuclear titanium complex $[\{Cp^*Ti(NMe_2\}_3(\mu\text{-}O)_3]$, when heated to 110 °C, undergoes β-H elimination, resulting in an imine ligand which bridges two of the titanium centres, eq 6.6:[5]

$$[\{Cp^*Ti(NMe_2\}_3(\mu\text{-}O)_3] \rightarrow [\{Cp^*Ti(NMe_2)(\mu\text{-}O)\}_3(\mu,\eta^2\text{-}CH_2NMe)] + HNMe_2 \quad (6.6)$$

Therefore we suggest that **10** may have the formula $(\equiv SiO)_2Ti_2(NMe_2)_2(\mu,\eta^2\text{-}CH_2NMe)_2$, where the imine ligands bridge the two titanium centers, (**10a, b**). Some possible structures are shown in Scheme 6.1. However, we cannot exclude that the siloxide ligands occupy bridging positions and force the imine ligands into azatitanacyclopropane coordination (**10c**). Finally, there is no direct evidence that the two titanium centers are associated with each other. Therefore **10d** is also consistent with all our spectroscopic and stoichiometric results.

Likewise, the structure of **11** is unknown but may also contain N-methylmethanimine ligands bridging the titanium centers, as in $(\equiv SiO)_2Ti_2(\mu,\eta^2\text{-}CH_2NMe)_2(\eta^2\text{-}CH_2NMe)$. In this case, isolated mono-titanium sites are less likely since the formation of **11** requires β-H elimination on one Ti center and extrusion of $HNMe_2$ on a second Ti center. Proposed structures are shown in Scheme 6.2.

Scheme 6.1 Possible structures for **10**

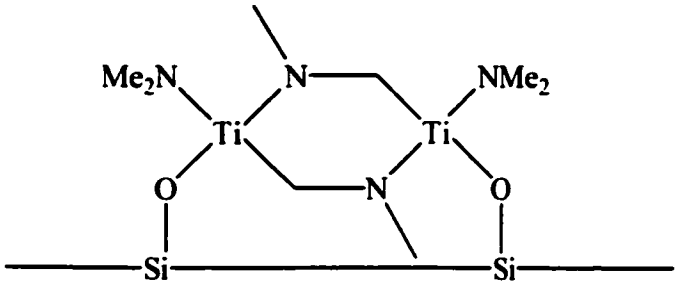

10a

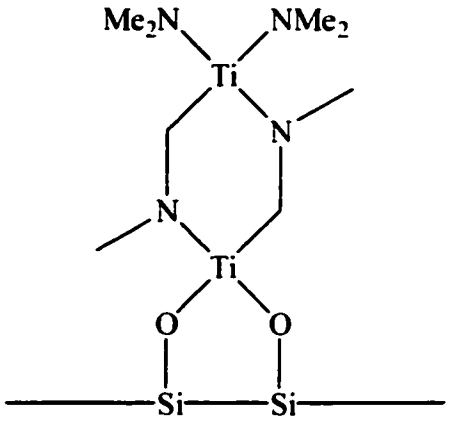

10b

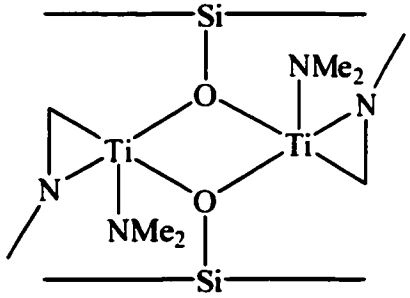

10c

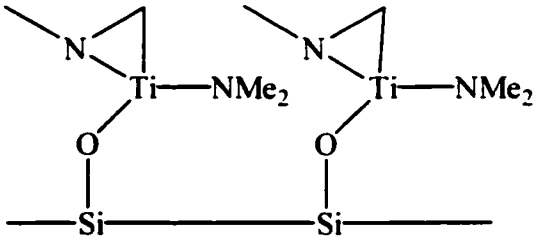

10d

Scheme 6.2 Possible structures for **11**

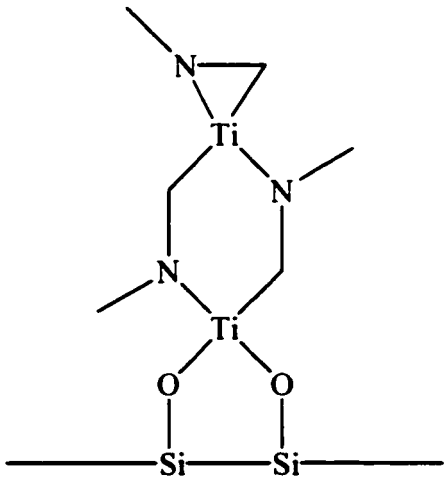

11a

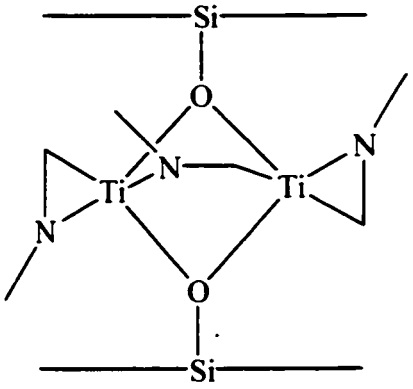

11b

Examination of the proposed structures sheds light on the analysis of Gordon and co-workers[1] of the different types of carbon contamination in TiN films. Deposition from $Ti(NMe_2)_4$ showed primarily titanium-bound carbon. The imine ligands produced during the formation of **10** and **11** contain Ti-C bonds. Thermal decomposition of these materials is almost certain to result in the introduction of "TiC" into the film.

6.3 Reaction of $Ti(NEt_2)_4$ with $(\equiv SiO)_2Ti{=}NEt$, 8

A fully loaded sample of $(\equiv SiO)_2Ti{=}NEt$, **8**, prepared by prolonged evacuation of $(\equiv SiO)_2Ti(NEt_2)_2$, was treated with excess $Ti(NEt_2)_4$. There was a rapid color change from pale yellow to orange. After desorption of unreacted material, new peaks appeared in the ν(CH) and δ(CH) regions of the IR spectrum, Figure 6.6. Their positions and intensities are consistent with the presence of diethylamido ligands on the surface. Identical spectral changes were observed when a sample of **8**, prepared by treating $(\equiv SiO)_2Ti(NEt_2)_2$ with NH_3, was exposed to $Ti(NEt_2)_4$, Figure 6.7. At the end of the reaction, after removal of unreacted $Ti(NEt_2)_4$, the samples contained up to 3.8 wt. % Ti, compared to 2.0 wt. % for samples of **6**. The sole gas phase product is $HNEt_2$, in an amount 0.46 $HNEt_2$ / Ti. These results suggest the occurrence of the reaction shown in eq. 6.7

$$(\equiv SiO)_2Ti{=}NEt + Ti(NEt_2)_4 \rightarrow (\equiv SiO)_2Ti_2(NEt)(N(Et)CHCH_3)(NEt_2)_2 + HNEt_2 \quad (6.7)$$

8 **2** **12**

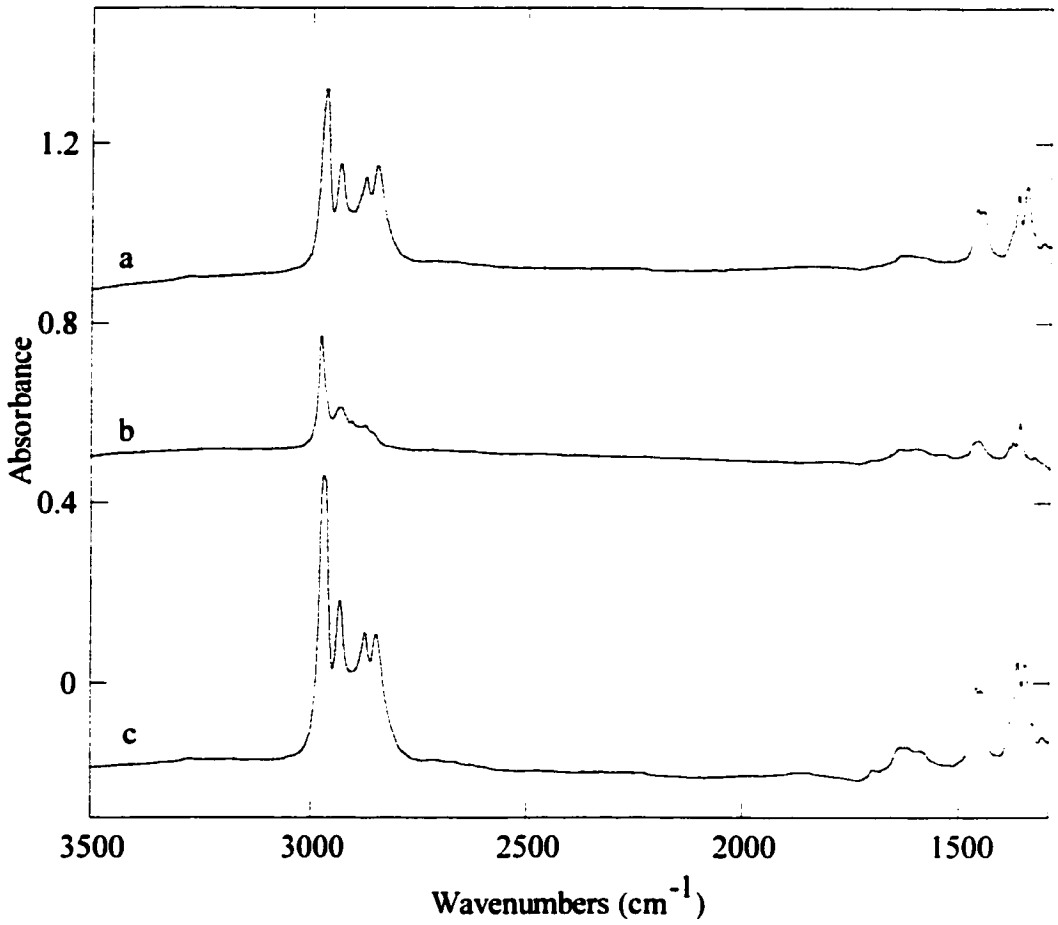

Figure 6.6 IR spectra of (a) $(\equiv SiO)_2Ti(NEt_2)_2$; (b) after evacuation to give $(\equiv SiO)_2Ti{=}NEt$; and (c) after addition of $Ti(NEt_2)_4$ to the sample from (b). Volatiles have been removed and a reference spectrum of silica-200 has been subtracted from each spectrum.

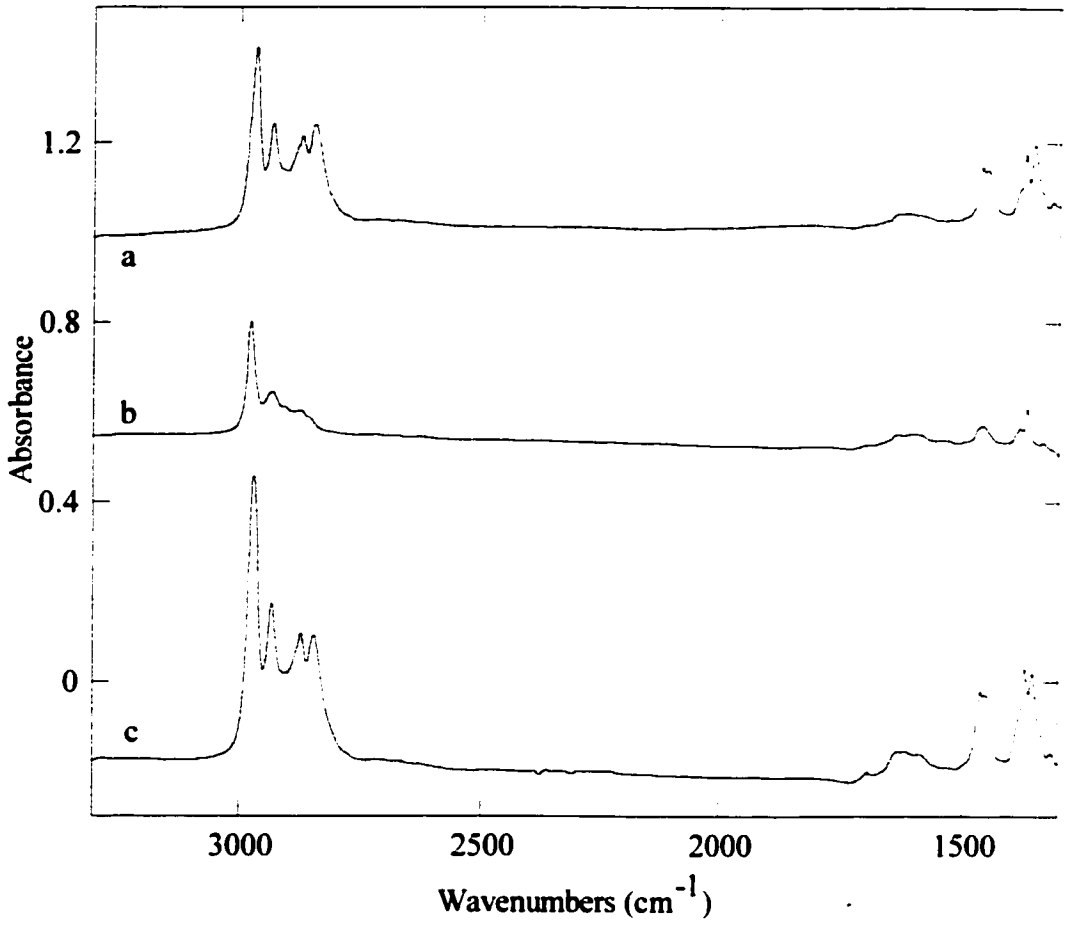

Figure 6.7 IR Spectra of (a) $(\equiv SiO)_2Ti(NEt_2)_2$; (b) after exposure to ammonia, followed by 12 hrs evacuation to give $(SiO)_2Ti{=}NEt$; and (c) after addition of $Ti(NEt_2)_4$ to the sample from (b). Volatiles have been removed, a reference spectrum of silica-200 has been subtracted from each spectrum and each individual spectrum offset.

Exposure of **12** to NH_3 resulted in a change in the appearance of the IR spectrum, Figure 6.8. The intensity of the ν(CH) bands decreased by ca. 25%. $HNEt_2$ was evolved in an amount corresponding to 0.9 $HNEt_2$ / Ti. Further exposure to NH_3 had no effect. These results suggest that the reaction of NH_3 with **12** occurs in the same manner as the reaction of NH_3 with $(\equiv SiO)_2Ti(NEt_2)_2$. The proposed reaction is shown in eq 6.8.

$$(\equiv SiO)_2Ti_2(NEt_2)_2(CH(CH_3)NEt)(NEt) \xrightarrow{NH_3} (\equiv SiO)_2Ti_2(CH(CH_3)NEt)_2(NEt) + HNEt_2 \qquad (6.8)$$

12 **13**

Once again, the structures of **12** and **13** are unknown. Possible bridging ligands for the dititanium surface complexes are the N-ethylethanimine, ethylimido and siloxide, Scheme 6.3.

These structures shed more light on the results of Gordon and co-workers.[1] Their research into TiN films deposited from $Ti(NEt_2)_4$ found that a majority of the carbon present in the films is in the form of organic, rather than titanium-bound carbon. Since N-ethylethanimine ligands have been shown to extrude C_2H_4, and since the resulting ethyl imido ligands contain no titanium-bound carbon, thermal decomposition should lead primarily to organic carbon.

6.4 Reaction of $(\equiv SiO)_2Ti{=}NEt$, 6, with $Ti(NMe_2)_4$

A sample of $(\equiv SiO)_2Ti{=}NEt$ prepared via evacuation of $(\equiv SiO)_2Ti(NEt_2)_2$ was treated with $Ti(NMe_2)_4$. As noted previously, a rapid color change from pale yellow to orange was observed as a result of the adsorption of $Ti(NMe_2)_4$ onto the silica surface. There was an immediate and

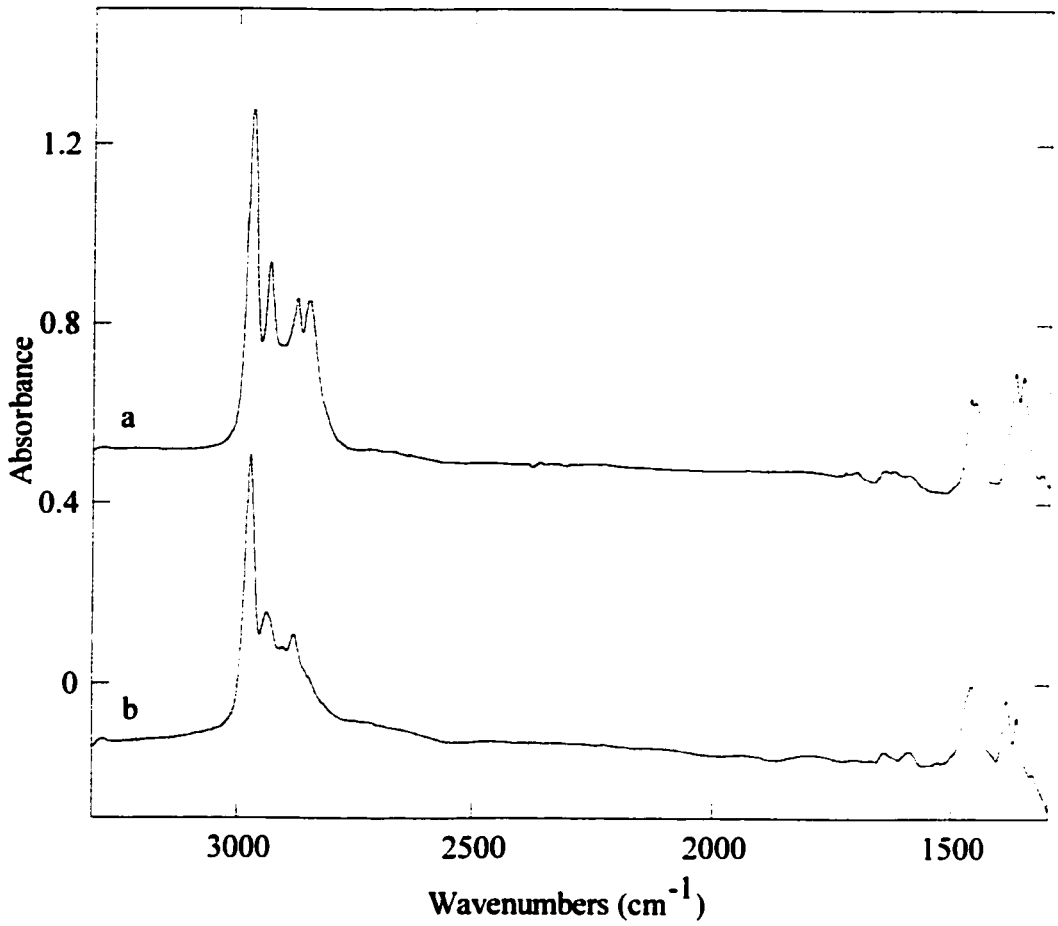

Figure 6.8 IR spectrum of (a) **12**; (b) after the exposure to 35 Torr NH_3 followed by 2 hours evacuation to give **13**. Volatiles have been removed, a reference spectrum of silica-200 has been subtracted from each spectrum and each individual spectrum has been offset.

Scheme 6.3 Possible structures for **12**.

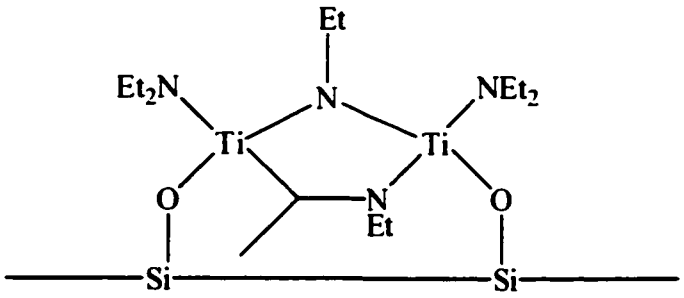

12a

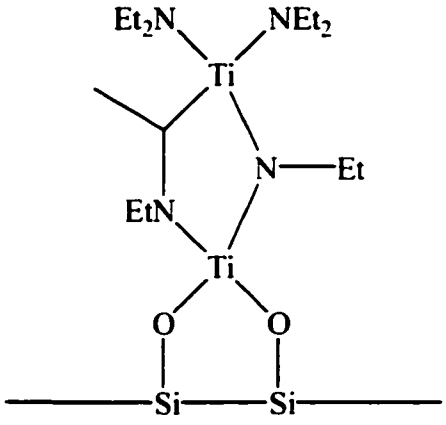

12b

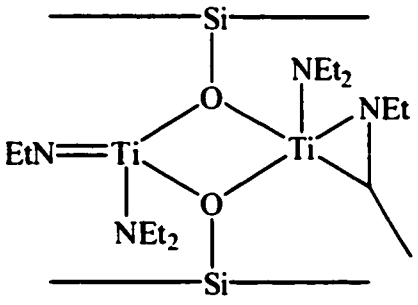

12c

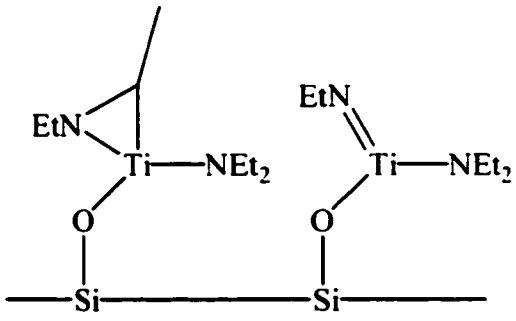

12d

rapid change in the IR spectrum, Figure 6.9, in addition to the release of 0.47 $HNMe_2$ / Ti into the gas phase. The final IR spectrum contains bands characteristic of dimethylamido ligands. At the end of the reaction, after removal of unreacted $Ti(NMe_2)_4$, the sample contained 3.7 wt. % Ti. compared to 2.0 wt. % Ti for samples of **6**. These results are consistent with the reaction shown in eq. 6.9:

$$(\equiv SiO)_2Ti{=}NEt + Ti(NMe_2)_4 \rightarrow (\equiv SiO)_2Ti_2(NMe_2)_2(NEt)(CH_2NMe) + HNMe_2 \quad (6.9)$$

8 **1** **14**

The product **14** may contain two titanium centers bridged by one ethylimido and one N-methylmethanimine ligand.

6.5 Conclusion

The imine and imide ligands formed upon reaction of **5** or **6** with ammonia, while unreactive to further exposure to ammonia, are reactive upon exposure to $Ti(NR_2)_4$. Grafting occurs in the absence of surface hydroxyl groups, resembling the spontaneous reactions of $Ti(O^iPr)_4$ with $(\equiv SiO)_xTi(O^iPr)_{4-x}$ (x = 1, 2) to yield dinuclear titanium species, eq 6.10-6.11.[6]

$$(\equiv SiO)Ti(O^iPr)_3 + Ti(O^iPr)_4 \rightarrow (\equiv SiO)Ti_2O(O^iPr)_5 + {}^iPrOH + C_3H_6 \quad (6.10)$$

$$(\equiv SiO)_2Ti(O^iPr)_2 + Ti(O^iPr)_4 \rightarrow (\equiv SiO)_2Ti_2O(O^iPr)_4 + {}^iPrOH + C_3H_6 \quad (6.11)$$

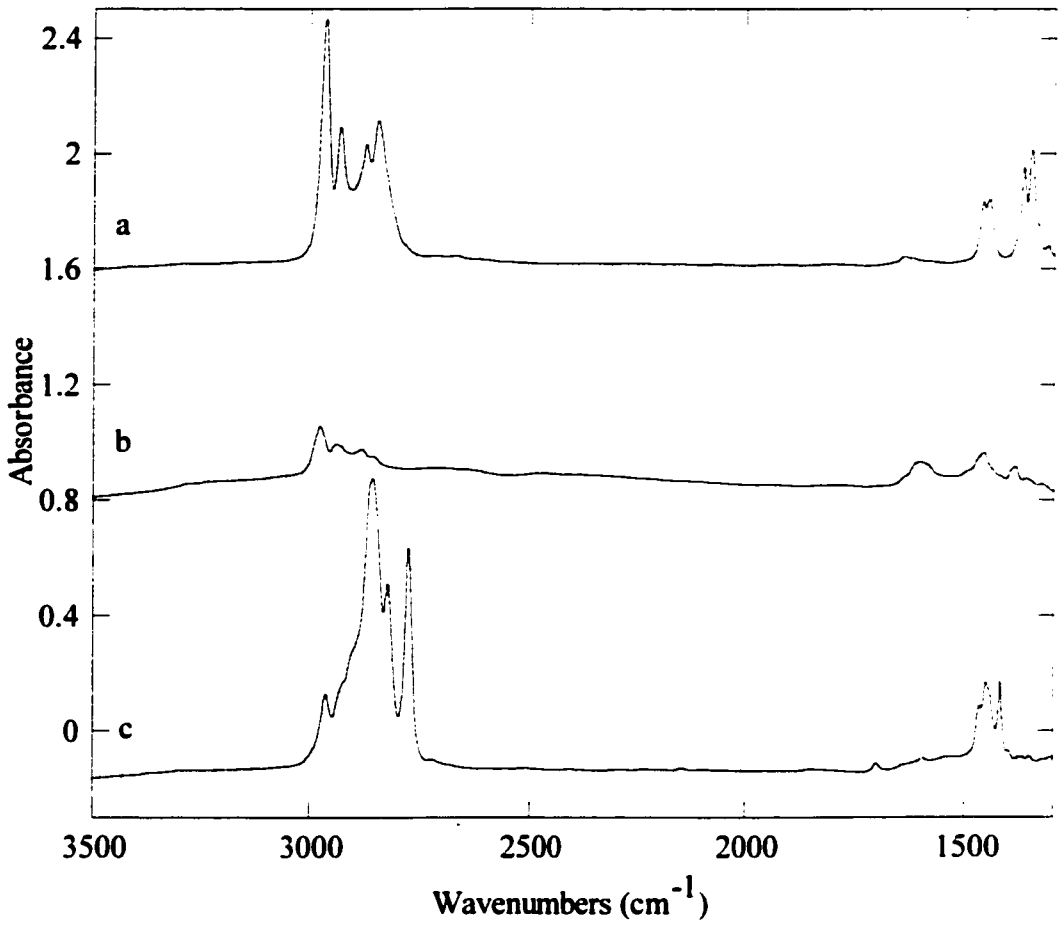

Figure 6.9 Spectra of (a) $(\equiv SiO)_2Ti(NEt_2)_2$, **6**; (b) after evacuation to give $(\equiv SiO)_2Ti{=}NEt$, **8**; and (c) after the addition of excess $Ti(NMe_2)_4$. All volatiles have been removed and a reference spectrum of silica-200 has been subtracted from each spectra.

Bridging imine and imido ligands are a probable source of carbon contamination during the CVD of TiN.[7]

It is known that the nitrogen in highly pure (low carbon) TiN films derived from $Ti(NR_2)_4$ comes exclusively from the added ammonia.[2] Under the conditions studied in this chapter, transamination by ammonia does not occur, although we cannot rule out its role under more CVD-like conditions.

6.6 References

(1) Fix, R. M.; Gordon, R. G.; Hoffman, D. M. *Chem. Mater.* **1990**, 235-241.

(2) Prybyla, J. A.; Chiang, C.-M.; Dubois, L. H. *J. Electrochem. Soc.* **1993**, *140*, 2695-2702.

(3) Baxter, D. M.; Chisholm, M. H.; Gama, G. J.; DiStasi, V. F. *Chem. Mater.* **1996**, *8*, 1222-1228.

(4) Ahmed, K. J.; Chisholm, M. H.; Folting, K.; Huffman, J. C. *J. Am. Chem. Soc.* **1986**, *108*, 989-999.

(5) Galakhov, M.; Gómez-Sal, P.; Martín, A.; Mena, M.; Yélamos, C. *Eur. J. Inorg. Chem.* **1998**, 1319-1325.

(6) Bouh, A. O.; Rice, G. L.; Scott, S. L. *J. Am. Chem. Soc.* **1999**, *121*, 7201-7210.

(7) Dubois, L. H. *Polyhedron* **1994**, *13*, 1329-1336.

Chapter 7

Nature of the chemisorption of $Mo(NR_2)_4$ on silica

7.1 Introduction

In modeling the initial stages of the deposition of TiN from $Ti(NR_2)_4$ (R = Me, Et), in the presence and absence of ammonia, tetrakis(dimethyl)- and -(diethylamido)titanium(IV) were grafted onto silica to generate supported bis(dialkylamido)titanium complexes. A spontaneous or NH_3-induced transformation was observed, catalyzed by unreacted hydroxyl groups present on the surface, which results in the extrusion of dialkylamine. When R = Me, an N-methylmethanimine ligand is formed. When R = Et, the corresponding imine, N-ethylethanimine is not observed, since it undergoes further loss of C_2H_4, resulting in the formation of a supported ethylimidotitanium complex.

In order to determine whether these transformations are unique for $Ti(NR_2)_4/SiO_2$ or generalizable to other metal dialkylamides, a study of the reactivity of $Mo(NR_2)_4$ (R = Me, Et) towards silica was undertaken. Molecular molybdenum(IV) dialkylamides display much the same reactivity that dialkylamidotitanium(IV) compounds do. Exposure to alcohols results in complete displacement of the amido ligands by alkoxy ligands.[1] while CS_2 undergoes quantitative insertion, resulting in the formation of tetrakis(dimethylcarbamate)- (E = O) or –(dimethyldithiocarbamate)molybdenum(IV), eq 7.1.[2]

$$Mo(NR_2)_4 + 4\ CS_2 \rightarrow Mo(S_2CNR_2)_4 \qquad (7.1)$$

Molybdenum nitride (both MoN and Mo_2N) are being investigated for use in a number of industrial areas. In high energy density energy storage devices it is being looked at as an electrode material.[3] As a catalyst, its activity in hydrodesulfurization is being investigated.[4] Its use in barrier layers in microelectronics is also being researched.[5]

7.2 Stoichiometry of grafting of $Mo(NMe_2)_4$ on silica

$Mo(NMe_2)_4$ is a volatile, purple solid. Exposure of silica pretreated at 500°C (silica-500) to an excess of $Mo(NMe_2)_4$ vapour, **15**, in a sealed reactor (base pressure < 10^{-4} Torr) at room temperature results in an irreversible chemisorption of the metal complex onto the surface. The silica, initially colourless, acquires a brown colour over the course of the reaction (ca. 45 min) while volatiles are released into the gas phase. After unreacted $Mo(NMe_2)_4$ was removed via desorption into a liquid nitrogen cold trap, the amount of chemisorbed Mo was found to be (3.78 ± 0.09) wt %. These values are highly reproducible, Table 7.1. The amount of chemisorbed Mo corresponds to 1.0 Mo/≡SiOH and a surface coverage of 1.25 Mo/nm^2.

During grafting of **15**, the sole gas phase product is $HNMe_2$, identified by GC and GC/MS. The amount of amine released during the reaction between $Mo(NMe_2)_4$ and silica was quantified by *in situ* gas phase IR spectroscopy and is also highly reproducible, Table 7.1. It corresponds to 1.0 $HNMe_2$ / Mo. Thus, the stoichiometry of the grafting reaction on silica-500 can be written as in eq 7.2:

$$\equiv SiOH + Mo(NMe_2)_4 \rightarrow (\equiv SiO)Mo(NMe_2)_3 + HNMe_2 \qquad (7.2)$$

15 **16**

Table 7.1 Analysis of silicas and volatiles resulting from exposure to $Mo(NMe_2)_4$ after complete consumption of surface hydroxyl groups.

Silica pretreatment temperature	Wt. % Mo	Mo[a] mmol / g	$HNMe_2$[a] mmol / g	Mo / ≡SiOH[b]	$HNMe_2$ / Mo
500°C	3.85	0.40	0.40	1.00	1.00
	3.65	0.38	0.37	0.95	0.97
	3.79	0.40	0.39	0.99	0.99
	3.75	0.39	0.41	0.98	1.05
	3.72	0.39	0.42	0.97	1.08
	3.90	0.41	0.40	1.02	0.98
Avg.	3.78 ± 0.09	0.39 ± 0.01	0.40 ±0.02	0.98 ± 0.02	1.01 ± 0.04
200°C	3.79	0.40	0.79	0.46	2.00
	3.75	0.39	0.77	0.45	1.97
	3.82	0.40	0.78	0.46	1.96
	3.86	0.40	0.82	0.47	2.04
	3.70	0.39	0.80	0.45	2.07
	3.90	0.41	0.81	0.47	1.99
	3.70	0.39	0.77	0.45	2.00
	3.85	0.40	0.81	0.47	2.02
	3.79	0.40	0.81	0.46	2.05
Avg.	3.80 ± 0.07	0.40 ± 0.01	0.80 ± 0.02	0.46 ± 0.01	2.01 ± 0.04

[a] Values normalized per g of silica.

[b] Based on a hydroxyl content of (0.40 ± 0.02) and (0.86 ± 0.02) mmol / g for silica-500 and -200 respectively. [6]

This 1:1 stoichiometry implies that the OH groups terminating the surface of silica-500 are isolated and capable of reacting with only one amide complex each, as was the case for grafting of $Ti(NR_2)_4$ (R = Me, Et).

Exposure of silica pre-treated at 200°C (silica-200) to the vapour of **15** also results in irreversible chemisorption. The colour change is identical to that on silica-500, from colourless or white to brown, and volatile organics are again released into the gas phase. Once the reaction was complete and the excess $Mo(NMe_2)_4$ removed to a liquid nitrogen cold trap, the molybdenum content was determined to be (3.80 ± 0.07) wt. % Mo, Table 7.1. These values are highly reproducible and correspond to 0.5 Mo/≡SiOH. As in the reaction with silica-500, the sole gas phase product is the corresponding amine, $HNMe_2$, identified by GC and GC/MS. The quantity of amine released is also reproducible, Table 7.1, and amounts to 2.0 $HNMe_2$/Mo. Thus, the stoichiometry of grafting of $Mo(NMe_2)_4$ onto silica-200 can be written as in eq. 7.3:

$$2\ \equiv SiOH + Mo(NMe_2)_4 \rightarrow (\equiv SiO)_2Mo(NMe_2)_2 + 2\ HNMe_2 \qquad (7.3)$$

15 **17**

This 2:1 stoichiometry implies that the OH groups terminating the surface of silica-200 exist in close proximity and react preferentially in pair-wise fashion, as was observed for the grafting of $Ti(NR_2)_4$ (R = Me, Et).

7.3 Infrared characterization of $Mo(NMe_2)_4$-modified silicas

Upon reaction of **12** with either silica-500 or -200, the intense ν(SiO-H) mode of silica, located at 3747 cm^{-1}, disappears, Figure 7.1. At the same time, new bands appear. The high frequency modes consist of bands in the C-H stretching and deformation regions. Qualitatively, the spectrum of **16** (on silica-500) is very similar to the spectrum of **17** (on silica-200).

The spectra of $(\equiv SiO)_nMo(NMe_2)_{4-n}$ (n = 1, 2) are very similar to reported spectra for $Ti(NMe_2)_4$[7,8] and $(\equiv SiO)_nTi(NMe_2)_{4-n}$ (Chapter 3). In the C-H stretching region, five peaks are visible, Figure 7.1b and Table 7.2. In the low frequency region of the spectrum not obscured by the absorbance of the silica matrix, the peak at 943 cm^{-1} (for $(\equiv SiO)_2Mo(NMe_2)_2$) is assigned is assigned to $\nu(NC_2)$. We note that the vibration at 600 cm^{-1}, which occurs in the spectra of $(\equiv SiO)_nTi(NMe_2)_{4-n}$ and assigned to ν(Ti-N),is not present in the spectra of $(\equiv SiO)_nMo(NMe_2)_{4-n}$, as expected. The ν(Mo-N) mode presumably lies at lower energy, outside the observable window.

7.4 NMR characterization of $Mo(NMe_2)_4$-modified silicas

The ^{13}C CP/MAS NMR spectrum of **17** consists of an extremely broad peak centred at ca. 47 ppm, Figure 7.2. It is assigned to the carbon present in the dimethylamido ligands, by comparison to the $^{13}C\{^1H\}$ NMR spectrum of $Ti(NMe_2)_4$ in C_6D_6 (44.4 ppm), as well as $(\equiv SiO)_2Ti(NMe_2)_2$ (43 ppm). The poor quality of the spectrum (signal-to-noise) cannot be explained by the small amount of carbon present, since spectra of $(\equiv SiO)_nTi(NMe_2)_{4-n}$ recorded under comparable conditions are much better resolved (Chapter 3). However, the electronic

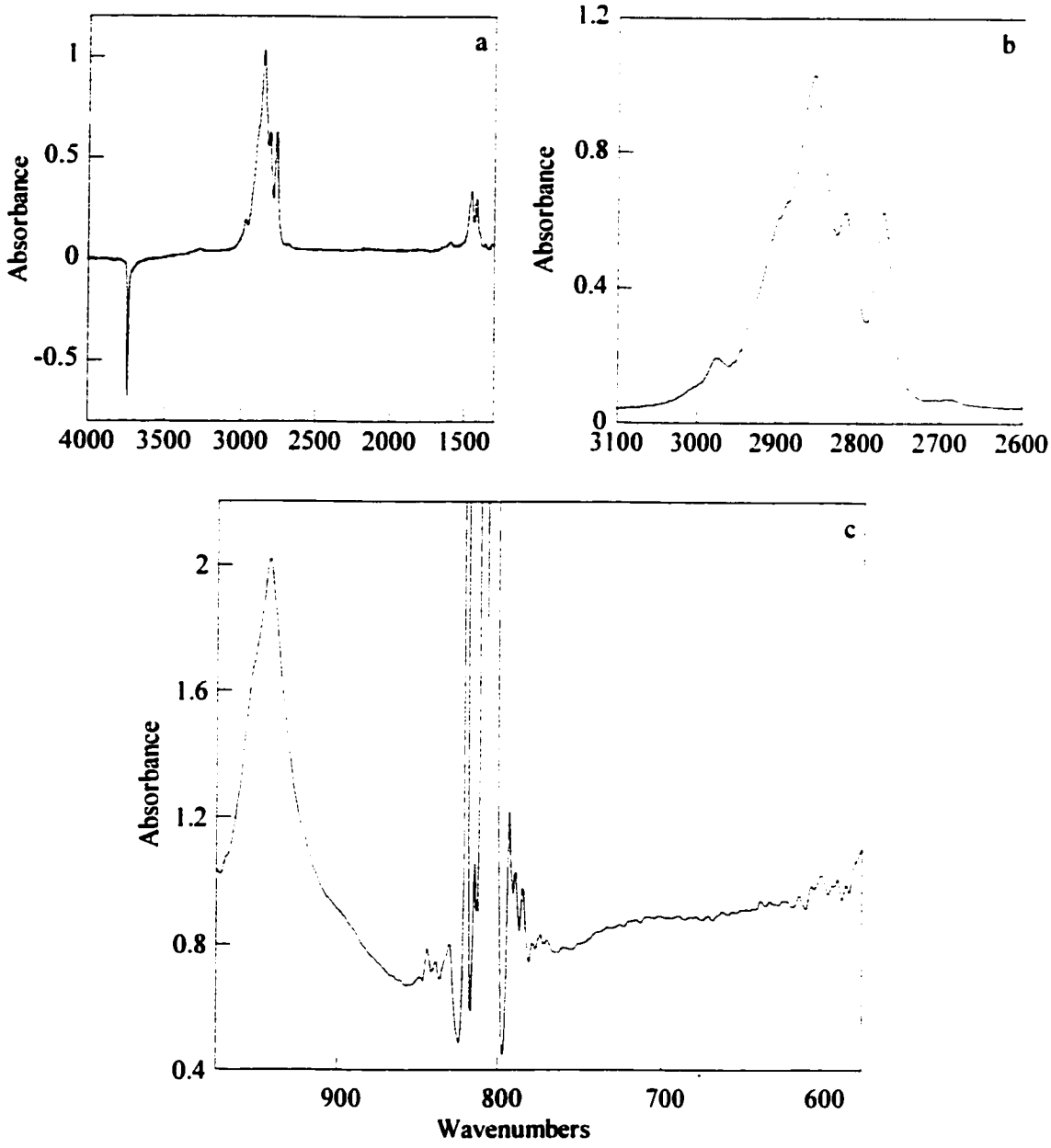

Figure 7.1 *In situ* IR difference spectra of regions of partial transmission of a self-supporting silica pellet after grafting of $Mo(NMe_2)_4$, **15**, onto silica-200. Excess **15** has been desorbed and the volatiles removed. A reference spectrum of silica-200 has been subtracted, thus negative peaks signify modes that disappeared upon reaction.

Table 7.2 IR modes of silicas modified with $Mo(NMe_2)_4$.

$(\equiv SiO)_nMo(NMe_2)_{4-n}$		Assignment[7,8]
n = 1	n = 2	
2973	2974	$\nu(CH_3)$
2899 sh	2893 sh	"
2859	2854	"
2818	2816	"
2768	2770	$\nu_s(CH_3)$
1465	1464	$\delta(CH_3)$
1450	1448	"
1416	1415	"
944	943	$\nu_s(NC_2)$

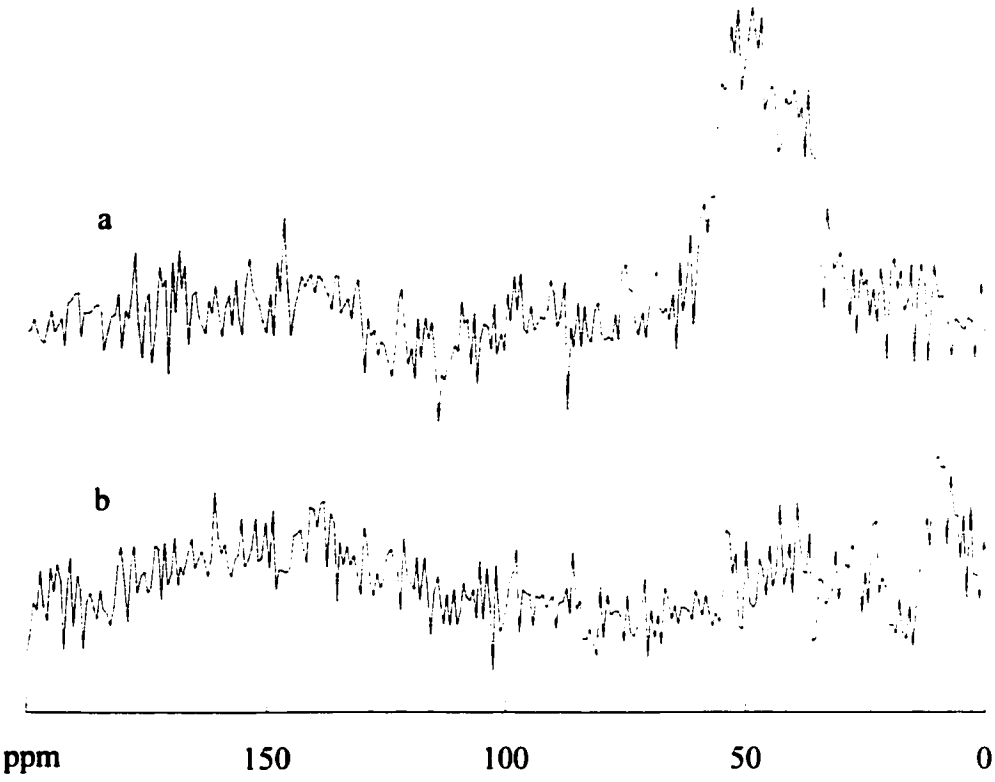

Figure 7.2 ^{13}C CPMAS spectrum of (a) $(\equiv SiO)_2Mo(NMe_2)_2$, **17**, (65,536 scans); and (b) silica-200 after exposure to $Mo(NEt_2)_4$ (123,400 scans).

structures of Ti(IV) and Mo(IV) are different. While d^0 complexes of Ti(IV) are necessarily diamagnetic, Mo(IV) is d^2. While molecular complexes $Mo(NR_2)_4$ are reported to be diamagnetic, as a result of interaction between the nitrogen lone pairs and d-orbitals on the Mo which lifts the degeneracy of the lowest-energy d orbitals.[2,9] this effect may be weakened in the surface complexes $(\equiv SiO)_nMo(NR_2)_{4-n}$ due to replacement of one or more amido ligands by the silica. The expected result would be a weak, broad or non-observable ^{13} CP/MAS spectrum.

7.5 Insertion of CO_2

A known reaction of molybdenum(IV) dialkylamides is the insertion of CE_2 (E = O, S) into the metal-nitrogen bond, and the quantitative formation of either dialkylcarbamates (E = O) or dialkyldithiocarbamates (E = S), eq 7.1.[2]

Exposure of **17** to excess CO_2 results in a rapid change in the IR spectrum, Figure 7.3. The ν(CH) region undergoes a drastic change, as does the $\delta(CH_3)$ region. The characteristic ν(C-H) pattern due to the dimethylamide ligands is replaced by a much less intense and less well-resolved pattern. Intense new bands appear in the IR spectrum which match those reported in the corresponding titanium molecular and silica-supported complexes, Table 7.3. The peaks at 1564, 1494, 1466 and 1409 cm^{-1} are assigned to $\nu_{as}(O_2C)$ and $\nu_s(O_2C)$. In the low frequency region, new peaks are seen at 964, 926, 905 and 652 cm^{-1}. The latter is assigned to $\delta(O_2CN)$ by analogy to the vibration at 650 and 660 cm^{-1} in $Ti(O_2CNMe_2)_4$ and $(\equiv SiO)_2Ti(O_2CNMe_2)_4$, respectively.

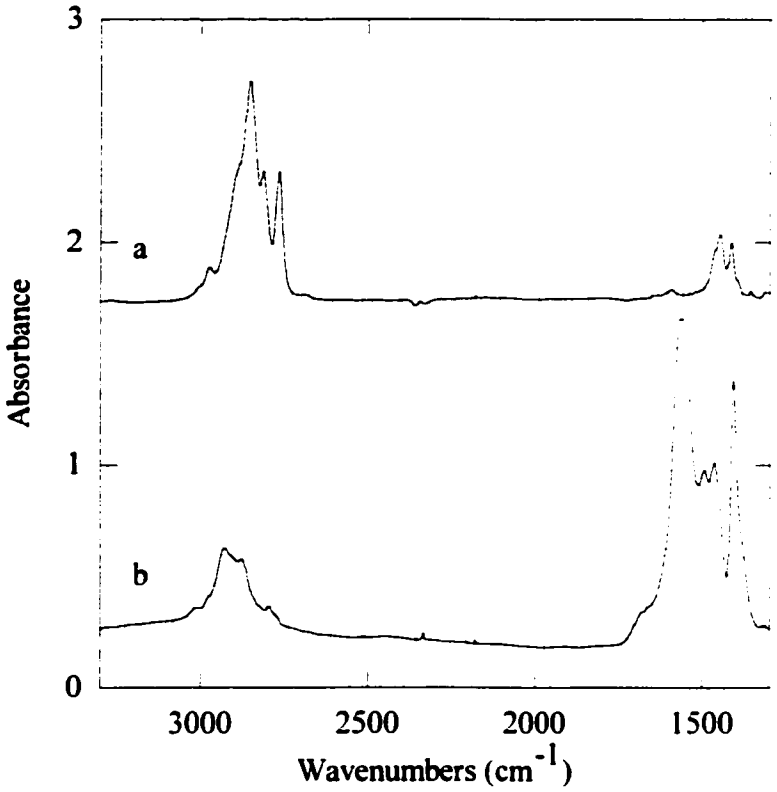

Figure 7.3 In-situ IR spectra of (a) $(\equiv SiO)_2Mo(NMe_2)_2$, **17**, and (b) after exposure to CO_2. In each case, a reference spectrum of silica-200 has been subtracted and all volatiles evacuated.

Table 7.3 Peak positions and assignments for $Ti(O_2CNMe_2)_4$, $(SiO)_2Ti(O_2CNMe_2)_2$, and $(SiO)_2Mo(O_2CNMe_2)_2$

$Ti(O_2CNMe_2)_4$[13]	$(\equiv SiO)_2Ti(O_2CNMe_2)_2$	$(\equiv SiO)_2Mo(O_2CNMe_2)_2$	Assignment[13]
1738			
1690	1700		
1589	1587	1564	$\nu_{str}(O_2CN)$ (bidentate)
1512			
1503	1500	1494	
	1461	1466	
1408	1416	1409	
1266	1276		
1170			
1153			
1058			
1042			
950	953	964	
		926	
865	867	905	
784			
650	660	652	$\delta(O_2CN)$
446			ν_{str}(M-O)
352			
250			

[a] Not observed due to intense absorbance of the silica lattice from 1000-1300, 775-850, and 400-600 cm^{-1}.

7.6 Grafting of $Mo(NEt_2)_4$ on silica

$Mo(NEt_2)_4$ is a volatile purple liquid. Exposure of silica-500 to vapour of $Mo(NEt_2)_4$, **18**, in a sealed reactor (base pressure < 10^{-4} Torr) results in an irreversible chemisorption of the metal complex onto the surface. The silica, initially colourless, acquires a yellow-brown colour over the course of the reaction (ca. 3 hrs) while volatiles are released into the gas phase. After unreacted $Mo(NEt_2)_4$ was removed via desorption into a liquid nitrogen cold trap, the maximum amount of chemisorbed Mo was found to reach 7.4 wt %, Table 7.4.

During grafting of **18**, the sole gas phase product is $HNEt_2$, identified by GC and GC/MS. The amount of amine released during the reaction between $Mo(NEt_2)_4$ and silica was quantified by *in situ* gas phase IR spectroscopy. Based on the average of 5 experiments at Mo loadings ranging from 3.8 to 7.4 wt. %, (1.5 ± 0.1) mol $HNEt_2$ was liberated per mol of grafted Mo. The results are summarized in Table 7.4. In comparison to the analogous grafting of $Mo(NMe_2)_4$ on silica-500 (Section 7.2), the maximum amount of Mo deposited from $Mo(NEt_2)_4$ exceeds the number of available hydroxyl groups by a factor of two. Furthermore, the amount of $HNEt_2$ generated during grafting exceeds the number of hydroxyls reacted by a factor of 1.5. Therefore, unlike the reaction of $Mo(NMe_2)_4$ with silica-500, grafting of $Mo(NEt_2)_4$ does not occur with a simple reaction stoichiometry. The mass balance on silica-500 is shown in eq 7.4:

$$\equiv SiOH + 2\ Mo(NEt_2)_4 \rightarrow (\equiv SiO)Mo_2(NEt_2)_3(N(Et)CHCH_3)_2 + 3\ HNEt_2 \qquad (7.4)$$

18 **19**

Table 7.4 Quantitative product analysis for the reaction of $Mo(NEt_2)_4$ with silica

Silica pretreatment temperature	wt. % Mo	Mo[a] mmol / g	$HNEt_2$[a] mmol / g	Mo / ≡SiOH[b]	$HNEt_2$ / Mo
500°C	7.4	0.78	1.10	1.9	1.4
	5.2	0.55	0.71	1.4	1.3
	4.2	0.44	0.70	1.1	1.6
	4.0	0.42	0.67	1.0	1.6
	3.8	0.40	0.64	1.0	1.6
Average					1.5 ± 0.1
200°C	7.5	0.85	1.62	0.9	1.9
	5.6	0.63	1.13	0.7	1.8
	4.4	0.50	1.10	0.8	2.1
	4.0	0.45	0.94	0.6	2.1
	3.7	0.42	0.80	0.5	1.9
Average					2.0 ± 0.1

[a] Values normalized per g of silica.

[b] Based on a hydroxyl content of (0.40 ± 0.02) and (0.86 ± 0.02) mmol / g for silica-500 and -200 respectively. [6]

Exposure of silica-200 to **18** vapor also results in an irreversible chemisorption of the metal complex onto the surface. The silica, initially colorless, again acquires a yellow-brown color over the course of the reaction (ca. 3 hrs) while volatiles are released into the gas phase. After unreacted $Mo(NEt_2)_4$ was removed via desorption into a liquid nitrogen cold trap, the maximum amount of chemisorbed Mo was found to reach 7.5 wt. %, Table 7.4.

During grafting of **18** on silica-200, the sole gas phase product is $HNEt_2$, identified by GC and GC/MS. The amount of amine released during the reaction between $Mo(NEt_2)_4$ and silica was quantified by *in situ* gas phase IR spectroscopy. Based on the average of 5 experiments for Mo loadings ranging from 3.7 to 7.5 wt. %, (1.96 ± 0.13) mol $HNEt_2$ were liberated per mol of grafted Mo, Table 7.4. In comparison to the analogous grafting of $Mo(NMe_2)_4$ on silica-200 (see above), in which the Mo loading at full coverage is one-half the number of hydroxyls, the maximum amount of Mo deposited from $Mo(NEt_2)_4$ is equal to the number of surface hydroxyls. However, the amount of $HNEt_2$ generated during grafting exceeds the number of hydroxyls reacted by a factor of 2.0. Therefore, grafting of $Mo(NEt_2)_4$ on silica-200 also does not occur with a simple reaction stoichiometry. The mass balance is shown in eq. 7.5:

$$2\ \equiv SiOH + 2\ Mo(NEt_2)_4 \rightarrow (\equiv SiO)_2Mo_2(NEt_2)_2(N(Et)CHCH_3)_2 + 4\ HNEt_2 \qquad (7.5)$$

18 **20**

7.7 Spectroscopic characterization of $Mo(NEt_2)_4$ modified silicas

Upon reaction of excess **18** with either silica-500 or -200, the intense ν(SiO-H) mode of silica, located at 3747 cm^{-1}, disappears, Figure 7.4. At the same time, new high frequency bands in the C-H stretching and deformation regions appear, Table 7.5. Many of the bands are very similar to those observed for $(\equiv SiO)Ti(NEt_2)_3$, **5**, with one significant exception.

An additional, intense peak appears at 1635 cm^{-1} in spectra of $(\equiv SiO)_nMo(NEt_2)_{4-n}$. Its frequency suggests that it may be a ν(C=N) mode, by comparison to the IR spectrum of N-methylmethanimine, which shows ν(C=N) located at 1661 and 1659 cm^{-1} in the gas phase and in an argon matrix, respectively.[10,11] We note that the IR spectra of $(\equiv SiO)_nMo(NMe_2)_{4-n}$, Figure 7.1, shows no features in this region.

The ^{13}CP/MAS spectrum of silica-200 modified with **18** is shown in Figure 7.2b. Peaks are expected at ca. 14 and 46 ppm for the ethyl groups of the diethylamido ligands. However, hardly any signal is discernable, even after an acquisition time of 48 hours for a sample loaded with 5.6 wt. % Mo. It appears that grafting $Mo(NEt_2)_4$ on silica produces a paramagnetic material.

7.8 Mechanism of grafting of $Mo(NEt_2)_4$ onto silica

The stoichiometry of grafting of $Mo(NEt_2)_4$ onto either silica-500 or -200 is not as simple as the grafting of $M(NR_2)_4$ (M = Ti, R = Me, Et; M = Mo, R = Me). Nevertheless, the first step is likely

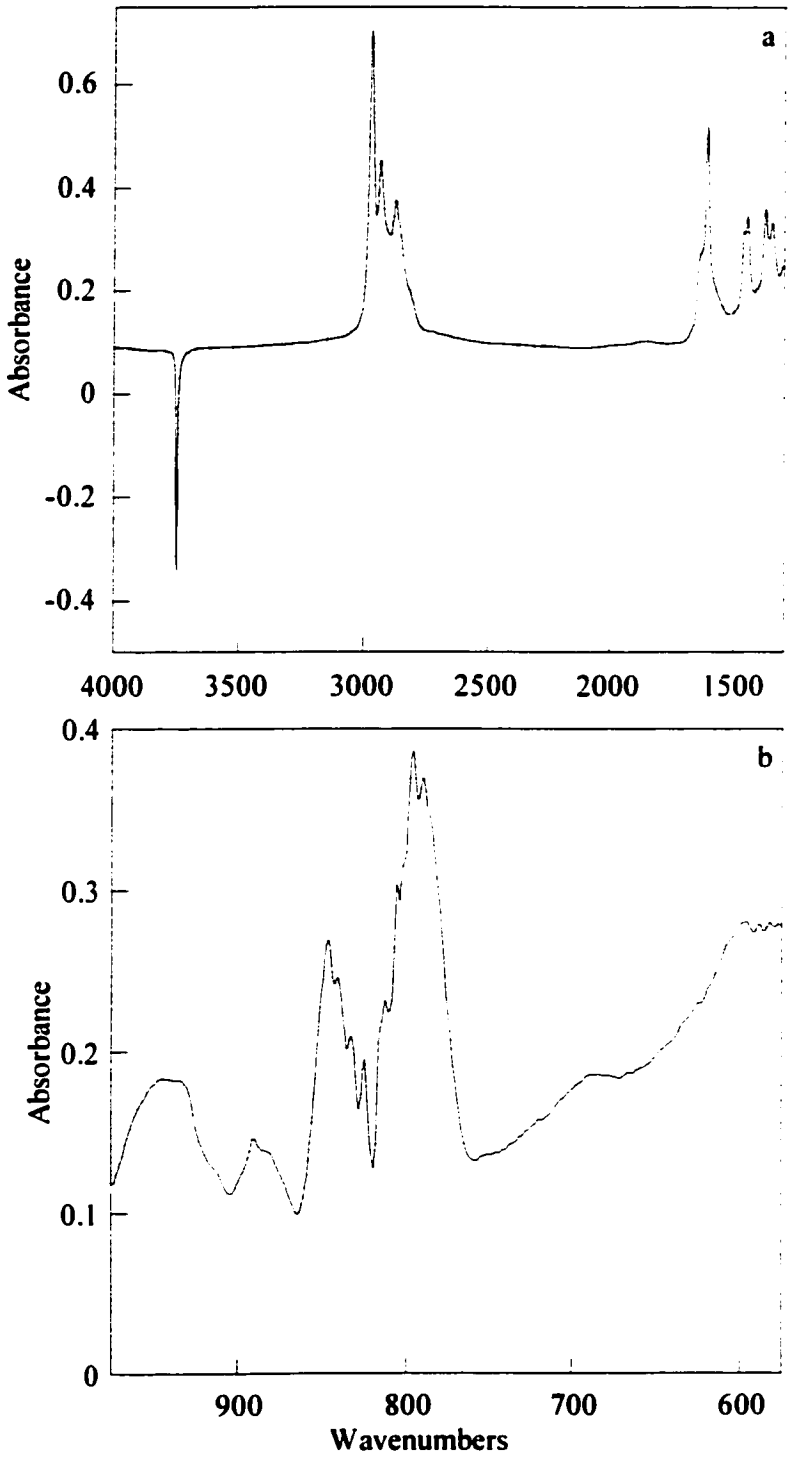

Figure 7.4 IR difference spectra of (≡SiO)Mo(NEt_2)$_3$. Volatiles have been removed and a background reference spectrum of silica-500- has been subtracted.

Table 7.5 Peak assignments in IR spectra of silica-500 modified with $M(NEt_2)_4$ (M = Ti, Mo)

$(\equiv SiO)Ti(NEt_2)_3$	Assignment[12]	$(\equiv SiO)Mo(NEt_2)_3$
2973	$\nu_{as}(CH_3)$	2969
2937	$\nu_{as}(CH_2)$	2933
2880	$\nu_s(CH_3)$	2872
2848	$\nu_s(CH_2)$	2855 (sh)
	$\nu(C=N)$	1635
1462	$\delta_s(CH_2)$	1463
1453	$\delta_{as}(CH_3)$	1450
1373	$\delta_s(CH_3)$	1375
1353	$\delta(CH_2)$	1349
992	$\nu_s(NC_2)$	
957	ν(Si-OM)	947
910		
882		880
616	ν(Ti-N)	

the reaction of $Mo(NEt_2)_4$ with the hydroxyl groups terminating the surface of the silica. Schemes 7.1 and 7.2. Whereas in the grafting of $Ti(NR_2)_4$ and $Mo(NMe_2)_4$, the resulting grafted dialkylamide metal fragments were stable, at least for several hours, for $Mo(NEt_2)_4$-modified silicas β-H elimination appears to occur spontaneously on the time-scale of grafting. These reactions are analogous to the spontaneous extrusion of $HNEt_2$ from $(\equiv SiO)_2Ti(NEt_2)_2$, Chapter 4. Once the N-ethylethanimine ligand is formed, further reaction with $Mo(NEt_2)_4$ occurs. The overall stoichiometry of grafting, as depicted in Schemes 7.1 and 7.2, is consistent with that shown in eqs 7.3-7.4.

The N-ethylethanimine ligand has two canonical resonance forms, Scheme 7.3. Evidence for a significant contribution from resonance form **II** lies in the intense band located at ca. 1635 cm^{-1} in the IR spectra of **19** and **20**. This bonding also implies a formal reduction of Mo(IV) to Mo(II), which result in an increased Mo-Mo bond order in the dinuclear products **19** and **20**.

7.9 Conclusion

In this chapter, the formation of two well-defined, silica-supported molybdenum complexes with the composition $(\equiv SiO)_nMo(NMe_2)_{4-n}$ (n = 1, 2), resulting from the reaction of $Mo(NMe_2)_4$ with silica, was documented. The value of n depends on the thermal pretreatment of the silica. On silica-500, $Mo(NMe_2)_4$ reacts with a single surface hydroxyl group (i.e., n = 1), whereas on silica-200, reaction occurs with pairs of hydroxyl groups (i.e., n = 2). IR spectroscopic characterization of the supported complexes is consistent with the retention of intact dialkylamido ligands, although the ^{13}C CP/MAS NMR spectrum shows evidence of

Scheme 7.1 Proposed mechanism for reaction of $Mo(NEt_2)_4$ with silica-500

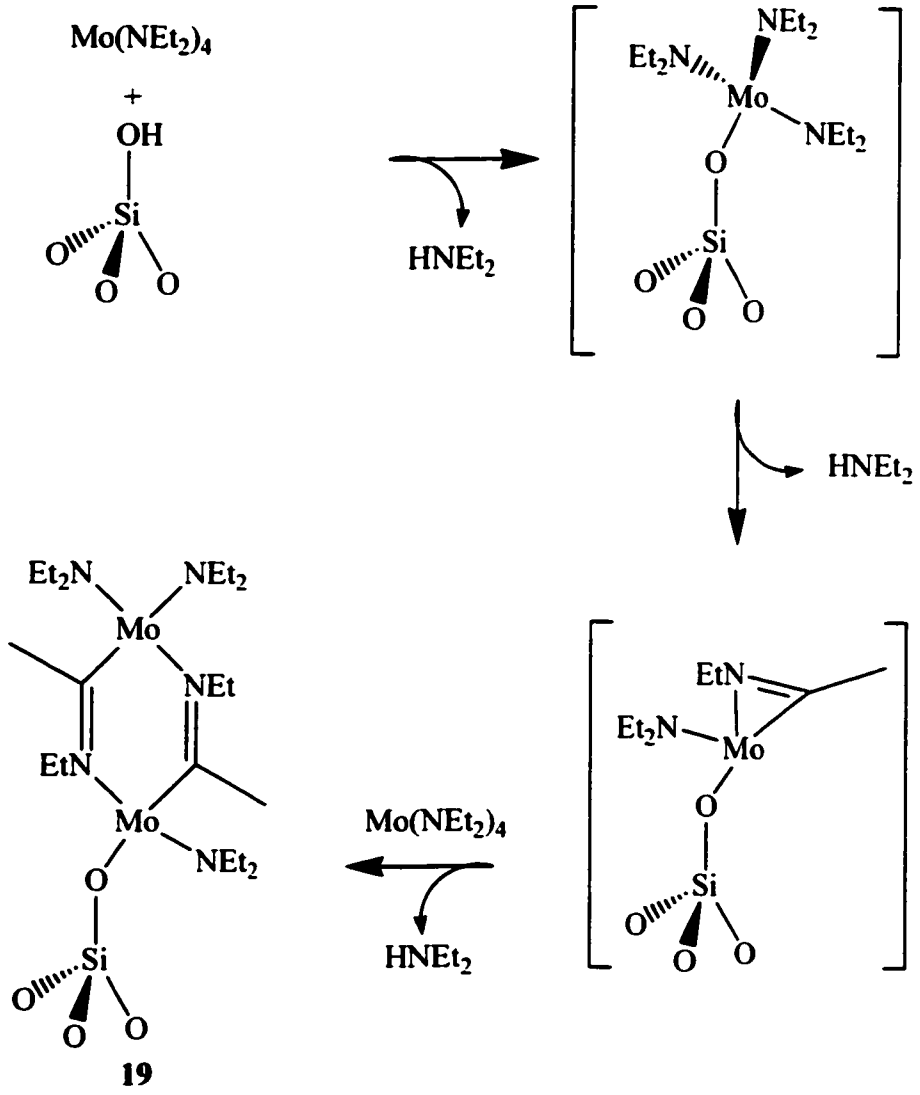

19

Scheme 7.2 Proposed mechanism for the reaction of $Mo(NEt_2)_4$ with silica-200

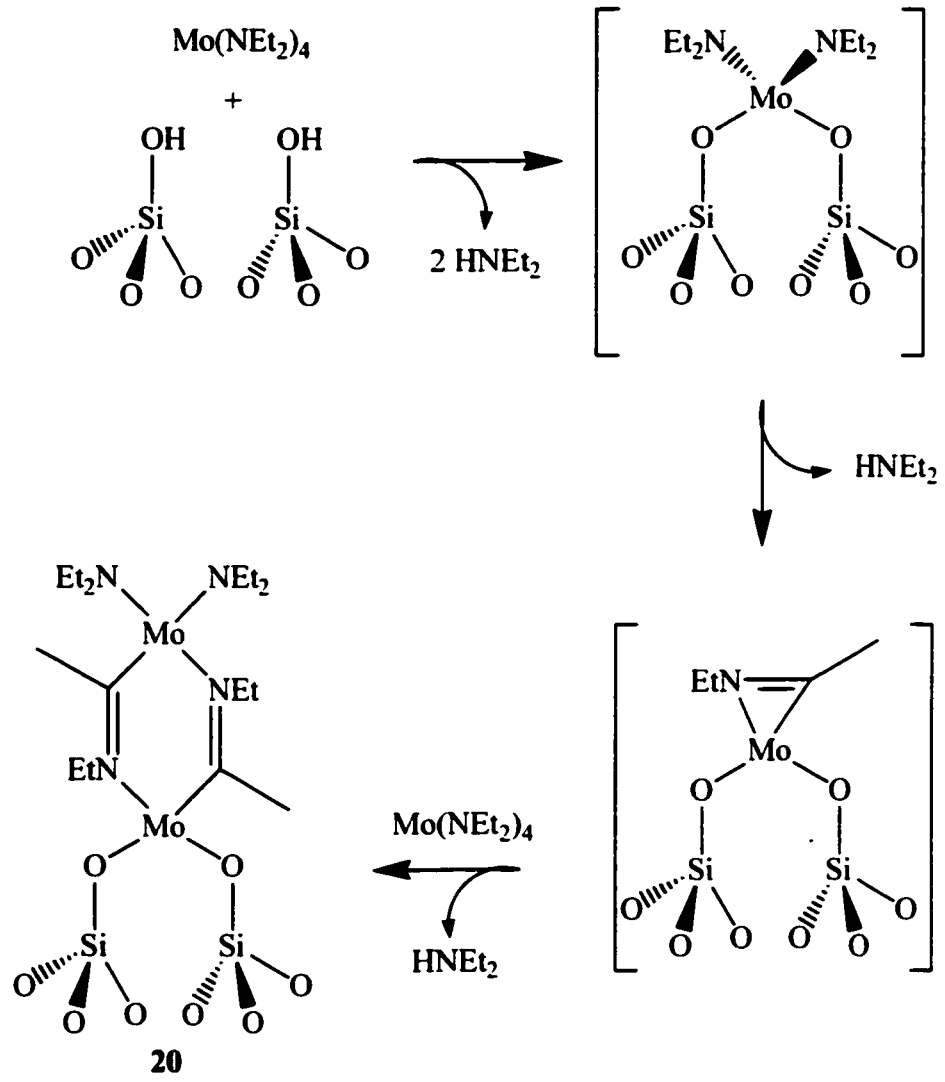

20

Scheme 7.3 Resonance structures of a bridging N-ethylethanimine ligand

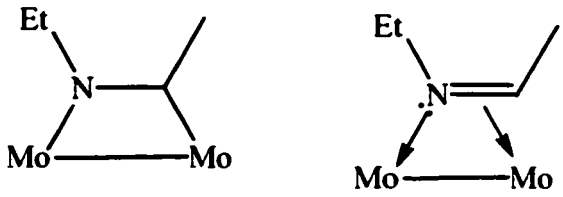

I II

paramagnetism and was therefore of limited usefulness in characterizing the ligands.

The reactions of $Mo(NEt_2)_4$ with silica are more complicated. While the initial step in the grafting is likely reaction with surface hydroxyls, further spontaneous β-H elimination results in further liberation of diethylamine and grafting of $Mo(Net_2)_4$ on the N-ethylethanimine surface complex. The molybdenum centres appear to have been formally reduced, since the amine ligands exhibit IR spectra consistent with substantial C=N double bond character, in contrast to titanium analogues which are closer to azametallacycles. The oxidation state of Mo was not determined, although NMR spectra suggest paramagnetism.

7.10 References

(1) Chisholm, M. H.; Reichert, W. W.; Thornton, P. *J. Am. Chem. Soc.* **1978**, *100*, 2744-2748.

(2) Bradley, D. C.; Chisholm, M. H. *J. Chem. Soc (A)* **1971**, 2741-2744.

(3) Roberson, S. L.; Finello, D.; Davis, R. F. In *Chem. Mater.*, *1990, 2, 150*: U. S. A., 1997.

(4) Markel, E. J.; Burdick, S. E.; II, M. E. L.; Roberts, K. L. *J. Cat.* **1999**, 136-147.

(5) Sun, S.-C.; Chiu, H.-T., Taiwan Semiconductor Manufacturing Company: U. S. A., 2000.

(6) Rice, G. L.; Scott, S. L. *Langmuir* **1997**, *13*, 1545-1551.

(7) Dubois, L. H.; Zegarski, B. R.; Girolami, G. S. *J. Electrochem. Soc.* **1992**, *139*, 3603-3609.

(8) Bürger, H.; Stammreich, H.; Sans, T. T. *Monatsh. Chem.* **1966**, *97*, 1276-1279.

(9) Chisholm, M. H.; Cotton, F. A.; Extine, M. W. *Inorg. Chem.* **1978**, *17*, 1329-1332.

(10) Stolkin, I.; Ha, T.-K.; Gunthard, H. H. *Chem. Phys.* **1977**, *21*, 327.

(11) Hinze, J.; Curl, R. F., Jr. *J. Am. Chem. Soc.* **1964**, *86*, 5068.

(12) Silverstein, R. M.; Webster, F. X. *Spectrophotometric Identification of Organic Compounds*; 6th ed.; Wiley: Toronto, 1998.

(13) Chisholm, M. H.; Extine, M. W. *J. Am. Chem. Soc.* **1977**, *99*, 782-792.

Chapter 8

General conclusions

Through analysis of the stability and reactivity of silica-supported titanium dialkylamide complexes, we have attempted to determine the manner by which carbon is incorporated into TiN films. Amorphous silica was used to model the surfaces of the silicon wafers most commonly used as substrates for TiN films. Exposure of $Ti(NR_2)_4$ (R = Me, Et) to silicas partially dehydroxylated at 500 and 200 °C results in the formation of well-defined tris- and bis(dialkylamido)titanium(IV) fragments. The dialkylamido ligands show reactivity towards CO_2 and ROH consistent with the behaviour of analogous molecular complexes in solution.

Spontaneous elimination of amine from the bis(dialkylamido)titanium fragments was discovered. the products were characterized as imine (R = Me, Et) and imide (R = Et) complexes. The transformations are catalyzed by surface hydroxyls.

Monoalkylamines, taking into account the lack of mobility enforced by the silica-titanium bond, react in a manner similar to their solution reactivity, forming mononuclear imidotitanium complexes upon exposure to the bis(dialkylamido) fragments. Exposure of the bis(dialkylamido)titanium complexes to dialkylamines results in the inducing of β-H elimination and the elimination of amine from the surface fragment. The resulting complexes are very similar to those produced spontaneously. Non-protic amines such as pyridine and triethylamine also accelerate this transformation.

Ammonia, on the other hand, does not display reactivity predicted by its solution reactivity. Instead, when exposed to ammonia, the bis(dialkylamido)titanium fragments undergo β-H elimination to form imine complexes. These imine complexes, as well as the ethylimidotitanium complex formed by evacuation of the N-ethylethanimino titanium(IV)

fragment, are unreactive towards ammonia, however, they are reactive towards $Ti(NR_2)_4$, forming binuclear titanium species.

Under CVD conditions, the N in clean (low carbon) films comes primarily from ammonia, indicating that transamination occurs and is efficient. Under the conditions of our study, β-H elimination of amine is the dominant reaction pathway. Further study of the activation barriers of both pathways will determine the optimum conditions for the CVD of TiN where β-H elimination is minimized.

The reactions of $Mo(NR_2)_4$ (R = Me, Et) with silicas partially dehydroxylated at 200 and 500°C was examined to probe the generality of β-H elimination from surface dialkylamidometal complexes. When R is methyl, the grafting on the surface hydroxyls is straightforward, and well-defined surface fragments with the stoichiometry $(\equiv SiO)_nMo(NMe_2)_{4-n}$ (n = 1 or 2 for silica-500 and -200, respectively) are formed. In contrast, $Mo(NEt_2)_4$ undergoes β-H activation at a rate comparable to that of its grafting, resulting in the formation of dinuclear supported molybdenum fragments.

It is becoming clear that caution must be exercised when predicting the result of the grafting of organometallic complexes on silica surfaces. While in many cases the grafting reaction is limited to the exchange of one (or more) ligands for a siloxy ligand, there is mounting evidence that not all reactions are this simple. The first well-documented example of grafting complexity was the deposition of $Ti(O^iPr)_4$ onto silica, where, at a rate comparable to that of the grafting reaction, disproportionation of two isopropoxide ligands occurs. The product is a dinuclear titanium complex with an oxo-bridge resulting from propene elimination. In an analogous manner, the grafting of $Mo(NEt_2)_4$ results in disproportionantion of two diethylamido

ligands, resulting in the formation of an imine-bridged dinuclear molybdenum complex accompanied by elimination of diethylamine.

List of Publications

1. Beaudoin, M. C.; Womiloju, O.; Fu. A.; Nait Ajjou, J. A.; Rice, G. L.; Scott, S. L. Silica-supported Alkylidene Complexes: Their Preparation, Characterization and Reactivity, Especially towards Olefins; J. Mol. Cat. A: Chem.; in Press.

2. Beaudoin, M. C.; Scott, S. L. Spontaneous Evolution of Silica-Supported Ti Amide Fragments to Imine and Imido Complexes; Organometallics; 2001; 20(2); 237-239.

3. Alladin, T.; Beaudoin, M. C.; Scott, S. L. Thermolysis of Silica-supported Bis(neopentyl) Complexes of Titanium and Zirconium; Inorg. Chim. Acta; in Press.

Claims to Original Research

This thesis contributes to the basic understanding of the mechanism of carbon incorporation during the LPCVD of TiN by reporting the composition and reactivity of silica-supported titanium(IV) complexes. By controlling the density of surface hydroxyls, we have been able to isolate tris- and –bis(dialkylamido)titanium(IV) fragments on the surface. These complexes spontaneously undergo β-H abstraction to give titanium(IV) imine and imido fragments, which have been previously proposed as intermediates in the deposition of TiN, but never isolated.

Through their reaction with ammonia, dialkylamines and aprotic amines, we have demonstrated an addition β-H activation pathway for the dialkylamidotitanium(IV) complexes. The resulting titanium(IV) imine complexes are stable to ammonia, yet are reactive towards $Ti(NR_2)_4$, resulting in imine- or imido-bridged bis(titanium) sites.

The imine bridges derived from $Ti(NMe_2)_4$ contain both Ti-C and Ti-N bonds, while the imido bridges in $Ti(NEt_2)_4$-based films contain solely Ti-N bonds. This difference may explain how different kinds of carbon, both organic and carbidic, are incorporated into TiN films.

We have demonstrated that, while tatrakis(dimethylamido)molybdenum(IV) complexes react with silica in a manner analogous to their Ti counterparts, $Mo(NEt_2)_4$ undergoes β-H activation at a rate comparable to that of grafting. The resulting surface complex contains both terminal amido ligands as well as imine ligands bridging two molybdenum centers.